Doctoral theses at NTNU, 2017:139

Espen Skjong

Optimization-based Control in Shipboard Electric Systems

Doctoral Thesis

Espen Skjong

ISBN 978-82-326-2350-1 (printed version)
ISBN 978-82-326-2351-8 (electronic version)
ISSN 1503-8181

Doctoral theses at NTNU, 2017:139

NTNU
Norwegian University of
Science and Technology
Faculty of Information Technology
and Electrical Engineering
Department of Engineering Cybernetics

NTNU
Norwegian University of
Science and Technology

NTNU

NTNU
Norwegian University of
Science and Technology

Espen Skjong

Optimization-based Control in Shipboard Electric Systems

Thesis for the degree of Philosophiae Doctor

Trondheim, June 2017

Norwegian University of Science and Technology
Faculty of Information Technology and Electrical Engineering
Department of Engineering Cybernetics

NTNU
Norwegian University of
Science and Technology

NTNU
Norwegian University of Science and Technology

Thesis for the degree of Philosophiae Doctor

Faculty of Information Technology and Electrical Engineering
Department of Engineering Cybernetics

ISBN 978-82-326-2350-1 (printed version)
ISBN 978-82-326-2351-8 (electronic version)
ISSN 1503-8181

Doctoral theses at NTNU, 2017:139

Printed by Skipnes Kommunikasjon as

Summary

With stringent, and globally sanctioned, environmental rules and regulations, dictating limits for allowed emissions of greenhouse gases and particle matter from combustion of fossil fuels, the marine vessel's efficiency has recently received a lot of attention. At the same time, in addition to meet environmental requirements from multiple stakeholders, ship owners strive to enhance revenue in an economically challenged market by reducing operational costs and gain competitive advantages. Examples of such competitive advantages are reduced environmental footprints, increased vessel/operational platform efficiency, operational flexibility and reliability, and higher Environmental Regularity Numbers (ERN). To asses the marine vessel's efficiency is complex and involves multiple disciplines. In this work, the main contributions are centered around the discipline automation and automatic control design, with the use of optimization-based control strategies to improve the (AC) shipboard power plant's efficiency. Two topics are covered in this thesis: Optimal harmonic mitigation using Model Predictive Control (MPC), and optimization-based unit commitment as part of Energy Management Systems (EMS). These two topics, although intertwined, represents different levels of power system control and contribute both to the efficiency of the shipboard power plant.

The thesis is divided into three parts. The first part, which is covered by Chapter 2, presents a review of the shipboard electrical power system's evolution. From the first successful use of shipboard electricity, marked by the use of electricity in *SS Columbia* in 1880 for illumination purposes, to present day with all-electric vessels using batteries, the shipboard power system has transitioned from containing few single-purpose passive components to containing many multi-purpose active components that rely on automatic control. Thus, the discipline automation and automatic control design plays an important part in the present stage of the shipboard electrical power system's evolution. Chapter 2 ends with a discussion of properties and challenges of the marine vessel's power system, including, among others, AC vs DC, integrated power systems and grid design, power electronics, harmonic pollution and electrical stability, and the increasing level of software complexity.

The second part of the thesis, which is covered by Chapter 3-5, addresses the problem of harmonic pollution and presents a novel harmonic mitigation strategy based on optimal control. The proposed method, which relies on a single, controllable Active Power Filter (APF), uses an MPC that (online) generates APF current references based on an optimization objective to minimize the total harmonic pollution in the whole power system – a system-level harmonic mitigation approach. Chapter 3 presents simulation results of the proposed method compared with two conventional APF control strategies using a two-bus shipboard power system with 6- and 12-pulse rectifier loads as test subject. The results demonstrate that the MPC is able to generate current references that better utilize the APF current capability for system-level harmonic mitigation, and is able to reduce the Total Harmonic Distortion (THD) beyond what is achieved with the conventional mitigation approaches. Chapter 4 introduces a system-level harmonic mitigation approach, also considering the control of a single APF, that is based on offline analytical optimization. The offline analytical optimization method is compared with the MPC in Chapter 3 and conventional mitigation strategies using a two-bus shipboard power system with 12-pulse rectifier loads as test subject. Non-idealities, such as parameter-mismatch and transformer saturation, are introduced in the simulation, and the results show that also in this case the MPC-based system-level harmonic mitigation method is superior compared to the offline analytical optimization and the conventional mitigation approaches. The last chapter in this part, Chapter 5, addresses an event-based system architecture with real-time implementation of a single-phase version of the MPC presented in Chapter 3 and 4 for system-level harmonic mitigation. Hardware-In-Loop (HIL) simulations using two desktop computers and a simulator demonstrate that the proposed system architecture and MPC implementation meet the real-time requirements for system-level harmonic mitigation.

The last part of the thesis, which is covered by Chapter 6, addresses the problem of unit commitment in an Energy Management System (EMS). Real power system data from three different vessels in operation, a ferry, a Platform Supply Vessel (PSV) and a seismic survey vessel, are extracted and analyzed with regards to diesel-generator-set (genset) loadings and genset running hours to shed light on potential fuel efficiency improvements. As demonstrated by the extracted data, the gensets in all three vessels run with non-optimal loading conditions relative individual gensets' Specific Fuel Oil Consumption (SFOC) curves. Two unit commitment methods, one based on

Mixed-Integer Linear Programming (optimization) and one based on logics, are presented and discussed. Moreover, three power system configurations are proposed; i) four fixed-speed gensets, ii) three fixed-speed genset and one variable-speed genset, and iii) four fixed-speed gensets and an Energy Storage System (ESS). The two unit commitment methods are compared by simulation studies of the three proposed power system configurations, using the real load profiles extracted from the three vessels during operation. The simulation results indicate that optimal EMS algorithms in combination with a revised power system configuration can increase the operational efficiency, in terms of fuel savings and reduction in genset running hours.

The last chapter in the thesis, Chapter 7, summarizes and concludes the work, and presents recommendations for future work.

Preface

This thesis is submitted in partial fulfillment of the requirements for the degree of philisophiae doctor (Ph.D.) at the Norwegian University of Science and Technology (NTNU). The research has been carried out at the department of Engineering Cybernetics (ITK), the Centre of Autonomous Marine Operations and Systems (AMOS) and Ulstein Power & Control AS (UPC) from August 2014 to June 2017. The work was supervised by Professor Tor Arne Johansen (ITK, AMOS), Professor Marta Molinas (ITK), Professor Asgeir J. Sørensen (department of Marine Technology, AMOS) and Dr.ing. Rune Volden (UPC). The research project was funded by Ulstein Power & Control AS, where the author is currently employed, and the industrial Ph.D. programme of the Norwegian Research Council, project number 241205.

Acknowledgements

My doctoral studies have truly been an amazing journey. After finishing my MSc in Engineering Cybernetics at NTNU in June 2014, I was given the opportunity to pursue the Ph.D. degree as a regular employee in Ulstein Power & Control AS. I owe my deepest gratitude to Rune Volden and Trond Berg in UPC for making this possible. Rune, who is currently my immediate manager in UPC, has given me his full support through thick and thin, and has believed in me since day one. His happy nature, sincereness and ability to identify and cultivate potentials, an *enabler* with the motto "Den som sover hopper vi over!", has been a great source of inspiration. I am grateful to call him a friend, and I could not have imagined a better manager than him.

I would also like to thank all my amazing friends and colleagues in UPC. Especially, I would thank Egil Rødskar, who has been a non-credited supervisor. He has been there for me whenever I needed a sparring partner. His rich and deep knowledge in shipboard power systems, his curiosity, calmness and thoroughness have amazed me.

I would humbly like to express my sincere gratitude to my supervisors at NTNU. Professor Tor Arne Johansen, who has been my main supervisor, has supported me every step of the way, and has offered me valuable guidance whenever called for. I would also like to thank Tor Arne for introducing me to Professor Marta Molinas, who has been my co-supervisor. She took sincere, profound interest in my research and devoted much of her time to support me in the field of electrical engineering. I am grateful for her guidance and support, both as a supervisor and as a friend. Even though formally a co-supervisor, I consider both Tor Arne and Marta as my main supervisors. Tor Arne and Marta combined have given me the best possible supervision in the pursue of the Ph.D. degree, and I owe them both my deepest gratitude. I would also like to thank my co-supervisor Professor Asgeir J. Sørensen, who has been encouraging and provided me with his great comments and valuable inputs. Dr. Jon Are Suul, who has been a non-credited supervisor, also deserves to be acknowledged. It has been a pleasure and honor to work with him, and he has supported me and guided me along with Marta when I was stuck in the field of electrical engineering. Jon Are himself is a source of inspiration, and I humbly thank him for all the support and guidance he has offered me during my research. I would also like to thank my colleagues and fellow students at ITK and AMOS, among others Dr. Frederik S. Leira, Dr. Torstein I. Bø, Dr. Mark Haring, Atle Rygg and Serge Gale, who have all contributed with valuable inputs and discussions. My hunting buddies, Runar S. Kjerstad and Simen K. Fylling, also deserves a thank for all the great times out on the hunting fields while I pursued the Ph.D. degree.

Furthermore, I would like to thank Dr. Juan José Valera, Prof.ssa Mariagrazia Dotoli and Professor Jan Tommy Gravdahl for accepting to be in the dissertation defense committee.

I can never find words to express my most profound gratitude to my family. I am indebted to my father Leif Kristian, who has taught me the practical side of engineering since I was a small boy, and encouraged me to do my homeworks properly. I am also grateful to my mother Oddhild, who has supported me and taught me right and wrong in life, and my brother Stian, my sister Karoline and their families for all the warmth and support.

Espen Skjong
Trondheim, June 2017

Contents

Summary iii

Preface vi

Contents x

Nomenclature xi

1 Introduction 1

1.1 Background and Motivation 1

1.1.1 The Problem of Harmonic Pollution 3

1.1.2 The Problem of Unit Commitment in Energy Management Systems 5

1.2 Structure of the Thesis and Main Contribution 7

1.3 Publications 9

Part I: Revisiting the Evolution of Shipboard Electrification **13**

2 The Marine Vessel's Electrical Power System: Past, Present and Future Challenges **15**

2.1 Introduction 15

2.2 The Birth of the Marine Vessel Power Grid 17

2.2.1 War of Currents 21

2.2.2 The Early Turbo-Electric Surface Vessels 24

2.2.3 The Early Submarines 28

2.3 Effects of World War I and II 30

2.3.1 "The Navy Oilers" 33

2.3.2 Submarines using Diesel-Electric Systems 33

2.4 Towards Today's Marine Vessel Power Systems 35

2.4.1 The Advent of Power Electronics and Variable Speed Converters . . . 36
2.4.2 Towards All Electric Ships (AES) . . . 38
2.5 Properties and Challenges of the Marine Vessel's Power System 43
2.5.1 AC vs DC . . . 44
2.5.2 Marine Vessel Power Systems and Microgrids . . . 46
2.5.3 Integrated Power System (IPS) and Grid Design . . . 48
2.5.3.1 Electrical Stability . . . 52
2.5.3.2 Radial and Zonal Grid Designs . . . 53
2.5.4 Power Electronics and Harmonic Pollution . . . 54
2.5.5 Energy Management Systems (EMS) and Energy Storage Systems (ESS) . . . 59
2.5.5.1 ESS Applications . . . 60
2.5.5.2 Standards and Guidelines . . . 64
2.5.5.3 Emission Free Operation . . . 65
2.5.6 Increasing Need for Measurements, Big-Data, and Software Complexity . . . 65
2.6 Conclusion . . . 69

Part II: Harmonic Mitigation **71**

3 System-Wide Harmonic Mitigation in a Diesel Electric Ship by Model Predictive Control **73**
3.1 Introduction . . . 73
3.2 Marine Vessel's Power Grid . . . 75
3.3 Model Predictive Control . . . 78
3.3.1 Power Grid Model . . . 79
3.3.2 Active Power Filter Constraints . . . 82
3.3.3 Formulating the MPC on Standard Form . . . 83
3.4 Implementation . . . 85
3.4.1 Power Grid Implementation . . . 86
3.4.2 MPC Implementation . . . 86
3.4.3 Closing the Control Loop . . . 88
3.5 Results . . . 90
3.5.1 Study Case 1 . . . 92
3.5.2 Study Case 2 . . . 94
3.5.3 Study Case 3 . . . 96

3.6 Conclusion 99

4 In search of the best method for system-wide harmonic compensation in isolated microgrids: MPC vs offline analytical optimization 101

4.1 Introduction 101
4.2 The Microgrid Under Investigation 104
4.3 Analytically Optimized APF Current 105
4.4 MPC Generated Filter Current Reference 110
4.4.1 Model Formulation 111
4.4.2 Cost Function 112
4.4.3 Constraints 113
4.5 Results 113
4.5.1 Ideal Simulation 115
4.5.2 Parameter Mismatch 119
4.5.3 Transformer Saturation 120
4.6 Conclusion 123

5 Real-time Model Predictive Control Architecture for System-level Harmonic Mitigation in Power Systems 125

5.1 Introduction 125
5.2 Problem Formulation 128
5.2.1 MPC Formulation 129
5.2.2 Control and Hardware Layers 131
5.2.3 Control Philosophy 131
5.3 System Architecture and Implementation 133
5.3.1 MPC Implementation 133
5.3.1.1 Optimization Horizon 133
5.3.1.2 Discretization 134
5.3.1.3 Integrator 135
5.3.1.4 NLP Solver 136
5.3.2 MPC Framework and Architecture 137
5.3.2.1 Engine 138
5.3.2.2 MPC 139
5.3.2.3 MPC Execution Timer 140
5.3.2.4 COM Transmitter 140
5.3.2.5 COM Receiver 141

5.3.3 Simulator Architecture 141
5.3.3.1 Engine 141
5.3.3.2 Measurement Simulator 143
5.3.3.3 Control Message Timer 143
5.3.4 Synchronization of Measurements 143
5.3.5 Communication Link 144
5.3.6 Implementation Aspects 145
5.4 Hardware in the Loop Test 145
5.5 Conclusion 150

Part III: Energy Management **153**

6 Approaches to Economic Energy Management in Diesel-Electric Marine Vessels **155**
6.1 Introduction 155
6.2 Data Extracted from Vessels in Operation 159
6.2.1 Ferry 160
6.2.2 Platform Supply Vessel (PSV) 162
6.2.3 Seismic survey vessel 166
6.3 EMS Algorithms 168
6.3.1 Objectives and models 169
6.3.2 Mixed Integer Linear Programming (MILP) Algorithms 172
6.3.2.1 4 fixed speed gensets 172
6.3.2.2 3 fixed speed gensets and 1 variable speed genset 173
6.3.2.3 4 fixed speed gensets and an ESS 174
6.3.3 Logic Algorithms 175
6.4 Results 176
6.4.1 Ferry 179
6.4.2 Platform Supply Vessel (PSV) 182
6.4.3 Seismic Survey Vessel 185
6.5 Conclusion 189

7 Concluding Remarks and Recommendation for Future Work **191**

References **220**

Nomenclature

Abbreviations

ABT	Automatic Bus Transfer
AES	All Electric Ship
AFE	Active Front End
AIP	Air Independent Propulsion
APF	Active Power Filter
AR	Active Rectifiers
AVR	Automatic Voltage Regulator
BESS	Battery Energy Storage System
CAES	Compressed Air Energy Storage
CAPEX	Capital Expenditures
DAE	Differential Algebraic Equation
DP	Dynamic Positioning
DPS	Dynamic Positioning System
ECA	Emission Controlled Area
EMS	Energy Management System
ERN	Environmental Regularity Numbers
ESS	Energy Storage System
ESWB/ESB	Emergency Switchboard
FFT	Fast Fourier Transform
FMEA	Failure Mode and Effect Analysis
FPGA	Field-Programmable Gate Array
HED	Hybrid Electric Drive
HIL	Hardware-In-Loop
IGBT	Insulated Gate Bipolar Transistor
IIoT	Industrial Internet of Things
IPS	Integrated Power System
LCC	Line Commutated Converter
LNG	Liquefied Natural Gas
ME	Main Engine
MILP	Mixed Integer Linear Programming

MMC Modular Multilevel Converter

MPC Model Predictive Control

MSWB/MSB Main Switchboard

MTTF Mean Time To Failure

MVdc Medium Voltage dc

NLP Non-linear Programming

NMPC Non-linear Model Predictive Control

OPEX Operational Expenditures

PEBB Power Electronics Building Block

PHS Pumped Hydro Storage

PMS Power Management System

PSV Platform Supply Vessel

pu/p.u. Per Unit (normalized quantity)

PWM Pulse Width Modulation

QOS Quality Of Service

SFOC Specific Fuel Oil Consumption

SMES Superconducting Magnetic Energy Storage

SOC State Of Charge

SOH State Of Health

THD Total Harmonic Distortion

UPS Uninterruptible Power Supply

VFD Variable Frequency Drives

VPN Virtual Private Network

VSC Voltage Source Converter

VSD Variable Speed Drive

CHAPTER 1

Introduction

Vision without execution is hallucination.
– Thomas Edison

This chapter, which will serve as a brief introduction to the topics addressed in this thesis, includes a short presentation of background information with the purpose of motivating and illuminating some of the aspects and incentives linked to efficiency in marine vessels. Furthermore, the chapter addresses the structure of the thesis and its main contributions and, finally, includes a list of main publications. A thorough overview of shipboard electrification is presented in Chapter 2.

1.1 Background and Motivation

From the maritime shipping in 2012, the International Maritime Organization (IMO) reported that global NO_x and SO_x emissions from all shipping represent about 15% and 13% of global NO_x and SO_x from anthropogenic sources. For CO_2, the total (global) and international shipping represent about 2.6% and 2.2%, respectively, of global CO_2 emissions [127]. In addition, IMO projects that, by 2050, the CO_2 emissions from international shipping could grow by between 50% and 100%, depending on future economic growth and energy developments.

On January 1st 2015, IMO introduced regulations and guidelines for Emission Controlled Areas (ECA) as an effect of changes implemented in the International Convention of the Prevention of Pollution from ships (MARPOL) Annex VI, *Regulations for the Prevention of Air Pollution from Ships* [128]. The ECA zones dictate strict requirements for allowable emissions of NO_x, SO_x and particle matter. The same year, the European Commission set out a new climate agreement (the *Paris Protocol*), with a long term goal of reducing global emissions by at least 60% below 2010 levels by 2050 [41].

In 2014-2015 the oil and gas industry started to face recession due to over-production and decreasing oil and gas prices. This recession had huge impact on suppliers of relating offshore services, such as supply-, seismic survey- and anchor handling vessels, as day rates decreased beyond nominal operation costs as a consequence of greater supply of services than demand. With stringent environmental requirements, only the most fuel economic vessels with high Environmental Regularity Numbers (ERN) were considered for charter.

These, among other incentives, have contributed to the discussion regarding efficiency of marine vessels and how they are operated, with the focus primarily resting on reducing the environmental footprints and operational expenses (OPEX). At the same time, the strive to enhance the vessel's reliability, and safety of crew and equipment during a vast range of different operations, is present. To analyze and propose improvements to increase the marine vessel's efficiency is a complex and highly multi- and inter-disciplinary challenge. From the smallest sensor to the materials used in the construction of the vessel's hull and superstructure, the challenge of increasing the vessel's efficiency involves the design of the ship and its power plant as well as the design, integration and interaction of various ship systems, e.g. the propulsion system, the Dynamic Positioning System (DPS/DP), the Energy/Power Management System (EMS/PMS), ballast- and cargo handling systems. In addition, requirements and regulations from various stakeholders, and the human aspect of controlling the ship through interactions with the ship's systems in a broad range of different operations play vital roles in the assessment of shipboard efficiency. It should be mentioned that the human aspect is especially challenging for the paradigm shift with autonomous vessels. The crew's experience and interaction with the ship's systems, and the way the crew act as system integrators with the ability to gather information used in the decision making process, must be implemented to seamlessly integrate the control of the various ship systems in a fully autonomous system solution.

With the focus fully directed towards an advanced vessel's power plant and its efficiency, a broad range of disciplines are involved, e.g. the fields of internal combustion engines, electric power generation, conversion and distribution, energy storage technology, control engineering, maritime operations, safety, rules and regulations. Hence, to assess the overall efficiency of a shipboard power plant is also a highly multi- and interdisciplinary challenge. In this thesis the main contribution is focused around the discipline automation and automatic control design, with the use of optimization-based control strategies to improve the (AC) shipboard power plant's efficiency. Two topics are covered in this thesis: Optimal harmonic mitigation using Model Predictive Control (MPC), and optimization-based unit commitment as part of EMS. These two topics are intertwined and both contribute to the efficiency of the shipboard power plant. Harmonic management can be part of a higher level system, such as EMS/PMS, where a number of different functions are combined to achieve reliable and efficient power generation and distribution. In the following these two topics are briefly introduced.

1.1.1 The Problem of Harmonic Pollution

Harmonic distortion (or harmonic pollution) is a stationary form of distortion caused by the presence of additional sinusoidal components or harmonic components at multiples of the fundamental frequency component carrying the electrical signal under consideration. Harmonic distortion can be defined as any deviation from the pure sinusoidal voltage or current waveform typically generated by an ideal voltage source with linear loads [10], and is contributing to active power losses, as well as reactive power, thus altering the efficiency of the power system. Most common sources of these distortions are non-linear loads such as multi (6, 12, 18, 24)-pulse rectifiers, Line-Commutated Converters (LCC), high frequency harmonics from Voltage Source Converters (VSC) and switch mode power supplies, saturated transformers and other magnetic components, and power system background voltage distortions. Figure 1.1 illustrates how an electrical signal (either voltage or current) can be distorted by harmonic pollution.

Harmonic pollution, which in addition leads to active power losses and reactive power, might introduce unwanted effects in a power system, which can cause other components to shut down to prevent taking damage. The content of harmonic pollution in a power system, Total Harmonic Distortion (THD), is calculated as the normalized quantity of harmonic contribution relative the fundamental frequency component, for both voltage and current, i.e.

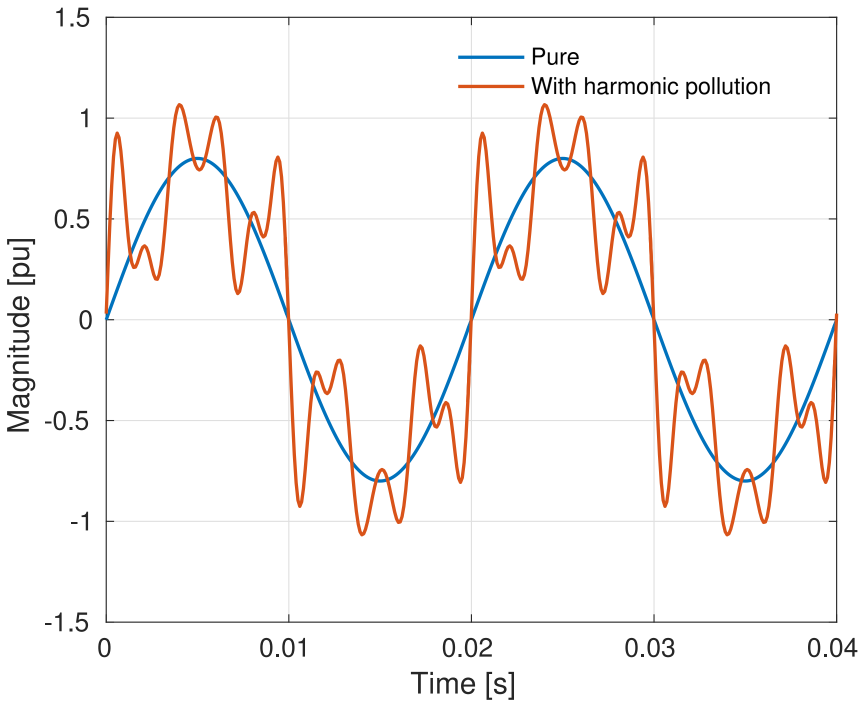

Figure 1.1: Illustration of harmonic pollution in an electrical signal: Harmonic content typically generated by 6-pulse diode rectifiers, where the harmonic frequency components are manifested as multiples of the fundamental frequency f given by $f_h = f \cdot h$, $h \in 6 \cdot (k \pm 1)$, $k \in \{1, 2, 3, \ldots\}$.

$$\begin{aligned} THD_V &= 100 \cdot \sqrt{\left(\frac{\sum_h V_h}{V_1}\right)^2} \quad [\%]\,, \\ THD_I &= 100 \cdot \sqrt{\left(\frac{\sum_h I_h}{I_1}\right)^2} \quad [\%]\,, \\ & h \in \{\text{harmonic frequency components}\}, \end{aligned} \tag{1.1}$$

where V_j and I_j are voltage and current amplitudes of harmonic frequency component j. $j = 1$ is the fundamental frequency component. Maximum allowed THD limits for current and voltage in a shipboard power system are strictly regulated by class rules [6, 36, 63], and THDs within allowed limits are commonly verified during commissioning by class representatives. Even though the design of the power system can, to some extent, limit the harmonic content in the system, conventional strategies for harmonic mitigation often involves use of active and passive filters, and control and coordination of these. In this thesis, a novel mitigation strategy using MPC to generate optimized Active Power Filter (APF) current references to control a single APF for system-level harmonic mitigation will be presented and discussed.

1.1.2 The Problem of Unit Commitment in Energy Management Systems

Figure 1.2 portrays an example of an one-line diagram for a typically advanced shipboard Integrated Power System (IPS), including four main engines and Battery Energy Storage Systems (BESS). The ability to plan the power production in such a shipboard power system is essential when it comes to the efficiency of the power production in terms of fuel consumption and emission of greenhouse gases. The scheduling of power producers, usually called unit commitment, must be conducted to follow class rules (or stricter requirements from other stakeholders) for a given operation. An example is power redundancy requirements through *spinning reserves*, i.e. being able to supply the (dynamic and static) aggregated (vital) load demand for a given operation in situations where one or multiple power producers are lost due to faults. Furthermore, power producers often have unit-specific optimal working conditions, thus, to optimize the power production, i.e. minimize the total fuel consumption and reducing total power producers' running hours, the power producers should be controlled as close to the units' optimal working conditions as possible. This is specified by the different units' Specific Fuel Oil Consumption (SFOC) curves.

A shipboard power system usually includes a PMS that is responsible for maintaining power balance by controlling the vessel's power plant at instantaneous time with the purpose of stabilizing voltage and frequency and meet the load demands. Examples of additional PMS functionality are (symmetric and asymmetric) load sharing (or load leveling), where the load is shared among the (online) power producers, and load shedding, where non-essential (non-vital) loads are disregarded in critical situations where the load demand exceeds the (online) power supply capability. With the in-

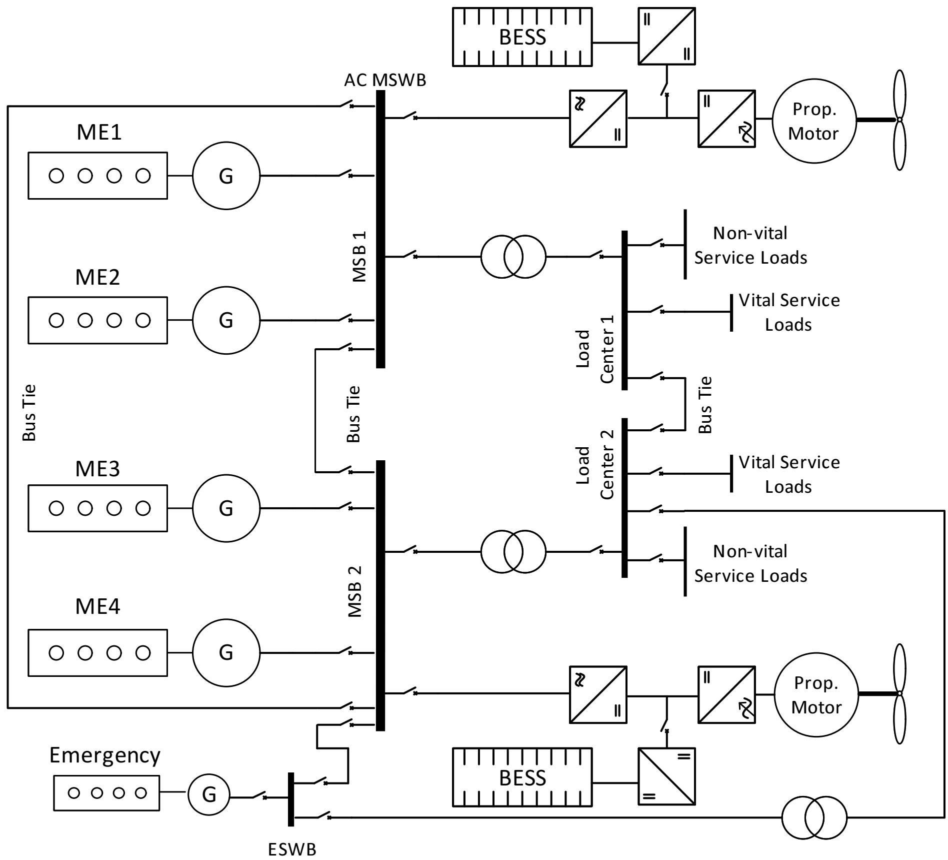

Figure 1.2: Example of an one-line diagram of a general (advanced) DPS 3 [57] Integrated Power System (IPS) with (ring bus) AC distribution, four Main Engines (ME) and Generators (G) connected to the Main Switchboard (MSWB), an emergency diesel-generator connected to an Emergency Switchboard (ESWB), and Battery Energy Storage Systems (BESS) in the propulsion drive units.

clusion of ESS, also the energy balance must be maintained, where the ESS units' State of Charge (SOC) are considered. An EMS, which often considers events in past and present along with future predictions/estimates, is often considered as part of a PMS that includes energy management functionality and control of ESS and/or different types of power producers along with additional supervisory functionality.

Scheduling of power producers, i.e. unit commitment, is often considered a manual operation and conducted by the crew. However, unit commitment with a range of different power producers and energy storages is a challenging task, where multiple aspects must be addressed. The way of manually scheduling the power producers may introduce human errors and poor decisions that do not support fuel efficiency and minimal environmental footprint through reduced emissions. This gives a foundation to include unit commitment in the EMS/PMS, either as an integrated autonomous solution or as a decision support tool. In this thesis, a unit commitment strategy based on Mixed Integer Linear Programming (MILP), with the purpose of optimally reduce fuel consumption and diesel-generator-set (genset) running hours, will be presented and discussed.

1.2 Structure of the Thesis and Main Contribution

This thesis is based on a collection of papers, where each chapter is self-contained. Furthermore, the thesis is divided into three parts where each part presents a topic. In the following, the main contribution of each chapter will be highlighted along with a presentation of the thesis' structure.

Part I: Revisiting the Evolution of Shipboard Electrification

- **Chapter 2:** This chapter presents a review of shipboard electrification, from the early use of electricity onboard ships, marked by *SS Columbia*'s lighting system in 1880, to modern shipboard power systems with different power generation- and distribution topologies. The chapter ends with a discussion of present and future trends and challenges towards all-electric ship (AES), including AC vs DC distribution and power system topologies (integrated/segregated), the use of power electronics and harmonic pollution, energy management and energy storage systems, emission free operations, the increasing need for measurements and software complexity, and cyber security.

Part II: Harmonic Mitigation

- **Chapter 3:** This chapter presents a system-wide harmonic mitigation strategy in AC shipboard power systems based on optimization. One Active Power Filter (APF) is optimally controlled to conduct system-wide harmonic mitigation to minimize the THD in all the power system's nodes. The optimization technique used is Model Predictive

Control (MPC), where a simplified model of the power system is used in the optimization scheme to predict the grid's future behavior. The output of the MPC are APF current references, which are fed to the APF's local PID controllers. Simulation results on a two-bus power system with 6- and 12-pulse loads are presented, and the system-wide harmonic mitigation approach based on MPC is bench-marked using conventional local filtering strategies.

- **Chapter 4:** This charter compares the optimal system-level harmonic mitigation strategy based on MPC from the previous chapter with an offline analytical optimization approach. The offline analytical optimization approach uses optimization to offline derive analytical expressions of optimal APF current references for system-level harmonic mitigation, which are based on system equations of the power system under investigation. Simulations of a two-bus shipboard power system with 12-pulse loads, uncertainties and non-ideal conditions, such as transformer saturations and parameter mismatch, are conducted to compare the MPC and the offline analytical optimization approach with the bench-marks from the previous chapter.

- **Chapter 5:** This chapter proposes a real-time implementation of the MPC for optimal system-level harmonic mitigation discussed in Chapter 3 and 4. The implementation is developed on a distributed topology, with one MPC per electrical phase in the power system, and utilizes an event-based architecture to keep cross-thread communication- and synchronization delays to a minimum. A low-overhead message protocol using UDP over Ethernet constitutes the communication between the different devices. The implementation is tested in a hardware-in-loop simulation, where a single phase power system simulator is implemented to interact with the MPC, to verify the real-time requirements are met.

Part III: Energy Management

- **Chapter 6:** Recently, the efficiency of diesel-electric marine vessels has been subject for discussion with focus on improving fuel efficiency, reducing the environmental footprint from emissions, as well as reducing running hours and maintenance costs. This chapter presents three different load profiles extracted from three different vessel during operation; i) a ferry, ii) a Platform Supply Vessel (PSV) and iii) a seismic survey vessel. The load profiles are analyzed and discussed with regards to power producer loadings, total number of running hours, total number of starts/stops of gensets and total fuel consumption. Furthermore, two new power system configurations are proposed; i) installation of an energy storage system and ii) changing one fixed-speed genset to variable speed. For these configurations, and the original configuration, two sets of Energy Management System (EMS) algorithms for unit commitment are implemented; one set based on logics, the other based on Mixed Integer Linear Programming (MILP). The EMS algorithms are run using the extracted data from the vessels to highlight potential fuel savings and reduction in genset running hours, as well as to compare logic-based EMS strategies with suitable optimization-based strategies, such as MILP.

The final chapter, **Chapter 7**, summarizes the final conclusions for the work presented in this thesis. The chapter ends with a presentation and discussion of recommendations for future work.

1.3 Publications

This thesis is based on results that were published or submitted for publications in journals in collaboration with colleagues. The publications that are included in this thesis and other related publications are listed in the following.

Publications included in the thesis:

[219] E. Skjong, E. Rødskar, M. Molinas, T.A. Johansen and J. Cunningham. ‘The Marine Vessel’s Electrical Power System: From its Birth to Present Day’. In: *Proceedings of the IEEE* 103.12 (Dec. 2015), pp. 2410–2424

[218] E. Skjong, J. A. Suul, A. Rygg, T. A. Johansen and M. Molinas. ‘System-Wide Harmonic Mitigation in a Diesel-Electric Ship by Model Predictive Control’. In: *IEEE Trans. Ind. Electron.* 63.7 (July 2016), pp. 4008–4019

[217] E. Skjong, R. Volden, E. Rødskar, M. Molinas, T. A. Johansen and J. Cunningham. ‘Past, Present, and Future Challenges of the Mar-

ine Vessel's Electrical Power System'. In: *IEEE Trans. Transport. Electrific.* 2.4 (Dec. 2016), pp. 522–537

[215] E. Skjong, T. Johansen, M. Molinas and A. J. Sørensen. 'Approaches to Economic Energy Management in Diesel-Electric Marine Vessels'. In: *IEEE Trans. Transport. Electrific.* 3.1 (2017), pp. 22–35

[221] Espen Skjong, Jon Are Suul, Tor Arne Johansen and Marta Molinas. *In search of the best method for system-wide harmonic compensation in isolated microgrids: MPC vs offline analytical optimization.* Submitted for publication

[214] E. Skjong, T. Johansen and M. Molinas. *Real-time Model Predictive Control Architecture for System-level Harmonic Mitigation in Power Systems.* Submitted for publication

Other related publications not included in the thesis:

[220] Espen Skjong, Marta Molinas and Tor Arne Johansen. 'Optimized current reference generation for system-level harmonic mitigation in a diesel-electric ship using non-linear model predictive control'. In: *2015 IEEE International Conference on Industrial Technology (ICIT).* IEEE Conference Publications. 2015, pp. 2314–2321

[202] A. Rygg, E. Skjong and M. Molinas. 'Handling System Harmonic Propagation in a Diesel-Electric Ship with an Active Filter'. In: *ESARS 2015 Conference on Electrical Systems for Aircraft, Railway, Ship Propulsion and Road Vehicles.* Mar. 2015

[224] Espen Skjong, Marta Molinas, Tor Arne Johansen and Rune Volden. 'Shaping the Current Waveform of an Active Filter for Optimized System Level Harmonic Conditioning'. In: *Proceedings of the 1st International Conference on Vehicle Technology and Intelligent Transport Systems.* 2015, pp. 98–106

[222] Espen Skjong, Miguel Ochoa-Gimenez, Marta Molinas and Tor Arne Johansen. 'Management of harmonic propagation in a marine vessel by use of optimization'. In: *2015 IEEE Transportation Electrification Conference and Expo (ITEC).* IEEE. 2015, pp. 1–8

[223] Espen Skjong, Jon Are Suul, Marta Molinas and Tor Arne Johansen. 'Optimal Compensation of Harmonic Propagation in a Multi-Bus Microgrid'. In: *International Conference on Renewable Energies and Power Quality (ICREPQ'16), Renewable Energy and Power Quality Journal (RE&PQJ)*. 2016, pp. 1–6

[216] E. Skjong, S. Gale, M. Molinas and T. A. Johansen. 'Data-Driven decision support tool for power quality measures in marine vessel power system'. In: *2016 IEEE Transportation Electrification Conference and Expo (ITEC)*. June 2016, pp. 1–8

[34] A. K. Broen, M. Amin, E. Skjong and M. Molinas. 'Instantaneous frequency tracking of harmonic distortions for grid impedance identification based on Kalman filtering'. In: *2016 IEEE 17th Workshop on Control and Modeling for Power Electronics (COMPEL)*. June 2016, pp. 1–7

Part I

Revisiting the Evolution of Shipboard Electrification

CHAPTER 2

The Marine Vessel's Electrical Power System: Past, Present and Future Challenges

The evolution of the use of electricity in marine vessels is presented and discussed in this chapter in an historical perspective. The historical account starts with its first commercial use in the form of light bulbs on the SS Columbia in 1880 for illumination, going forward through use in hybrid propulsion systems with steam turbines and diesel engines and then transitioning to the present with the first fully electric marine vessel based entirely on the use of batteries in 2015. Electricity use is discussed not only in the light of its many benefits but also of the challenges introduced after the emergence of the marine vessel electrical power system. The impact of new conversion technologies like power electronics, battery energy storage, and the DC power system on overall energy efficiency, power quality, and emission level is discussed thoroughly. The chapter, which is based on the merge of the reformatted versions of the articles [217, 219], guides the reader through this development, the present and future challenges by calling attention to the future research needs and the need to revisit standards that relate to power quality, safety, integrity, and stability of the marine vessel power system. These aspects are strongly impacted by the way electricity is used in the marine vessel.

2.1 Introduction

Starting with the earliest records of a commercially available shipboard electrical system which dates back to the 1880 with the onboard dc system at the *SS Columbia*, inventions such as the AC induction motor and the diesel engine have triggered new research and developments towards the end of the 19 century and the beginning of the 20th. In this period, the initial steps were given in research related to submarines, batteries, steam turbines and diesel engines. The two more important developments before WWI were the first diesel-electric vessel (*Vandal*) in 1903 and the first naval vessel with electric propulsion in 1912 (*USS Jupiter*). During the period of rising tension that preceded WWI the first cargo vessels with turbo-electric propulsion were conceived and developed in USA and UK. The outbreak of WWII stimulated new developments that brought the T2-tanker with turbo-electric propulsion into the picture. Also in this period, research on air independent propulsion (AIP) for submarines has been started and ended with the first submarine with AIP in the period that followed the end of the war. Nuclear powered vessels emerged in the end of the 50s and the first passenger liner to use alternating current was inaugurated in 1960 (*SS Canberra*), 70 years after the invention of the alternating current motor. In the period 1956-1985, the power electronics revolution triggered by the disruptive solid-state technology, marked the point of departure towards a new era for marine vessels; the era of the all-electric ships (AES). As a result of that, *Queen Elizabeth II* was inaugurated in 1987 with the first diesel-electric integrated propulsion system. And in the last two decades of the present time, the marine vessel community has witnessed the development of the first vessels having LNG as fuel. In January 2015, marking the milestone of the era of the *all-electric ship*, the world's first purely battery-driven car and passenger ferry *Ampere* has been placed in use (commissioned October 2014) and is being regularly operated in Norway.

This new era of electric marine vessels does not come without challenges, however. In what follows, the chapter highlights the different stages in the evolution of the marine vessel's development and the impact of electricity use in this evolution. Figure 2.1 indicates and guides the reader through the stages of development. The impact of new inventions and disruptive technologies as well as the impact of disruptive events in society such as wars, is discussed. Following the historical account, the chapter moves towards modern electric ship propulsion discussing the new challenges of moving towards hybrid AC/DC and pure DC power systems, the challenge of electrical stability, harmonic pollution, and power quality in stand-alone microgrids like the marine vessel, the role of battery energy storage systems, and the move towards emission free operation among others. Along with these challenges, potential solutions and possible roads to follow are presented.

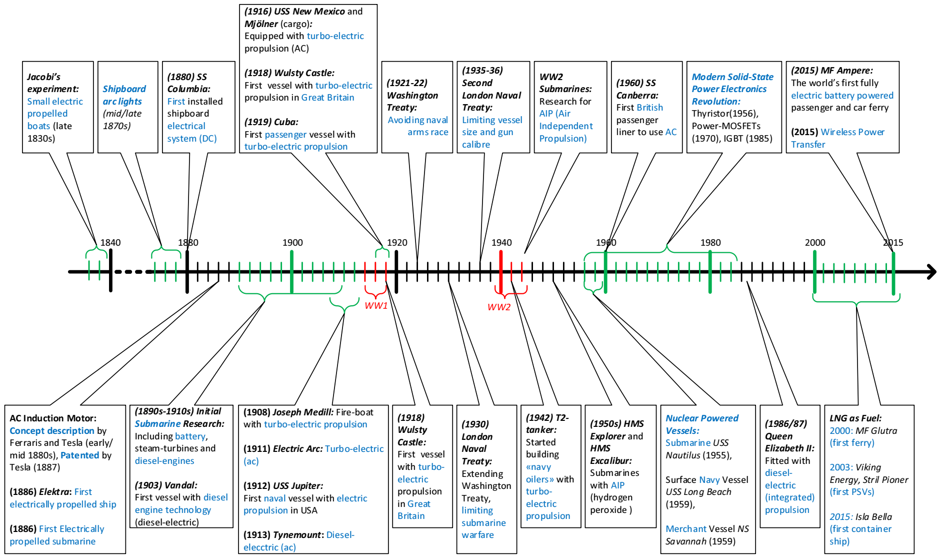

Figure 2.1: Historical highlights of the development of the Marine Vessel's Power System from 1830 to 2015 [219].

2.2 The Birth of the Marine Vessel Power Grid

In the late 1830s the German inventor Moritz Hermann von Jacobi (Yakobi [115]) invented a simplistic dc motor and conducted a couple of experiments with small boats able to carry about a dozen passengers with electric propulsion. The electric motor in his last experiment (about 1kW) was powered by a battery consisting of 69 Grove cells resulting in a speed of about 4 km/h. Due to the early motor design, which carried many imperfections, the invention was not adopted and used in any practical applications and was soon forgotten [115, 157, 203].

Commercially available electric systems first appeared on ships during the early 1870s in the form of gun firing circuits powered by battery cells. Electric call bells appeared on luxury passenger liners about the same time. The development of electric arc lamps by Charles Brush, Edwin Weston, Elihu Thomson, Hiram Maxim, and others for the illumination of streets and large public spaces in the mid/late 1870s was paralleled by the installation of electric arc searchlights on ships. Powered by steam driven generators, the primary function of such lights was to illuminate marauding attack boats and also to blind enemy gun crews during close engagements for some of

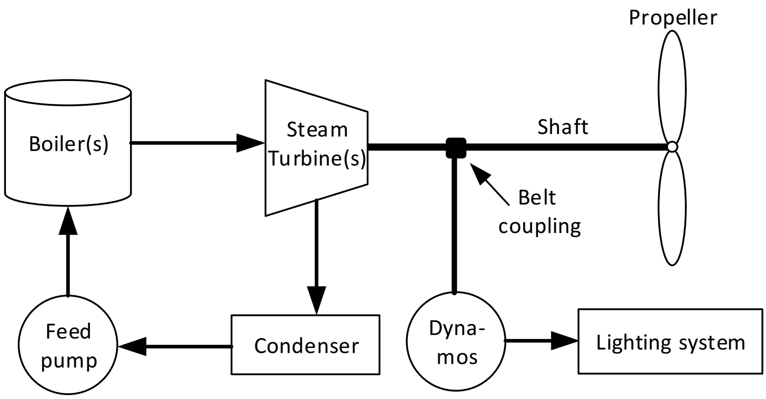

Figure 2.2: Simplified drawing of the propulsion and lighting system installed in *SS Columbia*, based on written description [104, 147, 156].

the early lamps were as bright as 11,000 candlepower. Most systems were direct current but alternating current systems were also employed [48, 153].

In the mid-1878 Thomas Edison (1847-1931) developed an incandescent electric light bulb for the consumer market. However, there were no commercial electrical system for generating and distributing electricity to end users. Edison knew that for the light bulb to achieve commercial success, he had to build an electric distribution system using direct current (dc), and his idea was a central power station with a system of electrical conduction radiating out of it, reaching multiple end users. After a successful demonstration in 1879, staged on his property in Menlo Park, New Jersey, where he had installed a lighting system to illuminate some of the houses and imaginary streets powered by a dynamo in his laboratory, he met skepticism from invited business leaders and potential investors. They were all reluctant to invest in the low-voltage dc system without more proof of the system's commercial viability [234]. Among the attendees was the president of the *Oregon Railway and Navigation Company*, Henry Villard, who, after the demonstration, immediately saw the benefits of the technological advancement demonstrated by Edison. One thing lead to another, and even though Edison didn't have any offshore installations in mind when developing the lighting system, Villard ordered an installation of the lighting system for his company's new steamship, *SS Columbia* (figure 2.3a), which was under construction by a shipyard in Chester, Pennsylvania.

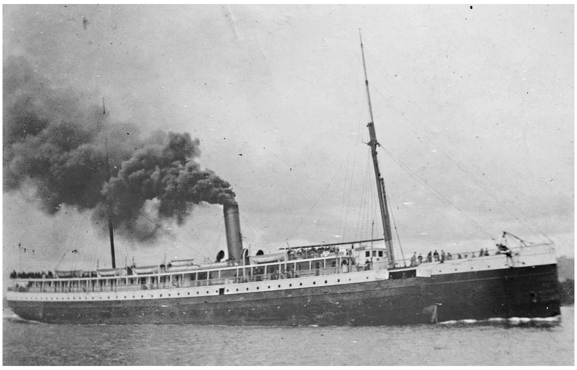

(a) Passenger and cargo vessel *SS Columbia* (1880-1907), owned by the Oregon Railroad and Navigation Company and later the Union Pacific Railroad, was the first ship with Edison's lighting system. Courtesy [229].

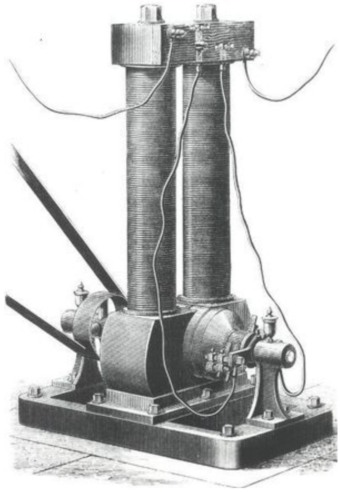

(b) Edison's belt driven "jumbo" dynamo (with the nick name *long-legged Mary-Ann* [71]) was one of the main components in *SS Columbia*'s lighting system. Courtesy [72].

Figure 2.3: Edison's lighting system first installed in a ship in 1880, aboard *SS Columbia*.

First electric light system installation in ships

After the installation of the new lighting system, the *SS Columbia* was equipped with 120 incandescent lights, which were distributed on several circuits and powered by four belt-driven 6kW dynamos (with small internal resistance and large bipolar magnets [71]), see figure 2.3b, connected to the steam-engine driving the single four-blade propeller through a mechanical shaft. The different circuits were secured by small lead-wires functioning as fuses. Each dynamo could supply 60 lamps, each rated 16 candlepower (1 candlepower is the radiating power of a light with the intensity of one candle). One of the dynamos was operated at reduced voltage for excitation of the three other dynamos' field magnets. The power system didn't include any instrumentation, thus any voltage adjustment was conducted by operators judging the brightness of the lamps in the engine room. Light switches were located in locked wooden boxes, and if the lights were to be turned on or off in the cabins, a steward had to come and unlock the boxes [104, 147, 156]. A simplified sketch of the propulsion and lighting system aboard *SS Columbia* is given in figure 2.2.

The installation of the light system aboard *SS Columbia* proved to be a success, the system worked as intended, and the story was published as a full-page article in *Scientific American* in its May 22nd 1880 issue [239]. Shortly after the success with the electric installation aboard *SS Columbia*, the *Edison Company for Isolated Lighting*[1] installed in 1883 an electrical system aboard a US ship, *USS Trenton* [163]. *USS Trenton*, was, as *SS Columbia*, a modern ship featuring both steel hull and a steam propulsion system with additional sailing rigs. The following year the *Bureau of Navigation* decided that the vessels *Atlanta*, *Boston*, and *Omaha* should be equipped with an electrical lighting system, and shortly after electric lighting became a standard feature aboard both military and commercial vessels. Even though the low-voltage dc electrical system (110V [111]) developed by Edison was only intended for incandescent lamps, and the fact that there are numerous competing claims about the pioneer of electrical installation aboard a ship, the period itself can be considered to mark the birth of the marine vessel's power grid.

Searchlights consumed the majority of power on Navy ships (as much as 50 kW) as compared to the lighting needs of passenger ships (10-20 kW) which did include some arc lamps for navigation purposes. That changed rapidly as electric power for ventilation and motorized gun turrets appeared on Navy ships in the 1880s. The lack of practical alternating current motors led to adoption of direct current as a standard to simplify the overall system. The same was true in many industrial applications until the early 1900s; as the available direct current motors were found to be more efficient than the alternating current designs of the day. Improved wiring and protective devices were also developed [153]. The first successful electrically powered vessel was the *Elektra*, a passenger ferry with a capacity of 30 persons, built by the German firm *Siemens & Halske* in 1885. Measuring 11 meters long by 2 meters wide, it was powered by a 4.5 kW motor supplied by batteries [211].

In the late 1880s, Nikola Tesla (United States), a former employee of Edison

[1] *Edison Company for Isolated Lighting* was a separate company in November 1881, which later, December 31 1886, was absorbed by the Edison Electric Light Company

who left Edison in 1885 [70], Galileo Ferraris (Italy) and Michael Osipowitch von Dilvio-Dobrowolsky (Germany) each had discovered the benefits of two alternating conductors with 90° phase difference (or three conductors with 120° phase difference), which could be used to rotate a magnetic field. This lead to the birth of the induction motor, demonstrated independently by Ferraris and also by Tesla in the early 1880s and patented by Tesla in 1887. Others claimed to have conceived independently the rotating field concept, among them Elihu Thomson, founder of the *Thomson-Houston Company*, and also Oliver Schallenberger of the *Westinghouse Electric & Manufacturing Company*. Charles Bradley, an inventor and entrepreneur in the electrical industry, demonstrated in 1888 an induction motor concept. Also, Frank J. Sprague, graduate of the US Naval Academy, researched electrical systems for US ships then worked for Edison to perfect mathematical estimation for system design and the three wire system for Edison. After leaving Edison he perfected in 1884 the first practical direct current electric motor. It could operate on incandescent electric lighting systems and won Edison's approval. He subsequently developed dc motors to a high state of efficiency for both industry and railways; such motors exceeded the efficiency of available ac motors for many years [48, 49, 201, 241].

2.2.1 War of Currents

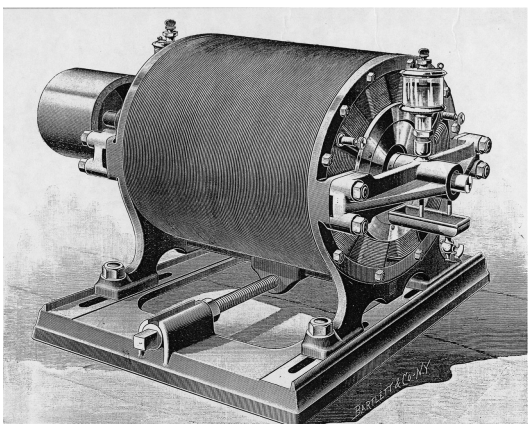

Figure 2.4: Nikola Tesla's ac induction motor demonstrated in 1887. Courtesy [174].

The invention of the ac motor had a cascade effect which lead to, among other inventions, a polyphase generator (figure 2.4) and ac distribution systems [51]. Tesla filed in 1887 two patents on the ac motor in October 1887, and three more patents pertaining to the system in November same year. One of Edison's greatest rivals, George Westinghouse (*Westinghouse Electric Co.*), acquired these patents [238] and with the help of Tesla the *War of Currents* [165, 236] began, with Edison on the dc side, and Westinghouse and Tesla on the ac side.

However, the war of currents put aside, the ac current had the ability to easily be transformed between different voltage levels, without rotating components as was needed for voltage transformation in dc, and could be transmitted at great distances by transforming the voltage to appropriate levels at relative low cost. The first long distance ac transmission in the world (12 miles, 4,000V) was realized in 1890 when Willamette Falls Electric company installed ac generators from Westinghouse while Edison struggled with the fundamental problem of line losses, founded on Ohm's law. The ac distribution had also, at the same time, been installed in Europe, and one example was the long-distance transmission in 1891 from Lauffen to Frankfurt am Main (100 miles) using three-phase ac at 25,000V [83]. An often missing part of the history of ac is the Hungarian research team consisting of the scientists Kàroly Zipernowsky, Ottò Blàthy and Miksa Déri, *ZBD*, who invented the closed core shunt connected ac transformer in 1884, revolutionized the grid using parallel connections (instead of series connections) to a main distribution line, and also electrified the Italian city of Rome in 1886. Westinghouse adopted much of the Hungarian scientists' work to take up the fight with Edison's dc systems [103, 129]. Not only had the ac inventions had an effect on the mainland power generation and distribution grids, but the inventions also gave support to more advanced use of electricity in ships.

In 1896, the US's *Brooklyn* was fitted with electrically operated gun mount elevators and subsequent ships were fitted with electrically operated deck machinery such as winches and cranes powered by 80 volt direct current systems [153]. It should be noted that, despite the success of the alternating current generation and transmission systems in both Europe and the United States, direct current continued to play a major role in land based power systems. There were a variety of reasons, the primary issue that of power factor. The early alternating current systems suffered substantial losses in the form of "reactive power" consumed by the magnetic fields of ac motors and transformers [48].

The percentage of useful power delivered by an alternating current system was and is known as the "power factor." In some early land systems that was as low as 80 or less. That situation led the legendary electrical engineer and mathematician Charles Steinmetz to favor the installation of direct current distribution wherever the load was sufficiently dense to justify the expense of the conversion substations that were required if a system were to reap the benefits of the large scale power generation and transmission that were attainable only with alternating current. Thus ac generation and transmission coupled to direct current distribution by mechanical conversion in substations was the norm in US cities and elsewhere until the 1920s. By that time, the expense entailed in large scale conversion combined with new developments in alternating current distribution and of steel with superior magnetic characteristics forced a change. The largest such system was the *New York Edison Co.* distribution system that supplied 90 percent of the utility power in Manhattan which grew to comprise a total of 41 substations in over 60 structures with a total of 282 mechanical converters before a change to alternating current was initiated in 1928. Elements of the old system remained in place however until late 2007 [48].

While the practices of urban power distribution do not translate directly to shipboard practice, some of the same concerns persist. For example, the direct current motor of the early 20th century still offered superior control of varying loads compared to ac motors. Power factor management was still an issue. The operation of large scale alternating current systems presented the need for synchronization of generators and certain types of motors. Still, the US, like the urban electrical utilities, began a change in favor of alternating current and began the use of three phase ac in 1932. Direct current control systems were larger and heavier; dc motors were more complex to construct. Alternating current was not a perfect solution; in an effort to reduce weight frequencies as high as 400 Hz were utilized but required mechanical converters in an era prior to the development of modern solid state equipment. It is said that was the reason that the British Navy retained direct current systems, although Germany followed the lead of the US with alternating current systems in the 1930s [153].

2.2.2 The Early Turbo-Electric Surface Vessels

During the last quarter of the 19th century, marine vessels with steam engines instead of sails as the primary propulsion became more common. In this period the shipbuilders experimented and fitted new vessels with many new technologies. The early propulsion systems were based on reciprocating steam engines, and with the advent of the steam turbines the ship's propellers were initially coupled directly to the prime movers (high-speed), often with poor results. As a result, in the early 1900s, technologies such as marine reduction gears and electric propulsion systems were developed to improve the propulsion system powered by the high-speed steam turbine prime movers. The United Kingdom was developing and perfecting mechanical-drive system employing reduction gears, while the United States focused on electric-drive systems [163, 184]. In 1908 the first merchant vessel *Joseph Medill* (a fire-boat) was built with a turbo-electric (dc) propulsion (400 shaft horsepower (shp)) [106, 115].

The first naval vessel with electric propulsion in USA was the collier *USS Jupiter*[2] in 1912. The collier was an experiment including both diesel engine propulsion, turbo-electric propulsion [115, 197] and direct coupled steam turbine propulsion (twin-screws). The *USS Jupiter* was a successful experiment, with its 3,500 horsepower (hp) *General Electric* turbo-electric propulsion system, which made headlines in the New York Times in the 3rd October 1909 issue [172], and the US decided to fit all the front-line battleships with the same propulsion system. Three *New Mexico* class battleships powered by turbines were ordered in 1914, but while under construction it was decided that the lead ship, *USS New Mexico*, should be equipped with turbo-electric drive system and be the first vessel to convert to turbo-electric propulsion [2].

The *New Mexico* used two 11.5MW, 3,000V/4,242V dual voltage, variable frequency ac generators that powered four 7,500hp 24-/36-pole induction motors [163], and was able to maintain a speed of 21 knots [250]. The vessel also had six 300kW auxiliary turbo-generators for lighting and non-propulsion electrical machinery [2]. The *USS New Mexico*'s main switchboard is shown in Figure 2.5a. It is important to note that there were no power electronics in the early 1910s, hence, the vessel's speed was controlled

[2] *USS Jupiter* was from 1920-'22 converted to the first aircraft carrier in the US and renamed *USS Langley* [13, 161, 163, 257]

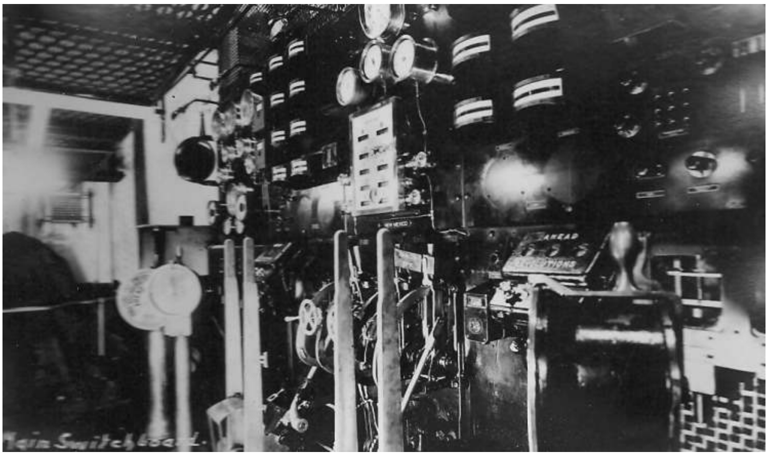

(a) *USS New Mexico*'s main switchboard and control station. Change of speed and direction was done with manual levers. Courtesy [2].

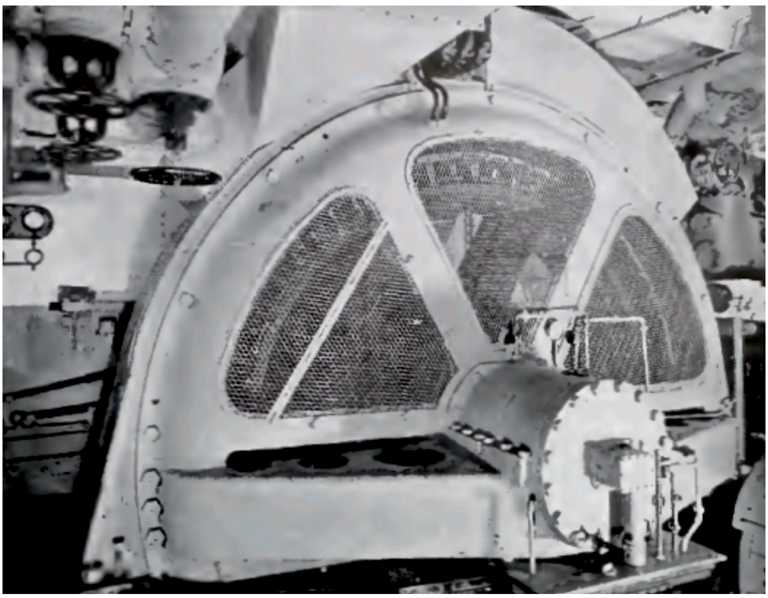

(b) *Cuba*'s 3,000 horsepower, 1,150 volt, 1,180 ampere electric propulsion motor. Courtesy [16, 69].

Figure 2.5: *USS New Mexico* was one of the first US vessels with turbo-electric propulsion. *Cuba* was the first passenger vessel in the world with turbo-electric propulsion.

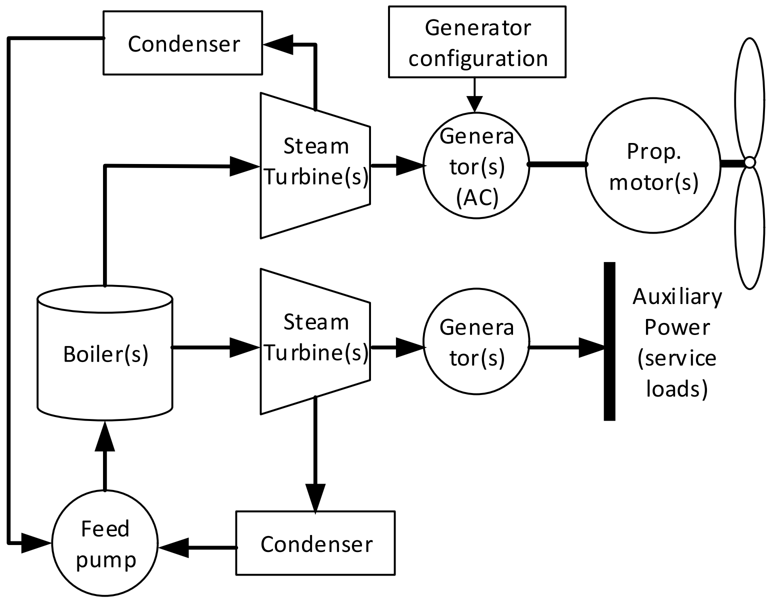

Figure 2.6: Simplified drawing of the turbo-electric generation and distribution system installed in *USS New Mexico*, based on written description [163, 250].

through a complex combination of varying the frequency (speed), voltage of the generator sets and changes in pole configuration. The turbo-electric propulsion was a very effective system with a number of benefits. The shaft alley onboard a turbo-electric vessel was much shorter, and less of a target, than a typical steam-powered vessel [257]. The fuel economy was also substantially improved, and the electric motor was faster to reverse because there wasn't need for rerouting steam through a separate turbine. All the benefits, however, came at the cost of weight, since the electric motor weighed considerably more than a reduction gear and a longer shaft. Figure 2.6 shows a simplified drawing of the *USS New Mexico*'s turbo-electric generation and distribution system, illustrating integration on the steam side of the system.

The passenger vessel *Cuba*, originally built in 1894 as *SS Yorktown*, after being sold and renamed a couple of times, was wrecked in 1916 and rebuilt with turbo-electric propulsion in 1919 and was then the world's first passenger vessel with that propulsion system [16, 69]. Figure 2.5b shows the *Cuba's* electric propulsion motor. The use of turbo-electric propulsion was not only taking place in the United States. In Europe the Swedish enterprise *Rederiaktiebolaget Svea*, which was located in Stockholm, started equipping ships, that had steam machinery, with turbo-electric propulsion. In 1916, in the same period *USS New Mexico* was equipped with the new propulsion system, *Rederiaktiebolaget Svea* built two sister ships, *Mjölner* and *Mimer* (cargo ships). *Mimer* was fitted with triple-expansion engines while *Mjölner* got two Ljungström radial-flow reaction turbines, invented by the Swedish engineer Fredrik Ljungström and patented in 1894 [37], driving electric generators [225]. The total power output from the turbines running at 9,200 revolutions per minute (rpm) was 800kW, with a voltage level of 500V. Two induction motors, one on each side, were running at 900rpm and drove the single propeller shaft through single-reduction gearing at 90rpm. The first turbo-electric ship constructed in Great Britain was the cargo ship *SS Wulsty Castle* in 1918, which used the same type of machinery.

The steam-engine was a well adapted solution to generate electricity, however due to the fact that as much as 90% of fuel's energy was wasted on heat, the oil industry was in search for a more economical engine solution fueled on oil. The solution came with Rudolf Diesel, a German inventor and mechanical engineer, which developed the diesel engine (patented in 1892) [39, 243]. Diesel marketed the technology to oil industries all around the world, and granted Emanuel Nobel exclusive licenses to build his engine in Sweden and Russia [245]. In 1902 it was suggested to install diesel engines in the river barges to transport oil from the lower Volga to Saint Petersburg and Finland, and in 1903 the vessel *Vandal* was launched, which was the first vessel equipped with the new diesel engine technology, in addition to being the first vessel featuring diesel-electric propulsion. The vessel's power plant consisted of three 3-cylinder 120hp diesel engines which ran at constant 240 rpm. The electrical transmission was controlled by a tram-like lever which varied the propeller (three screws) speed from 30 to 300 rpm [115, 193]. Even though the Russian river tanker *Vandal* was also the first vessel equipped with a fully functional diesel-electric transmission [91], the use of diesel-electric systems didn't catch on until the entry of the World War I submarines.

Another vessel that can be mentioned is the passenger vessel *Electric Arc* built in 1908 as an experiment with alternating current. The vessel, which probably was the first experimental vessel with ac, originally featured a gas engine that was replaced by a petrol engine (45bhp, 700rpm) driving the alternator (4- and 6-poles winding). This vessel illustrated that electric drive with ac was possible, and was followed by the cargo vessel *Tynemount* in 1913 with diesel-electric ac propulsion. Two diesels of 300hp running at 400rpm; the port side diesel drove a 6-pole alternator and its shunt-wound exciter, and the starboard diesel drove a generator which was wound for eight poles [115]. The electrical system worked well for light loads, however, the propeller pitch was too coarse and required more power than the generators were able to supply, resulting in a breakdown of the engines.

2.2.3 The Early Submarines

Marine electrical installations gave, in many cases, a foundation of new-thinking and innovation. In addition to new propulsion systems, the marine power grid made it possible to supply a *service load*, including new navigation- and communication systems as well as light systems. Naval vessels were also equipped with more advanced and precise weapon systems than before, powered by the vessels' power generating units. In the wake of the surface vessels' success using electric systems, and with the advent of the battery (voltiac cell), which was introduced in the early 1800s by Alessandro Volta [155, 256] and developed further for practical use, the innovations also found their way to submarines. The French Navy was considered to be the most enthusiastic advocate for submarines in the late 1800s, and in 1863 the French Navy launched the very first submarine that did not rely on human power for propulsion. The submarine, 140 feet long, 20 feet wide and displacing 400 tons, was designed by Charles Brun and Simèon Bourgeois and named *Le Plongeur*[3]. The propulsion system consisted of a 80 horsepower direct-drive engine run by 180 psi compressed air stored in tanks throughout the vessel [82, 260], and the buoyancy was controlled by regulating the vessel's inner volume by pistons running in and out of the hull. Even though the submarine was state of the art at that time, it was difficult to maneuver, and movements of the crew could send the vessel into severe roll motions. Due to its ineffectiveness the *Plongeour* was set aside.

During the 1880s a lot of inventors around the world were caught up developing the submarine and make it reliable and commercial available. In 1885 the American inventor Josiah H. L. Tuck made a submarine, named *Peacemaker*, which used a chemical (fire-less) boiler with 1500 pounds of

[3] Meaning "*The diver*" in French.

caustic soda to generate steam to its engine and provide five hours endurance (turbo-electric). However, his days of innovation came to an end when his relatives had him committed to an asylum for insanity [82, 261]. The same year, the French designer Claude Goubet started his demonstration of electric propelled submarines by building two small private venture vessels, *Goubet I* in 1885 and *Goubet II* in 1889. Both vessels showcased the benefits of electric propulsion, but were otherwise unsuccessful regarding maneuverability. In 1886 the submarine *Nautilus* was built in Tilbury with two electrical motored twin-screws. In 1888 the *Gymnote* (59 feet long, displacing 30 tons) was built with a 50hp motor resulting in a speed of about 7 knots [115]. From this point on, electric propulsion came to be the common factor between the different submarine designs, as solutions involving compressed air and compressed steam did not provide the necessary response to achieve the needed maneuverability when diving.

In the late 1890 and the early 1900s many nations were occupied by making their own naval submarines for warfare with a range of different weapon system designs, including torpedoes, air cannons, and large calibre guns. The French Navy was independently developing its own submarine, while the Royal Navy and the US based much of their work on John Phillip Holland's prototypes. Holland, originally a school teacher, made different submarine prototypes involving combustion engines for surface use and batteries for diving operations. Holland also challenged the original designs to overcome the stability and maneuverability problems with the solution of a small net positive buoyancy, ballast tanks and diving planes [82]. The use of combustion engines to charge the battery proved to be a valid option, as turbo-electric systems required the submarine to come to a stop before submerging, which made dive operations slow. Even after the steam-plants had been shut down, the power system retained a lot of heat, which made the climate within the submarine almost unbearable. In addition, when surfacing, starting the steam plant was a slow process, due to the fact that the boilers had to be reheated. In the early 1900s almost everyone had adopted the idea of using combustion engines to charge the batteries. Both gasoline and pre-diesel internal combustion engines were used, and a lot of research was directed towards engine construction, including both 2- and 4-cycle (stroke) engines with different number of cylinders. The German Navy used a *MAN* 4-cycle diesel, with 850-1,000 brake horsepower (bhp), which powered nearly all World War I submarines. Initially, the US used the 4-cycle *Vickers* diesel engine, either 4-cylinder 275bhp or 6-cylinder 300bhp, which was built by *Electric Boat* closely associated with *Vickers* and completed at the *New London Shop and Engine Company* (NELSECO). Also in Sweden, around 1913, the Swedish firm *Polar* begun to manufacture 4-cycle submarine engines [88]. Although a lot of effort was directed towards the engines and propulsion systems, no one had solved the problem restricting the duration of dive operations due to limited oxygen supply. The engines could not be run underwater to charge the batteries, and the crew needed fresh, breathable air.

2.3 Effects of World War I and II

After the end of World War I, a naval arms race was led by the US, Great Britain and Japan, where the three nations all commenced large-scale capital ship efforts [163]. This arms race was unfortunate, increasing the possibility for another war. Between 1921 and 1922 the world's nine largest naval powers were gathered for a conference in Washington D.C., invited by the US Secretary of State, Charles Evans Hughes, to discuss naval disarmament and solutions to relieve the growing tensions in East Asia [177]. Great Britain, Japan, France and Italy were invited to the conference in effort to reduce the naval capacity, while Belgium, China, Portugal and the Netherlands were invited to join in discussions on the tense situation in the Far East. The results from the Washington Naval Conference were three major treaties; the *Five-Power Treaty*, the *Four-Power Treaty* and the *Nine-Power Treaty*, all commonly known as part of the *Washington Treaty*. The cornerstone of the naval disarmament program, in effort to ending the arms race, was the *Five-Power Treaty*, involving the US, Great Britain, Japan, France and Italy. The politics put aside, the *Five-Power Treaty* gave strict regulations for each of the countries involved to maintain a number and size limits (set ratio of warship tonnage) on capital ships. In addition, the treaty also spelled the end of turbo-electric propulsion for war ships by prohibiting the reconstruction of ships [257], meaning a cancellation of any plans to rebuild existing US battleships with turbo-electric drives, and also prohibiting construction of new naval vessels[4][5]. From this point on, most of the existing US vessels were powered by geared turbines.

As the treaty covered only naval vessels, the development of turbo-electric

[4]Sometimes referred to as the *treaty's building holiday* [206].

[5]All battleships and cruisers retained under the treaty were allowed the addition of 3,000 tons for providing means of defence against air and submarine attacks [113].

propulsion continued, but was not, however, used for naval surface vessels. Geared steam-turbine propulsion became predominant for large warships, however, electric propulsion was still being used, especially for passenger vessels and ice breakers with separate power systems supplying the propulsion loads and the ship's service loads.

In 1930 a new naval conference was held in London, with the effort to extend the *Washington Treaty*. The participating nations were the US, Great Britain, France, Italy and Japan. The result from the conference was the *Treaty for the Limitation and Reduction of Naval Armament*, commonly known as the *London Naval Treaty*, which regulated submarine warfare and limited naval shipbuilding by extending the *Washington Treaty*'s building holiday another five years [231]. The treaty was signed by all five nations, despite Japan's growing overseas ambitions which, in secret, exceeded the treaty's limits on improvements and refitting of some of the nation's battleships [206]. The *Second London Naval Disarmament Conference* was held in 1935-1936 in effort to limit growth in naval armaments. The following treaty, the *Second London Naval treaty*, limited the maximum size of the participating nation's ships and the maximum calibre on the guns they could carry. The treaty also included an "escalator" clause that allowed the members to match tonnage and armament increases by nonmembers. However, an agreement on a maximum allowed number of warships was prevented. The reason being Japan's withdrawal from the treaty after refusing to continue with the quantitative "ratio" system of limitation which had existed since 1922 [119]. Japan, which had interest in expanding the empire into East-Asia and China, proposed parity among the three major naval powers, with no restrictions on the type of warships allowed. This was in short rejected by the US and Great Britain, fearing to lose naval superiority over Japan which would cede Asia to Japan and threaten the security of Australia, New Zealand and the Philippines [161].

After Japan abrogated the treaty, after giving a two-year notice in 1934 refusing to renew the existing treaty, the naval construction and arms race ensued and the US began to design and build new battleships. However, the battleship designs of the late 1930s did not feature turbo-electric propulsion systems despite its advantages. A major reason being vulnerability to electrical short-circuits that could result from battle damage increasing the likelihood to be knocked out of operation - *survivability* - and added weight which could instead be used more wisely, i.e. to carry more guns and armor.

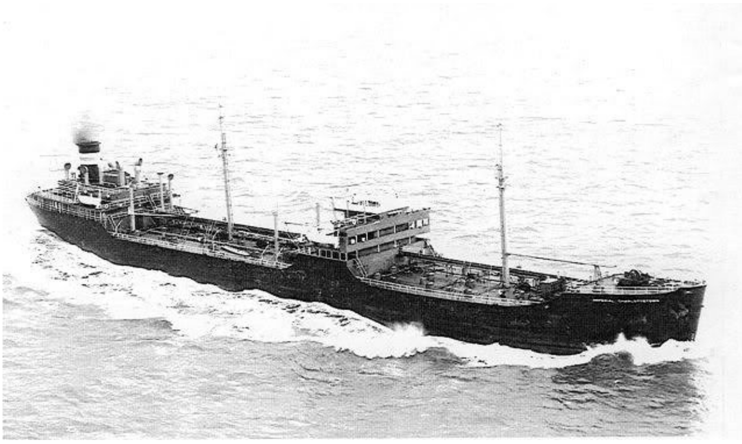

(a) The *Sag Harbor*, built for USMC by the *Sun Shipbuilding and Dry Dock Company* in 1944. Courtesy [259].

(b) *USS K-5* (built 1914) underway on the Mississippi River, 1919. The vessel was built by the *Fore River Shipbuilding* and launched 17 March 1914. Courtesy [226].

Figure 2.7: World War vessels, the T2 tanker (World War II) and the USS K-5 submarine (World War I), both with electric propulsion.

In fact no other nations at that time had naval surface vessels with turbo-electric propulsion [206]. Germany originally had plans to use turbo-electric drives in the battleships of the *Bismarck* class, however, *Siemens-Schuckert Werke* in Berlin did not accept the contract because of a fear that it could not meet certain technical requirements. Hence, the battleships of the *Bismarck* class were built with reduction-gear systems [92, 161].

2.3.1 "The Navy Oilers"

One of the more important vessels using turbo-electric propulsion built during World War II was the T2 tanker. The T2 tankers, see figure 2.7a, ("navy oilers") were crucial for maintaining the upper hand in the war by transporting oil to the navy vessels around the world. The most common type of the T2 tanker was the United States Maritime Commission type T2-SE-A1, which was overall 523.5 feet long, with a beam of 68 feet [95]. Between 1942 and 1945 481 tankers of this type were built, with propulsion provided by a turbo-electric drive [1, 242]. The propulsion system consisted of a steam-turbine generator connected to a propulsion motor to drive the propeller, hence, the need for a large main reduction gear was obviated. At this time the turbo-electric propulsion system was not a new invention, as all the capacity to manufacture reduction gears was committed to supplying the naval fleet, the use of turbo-electric propulsion was a natural choice resulting in an average production time from laying the keel to sea trials to about 70 days. The T2 (A1 type) tanker's propulsion system delivered 6,000shp , with a maximum power of 7,240hp resulting in a rated top speed of about 15 knots with a cruising range of about 12,600 miles.

2.3.2 Submarines using Diesel-Electric Systems

During World War I the submarines proved to have a significant impact, as the German Navy's submarines (u-boats) saw action in the war on Allied commerce, often referred to as the *Handelskrieg*. In this period, the battery technology and diesel-electric systems were primitive, and the submarines were designed to be more of a surface vessel with the ability to dive when needed. The submarine design included more or less a triangular cross section of the hull with a distinctive keel and bow, like the USS K-5 shown in figure 2.7b. The propulsion system consisted of a diesel-electric system to charge the main batteries (lead batteries) on the surface using the propulsion motors as generators. The batteries were solely used during submerged

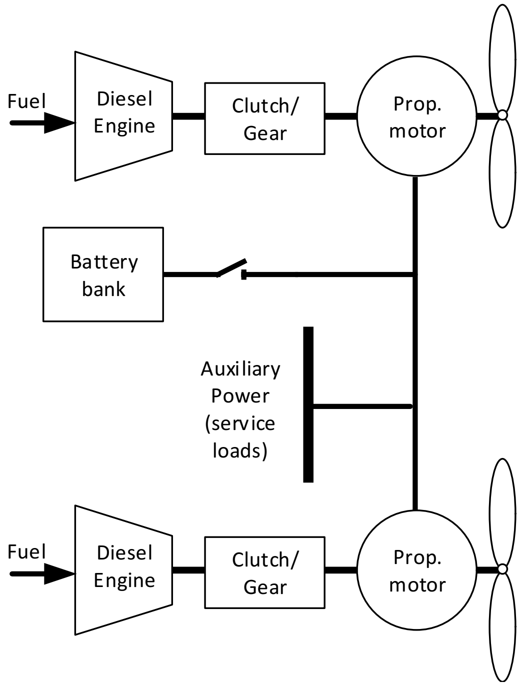

Figure 2.8: Simplified drawing of a common diesel-electric configuration in World War I and II submarines. Propulsion motors acted as generators driven by diesel engines on surface.

operations for both propulsion and service loads such as lights and instrumentation. Figure 2.8 shows a simplified sketch of such a configuration. The maximum duration of underwater operations was heavily dependent on the vessel's speed. At a very slow speed of about 2 knots, the vessel could be submerged for around 48 hours, while at a higher speed, about 6-8 knots, the vessel could only be submerged for around an hour [32]. World War I was the first war using submarines, and is often referred to as *The Submarine War*.

When World War II broke loose, a lot of research had been conducted towards the diesel engine, the electric motor and battery technology. Even though the *Versailles Treaty* (1919), among other things, banned Germany from having submarines (and air force) [182], the German Navy, *Kriegsmarine*, started constructing submarines in the early 1930s. To increase the duration of submersed operations a German engineer, Dr. Helmut Walter of Kiel's *Germaniawerft*, proposed a radical new technology for providing oxygen to the submarine's engine whilst submerged. Using high-purity hydrogen peroxide (H_2O_2) as an oxidant, the oxidant was decomposed using a permanganate catalyst to yield high temperature steam and free oxygen. This oxygen was then injected into the diesel engines, enabling the diesel engines to run underwater and charge the batteries. The exhaust from the engines and the steam from the oxygen production were ejected. Dr. Walter made a prototype, which was scaled by the *Kriegsmarine*. Although seven Type XVIIB H202 vessels were built, they never saw combat due to Germany's defeat in 1945. In the 1950s Great Britain, with the help of Dr. Walter and some of his key personnel, created two high speed boats, *HMS Explorer* and *HMS Excalibur*. However, the highly concentrated hydrogen peroxide fuel created a safety hazard, and the vessels were decommissioned in the 1960s. This was not the end for Dr. Walter's technology as both the US and the Soviet Union adopted his technology, and started research on Air-Independent Propulsion (AIP) systems [258]. The research on AIP systems started by Dr. Walter is still an important research topic in the sense of electric power generation for underwater vehicles, including, among others, closed-cycle diesel engines [84, 85, 86], closed-cycle gas and steam turbines [40, 96, 114], Stirling-cycle (adiabatic) heat engines [185, 191] and fuel cells [152, 207], and a range of different patents are filed within the topic.

2.4 Towards Today's Marine Vessel Power Systems

After World War II and toward present time, new innovations and stringent requirements with regards to fuel efficiency, reliability, maneuverability (variable speed propulsion) and air pollution (emissions) led the way towards today's marine vessel power system solutions. With an increasing need for electricity, as a result of more electrical loads with different power requirements (i.e. voltage levels, dc/ac, etc.) the technical advances in power electronics found their way to the shipboard power system, with the result of the marine vessel power system slowly converting towards an All Electric Ship (AES).

2.4.1 The Advent of Power Electronics and Variable Speed Converters

The next technological advance paving the way for the modern marine vessel's power systems may be seen as the advent of modern power electronics. The history of power electronics started with the American inventor Peter Cooper Hewitt, who in 1902 invented the glass-bulb pool-cathode mercury arc rectifier [110], as a result of experiments with a mercury vapor lamp which showed the current flowed in only one direction, from anode to cathode, giving rectifying action. His invention was quickly adopted by the industry, finding its way to applications in battery charging and electrochemical processes. The technology was also adapted in power grid control, and by retarding the firing angles, the rectifier circuit could also be operated as a line-commutated inverter. In 1926 *General Electric* invented the thyratron, or hot-cathode glass bulb gas tube rectifier, which was the forefather to the thyristor. In 1934 the thyratron was used in a motor drive for speed control of induced draft fans in the *Logan Power Station*, which was the first variable-frequency ac installation in history. The diode version of the thyratron, the phanotron, was used in the *Kramer* drive in 1938, where the phanotron bridge replaced the rotary converter for slip power rectification. In 1947 the bipolar point contact transistor was invented by Bardeen and Brattain followed by the bipolar junction transistor (BJT) in 1948 by Shockley, all working in *Bell Telephone Laboratory*. The same laboratory also invented the PNPN triggering transistor in 1956, which later was defined as a thyristor or silicon controlled rectifier (SCR), and in 1958 *General Electric* introduced a commercial thyristor, including the TRIAC (integrated anti-parallel thyristor) and the gate turn-off thyristor (GTO). The invention of the thyristor marked the beginning of the modern era of power electronics, often referred to as *the modern solid-state power electronics revolution* [27, 28, 29, 30]. In the late 1970s power MOSFETs became commercially available, and in 1985 the Insulated Gate Bipolar Transistor (IGBT) was commercially introduced by *General Electric*. The IGBT is basically a hybrid MOS-gated turn on/off bipolar transistor that combines the properties of MOSFET, BJT and the thyristor [17].

From the early power electronic inventions a range of different devices were made to convert, transform and do frequency adjustments to gain effective and economical power distribution systems. The *SS Canberra*, launched in 1960, was the first British passenger liner to use alternating current as power. The vessel was originally an ocean liner, intended to sail between the United Kingdom and Australia (*The Orient Line*). However, due to the arrival of jet airlines, the vessel was adapted to cruising. The vessel was equipped with two *British Thomson-Houston* (AEI[6]) synchronous three-phase 6,000V air-cooled electric motors providing 85,000hp (63,000kW) running twin screws, which were the most powerful turbo-electric powered units ever installed in a passenger ship, giving the vessel a speed of about 27.5 knots. The two electric motors were supplied by two 32,200kW steam-turbine driven alternators. In addition, the vessel was equipped with four steam-turbines providing auxiliary power, each driving a 1,500kW, 440V, three-phase, 60Hz alternator and a tandem driven 300kW exciter for the main propulsion alternators. In addition to the twin screws, the vessel was equipped with a bow propeller to make the maneuvering in port and docking easier [52, 53, 162]. *SS Canberra* is considered a legend, having an important role in the Falklands war starting in 1982 [255], but was scrapped in 1997 due to high running costs and age. The power system installed in *SS Canberra* was state of the art, with separated power generation for main propulsion and service loads (auxiliary power), and still today many vessels use this kind of separated power generation.

From approximately 1980 the use of power electronics in vessel's propulsion systems became a very common method for improving fuel efficiency [139, 164]. A high-profile example is the ocean liner *Queen Elizabeth 2* (QE2), which was built in 1968 for *Cunard Line*, originally steam powered. After experiencing mechanical problems in 1983, and an electrical fire in 1984, *Cunard* decided to convert her from steam to diesel. The conversion to diesel-electric propulsion would improve the fuel efficiency and was expected to save *Cunard* £12 million a year in fuel costs [189]. The vessel was fitted with 9 German *MAN B&W 9L58/64* 9-cylinder engines, each weighting about 120 tons, all connected in a diesel-electric configuration, each driving a generator rated 10.5MW at 10kV [240]. The electrical plant, in addition to powering the vessel's auxiliary loads (and hotel services) through transformers, drove two synchronous salient-pole 44MW *GEC*[7] propulsion motors (each weighting more than 400 tons), which, one on each propeller shaft, drove two five-bladed variable-pitch propellers. A simplified drawing of the ship's electric configuration is given in figure 2.9. The vessel's service

[6] *Associated Electrical Industries*
[7] *General Electric Company*

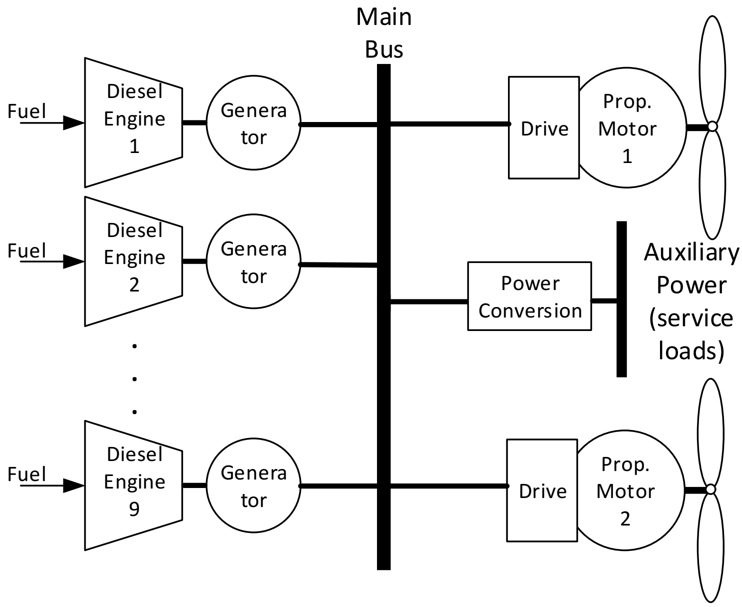

Figure 2.9: Simplified drawing of *RMS Queen Elizabeth 2*'s integrated diesel-electric power grid.

speed of 28.5 knots could be maintained using only 7 of the diesel-electric sets. At this speed the fuel savings were about 35% compared to the old machinery. The maximum power output from the power plant was 130,000hp, in comparison with the old machinery's 110,000hp. The vessel is still functional today, laying in Dubai after plans for it to become a luxury hotel in Asia stalled [171].

2.4.2 Towards All Electric Ships (AES)

Not only did passenger and cruise vessels convert to diesel-electric systems. Also offshore vessels such as Platform Supply Vessels (PSV), anchor handling and a range of special vessels adopted a diesel-electric configuration in the 1980s. Due to an increase in electric equipment and systems used for different operational profiles - a transition towards All Electric Ships (AES) [181], the vessels needed reliable power generation which could supply the often rapidly varying load profiles. Also the introduction of Dynamic Positioning (DP) systems, in which interest started to grow with the offshore drilling in the 1960s when drilling moved to deeper waters where jack-up barges could no longer be used, added requirements for the power systems. The DP system was originally designed for station keeping, which today has been further developed to include a number of different features and functionality [80, 228]. The DP system requires a fast acting power system that can supply the propulsion system's load profile to keep the vessel at the desired coordinates. In addition to DP systems, the advent of different thruster designs, such as azimuth (azipod) and bow thrusters, all increasing the vessel's maneuverability, changed the load profile of a vessel and required its power system to be able to supply the necessary load profiles in relatively different operations while keeping the fuel consumption at a minimum. With the advent of modern power electronics, and the application of the thyristor to power control in the 1970s, new systems and electrical equipment could be powered, and the power generation in a diesel-electric configuration could be realized with high efficiency and at appropriate safety levels. In vessels, such as the PSVs and naval vessels, the power system had to include more than one primary mover to generate power to the propulsion system, and due to limited space, maximum weight limits and high reliability requirements the power system design changed from a radial to a zonal design.

Although diesel-electric power generation can be considered to be the most common system in today's shipboard power grids, there exist other solutions using alternative fuel. Prime movers using Liquid Natural Gas (LNG) and nuclear steam-turbine plants (turbo-electric or geared configuration) have both been explored and used, LNG for reducing air pollution and nuclear as more or less an *infinite* power source cultivating AIP:

- *USS Nautilus* was the first nuclear-powered submarine, commissioned in 1954 (cold war submarine) [188, 198].
- *USS Long Beach* was the first nuclear-powered navy surface vessel, launched in 1959 [188].
- *NS Savannah* was the first nuclear-powered merchant (passenger-cargo) vessel, launched in 1959 [68, 248].
- *MF Glutra* was the first LNG-powered vessel in the world. The ferry was set in operation in 2000 [8].

- *Viking Energy* and *Stril Pioner* were the first LNG-powered cargo vessels, both launched in 2003 [62, 178, 205].
- *Isla Bella* was the first LNG-powered container ship, launched in 2015 [208].

For economical reasons, some vessels, with varying operational modes and propulsion load profiles, have adopted a Hybrid Electric Drive (HED) system (sometimes referred to as the *power take-in/power takeoff architecture* [163]), which adds a propulsion motor to the gearbox of a mechanical drive propulsion system. This is done to allow the electrical distribution system to power the propulsion system at low speed. Mechanical propulsion engines are in general least effective at low speed, and by using the electric propulsion a considerable amount of fuel can be saved while operating at low speed (low propulsion power demand) [65]. An example of a vessel using a HED system is the *USS Makin Island*, a *Wasp*-class amphibious assault ship, which was commissioned in 2009. The ship is equipped with two 35,000shp gas-turbines (*General Electric*) and six 4,000kW diesel generators (*Fairbanks Morse*). The vessel uses two auxiliary propulsion motors powered by the ship's electrical grid (diesel-electric) at low speed (up to 12 knots), while at higher speeds the gas-turbines are used [247, 249]. Since such amphibious ships spend about 75% of the time at speeds lower or equal to 12 knots, the diesel-electric propulsion is used a majority of the time, saving both fuel and wear and tear on the vessel's primary engines. Figure 2.10 shows a simplified drawing of such a hybrid system, where a mechanical engine and an electric propulsion motor are both connected to the gearbox driving the propeller shaft.

New technologies such as fuel-cells and Battery Energy Storage Systems (BESS) using renewable energy have also been explored. In January 2015 the world's first fully electric battery powered passenger and car ferry, *MF Ampere*, was set in operation (commissioned and delivered October 2014) in Norway. The vessel was a joint development between the Norwegian ferry company *Norled AS*, the shipyard *Fjellstrand* and *Siemens AS*. The vessel, which was certified by *DNV-GL*, is powered by a lightweight *Corvus* Energy Storage System (ESS), weighting only 20 metric tons, and supplies all the vessel's power demands while at sea [46, 209]. The vessel, which is 80 meters long, can carry 120 cars and 360 passengers, and the ferry's crossing, which goes between Oppedal and Lavik, near Bergen, Norway,

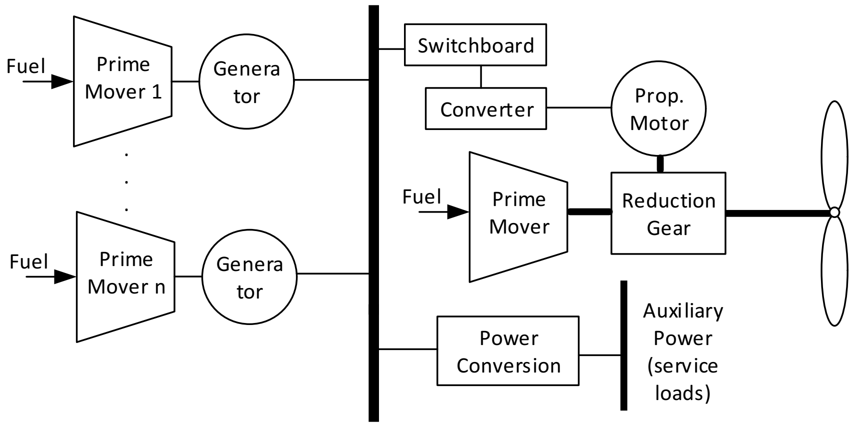

Figure 2.10: Simplified drawing of a hybrid grid. Diesel-electric propulsion is used for low speeds while the prime mover is used for high speeds [163].

takes about 30 minutes. The ship's batteries, which are approximately 1MW combined, are charged on each side of the route using the villages' electric grids, which distribute hydro-generated power. Due to fast charging and to avoid overloading the electrical grids in the villages, the charging systems contain battery packs (battery energy storage systems), which are charged by the villages' electrical grid while the vessel is at sea. The vessel's hull is optimized to be energy effective, and each port is equipped with a docking system which uses vacuum mounts to keep the ferry at rest without using the vessel's propulsion. Figure 2.11 shows a simplified one-line diagram of the ferry's power system.

The implementation of ECA (Emission Controlled Area) zones at different areas along coastlines defines a set of strict requirements for acceptable emission levels from diesel engines, and in this way pushing the development of shipboard power systems towards more environmental friendly solutions. IMO is defining the standard for emissions in the ECA zones by the *MARPOL Annex VI*, which make designers and engine manufacturers look into improving performance of engines and the way they operate in a power system. The focus on improving the solutions by reduction of losses and best possible utilization of the generated power has introduced centralized and distributed dc solutions as presented by *Siemens* (*BueDrive-PlusC*) [212] and *ABB* (*DC-grid*) [3]. This development is in line with an increasing demand for batteries as part of power system solutions for ships in order

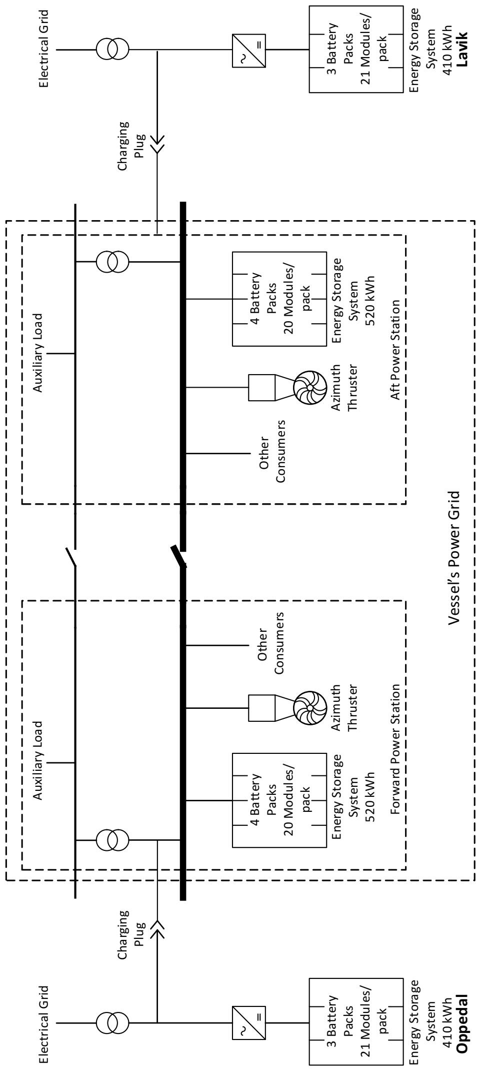

Figure 2.11: Simplified one-line diagram of *Norled*'s *MF Ampere* all electric battery ferry [46]. Each side of the ferry's crossing contains an energy storage system, which is charged while the vessel is at sea, to not overload the village's electrical grid when the ferry is charging its batteries.

to meet the emission requirements, and has also made class societies, such as *DNV-GL*, develop new rules for use of large battery systems in ships, as was done for the *Ampere* ferry.

2.5 Properties and Challenges of the Marine Vessel's Power System

Electrical power systems for marine vessels have existed for more than 100 years, and history has shown a high level of research and innovation, to bring the early applivations of shipboard electricity of the 1880s to modern power systems. Vessels today often consist of an ever increasing electrical load: The majority of the propulsion systems and auxiliary loads, such as weapon systems in naval vessels, hotel and service loads in a cruise vessel, and station-keeping (DP) systems for subsea operations, are of an electrical type. The power is, in general, generated from prime movers using e.g. diesel and/or gas, or from nuclear plants with a turbo-electric configuration. In many modes of operation the power systems need to be reliable and exercise a high level of survivability. The *Naval Sea Systems Command* states the design philosophy for naval power systems very well [65, 66, 170]:

> *The primary aim of the electric power system design will be for <u>survivability and continuity of the electrical power supply</u>. To insure continuity of service, consideration shall be given to the number, size and location of generators, switchboard, and to the type of electrical distribution systems to be installed and the suitability for segregating or isolating damaged sections of the system.*

This design philosophy does not only apply to naval ships. Vessels that exercise dangerous operations, such as DP operations near offshore structures, or operations in which in general, any failure could have a high economical or environmental consequence, need power systems with high levels of reliability and survivability and electrical stability.

On the commercial side the vessels should be fuel efficient, thus keeping the emissions (air pollution) to a minimmum and the fuel costs low. One of the most critical issues facing ship owners and builders today is stricter regulations for emissions, such as the *International Maritime Organization's* (IMO) *MARPOL* air pollution regulations [128, 163]. Due to these stringent exhaust emission regulations, a lot of focus has been devoted toward technology such as exhaust catalysts, electronically injected common rail diesels, and waste-energy recovery, such as heat-exchange systems. Also alternative fuel, such as LNG, has also found its way to a broader market.

Properties (and requirements) such as reliability, survivability, and continuity of electrical power supply, sustainability, and efficiency can all be related to the power system's design, electrical stability, and manner of operation. In the following some of the aspects of the shipboard power system's ongoing design trends, properties, and challenges will be discussed. For a thorough introduction to the most common shipboard power system designs it is referred to [181].

2.5.1 AC vs DC

The early shipboard power systems were of a dc type, but with the introduction of the ac motor this changed and ac became the main trend in shipboard power system designs. One of the reasons for this was that the early dc systems (without power electronics) needed rotating devices to transform the power from one voltage level to another [105]. The ac power system has been the most used power system in marine vessels, but now, with modern power electronics and other technological advantages, the discussion of using dc or ac distribution in shipboard power systems has been brought to the table and some of the key points whether to use ac or medium-voltage dc (MVdc) are (adopted from [18, 65, 192, 230]):

- **Impedance:** MVdc power systems are capable of providing greater energy dynamics than the classical ac power systems due to elimination of many components for power conversion and optimizing the use of the cables (only ohmic resistance). The dc distribution doesn't experience skin effect in the power transmission, as is the case in ac transmission. Also, due to the lack of a fundamental frequency, the dc system does not have a power factor, and depending on the voltage levels, the weight of cables may decrease for a given power level. Unlike the dc system, the ac system has reactive currents that increase the losses, which thus reduce the energy transportation capability. Cable impedance in an ac system causes a current-dependent voltage drop along the cable, however the impedance of the cable automatically limits the short-circuit currents. In dc systems only the (very low) ohmic resistance of the cables limit the short-circuit currents, thus all parts of the power system are equally effected by a short-circuit at an arbitrary position. This effect, and the missing natural zero-crossing of the ac current makes it hard to break a connection (bus-tie/circuit breaker) or even limit the dc current, which may endanger power converting devices that contain power electronics.

- **Prime mover speeds:** In dc systems the speeds of the prime movers can be altered, as the prime mover speeds are largely decoupled from the power quality of the grid. Since frequency control is not a concern, the prime movers can run at optimized speeds (relative power demand with the objective of increased fuel efficiency) connected to generators with an arbitrary number of poles.

- **Connection of parallelled power sources:** In ac systems parallelled power sources must be both voltage and phase matched before being connected to the power system. In a dc system the phase matching is not needed, resulting in a faster power generation response time.

- **Power Electronics Conversion System:** In dc systems, medium or high frequency transformers (dc-ac-dc electronic transformers) can be used resulting in a smaller footprint. On the other hand, in ac systems the transformers make an easy and reliable adaption of the voltage levels, however the conversion system often includes a dc-link stage. Hence, using a cable connection instead of the internal direct connection of the dc-links between the source- and load-side of the converter leads to a dc grid. Linking the dc-links from the converters directly will demand a sufficiently high dc-link voltage in the order of 10kV. Using back-to-back converters with internal dc-links, which are state of the art, this dc-link voltage can be reduced by adapting to the high ac-side voltage by a transformer, at the cost of increased weight and space and reduced efficiency.

- **Fault currents and circuit breaker technology:** In dc systems the fault currents can be controlled to levels considerably lower than in ac systems. This is because power electronics can be used instead of conventional circuit breakers. Lower fault currents will also reduce damage during faults. On the other hand, the ac systems can use much simpler circuit breaking technology than dc systems as electrical arcs clear at zero-crossing of the current.

- **Acoustic signature:** The dc system does not have a significant acoustic signature, as is the case with ac systems due to a common fundamental frequency. This can be an important feature for naval vessels. However, the constant magnetic field created by dc current can leave a residual magnetic field in ferrous materials, which contributes to the overall ship magnetic signature. This tends to be, among other things, a disadvantage with regards to mines and sensor/equipment interference.

- **Weight and space:** In dc systems, high-speed gas turbines can be used in conjunction with high-speed generators, without the need for reduction gears for frequency control, which is often the case in ac systems. A mated high-speed gas turbine and generator enables a shorter generator with reduced footprint. This is desirable due to space and weight savings. For constant power, the dc system needs only two conductors compared to the ac system, which needs three. Removing one conductor is beneficial due to weight savings.

New technological advances, such as the modular multilevel converters (MMC) can, in special configurations, solve many of the issues and challenges of dc power grids, thus making the dc system a more interesting solution in shipboard power systems than before. Even though the MVdc solution may lead to reduced weight, increased efficiency, and offer high-energy transport capability at low losses, challenges such as short-circuit currents, dc-breaker technology, and system standardization must be solved [230]. The different power system solutions, whether it is pure ac, a hybrid between ac and dc or pure dc, have different properties, advantages and disadvantages. The choice of power system (pure ac, ac/dc or pure dc) will be strongly dependent on, among others, available technology and different components from different manufacturers, developer and customer preferences, most economical solution, type of equipment connected to or powered by the power system, possibilities for energy storage, space and weight requirements, the level of redundancy and rules and regulations from classification entities. These aspects, along with an economical point of view, will influence in shaping the power system solution.

2.5.2 Marine Vessel Power Systems and Microgrids

Microgrids are electrically and geographically small power systems capable of operating connected to, or islanded from, a national grid [109]. In islanded mode, the microgrid has strict requirements imposed such as energy independence and service quality for an extended period. Marine vessel's power systems are indeed microgrids; they are isolated (and islanded) while at sea) and part of a terrestrial grid while docking and connected to shore power. Shipboard power systems have a lot in common with terrestrial stand-alone microgrids; many of the methods and a lot of equipment and components are the same [254]. In addition many control strategies and design principles used in microgrids may be applicable for shipboard power systems, and also the other way around. Examples of such control strategies and design principles are voltage and frequency control schemes, power quality improvement strategies, power sharing methods for multiple distributed generators, and energy management systems [9, 141, 144, 151, 251]. A thorough overview of technical cross-fertilization between terrestrial microgrids and ship power systems is presented in [109]. Some of the main differences between a shipboard micrigrid and larger terrestrial (commercial) grids are summarized in the following [65, 109]:

- **Frequency:** The shipboard power system's fundamental frequency cannot be assumed constant. Due to limited rotational inertia of the prime movers and the generators, rapid load changes can cause fast acceleration and deceleration of the motor shafts, which causes frequency fluctuations. Such fluctuation may last for a couple of seconds until the speed of the shafts reach a steady state that coincides with the reference frequency.

- **System analysis:** In analysis of a commercial grid all the system's time constants are quantified and used to analyze the problem by time-scale separation. However, such analysis is not easy to conduct in a shipboard power system due to the principal time constants for motor dynamics, electrical dynamics, and controls which all lie in the same time range of milliseconds to seconds.

- **Planning of power generation:** In a commercial grid the power delivered by each generating unit is scheduled. The difference between consumed and produced power is regulated through equipment acting as swing generators. This is not the case in a shipboard power system as all the generators share the active and reactive power through fast exchange of load-sharing information, which amplifies the paralleled generators' dynamics. Hence, instead of generator scheduling the shipboard power generation exhibits load sharing, which is often realized by generator droop control.

- **Electrical distances and load flow:** In the commercial power sector it is important to model the electrical distances (transmission lines) in the power distribution to achieve the right dynamics and proper voltage regulation. This is not the case in a marine vessel's power system as the electrical distances are short, thus trivializing the load-flow problem. The short electrical distances result in low impedance which increases the coupling between the different parts of the power system. Hence, to strengthen coupling between devices and subsystems the assurance of stability needs proper attention.

- **System's size and extent:** Due to the shipboard power system's limited extent, a higher level of centralized control can be applied than in commercial systems. The shorter electrical distances also facilitate easier synchronization of data and measurement retrieval than in a commercial grid.

- **Load profile:** In a shipboard power system the load profile is often rapidly changing due to the power demand from the propulsion system and other high-rated systems and equipment. Hence, the power (both active and reactive) is changing more rapidly in a shipboard power system than in commercial distribution systems.

- **Single line faults:** A shipboard power system is designed to continue operation with a single phase (line) to ground. For safety reasons such medium voltage systems always include high impedance grounding systems.

- **Environmental effects:** A shipboard power system must be able to operate in a tough environment, which is characterized by vibrations, shock and motion dynamics, and should survive salinity and moisture.

2.5.3 Integrated Power System (IPS) and Grid Design

In an *Integrated Power System* (IPS), or *integrated-electric ship*, all the required power, for the vessel's propulsion and auxiliary (service) loads, is generated and distributed by the same main generators. In comparison, in a conventional (segregated) *electric-drive* vessel power system, the propulsion and the auxiliary loads are separately powered by dedicated generators [181]. Fig. 2.12 illustrates the main structural difference between the conventional (segregated) power system and the IPS.

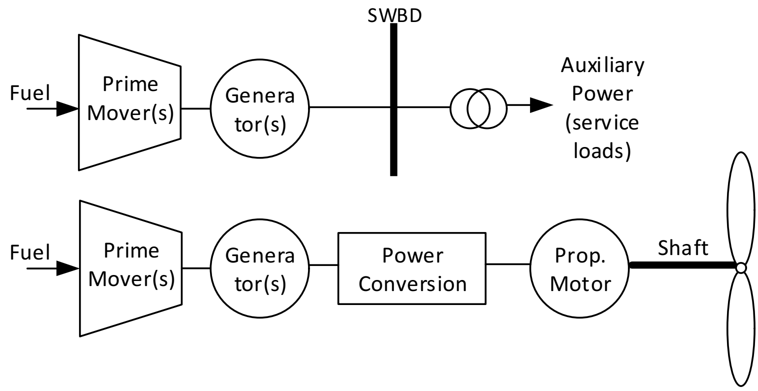

(a) Conventional *electric-drive* power system: Separated, or segregated, power generation for propulsion and auxiliary loads.

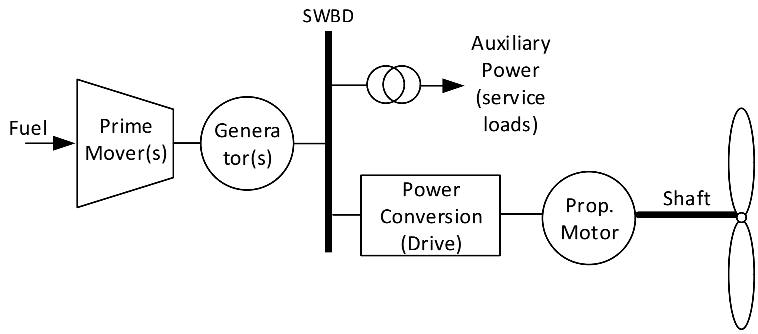

(b) Integrated power system (IPS): Integrated power generation for propulsion and auxiliary loads.

Figure 2.12: Simplified drawing illustrating the main structural difference between conventional and integrated power systems.

The propulsion system in a conventional power system was originally a mechanical-drive system with reduction gears connecting the prime movers to propeller shafts. Many vessels were converted to electric propulsion to gain faster response, which resulted in the separated conventional electric-drive power system. Even today there exist numerous vessels with this kind of power system. As Fig. 2.12a indicates, the conventional power system consists of two separated subsystems; one for propulsion and one for auxiliary loads. Due to the separation between the subsystems, the engines of each subsystem are only connected to their respective systems and can only be used within that subsystem. This configuration has been the leading design for ensuring maneuverability; almost 90% of the vessel's generated power is locked into the propulsion system [139]. However, this separation, where the majority of the vessel's power supply are limited to the propulsion system, can be a disadvantage as the propulsion power is not available for other mission specific systems.

To tackle the disadvantage with the conventional power system, the IPS was introduced as a solution. Instead of separating power generating units into stand-alone subsystems, the IPS shares all generated power from all the generators on an integrated power grid, which distributes the power to all individual consumer systems located throughout the grid in a utility fashion. The IPS's ability to share the generated power between all (online) consumers is also an important property for easing aftermarket installations of electric equipment, as new equipment is simply connected to the distribution grid. The property of power sharing is the main advantage of IPS, and improves power flexibility (operational flexibility) and availability. At low- and medium-speed ranges, the IPS can generate the same amount of power as a conventional power system with fewer running prime movers. This is preferable both from an economical and an environmental point of view, as fewer running generator sets (gensets) will enhance the fuel efficiency and reduce exhaust emissions. By starting and stopping gensets relative to the vessel's power demand, the IPS provides a stepped power generation, and by equipping a vessel with gensets of different power ratings, the power production could be optimized to avoid low non-ideal loading conditions of the prime movers. However, this is seldom the case since all or multiple gensets in a vessel are often of same size to make maintenance and access to spare parts easier. In addition, if the IPS operates with open bus-ties (see Fig. 2.13), both sides should have the same power generating capacity. The future shipboard power system may have an elegant solution to the optimal prime mover loading problem involving Energy Storage Systems (ESS) [108, 120], that can store excess power to achieve ideal prime mover loading conditions, which, among other scenarios, can be used to give a *green* approach to harbors without emissions.

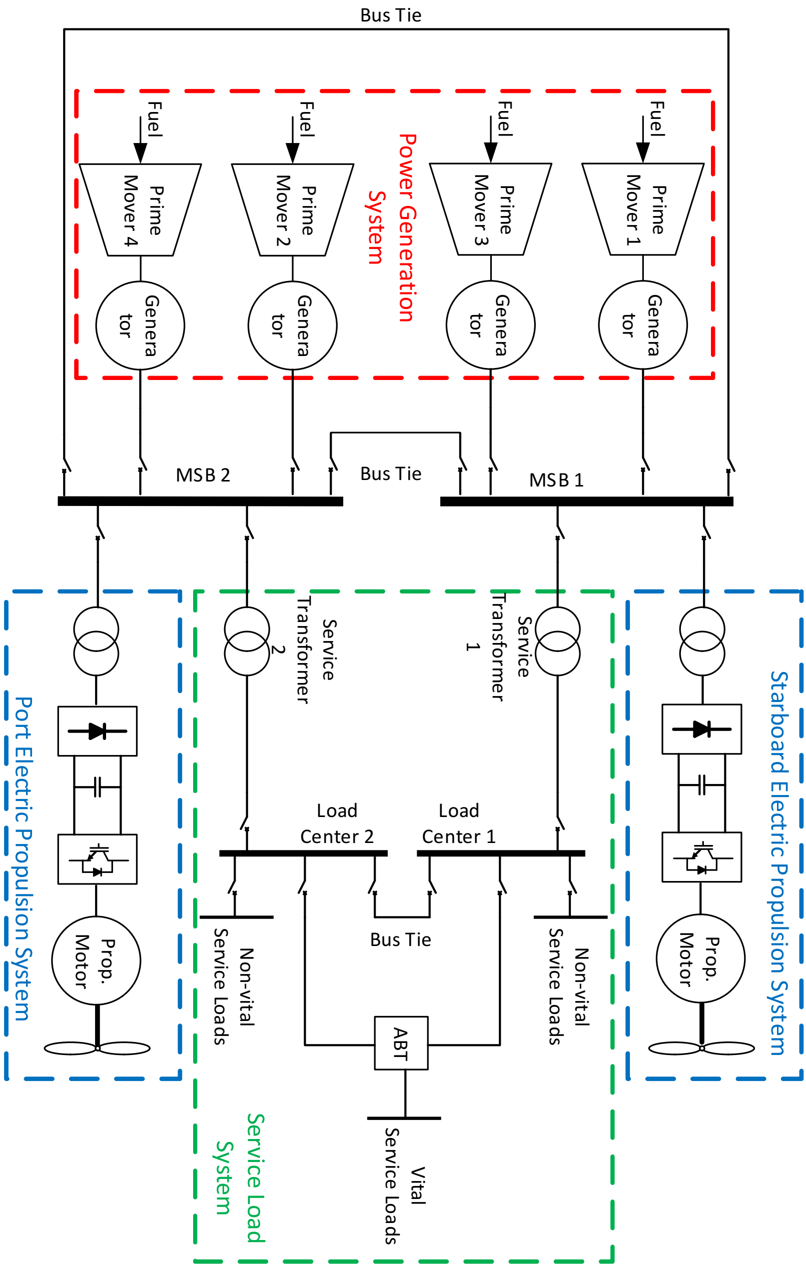

Figure 2.13: Example of a typical redundant IPS for PSVs and small-medium naval ship. Redundancy for bus-tie breakers connecting Main SwitchBoard (MSB). Redundant power supply for vital loads using Automatic Bus Transfer (ABT) [139, 181].

2.5.3.1 Electrical Stability

Reliability, dependability, and survivability are important properties for many shipboard power systems. A naval vessel must be able to survive an attack where parts of the power system are down, but still be able to bring the ship away from the situation and have the power needed for initiating defense measures. An offshore vessel conducting a station-keeping operation (DP) near offshore structures needs to survive single faults and have the power needed to bring the vessel to a safe position away from the structures. In the same way, a deep-sea drilling vessel must have a reliable power system that survives faults and maintains station-keeping to avoid critical situations that can harm both equipment and crew.

- **Reliability** is often explained as a fail-safe operation [139], and the term *system reliability* is a standard measure for the effect of component failures and internal errors and is calculated using component mean time to failure (MTTF) statistics and static dependency analysis [266].

- **Dependability** is given as the system's ability to continue operation despite component failures, internal errors and exogenous disruptions.

- **Survivability**, on the other hand, is mostly used for naval vessels and military applications and deal with continuity of vital services during major disruptions associated with battle and damage control operations.

In many settings the terms are mixed together, and reliability often comprises both dependability and survivability. To achieve a reliable IPS, which cultivates both dependability and survivability, the most used design principle is redundancy, however, spatial separation and manual backup systems have also been used to a great extent.

An often used redundant *two-split* IPS design for small and medium size vessels is shown in Fig. 2.13. As can be seen, the power generating units are split in pairs, each pair connected to a switchboard (MSB 1 and 2), and the switchboards are connected through redundant bus-ties. Each switchboard supplies one propulsion system, and both switchboards are serving the service loads. The load center is split in two switchboards. The vital service loads have redundant power supply from both switchboards using an Automatic Bus Transfer (ABT) unit, while the non-vital loads are served by one of the switchboards, one on each side of the vessel. Depending on the vessel type and class regulation from classification entities, the IPS may include an emergency generator supplying vital loads, and in some cases part of the propulsion loads. The bus-tie between the load center switchboards has the ability to connect the switchboards if, for instance, one of the service transformers fails. The IPS is equipped with many breakers, which may be used to isolate faults from propagating through the grid and causing a complete blackout. Hence, this property, *reconfigurability*, is important for achieving the needed system reliability, and is closely related to the IPS's practical design and installation, as well as fast and reliable fault detection systems that are able to invoke protection schemes isolating the faults.

2.5.3.2 Radial and Zonal Grid Designs

Traditionally, the practical solution to provide redundant power distribution was to install alternate power routes between components using longitudinal cables connecting vital loads to multiple switchboards. This solution, a *radial* distribution, was shown to be a bulky and heavy solution with the ever-increasing number of vital electrical loads. As a solution, the *zonal* distribution grid was introduced in the 1990s, where the redundant power supply was realized by providing vital loads with alternate power routes using shorter transverse feeder cables from port and starboard switchboards [139, 266]. This may be seen as stretching the switchboards along the vessel's longitudinal axis, one switchboard for starboard side and one for port side. Bus-ties are used to isolate faults, or segregate parts of the switchboards. With this solution, the long feeder cables in a radial system are removed, with the effect of reduced cost and weight - which again leads to lower fuel consumptions and emissions. The zonal distribution topology is usually adopted in the IPS design philosophy, enabling easier aftermarket installations of equipment and more flexibility regarding installation of redundant solutions for achieving a design with the needed level of reliability and survivability at relatively low cost. An illustration showcasing the differences between radial and zonal grids is given in Fig. 2.14.

It is expected that tomorrow's power system design solutions will be completely different from today's solutions. Future shipboard power systems

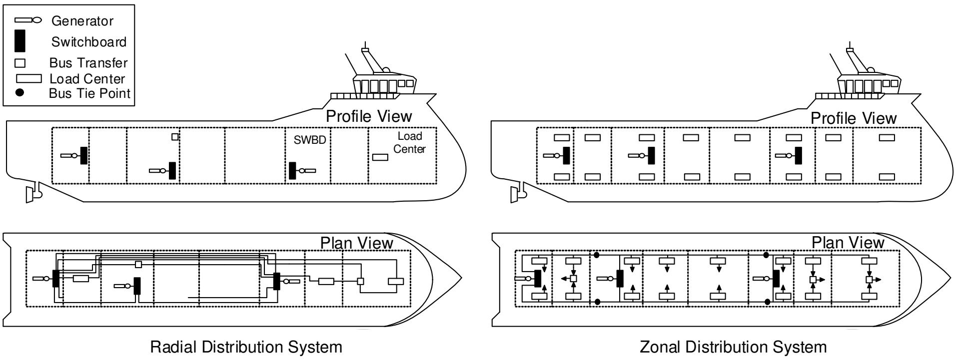

Figure 2.14: Comparison of *radial* and *zonal* power distribution systems in a marine vessel [65].

should aim for a higher quality of service (QOS), increased reliability and efficiency as key requirements, which may be achieved by, among other means, a completely new design strategy, advanced monitoring of system health and state as part of new sensor technology, and advanced and efficient stability and power quality improvement methods and devices.

2.5.4 Power Electronics and Harmonic Pollution

Electricity enables a more flexible way to utilize energy than any other energy source. Technology such as information systems, radar and sonar systems, advanced motion compensation, and military precision weaponry would not be possible without electricity. Future predictions show that more and more equipment is of an electrical type, and the marine vessel is asymptotically converting towards an *All-Electric Ship* (AES), where all installed equipment and systems are of an electrical type [75, 181]. The broad variety of electrical equipment and systems connected to the power system require different power conversions. Some of the equipment and systems are powered by ac, while others are powered by dc. In addition, the needed (and rated) voltage levels may span from a few volts to thousands of volts, and different systems and equipment may require different frequency levels. Almost 90% of the vessel's generated power may at some points go to the propulsion systems [139], flowing through power electronics devices. Power electronics is at the heart of power conversion, and, because of this, the IPS includes numerous different power electronics devices to be able to supply the right form and level of power to the connected systems and equipment. The shipboard electrical power demand continues to increase, from tens of MW and in some cases even greater than 100MW [75]. However, such high power ratings lead to power electronic devices that are both heavy and have a large footprint. This is a real handicap for serving high power demands. In general, in the given order of priority, size, losses, cost, and weight are interrelated factors that limit acceptable applications of power electronics.

An important power electronic device is the converter/inverter, which is able to convert the electric power from one form to another, i.e. ac/dc, ac/ac, dc/ac, dc/dc. The necessary power for each load, or group of loads with the same power requirements, are in an IPS converted at *point-of-use*. In fact, almost all power sources and loads need a converter. Pulse-Width-Modulation (PWM)[8] has been widely used for modulating small- and medium size converters. A switch-mode power electronics converter, which consists of switches that are either on or of, uses PWM to control the time the switches are on and off, and by this, the converter (which in fact is an array of switches) can be programmed to produce voltage and current waveforms, different power factors, and obtain a desired frequency from a range of different input waveforms. From this point of view, there is little difference between motor drives, power supplies, and active power filters, and the composition of power electronics in such devices can be generalized to form a Power Electronics Building Block (PEBB) [74, 76]. These building blocks are intended to minimize the number of different power electronics devices in a power system and can be mass-produced due to their generality. The general design will also allow the power electronics to be tightly packed, which will reduce weight and footprint. The blocks may be controlled by different algorithms and software solutions, through a general interface (communication protocol), and can be changed in the field, depending on operational status or mission type. The blocks can easily be installed (plug and play) with an interface which allows information sharing between the components. Depending on the way the blocks are connected to each other, different algorithms may be deployed as part of a configuration scheme; and, depending on the power system's status and classification requirements, different algorithms may be enabled to perform functions such as power conversion, harmonic mitigation (as an active fil-

[8] Often realized with a hysteresis control scheme.

ter), active or reactive power control, or inherit a simple breaker's properties to isolate faults. Due to its generality, a wide range of different modelling and simulation tools may be developed around this block, which will ease power system design and realization dramatically, thus ensuring stability, reliability and efficiency. An important part of developing PEBB is the continuation of improving power electronics in the sense of minimizing weight, size, and losses, to achieve components that can handle more heat and have faster dynamic response with increased power ratings. The PEBB is seen as tomorrow's solution for advanced power systems. Even though a lot of research and development has been devoted to realizing such a standardized building block, a general solution has not yet become available on the market.

A lot of research has also been conducted towards power semiconductor devices, which consist of a variety of diodes, transistors, and thyristors. New designs have produced components with better performance and lower losses, but few of the designs have reached the market. Also silicon carbide (SiC) has been devoted attention due to the material's properties which leads to lower switching losses, high voltage and high temperature capabilities. SiC devices are expensive, but have a huge impact on converter size, losses, weight, cooling requirements and potential for high PWM frequencies [65, 73, 75].

The composition and use of different power electronics to make a general PEBB will affect the shipboard power system in many ways. The transition from early solutions using Line Commutated Converters (LCC) and Cycloconverters to today's PWM Voltage Source Converters (VSC) had many advantages, including lower harmonic pollution, four-quadrant operation and converter reversibility [145]. It is also expected that the introduction of the PEBB will lead to an increased power quality: The PEBB can be designed and controlled to achieve redundant and reliable solutions, with fewer building blocks, which minimize losses and keep the power quality higher than what is achieved in today's solutions. However, power electronics in general are non-linear elements, with non-linear behavior, and are in most cases sources of harmonic pollution. In thyristor-based devices (which is often the case in motor drives) the harmonic spectrum is not dependent on impedance, thus introduces characteristic harmonic pollutions relative to the devices' different designs. In a 6-pulse converter, the characteristic harmonics are of 5th, 7th, 11th, 13th, etc. order, and in a 12-pulse converter, the characteristic harmonics are of 11th, 13th, 23rd, 25th, etc. order. In a voltage source converter (VSC), which is not based on thyristors, these characteristic harmonics do not occur, and motor drives consisting of VSCs instead of thyristor-based drives may solve the problems with the characteristic harmonics. However, the VSC introduces harmonics dependent on the modulation frequency, which may be 1kHz or higher. LCL filters are often used to suppress the harmonics generated by the VSC, but LCL filters are passive devices and tuned for a given modulation frequency. If, for some reasons, the VSC changes its modulation frequency the LCL filters have to be re-tuned. In addition, the harmonics from a VSC may cause harmonic resonances due to interaction with passive filters [112]. Hence, harmonic pollution can, to some extent, be suppressed by design, but the ever-increasing number of electrical devices, which are directly or indirectly dependent on power electronics, will introduce even more non-linear elements into the power system, making harmonic mitigation and power conditioning devices a necessity.

Harmonic pollution is defined as any waveform with frequencies that are multiples of the fundamental frequency, and is measured as *Total Harmonic Distortion* (THD), which is a normalized quantity describing the relation between the amplitudes of the harmonic frequencies and the amplitude of the fundamental frequency. Most shipboard power systems today are affected by harmonic pollution in some or another way [112]. Harmonic pollution, which impairs the power system's power quality, leads to higher fuel consumption and emission. Harmonics are closely connected to reactive power, and high levels of harmonics may lead to equipment and system break down, and even cause catastrophic events like explosion and fire[112]. Theoretically, this can, in the worst case, cause a complete blackout as a result of voltage collapse. A complete blackout may occur due to high levels of harmonic pollution, but is usually caused by operational mistakes. The term *voltage dip ride through capability* is often used to describe the consumers' ability to cope with faults and malfunctions where in worst case it must be assumed that the voltage becomes zero until the faults are fixed or isolated. Examples of such malfunctions and failures may be short circuits and high inrush currents while starting large motors. The allowed voltage drop is dependent on the vessel and its operations and is set by classification entities [25].

In DP-operations (e.g. DP2 [57]) with closed bus-ties, assessments regarding voltage dip ride through capability must be conducted as part of FMEA to assure continued operation after faults or malfunctions occur. Many DP-operations (station-keeping operations) are performed with open bus-tie, splitting the power system in two, thus minimizing the chances for a complete blackout. This is not an economical nor an efficient solution, as splitting the power system in two requires an increased number of online prime movers for power generation, and also requires multiple separated power management systems (PMS). Harmonic mitigation is therefore not only important for the power system's efficiency, but also for its stability and reliability. Harmonic mitigation and power conditioning is a active research topic, and many active and passive filter solutions have been proposed [10]. Passive filters do not have the ability to change their tuned frequency, and due to changes in power system configurations (and changes in load profiles) as a result of different operational requirements and mission types, passive filters are not always a good solution for harmonic mitigation as a change in the harmonic spectrum requires a re-tuning of the filters. An active filter, on the other hand, has the ability to mitigate any frequency spectrum, the only limitation being the bandwidth of its controller, thus increasing flexibility for changes in the power system's harmonic frequency spectrum. Active filters have also a smaller footprint than passive filters, which is a desired property in marine vessels. Active filters are expensive devices, thus location of installation in a power system is important for maximum utilization (and mitigation) of the filter's power rating. A conceptual method using optimization (Model Predictive Control) to perform system level harmonic mitigation has also been proposed [218, 220, 222, 224]. Active filters come in many forms, and can be part of e.g. a propulsion system's motor drive, realized as controlled Active Front End (AFE) converters or simply stand-alone devices. Harmonic mitigation (and power conditioning) is, as earlier mentioned, important for achieving an efficient and reliable power system, and the harmonic pollution problem is also expected to be an issue in future power systems, consisting of even more non-linear components. As of today, there are no classification entities that require real-time THD surveillance, which would be an important measure for detecting potential stability issues as well as performing fuel efficient operations. THD requirements are checked by classification entities during the vessel's commissioning and certification using handheld measuring devices. The future power system, where reliability and efficiency are cultivated, may require real-time THD surveillance and power conditioning devices (possible consisting of PEBBs), which may be backed on optimization for system level harmonic mitigation, to comply with stringent air pollution regulations, as well as achieving higher reliability in terms of blackout-prevention due to increased power quality.

2.5.5 Energy Management Systems (EMS) and Energy Storage Systems (ESS)

Planning power generation, *energy management*, is important for achieving an economical and efficient power generation with optimal prime mover loading conditions, thus keeping the fuel consumption at a minimum. In ac power systems, the prime movers are speed-controlled, mostly connected to fixed speed generators, to maintain a desired (and designed) frequency within allowable variations (deadband). As the prime movers' speeds are more or less fixed due to frequency control, the loading of each prime mover determines the fuel efficiency in terms of amount of fuel per delivered amount of useful energy - Specific Fuel Oil Consumption (SFOC) $\frac{g}{kWh}$. The prime movers often experience speed deviations as an effect of dynamically changing load profiles (active and reactive power demand), in which affects the inertia on the shafts between the prime movers and the generators. If such prime mover speed variations result in frequency fluctuations exceeding the allowed deadband, the prime mover needs to be isolated and shut down. Large negative frequency fluctuations can also be an indication of the running prime movers are unable to meet the load demand, thus additional supervisory steps should be taken to either shed non-essential loads or spin up idle prime movers, and after synchronization connect them to the power system. Because of speed variations and allowed frequency fluctuations within a designed deadband, the frequency in shipboard ac power systems cannot be assumed constant.

In addition to frequency fluctuations, the speed variations on the motor shafts will also increase wear and tear leading to higher maintenance costs. Controlling the prime movers to track a constant speed greatly affects the power generation as an optimal increase or decrease in power generation is related to starting and stopping prime movers in a *stepwise* (ac) power generation [50]. As the load demand must be met at all times this means that prime movers running at low non-optimal loading conditions is often the case in shipboard ac power systems. To increase the fuel efficiency related to the power demand, the prime mover loading could be increased and power stored to be used in situations where the power demand surpasses the power generation. An example would be to provide the difference between consumed and generated power while additional prime movers are being started and connected to the power system to meet an increasing power demand.

In dc power systems, where the power distribution is conducted on dc grids, the prime movers may run at varying speeds to meet the power demand. As in ac systems, the voltage level is maintained by controlling the generators excitation fields. Due to the flexibility of being able to change the prime movers' speeds, the power generation will adopt a more *stepless* behaviour than in ac systems. However, prime movers running outside their optimal speed ranges are prone to wear and tear, and especially at low speeds the combustion is not optimal and will increase sooting of the prime movers, thus increasing maintenance costs. At high speeds the fuel consumption is not in line with the produced power (non-linear relationship between fuel consumption and produced power), thus reducing the fuel efficiency which leads to increased fuel costs and emissions. As with ac power system, the dc power system could also benefit from a ESS that facilitates optimal operation of the prime movers.

2.5.5.1 ESS Applications

Many suitable ESS technologies that facilitate a more economical and redundant operation in a marine vessel are available on the market today. The choice of ESS technology is related to area of application, energy density, size, weight, and cost, expected lifetime, charge/discharge rates, and other functional requirements. Examples of ESS technologies are Battery Energy Storage System (BESS), Compressed Air Energy Storage (CAES), flywheels, Superconducting Magnetic Energy Storage (SMES), capacitors (including ultra-capacitors) and Pumped Hydro Storage (PHS) [265]. Depending on the power system (ac or dc) most ESS technologies need power conversion devices that convert the power from and to the power system for charging and discharging purposes. An obvious application of a ESS would be to serve as a backup power source similar to an Uninterruptible Power Supply (UPS), which sets strict requirements to the ESS technology's energy density and rate of discharge. This type of application can be beneficial for many marine operations. An example would be an offshore vessel conducting a DP-operation alongside an offshore structure that experiences faults that cause power losses which may lead to a blackout. The ESS may in this case be crucial for powering the propulsion system for a short period of time to be able to reposition the vessel at a safe distance away from the structure to get the time-window needed for isolating the faults and to re-power the vessel.

Many power consuming systems and equipment on a vessel do not have a flat load profile. Propulsion systems, while conducting station-keeping, have a load profile which correlates with waves and ocean currents. Weapons systems aboard a naval vessel may give a pulsed load profile at irregular time instants, which would be more or less impossible to predict. Due to the vessel's dynamic load profile, the energy management is not an easy task, and, as earlier mentioned, often more prime movers are running than are actually needed to be sure of serving the load demands. One application of the ESS, which is a feature that is sought for in a shipboard power system, is *load shaving* or more precisely *peak shaving* [180]. By using the ESS to flatten the vessel's total load profile, energy management, in terms of starting and stopping generators, would be easier, and fewer prime movers have to be on line to meet a potential high and instant power demand. Under low non-ideal loading conditions the ESS charges, and while the load demand exceeds the power generation capabilities the ESS discharges. Whether the power system is dc or ac, the prime movers can be run at optimal speed for maximum fuel efficiency. This feature, peak shaving, may be seen as one of the strongest arguments for installing a suitable ESS in a shipboard power system, as peak shaving may result in a lower fuel consumption (and emission) due to the need for fewer running gensets.

Another interesting application of ESS, dependent on ESS technology employed, is harmonic mitigation [56, 139]. Depending on the ESS' speed of discharge, it may be used to suppress harmonic pollution. The ESS may also be used to charge a dc capacitor in an active filter, which strengthens the filter's capabilities, and thus enables the filter to use active power in harmonic mitigation. Also frequency control by use of ESS has been proposed [179]. As an example, an ESS such as BESS may be installed alongside an Active Front End (AFE) (Figure 2.15), which is a realistic scenario if for instance the ESS is part of a motor drive. In this case, when the ESS is installed alongside an AFE, the ESS could attain application flexibility, thus being able to do harmonic mitigation, peak shaving, and even act as a reactive power source or consumer to increase the power system's voltage

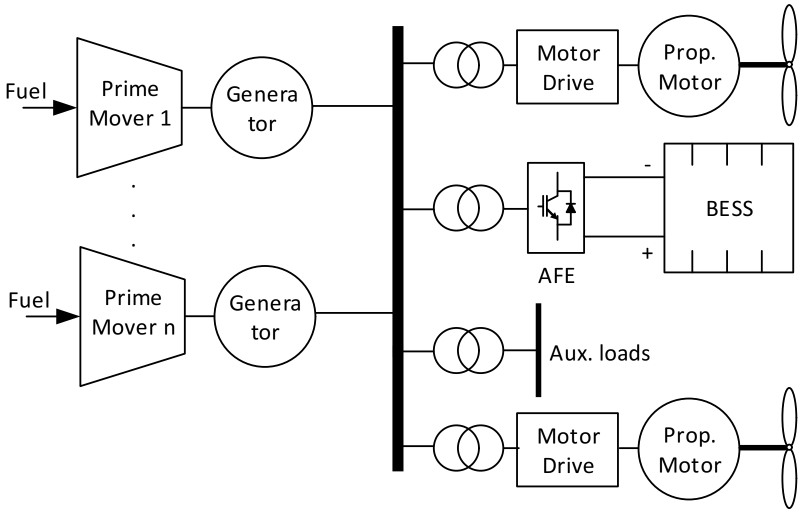

(a) Battery Energy Storage System (BESS) connected to the main bus (switchboard) in an IPS configuration. An Active Front End (AFE) is installed alongside the BESS as a solution for supervision and BESS control purposes.

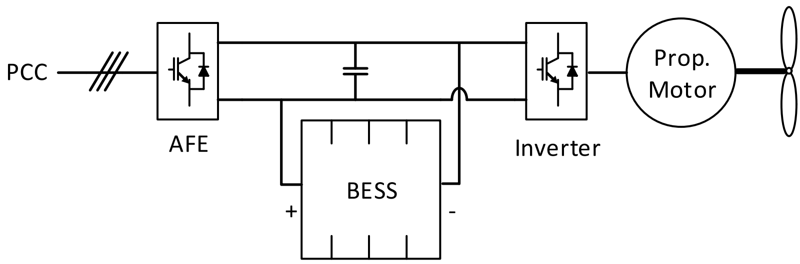

(b) Battery Energy Storage System (BESS) as part of a motor drive for propulsion systems [139]. Point of Common Coupling (PCC) refers to e.g. the vessel's main switchboard. An Active Front End (AFE) is part of the depicted motor drive and supervises charging and discharging of the BESS.

Figure 2.15: Simplified illustrations of different installations of Battery Energy Storage Systems.

stability margins. Figure 2.15 showcases two different locations in the grid for installing a BESS. The BESS may be installed alongside an AFE or other power electronic devices which supervise the BESS state of charge (SOC) and state of health (SOH), and control charging and discharging dependent on the load demand and the BESS' SOC.

Even though the advantages of ESS in shipboard power systems are many, it doesn't come without challenges. Many of the available and suitable ESS technologies are expensive solutions, and are dependent on power conversion devices relative to ac or dc power systems. An effective solution, which was illustrated in Figure 2.15b, is to install an ESS, such as BESS, as part of motor drives, thus eliminating the need for additional power conversion devices, reducing weight, footprint, and costs [139]. For BESS the available battery technology also introduces challenges, as the battery packs are heavy (relative to power capacity) and in many cases have a large footprint. Despite weight and volume, the BESS may allow removal of one prime mover from a vessel, which justifies the use of BESS. Another issue is the battery packs' lifetime. Rapid charging and discharging of battery generates a lot of heat, which can be seen as losses, and may have critical effect on the battery's life. Thus a possible realistic outcome is that the battery pack dies before the BESS manages to pay back the installation costs by reduced fuel consumption. In some applications ultracapacitors or fuel cells can switch places with the battery pack, giving the energy storage system different properties such as increased lifetime, charge/discharge speed, energy density relative to footprint and weight, etc. Also hybrid energy storage systems, including different energy storage devices, may also be interesting possibilities, thus increasing applications and system flexibility [138, 194].

When moving towards all electric-battery powered vessels, a new emerging technology -the inductive charging technology- has attracted the attention of the marine vessel community and the old concept of *Inductive Power Transfer* has re-emerged for contactless battery charging of marine vessels [31, 47, 154]. Significant progress toward the development of commercial solutions for wireless charging is already on its way for high power wireless transfer in the MW range [101]. This technology will greatly benefit coastal vessels operating with a tight schedule as it will significantly reduce charging time and improve reliability. This will bring unavoidable challenges to the local power grid from which high power will be tapped in a short time to charge the vessel's battery packs. This impending impact on the local electrical grid will require grid reinforcements and new solutions that will require collaborative efforts between the utility and marine vessel sectors.

2.5.5.2 Standards and Guidelines

Many classification entities and interest groups impose strict regulations and set forth guidelines for redundancy for many types of marine vessels to avoid total loss of maneuverability. This is mostly the case for offshore vessels, like PSVs, but the requirements can also be found for passenger vessels and cargo vessels transporting hazardous materials. The *International Marine Contractors Association* (IMCA) [121] states (for an offshore vessel) that *if there is a realistic chance of the bus-ties not opening or not opening fast enough then the switchboard should be split for the work* (two-split in Figure 2.13), *and if so the power system must include an independent power system* (Power/Energy Management System - PMS/EMS) *for each individual split* [123]. Furthermore IMCA states that *for a diesel-electric vessel a task appropriate mode could mean operating with closed bus-ties, whereas a critical activity mode of operation may require open bus-tie configuration* [124]. These guidelines are based on risk assessments (Failure Modes and Effect Analysis - FMEA) and fault tolerance (isolation of faults) dependent on classification and control system redundancy [122]. DNV-GL (earlier DNV) [59] describes that the traditional interpretation of the DP-3 requirements has been to run the power system as separated (segregated) subsystems with open bus-tie breakers. This is backed on IMO [125] MSC/Circ.645 guidelines for vessels with dynamic positioning systems, which states that *for equipment of class 3 the power system should be divisible into two or more systems such that in the event of failure of one system, at least one other system will remain in operation* [126]. However, closed bus-tie DP operations have economical, technical, operational, and environmental benefits, thus some DP operators run the power system with closed bus-ties for as large periods of operation as possible [57, 58]. ABS [4] also refers to the IMO MSC/Circ.645 guidelines, and states that these guidelines should be followed in the design of DPS-2 (DPS - Dynamic Positioning System) and DPS-3 systems where loss of position is not allowed to occur in the event of a single fault [5]. For ships normally operating in transit, such as tankers and cargo ships, the equivalent concept is redundant propulsion as described in e.g. DNV-GL's class notation RP. In short, all these regulations and guidelines state that, dependent on the vessel's classification, one should not loose maneuverability, and due to the fact that it has been difficult to both engineer completely fail-safe power systems and prove that there is no chance for power losses impairing the maneuverability, the trend has been to operate the power systems with open bus-ties (a split power system). This type of operation increases the number of needed online prime movers, which results in lower efficiency (higher fuel consumption) and increased emissions. To be able to close the bus-ties in all operational scenarios would be a necessity for future power systems with increased efficiency and stringent emission requirements. To achieve this, the power systems must be equipped with stability-improving systems and devices that, in a safe way, handle faults without harming the rest of the power system. Such systems may involve harmonic mitigation, reactive power control, voltage and frequency control, peak (load) shaving, UPS systems and advanced power system segregation and fault-isolation systems. In order to take advantage of new technological developments to increase operational flexibility without increasing risk, DNV-GL recently introduced the DYNPOS-ER (Enhanced Reliability) notation for DP class 2 and 3 vessels.

2.5.5.3 Emission Free Operation

In tomorrow's shipboard power systems the BESS (or another suitable ESS) may be essential to cultivate reliable and efficient power systems (both ac and dc), and applications such as harmonic mitigation, peak shaving, reactive power control (voltage stability), voltage and frequency control, and backup power can simply be different algorithms deployed to a PEBB-based ESS. It is also expected that in the near future harbors may require an emission-free approach for vessels to load and unload, thus an ESS may be part of a larger *green* system keeping the air pollution (emission) in harbors at a minimum. In addition, the EMS must be intuitive and easy to understand, and provide supportive and advisory actions which are trusted by the operators. Many EMS systems today are hard to understand, as a result they are disregarded by the operators and kept out of the control loop with the effect being an inefficient power system. A lot of work remains to map the operators' behaviors and interaction with the system to make an optimal, reliable, and trustworthy interaction for efficient and economical control of the shipboard power systems.

2.5.6 Increasing Need for Measurements, Big-Data, and Software Complexity

To achieve a reliable and efficient shipboard power system, many different measurements are needed. Active power measurements (voltage and current measurements) are important for the EMS to be able to meet the load demand, and an ESS needs power measurements for conducting peak shaving. In ac distribution systems reactive power measurements (voltage and current measurements) are important for voltage stability assessments, and give a measure of the system's efficiency. Frequency measurements are needed in ac distribution systems as feedback to the prime movers' speed controllers. Voltage measurements are needed for controlling the generators' excitation fields, which are done by Automatic Voltage Regulators (AVR), and also for transformers and power converters connecting equipment and subsystems (including energy storage systems) to the power system need voltage measurements. When starting a prime mover and connecting it to the grid in a synchronization process both phase and voltage measurements are needed. Voltage measurements with high sampling frequency are needed for harmonic mitigation, to assure voltage quality within boundaries set by classification entities. These are only a few examples of needed measurements.

Many parts of the power system have high real-time demands (high sampling frequency demands) for measurements. Harmonic mitigation using Active Power Filters (APF) and power converters such as Active Front Ends (AFE) are examples of systems that require (internal or external)a high rate of sampling measurements. In addition, fast hardware and software is required to process the measurements in real-time to be able to utilize the information for control purposes. Redundancy in measurement devices (sensors) is also a requirement for achieving a reliable system. If one measurement device goes down another has to take over to keep the needed information to the system flowing. Redundancy in measurement devices comes in many forms, and a common approach in systems that relies on correct information is to have a minimum of three measurement devices and use voting algorithms to assure the correctness of the measurement information.

Some measurements may be contaminated by noise, and communication delays between taking the measurement and sending it to the subscribing system may make the information no longer valid. Thus the use of filtering techniques for removing noise, and estimators for estimating biases and transport delays may in some cases be a necessary requirement for optimal control, giving the subscribing system correct and valid information. Advanced signal processing methods may also be used to detect and solve measurement drop-outs as part of a solution to redundancy requirements for improving system reliability.

With increasing system integrity that cultivates both efficiency and reliability of the shipboard power system, there is also an increasing need for measurements. The present trend shows that more and more devices and subsystems are given an IP-address and system information and measurements are broadcast on a local network in the vessel in a cloud-based architecture - *The Industrial Internet of Things (IIoT)*. As a consequence the future system integrity may involve consumer systems planning their power consumption, which is available information for the EMS for use in power generation planning.

With the expected enormous amount of data as a consequence of an increase in measurement devices and broadcasting of system information to get more efficient and reliable control, problems such as limited network throughput and data processing resources may appear. Maybe the most frightening issue is that when all the vessel's systems "come online", the vessel is vulnerable to cyber-attacks. Even though an increase in available system information, measurement data, and distributed control may be beneficial for controlling the vessel's power system in an optimal, reliable, and efficient way, the development of the future shipboard power systems have to address the *Big-Data* challenge in the design of its architecture and assure cyber-security. There exists a range of different types of cyber-attacks, some of which are based on gaining access to data and information, and others that are disruptive and intended to take over or break down a system. The latter may have catastrophic consequences if they enable the attacks that gain control over the vessel's power and propulsion system. A small selection of potential external and internal cyber-attacks will be treated separately in the following:

- ***External cyber-attacks*** can be classified as cyber-attacks originating remotely from the marine vessels. There are different strategies for protecting the vessel from such attacks. A vessel's access point to the rest of the world and potential remote systems, which normally is a 3 layer switch, has authentication and VPN capabilities which provide basic security. The switch can also limit input and output network ports, which restrict the communication channel. By enabling only output ports, the vessel data can be encrypted and exported to e.g. onshore fleet management systems without allowing any input traffic from a potential cyber-attack. A practical approach is described by DNV-GL [60], where the main access point to remote systems is to be powered on only when allowed by the vessel's crew. Another form of attack is related to connection to other equipment or systems that are infected. An example of such a case might be the vessel's shore power connection while docking, where the shore power is altered to harm the vessel's power system and put the vessel out of operation. Another example could be infection of onshore fleet management systems, or other vessels within the same fleet that have dedicated ship-to-ship communication equipment.

- ***Internal cyber-attacks*** can be classified as attacks originating within the marine vessel. This could either be a passenger or trusted insider (crew) that gains control over, or infects, one of the vessel's distributed control system nodes. The cyber-attacks could be based on maleware delivery by a USB stick or different internal access interfaces such as an Ethernet that connects the vessel's office network to the control system network. These types of attacks are more difficult to handle, however procedures such as disabling unused potential access points (such as USB connections) and limiting input and output ports on the router that connects the office network to the control system network can reduce the risk of internal cyber-attacks. If one of the distributed control nodes gets infected it is important to isolate that controller from the rest of the system. However, to quickly realize and identify the attack before any harm is done might be a challenge, which puts stringent requirements on the vessel's distributed control system's middleware to limit potential attacks [78]. Such requirements can be based on each control node's accessibility and level of security clearance to distribute control actions to the rest of the vessel's control nodes. If for instance the middleware detects that one of the control nodes tries to control parts of the system outside the controller's security clearance, e.g. the vessel's prime movers or propulsors, it might be considered as an attack, which should trigger isolation procedures and alert the crew. In addition, it is essential to keep operation systems and firmware up to date to be more resistant to cyber-attacks.

There is a drive towards increased fuel optimality, reduction of emissions, increased safety, and performance and operational flexibility. The technologies that are supporting this development tend to increase system complexity, which has consequences for ship designers, ship builders, ship owners, crew and other stakeholders such as classification societies and authorities. Like the automotive and aerospace industries, the electric power plant is a highly computer controlled system with advanced functionality offering endless user configurations and options embedded in software. The control of the power plant itself is also integrated with the control of power consumers, e.g. [158]. This leads to more complex processes with new tasks, skills and training required by the crew. Due to the safety-critical nature of the ship's power plant and electric system, the maritime industry is looking to learn from the automotive, aerospace, and defense industries that have experienced the paradigm shift due the huge impact of information and communication technology. This has led to new standards, certification, and classification schemes related to integrated systems development and more extensive use of simulator-based training and verification technologies, [23, 131]. Future visions for unmanned and autonomous shipping, [61, 200], are indicators of the opportunities and challenges that are emerging.

2.6 Conclusion

The evolution of the development of marine vessels, from the earliest introduction of electricity in commercial vessels with the *SS Columbia* in the 1880 to the new era of the all electric ship marked by the *Ampere* ferry, has been presented in this work. The use of electricity in marine vessels which started far from the idea of an electric power system on board, has however spurred the developments of electric propulsion systems, and the concept of the integrated power system. As new needs arose (raising cost of fuels and need for improved fuel efficiency) and new inventions emerged, electricity moved from illumination to propulsion systems and energy storage, gradually shaping the emergence of an electric power grid within the marine vessel. The evolution of the marine vessel electrical power system, in this way shaped also the evolution of several electrical technologies, that were customized for use in vessels. And the move appears likely to continue as the Ampere example shows, towards fully electric ships with compact electric components, far from the solution but not from the idea of the first experiment of DC electric boat by von Jakobi. More than 150 years after this first experiment, and through a trajectory of diverse technological developments, the concept of fully electrically driven ships seems to not have gone forgotten.

The electrical system of today's marine vessels can be compared to a land-based stand-alone microgrid system, with which the marine vessel power system shares many common features. Present and future challenges include issues such as harmonics, power quality, fault handling, and stability. These issues will be as relevant during normal operation of the marine vessel as they are at commissioning today. Many of the features required today to handle the modern land-based electrical system (smart grid) will be a necessity in marine vessels as the use of electricity becomes more intensive. Characterization of the marine vessel electrical grid through real-time measurements, and the monitoring of fundamental parameters such as impedance in addition to fundamental and harmonic currents and voltages, will be essential to ensure the safety, integrity, and stability of the marine vessel power system. Lately, re-emerging wireless power transfer for battery pack charging in vessels will make the link between the land-based power grid and the marine vessel power grid even tighter and will create a new form of interaction. Ultimately, as the use of all electric ships becomes widespread, the electric vessel will become a part of the land-based power grid as a high impact electric load, thus bringing new challenges. This work aims at anticipating the potential new challenges and the associated research needs for the future by stimulating the discussion and identifying synergies between the modern power grid and the electrical grid of the marine vessels today.

Part II

Harmonic Mitigation

CHAPTER 3

System-Wide Harmonic Mitigation in a Diesel Electric Ship by Model Predictive Control

This chapter, which is based on the reformatted version of [218], proposes a system-oriented approach for mitigating harmonic distortions by utilizing a single Active Power Filter (APF) in an electrical grid with multiple buses. Common practice for control of APFs is to locally compensate the load current harmonics or to mitigate voltage harmonics at a single bus. However, the operation of an APF in a multi-bus system will influence the voltages at neighboring buses. It is therefore possible to optimize the APF operation from a system perspective instead of considering only conventional local filtering strategies. For such purposes, Model Predictive Control (MPC) is proposed in this work as a framework for generating APF current references that will minimize the harmonic distortions of the overall system within a given APF rating. A diesel-electric ship, with two buses supplying separate harmonic loads, with an APF located at one of the buses, is used as study case. The operation with on-line MPC-based optimization of the APF current references is compared to two benchmark methods based on conventional approaches for APF control. The results demonstrate that the MPC generates current references that better utilize the APF current capability for system-wide harmonic mitigation.

3.1 Introduction

Harmonics are any deviation from the pure sinusoidal voltage or current waveform typically generated by an ideal voltage source with linear loads [10]. In a diesel-electric ship power system, the main source of harmonics is usually the diode rectifier stages of Variable Frequency Drives (VFDs) for controlling the propulsion motors. A wide variety of VFDs are in use today depending on the power level, the pulse-number of the rectifiers and the system design, each of them generating different harmonic distortion levels [79, 94, 181].

Harmonic distortions in a power system can be mitigated by installing passive filter solutions (i.e. inductive and capacitive filters) that will reduce the impact of harmonic load currents on the rest of the system. For large nonlinear loads with known harmonic spectra, tuned harmonic filters for dominant low-order components are commonly applied [183, 232]. Such configurations can also include high-pass filters for mitigating a wider range of higher order harmonics. However, passive filters must be carefully designed to avoid resonances causing amplification of other harmonic components, especially when the installation is exposed to parameter variations or frequent changes in system configuration [262]. Furthermore, the amplitude of the harmonic current components generated by a diode rectifier will depend on the active power needed by the loads. Thus, a set of shunt-connected passive filters cannot be effectively adapted to the wide range of variations in propulsion loads on-board an electrical ship. Another alternative for passive harmonic mitigation is to apply series connected wide spectrum filters [79]. However, such filters must be installed in each of the propulsion loads, and will not mitigate harmonics generated by smaller VFD loads in the system.

High harmonic distortion levels in a system with dominant VFD loads can also be avoided by applying Active Rectifiers (ARs) instead of diode rectifiers. However, this solution is still more costly and has also higher losses than passive rectifiers. Another option to deal with harmonics without resorting to passive filters or diode rectifiers with high pulse numbers and complex multi-winding transformers for all VFD loads, is the use of Active Power Filters (APFs). The common practice in active filtering is to use the APF for local compensation by applying a current reference equal to the harmonic and reactive current components of the non-linear load [10]. However, when there are multiple non-linear loads distributed on multiple buses in a system, like in a marine vessel grid, minimizing the total harmonic distortion in the system will no longer be possible with the local filtering approach. In such grid configurations, with several and dispersed sources of harmonics, approaches for controlling APFs with the objective of system-wide harmonic mitigation represents an interesting option that has not yet been systematically pursued.

Optimization techniques can provide a general framework for generating optimal current reference waveforms for an APF with the objective of minimizing the overall total harmonic distortion (THD) in a system. Significant research efforts have recently been directed towards application of Model Predictive Control (MPC) to the local control of power electronic converters, including APFs [42, 93]. However, the potential for utilizing MPC in system-wide harmonic mitigation with an APF still remains to be exploited.

In this chapter, application of MPC is thoroughly investigated for system-wide harmonic conditioning with a shunt-connected Voltage Source Converter (VSC), controlled as an APF, based on the original idea presented in [220, 222, 224]. The previously presented studies on this topic were preliminary explorations of the capability of the MPC for minimizing the total harmonic voltage distortion (THD_V) in the load buses of a marine vessel power grid, based on simplified models with ideal current sources. Although the results in [220, 222, 224] indicated that APF current references generated by a system-wide MPC-based approach can improve the THD_V at the main buses compared to local filtering approaches, the impact of accurate load models and the implementation of the APF were not taken into account. A revised and improved closed-loop implementation of MPC for optimal harmonic mitigation is presented in this work, and demonstrated in a model of a marine vessel power grid implemented in MATLAB/Simulink with detailed models of VFD rectifiers and the APF. The APF performance with the proposed system-wide control approach is compared to the results with traditional local filtering and an ad-hoc solution proposed in [202]. The same trend as observed in the previous works is confirmed, with consistently improved system-level THD_V when the MPC approach is used to calculate the APF current references. Furthermore, the results highlight the advantages of the MPC compared to the solution from [202], namely the higher degree of freedom and flexibility, the ability to impose APF current saturation (constraints) and the ability to find an optimal current reference for an APF in a complex power grid with more than two buses.

3.2 Marine Vessel's Power Grid

Diesel-electric power generation and propulsion for marine vessels was commercialized and fully adopted by the offshore industry in the mid 1990s, with industry partners for power solutions at the helm. For an offshore operation vessel, the power demand, i.e. the vessel's power profile, is given by the vessel's momentarily assignment, e.g. transit, station keeping with Dynamic Positioning (DP) or anchor-handling. Diesel-electric vessels have introduced a flexibility of power generation when needed, compared to mechanical drive vessels where the prime mover is directly connected to the propeller via mechanical gears and long shafts. Therefore, diesel-electric operation has contributed to cultivating a *green environment* philosophy where the fuel consumption, and thus the exhaust emission, is in line with the power demand [181]. Diesel-electric power generation has also introduced advanced redundant power grid designs, e.g. ring bus designs, which satisfy requirements set by classification entities, such as ABS, Lloyd's Register and DNV GL [64]. This favors an increased number of installed generators with lower power ratings, facilitating a more *step-less* power generation compared to vessels with redundant mechanical drives.

The power grid under investigation in this work is based on a simplified equivalent of a marine Platform Supply Vessel (PSV) power system with two buses and two propulsion loads, operating with closed bus-tie breaker. The simplification is justified from the fact that these loads are typically responsible for the dominant part of the power consumption and the dominant harmonic distortions. A single-line diagram of the assumed power grid configuration is shown in Figure 3.1. In the investigated operating conditions, the vessel has only two generators in operation, one connected to each bus, *Bus 1* and *Bus 2*, respectively, since this is assumed to be the worst case for voltage distortions in the system. One propulsion motor supplied through a VFD is connected to each bus. The VFD has either a 6-pulse or a 12-pulse diode rectifier interfaced to the bus, and a voltage source inverter for controlling the motor driving the propeller. A transformer is included to provide galvanic isolation and for phase shifting in case of a 12-pulse rectifier. A series impedance is included between the two buses. Finally, the active filter is connected to bus 2 as seen in the Figure 3.1. Table 3.1 lists the most important details of the power grid under investigation, where the adopted pu base values are referred to the generator ratings.

The maximum allowed total harmonic distortion in a marine vessel's power system is regulated by classification entities. DNV GL follows IEC 61000-2-4 Class 2, which implies that the total harmonic voltage distortion (THD_V) shall not exceed 8% [63]. In addition, DNV GL requires that no single order harmonic voltage component shall exceed 5%. Similarly, Lloyd's Register requires that the THD_V at any ac switchboard or section board is below 8%

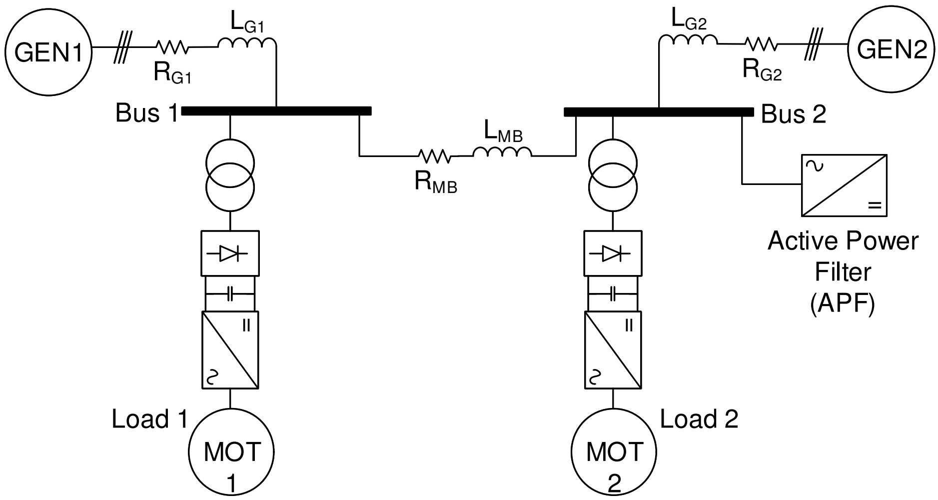

Figure 3.1: Simplified diagram of the power grid under investigation, including two generators, two loads and an active power filter.

Table 3.1: Power grid parameters, with generator rating as pu-base.

Parameter	Value		
L_{G1}	20% [pu]	**Generator 1**	1MVA
L_{G2}	20% [pu]	**Generator 2**	1MVA
L_{MB}	4% [pu]	**Motor 1**	1MVA
R_{G1}	$10\% \cdot L_{G1} \cdot \omega$ [pu]	**Motor 2**	1MVA
R_{G2}	$10\% \cdot L_{G2} \cdot \omega$ [pu]	**Active filter**	200kVA
R_{MB}	$10\% \cdot L_{MB} \cdot \omega$ [pu]	**Voltage (RMS)**	690V, 50Hz

(unless specified otherwise) of the fundamental, considering all frequencies up to 50 times the supply frequency. Within this requirement, no voltage component at a frequency above 25 times the supply frequency should exceed 1.5% of the fundamental of the supply voltage [150]. American Bureau of Shipping (ABS) recommends that the THD_V should not exceed 5%, as measured at any point of common coupling (PCC), with any individual harmonic voltage not exceeding 3% of the fundamental voltage value. The range of harmonics to be taken into account should be up to the 50th harmonic [6]. Bureau Veritas (BV) has similar rules and regulations [36]. However, the classification entities do not provide a clear set of requirements regarding total harmonic current distortion (THD_I) at any specific points, as harmonic current distortions do not propagate the power grid as easily as harmonic voltage distortions due to impedances in the system. Thus, this work will focus on harmonic voltage distortions at the main buses of the system, intending to comply with the classification requirements according to ABS.

3.3 Model Predictive Control

In this work, Model Predictive Control (MPC) is utilized to achieve optimal APF control for system-wide selective harmonic mitigation in a power grid, by generating APF current references optimized within the APFs current rating [220, 222, 224]. The main idea of MPC is to calculate the control action for a process/system using a (usually simplified) model to predict the system's future behavior. The model is initialized by measurements of the system's current state, and at each sampling interval the control action is obtained by solving online a constrained finite horizon optimal control problem [190]. The control action is extracted from the resulting finite control sequence yielded from the optimization and given to the system to close the control loop. Depending on the MPC's computational costs, there might be a non-negligible time delay between the initialization of the model and the resulting calculated control sequence, which must also be taken into account in the implementation.

The MPC's accuracy and computational costs are dependent on the model of the system and the availability and accuracy of real-time measurements. To model a system perfectly is in most cases an impossible task. In addition, modelling all dynamics, if possible, usually result in a large and complex model with high computational costs, that often requires more measurements. Therefore, a compromise between accuracy and computational costs must be made when designing MPC schemes. In general, the model applied for MPC should be as simple as possible while containing all dynamics needed to satisfy the control objective within the control horizon and the level of discretization. The horizon's length is dependent on the control objective, and the level of discretization should be chosen with respect to the fastest dynamics that should be controlled. A thorough overview of dependable embedded MPCs is given in [132].

In the literature it has been reported MPC implementations with good real-time properties [89, 148, 263], and some research has also been conducted to explore the use of optimization and MPC in the field of electrical engineering [90, 93, 146]. The MPC formulation described in this section is based on the models and approaches from [220, 222] and [224]. However, the implementation and the formulation of the objective function are further improved to benefit from the MPC's flexibility in the search for the optimal filter current injection. In the following, the power grid model and the active filter constraints used in the development of the MPC are discussed before the MPC formulation is presented on standardized form.

3.3.1 Power Grid Model

As mentioned, MPC depends on a model of the system for calculating the optimal control actions. The main 690V busbars and loads in diesel-electric ships are usually three-phase three-wire systems. Thus, there will be no path for zero-sequence currents and the system could be modelled in the $\alpha\beta$ frame (by using the Clarke transform) while ignoring zero sequence components [10]. This would imply a reduced dimension of the problem formulation for the MPC compared to modelling in the *abc* frame, and could be beneficial for reducing computational costs (for real-time implementation). However, representation in the $\alpha\beta$ frame implies that the current limit of the APF in the α-axis will depend on the current in the β-axis and vice versa. Since functionality for such limitations are not included in the MPC software used in this work, the MPC formulation will be based on the *abc* frame. In the following, subscript a, b and c are used to denote the *abc* phases of each voltage and current component. The vectors $\mathbf{v}$ and $\mathbf{i}$ are used to represent the voltages and currents, respectively, given in the *abc* frame.

Figure 3.2 shows a simplified power grid model approximating the marine vessel's power grid discussed in section 3.2, with parameters adopted from Table 3.1. The shunt capacitors indicated in the figure are included to decouple the states representing currents in the inductances, but can also be considered as an equivalent representation of the cable and busbar capacitances. The capacitor voltage states will represent the busbar voltages used for assessing the THD_V in the system.

In this work, a simplified generator model with fixed voltage amplitude behind an impedance is used for the modelling and simulations. The per unit generator impedance is selected to be within the normal range for sub-

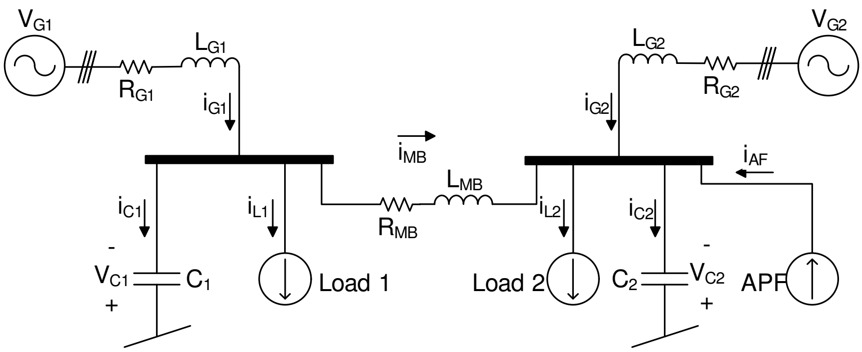

Figure 3.2: Simplified power grid model used to design the MPC for harmonic mitigation.

transient reactances of synchronous machines, according to [55]. A constant fundamental frequency model is also assumed, i.e. $\omega := 2\pi f(t) = 2\pi f$ where f is the nominal fundamental frequency. In reality, the frequency of a ship power system will not be constant and the synchronous generators will have voltage controller dynamics as well as small internal voltage distortions due to the physical construction. However, the applied simplified model can be considered sufficient to demonstrate the steady state system-wide optimization achieved with the MPC without depending on simulations with large mechanical and electromechanical time constants. The MPC is also partly able to reject un-modelled disturbances since the internal system model will be continuously updated through closed-loop feedback. Furthermore, the MPC can easily handle frequency variations as long as the harmonic analysis in the control system is frequency-adaptive. If necessary, a simple dynamic frequency model, can also be embedded in the MPC, as proposed in [222].

Assuming 6-pulse rectifiers are part of the marine vessel's propulsion system, the loads will introduce non-linear conditions drawing harmonic current of order 5, 7, 11, 13, etc. from the generators [10]. Hence, the load model used in the MPC can be modeled as ideal current sources,

$$\mathbf{i}_L(t) = \begin{bmatrix} i_{L,a}(t) \\ i_{L,b}(t) \\ i_{L,c}(t) \end{bmatrix} = \begin{bmatrix} \sum_i I_{L,i} \sin\left(i\left(\omega t + \phi_{L,i}\right)\right) \\ \sum_i I_{L,i} \sin\left(i\left(\omega t + \phi_{L,i} - \frac{2\pi}{3}\right)\right) \\ \sum_i I_{L,i} \sin\left(i\left(\omega t + \phi_{L,i} + \frac{2\pi}{3}\right)\right) \end{bmatrix}, \quad \forall i \in \{6k \pm 1 | k = 1, 2, \ldots\}, \tag{3.1}$$

which includes the assumed harmonic components, i, to be mitigated, with phase shifts $\phi_{L,i}$ and amplitudes $I_{L,i}$. Note that the load model, (3.1), does not include the fundamental current components. If the marine vessel's power grid includes elements that generate other dominant harmonic components, the load models and the harmonics to be mitigated by the MPC can be changed accordingly.

The APF in Figure 3.2 should be controlled to suppress the harmonic content of the generator currents in order to minimize the voltage harmonics at the main buses. The APF currents in all three phases, $i_{AF,a}$, $i_{AF,b}$ and $i_{AF,c}$, are kept as free variables and are optimally calculated by the MPC. This decision gives total authority to the MPC, allowing the MPC to phase shift and alter the different harmonic components of the filter currents in any possible way to achieve the best possible harmonic mitigation. This is an important property when the APF is reaching its peak current limits.

The power grid's dynamics can be derived using Kirchhoff's laws and be stated as

$$L_{G1}\frac{d\mathbf{i}_{G1}}{dt} = -R_{G1}\mathbf{i}_{G1} - \mathbf{v}_{C1} \tag{3.2a}$$

$$C_1\frac{d\mathbf{v}_{C1}}{dt} = \mathbf{i}_{G1} - \mathbf{i}_{MB} - \mathbf{i}_{L1} \tag{3.2b}$$

$$L_{MB}\frac{d\mathbf{i}_{MB}}{dt} = \mathbf{v}_{C1} - \mathbf{v}_{C2} - R_{MB}\mathbf{i}_{MB} \tag{3.2c}$$

$$C_2\frac{d\mathbf{v}_{C2}}{dt} = \mathbf{i}_{MB} + \mathbf{i}_{G2} - \mathbf{i}_{L2} + \mathbf{i}_{AF} \tag{3.2d}$$

$$L_{G2}\frac{d\mathbf{i}_{G2}}{dt} = -R_{G2}\mathbf{i}_{G2} - \mathbf{v}_{C2}. \tag{3.2e}$$

As seen from these equations, the bus voltages are provided in the model by the capacitances, and the differences between the two bus voltages determine the current flowing in the main bus impedance ($\mathbf{i}_{MB}$). For the MPC implementation, (3.2) does not include the fundamental components since the MPC only regards harmonic components. It should also be mentioned that potential voltage distortions originating from the generators or from other components in the systems that are difficult to measure, will affect the harmonic generator currents. Thus, the MPC will indirectly attenuate the effect of such disturbances since they will be contained by the feedback signals used to initialize the internal model of the MPC.

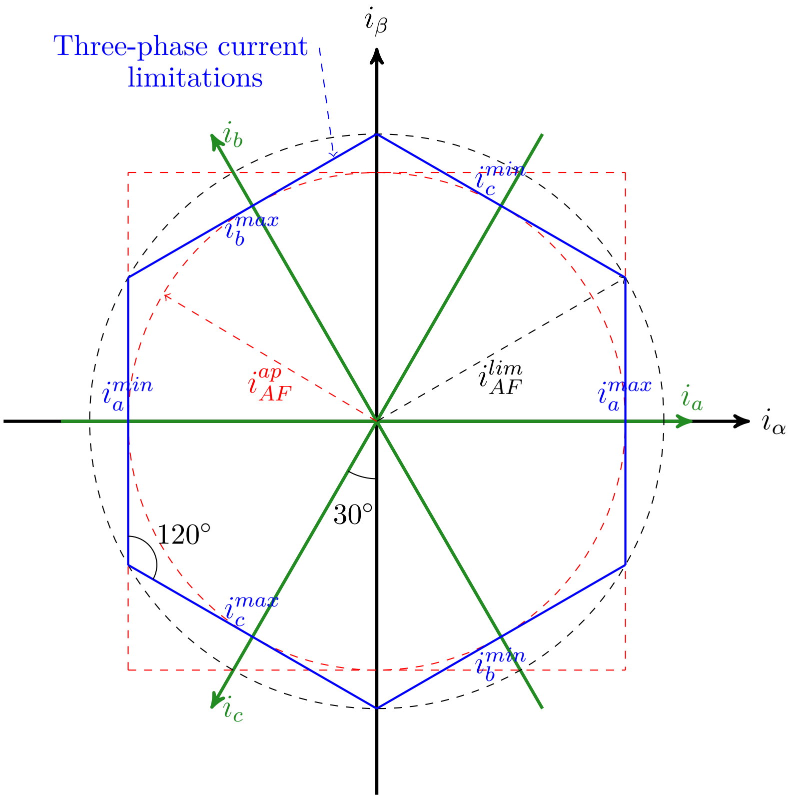

Figure 3.3: Active power filter constraints: Three-phase three-wire system represented in the $\alpha\beta$ and *abc* frames [237].

3.3.2 Active Power Filter Constraints

The APF's current and voltage limits are determined by its physical components. In general, the semiconductor devices, usually IGBT modules containing anti-parallel diodes, determine the current rating, while the voltage rating of the dc-side capacitor limits the maximum voltage available to inject current harmonics into the grid. The current limitations will be the same for all three phases, as illustrated in the *abc* frame by the blue hexagon in Figure 3.3 [237]. These limits should be included in the MPC formulation to avoid unwanted effects from saturation of filter current references (i.e. current clipping). Inclusion of the current limits in the MPC will also ensure that the utilization of the current capability will be optimized. By this, the

MPC will be able to optimally calculate APF currents close to the APF's limits without saturation effects impairing the harmonic conditioning.

The current constraints given by the hexagon in Figure 3.3 can be formulated in the *abc* frame as

$$i^{min} \leq i_j \leq i^{max}, \quad \forall j \in \{a, b, c\}, \tag{3.3}$$

where $i^{min} = -i^{max}$. The constraints given in $\alpha\beta$ form can be found in [220, 222, 224].

As mentioned, the MPC model could be developed in the $\alpha\beta$ frame for a more effective implementation of the system model. However, the implementation of the current constrains are more complicated in the $\alpha\beta$ frame. Therefore, it is preferred in this case to implement the MPC in the *abc* frame.

3.3.3 Formulating the MPC on Standard Form

With the formulation of the model and the APF's constraints, which was discussed in section 3.3.1 and 3.3.2, the MPC at time t with a control horizon of length T can be written on standard form as

$$\begin{aligned} \min_{\mathbf{x}(t),\mathbf{z}(t),\mathbf{u}(t)} \quad & V(\mathbf{x}(t),\mathbf{z}(t),\mathbf{u}(t)) = \\ & \int_{t_0}^{t_0+T} l\left(\mathbf{x}(t),\mathbf{z}(t),\mathbf{u}(t)\right) dt \\ \text{s.t.} \quad & \\ & \dot{\mathbf{x}}(t) = \mathbf{f}\left(\mathbf{x}(t),\mathbf{z}(t),\mathbf{u}(t)\right), \\ & \mathbf{g}\left(\mathbf{x}(t),\mathbf{z}(t),\mathbf{u}(t)\right) = 0, \\ & \mathbf{h}\left(\mathbf{x}(t),\mathbf{z}(t),\mathbf{u}(t)\right) \leq 0, \\ & \forall t \in [t_0, t_0 + T], \end{aligned} \tag{3.4}$$

where $V(\cdot)$ is the objective function defining the objective of the optimization, $l(\cdot)$ is the stage cost function and $\mathbf{f}(\cdot)$ represents the power grid's dynamics given by (3.2). $\mathbf{g}(\cdot)$ represents the MPC's equality constraints, in which includes algebraic equations such as the load models given by (3.1). $\mathbf{h}(\cdot)$ represents the MPC's inequality constraints, which includes the filter's current limits given by (3.3). The dynamic state vector, $\mathbf{x}$, is given by the power grid's dynamic equations, and by omitting the time notation (t), it can be stated as

$$\mathbf{x} = \left[\mathbf{i}_{G1}^\top, \mathbf{i}_{G2}^\top, \mathbf{i}_{MB}^\top, \mathbf{v}_{C1}^\top, \mathbf{v}_{C2}^\top\right]^\top, \tag{3.5}$$

where $\mathbf{i}_{G1}$ and $\mathbf{i}_{G2}$ are the harmonic generator (source) currents to be compensated, $\mathbf{i}_{MB}$ is the main bus current and $\mathbf{v}_{C1}$ and $\mathbf{v}_{C2}$ are the bus voltages in Figure 3.2. The load currents $\mathbf{i}_{L1}$ and $\mathbf{i}_{L2}$ can be expressed by the algebraic state vector $\mathbf{z}$,

$$\mathbf{z} = \left[\mathbf{i}_{L1}^\top, \mathbf{i}_{L2}^\top\right]^\top. \tag{3.6}$$

The control vector, $\mathbf{u}$, which consists of the filter currents, is given by

$$\mathbf{u} = \mathbf{i}_{AF} = \left[i_{AF,a}, i_{AF,b}, i_{AF,c}\right]^\top. \tag{3.7}$$

One should note that (3.2) can be written on state space form, i.e.

$$\begin{aligned} \dot{\mathbf{x}} &= \mathbf{A}\mathbf{x} + \mathbf{B}\mathbf{u} + \mathbf{E}\mathbf{z}, \\ \mathbf{y} &= \mathbf{C}\mathbf{x}, \end{aligned} \tag{3.8}$$

with $\mathbf{x}$, $\mathbf{z}$, and $\mathbf{u}$ as given above. $\mathbf{z}$, which contains the harmonic load current models, can be considered a disturbance vector. With this state space formulation, the linear function $\mathbf{f}(\cdot)$ in (3.4) can be written as $\mathbf{f}(\cdot) = \mathbf{A}\mathbf{x}+\mathbf{B}\mathbf{u}+\mathbf{E}\mathbf{z}$. Even though both the function $\mathbf{f}(\cdot)$ and $\mathbf{h}(\cdot)$ in (3.4) are linear, the function $\mathbf{g}(\cdot)$, which contains the equality constraints, is non-linear due to the non-linear harmonic load current models (algebraic states implemented as equality constraints). Hence, already from this consideration, the MPC is non-linear.

The objective of the MPC is to conduct selective harmonic mitigation in the power grid. Harmonic pollution may induce vibrations and torque changes in the generator shafts, depending on the generators' inductance. To reduce wear and tear on the generators, the harmonics in the generator currents (source currents $\mathbf{i}_{G1}$ and $\mathbf{i}_{G2}$) should be compensated. A convex stage cost function which addresses the harmonic pollution in the generator currents can be stated as

$$\begin{aligned} l\left(\mathbf{x},\mathbf{z},\mathbf{u}\right) = & \, \mathbf{i}_{G1}^{\top}\mathbf{Q}_1\mathbf{i}_{G1} \\ & + \mathbf{i}_{G2}^{\top}\mathbf{Q}_2\mathbf{i}_{G2} \\ & + (\mathbf{i}_{AF,a}+\mathbf{i}_{AF,b}+\mathbf{i}_{AF,c})^{\top}\mathbf{Q}_{abc}(\mathbf{i}_{AF,a}+\mathbf{i}_{AF,b}+\mathbf{i}_{AF,c}) \\ & + \mathbf{u}^{\top}\mathbf{Q}_u\mathbf{u}, \end{aligned} \tag{3.9}$$

with diagonal weight matrices given by

$$\begin{aligned} \mathbf{Q}_1 &= \mathrm{diag}([q_1,q_1,q_1]),\ \mathbf{Q}_2 = \mathrm{diag}([q_2,q_2,q_2]), \\ \mathbf{Q}_u &= \mathrm{diag}([q_u,q_u,q_u]),\ \mathbf{Q}_{abc} = \mathrm{diag}([q_{abc},q_{abc},q_{abc}]). \end{aligned} \tag{3.10}$$

The last part in (3.9) is added to punish utilization of large filter currents (amplitudes), which will make it easier for the MPC to use phase shifting in the search of the optimal harmonic mitigation [220]. The third part is added to avoid solutions that relies on zero-sequence filter currents. Because punishment of large filter currents is of lesser importance than minimization of the harmonic pollution and avoiding optimal solutions that rely on zero-sequence filter currents, the weights should be selected so that $q_{abc} > q_1, q_2 > q_u$. Since the load model in (3.1) as used by the MPC does not include the fundamental components, the objective is to minimize the source current, where perfect harmonic cancellation would yield $\mathbf{i}_{G1} = \mathbf{i}_{G2} = \mathbf{0}^{3\times1}$.

The weighting of the harmonics from the different buses, q_1 and q_2, could be modified to also include a weighting relative the amount of harmonics originating from each load, i.e.

$$\begin{aligned} q_1 &= k_1 \cdot \sum_i I_{L1,i} \\ q_2 &= k_2 \cdot \sum_i I_{L2,i}, \end{aligned} \tag{3.11}$$

where k_1 and k_2 are weighting constants and i are the harmonics to be mitigated. In this way, the MPC could be designed for prioritizing harmonic mitigation on the most polluted bus, or according to any other criteria suitable for a specific system. However, further discussions or analysis of such possibilities are outside the scope of this work.

3.4 Implementation

With references to section 3.2 and section 3.3, where the power grid and the MPC formulation were presented, respectively, the implementation of the simulation environment will be discussed in this section. Before discussing the closed-loop interaction between the MPC and the power grid, the power grid simulation model and the MPC implementation are separately addressed.

3.4.1 Power Grid Implementation

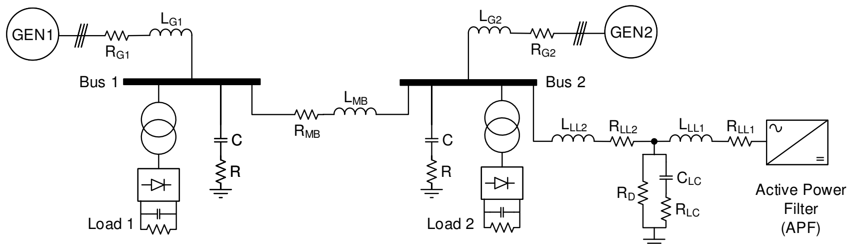

Figure 3.4: Power grid implementation in MATLAB/Simulink, with parameters given in Table 3.1 and Table 3.2.

The power grid, which was presented in Figure 3.1 with properties given in Table 3.1, is implemented in MATLAB/Simulink using the SimPowerSystems library. For ensuring fast and robust current reference tracking in a simple way, the APF control is based on a traditional phase current hysteresis controller [33, 137]. The hysteresis band is in this case set to 0.15 [pu] (relative the APF's rating), and the resulting average switching frequency is approximately 17.5kHz. The active filter's DC link voltage reference is set to approximately 1240V ($1.1 \cdot 2 \cdot \frac{\sqrt{2}}{\sqrt{3}} \cdot 690V$), and a PI controller is used to control the DC link toward its reference [10]. An LCL filter with passive damping is inserted between the active filter and bus 2 to suppress switching noise from the active filter. To avoid unrealistic high frequency oscillations in the system, the parasitic bus capacitances are modelled as shunt RC elements placed on each side of the bus-tie connection. An illustration of the power grid implementation is given in Figure 3.4, with the most important parameters listed in Table 3.1 and Table 3.2.

3.4.2 MPC Implementation

The MPC formulation addressed in this work is implemented using the software environment ACADO (Automatic Control and Dynamic Optimization) [116], which is a higher-level toolkit than the CasADi framework [14] used

Table 3.2: Power grid implementation details.

Parameter	Value
AF DC link	1240V
AF DC capacitor	236μF
AF hysteresis frequency	$\approx$ 17.5kHz
AF hysteresis band	0.15 [pu] (relative APF rating)
Shunt RC	$R = 2\Omega$, $C = 1\mu$F
LCL filter	$L_{LL1} = L_{LL2} = 0.4$mH,
	$R_{LL1} = R_{LL2} = 0.02\Omega$,
	$C_{LC} = 40\mu$F, $R_D = 120\Omega$, $R_{LC} = 10\Omega$

in [220, 222, 224]. Using ACADO, the MPC formulations are implemented in standard form, and the toolkit builds the MPC using user-specified shooting techniques, e.g. single shooting, multiple shooting or collocation [22], and solvers such as qpOASES [81]. The ACADO toolkit also provides a code-generation tool for generating efficient MPC-implementations in C and MATLAB [117]. The main reason why ACADO is used in this work to realize the MPC is the toolkit's fast prototyping properties and the code-generation feature, which can generate an efficient MATLAB implementation of the MPC and make the integration with the power-grid implementation in MATLAB/Simulink less cumbersome. The main details of the MPC implementation are listed in Table 3.3.

Table 3.3: MPC implementation details.

Parameter	Value
Time horizon T	12.5ms
Discretization N	220
Discretization type	Multiple Shooting
Integrator	Runge-Kutta 4 (RK4)
Hessian Approximation ($\nabla^2_{\mathbf{x}}\mathbf{f}(\cdot)$)	Exact Hessian
Solver	qpOASES
Number of iterations	5
Stage cost weights	$q_1 = q_2 = 1000$,
	$q_u = 1$, $q_{abc} = 0$
AF current limit	$i^{ap}_{AF} = 1[pu]$ (of APF rating)

As indicated in Table 3.3, the MPC's optimization horizon is set to 12.5ms, which is slightly longer than half a period for the fundamental frequency of 50Hz. Even though the fundamental period is 20ms, the MPC is set to run every 10th ms to achieve a faster closed-loop feedback and be able to correct for model/process mismatches. Thus, only the first 10ms of the MPC's resulting control horizon will be used to provide an optimal APF current reference. The additional 2.5ms are included to keep future changes in account, and provide an overlap between the control horizons. This is an important property for achieving continuous optimality between each MPC cycle [190].

The filter currents in the MPC model are kept as free variables, as was described in section 3.3.1, giving the MPC full flexibility and authority when searching for the optimal harmonic mitigation. Hence, the quality of the harmonic mitigation is dependent on the MPC's discretization. In addition, the level of discretization has significant influence on the MPC's real-time properties. However, details regarding real-time implementation of the MPC on suitable industrial control platforms is outside the scope of this study. In the following, the discretization is chosen to be 220 samples for each 12.5ms, which gives a discretization step-size that allows for reasonably accurate analysis up to about the 37th harmonics.

3.4.3 Closing the Control Loop

Using the MPC and the power grid model, a closed loop APF control for system-wide harmonic mitigation can be obtained. A block diagram illustrating the simulated system is given in Figure 3.5. Instantaneous measurements are used to initialize the MPC's internal model before each new cycle. The **FFT** (moving horizon) block is used to extract measurements, i.e. amplitudes and phase angles, from the load currents, originating from the **Power Grid** block. The output from the **FFT** block and the instantaneous measurements are sampled with the same clock signal as the rest of the system in the **Sample & Hold** block, which synchronizes the measurements with the MPC. The output from the **MPC** block is discrete filter currents (vectors) in the *abc* frame. These vectors are sent to the **Evaluation** block which ensures that the filter currents are within the APF's constraints. As filter current references containing zero-sequence components cannot be tracked by the APF, any zero-sequence components are removed from the current references before they are provided to the APF's hyster-

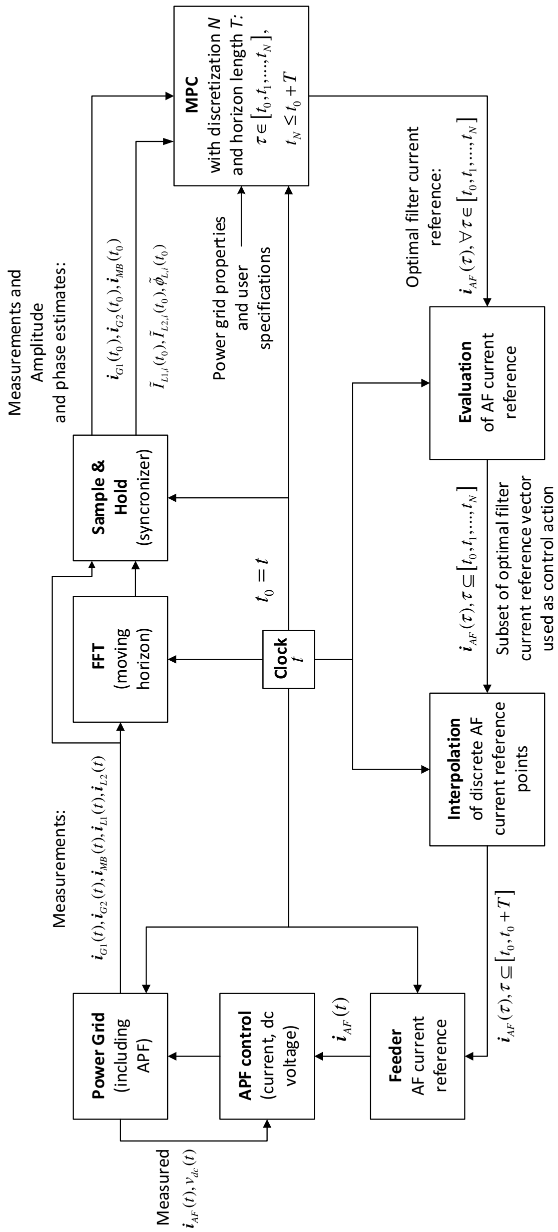

Figure 3.5: Functional overview of the closed-loop implementation in MATLAB/Simulink.

esis controllers. As an alternative to use the zero-sequence penalty in the MPC's objective function, which was given as the third term of (3.9), the **Evaluation** block is equipped with additional functionality that transforms the filter current references to the $\alpha\beta 0$ frame, where the zero-sequence current components are removed. The APF's constraints, which were shown in Figure 3.3, are imposed before transforming the resulting filter current references back to *abc* form. Since zero-sequence current components are equal for all three-phase [10], the elimination of zero-sequence currents will not destroy the optimality of the filter current reference calculated by the MPC.

Table 3.4: Closed Loop implementation details.

Parameter	**Value**
MPC cycle	100Hz
Power grid simulation step-size	2μs

After evaluating the filter currents, the **Evaluation** block extracts a subset of the filter currents to be used. The length of the extracted subset is relative the MPC's run cycle. The subset of the filter current vector is then sent to the **Interpolation** block, which interpolates the points in the filter current vectors to get the same discretization as used in the simulation environment. The resulting filter current vectors are sent to the **Feeder** block, which feeds the **APF control** block with one point (one for each phase) at the time. The **APF control** block includes the local control loops used to operate the APF in the power grid, including phase current hysteresis controllers and a dc-voltage PI controller providing the fundamental frequency active current reference. A global clock is used in the simulation to synchronize all time dependent blocks, including the electrical system. The MPC's run cycle and the simulation step-size are given in Table 3.4.

3.5 Results

To validate the selective harmonic conditioning using the MPC formulation discussed in section 3.3, two methods for active filter current reference generation are applied as benchmark cases:

- BM1: $\mathbf{i}_{AF} = \mathbf{i}_{L2}^{h}$
- BM2: $\mathbf{i}_{AF} = \mathbf{i}_{L1}^{h} + \mathbf{i}_{L2}^{h}$,

where $\mathbf{i}_{L1}^{h}$ and $\mathbf{i}_{L2}^{h}$ are the selected harmonic currents from load 1 and load 2 in the *abc* frame, respectively, to be suppressed by the active filter. As can be seen, BM1, which is named *local filtering* in [220, 222, 224], only considers the load connected to the same bus as the APF. This approach is considered as a standard strategy for harmonic mitigation. The second benchmark case, BM2, is an ad-hoc method for harmonic mitigation in a two-bus system proposed in [202]. This approach attempts to mitigate the harmonics in the system by using the sum of the harmonic content from both loads as the current reference for the APF. Thus, the grid impedances are not considered, and this approach will only obtain a direct compensation of the load harmonics if the bus impedance is zero. It should be noted that this approach is not established or commonly applied for APF control in multi-bus systems but it is included as a reference case for providing a more fair basis of comparison for the MPC than what is achieved with BM1.

Three different study cases are simulated for the two benchmark models and the proposed MPC:

1. **Bus 1:** 6-pulse rectifier load. **Bus 2:** 6-pulse rectifier load. The loads have equal power demand.
2. **Bus 1:** 12-pulse rectifier load. **Bus 2:** 6-pulse rectifier load. The load at bus 1 has higher power demand than the load at bus 2.
3. **Bus 1:** 12-pulse rectifier load in parallel to a single-phase rectifier load. **Bus 2:** 6-pulse rectifier load. The aggregated loads at bus 1 has higher power demand than the load at bus 2.

The configuration of the power grid used in the simulations was given in Table 3.1, and the harmonic components to be mitigated are the 5th, 7th, 11th and 13th. The 5th and 7th harmonic components will be the dominant harmonics in a load with a 6-pulse rectifier while the 11th and 13th harmonic components are dominant in a load consisting of a 12-pulse rectifier. The filter current limits for harmonic current injection are set to 1 [pu] in all phases (referred to the APF rating), as mentioned in Table 3.3. For each case the resulting THD_V values averaged for all three phases of each bus and key information about the system configuration are summarized in tables, and two figures are presented: The first two plots in the first figure showing the filter output current (measured after the LCL filter) and its reference, while the two last plots show the resulting generator currents. All results are plotted only for phase a. The second figure shows the frequency spectra of the bus voltages and generator currents for phase a up to the 50th harmonic - all harmonics given in percentage of the fundamental component. The results from each case are discussed in the following.

3.5.1 Study Case 1

The first study case is a scenario where both loads are equal, both with 6-pulse rectifiers, and connected to the grid. As shown in Table 3.5, the power demands from each load are set to 5% of their power ratings. As expected, the THD_Vs presented in Table 3.5 for BM1 and BM2 are not equal as BM1 only considers harmonic mitigation for bus 2 while BM2 considers both buses. As BM1 only considers the local load connected to bus 2, harmonic currents from load 1 will be unsuppressed and flow through the grid, from one bus to the other, resulting in higher THD_Vs than BM2 and the MPC. BM2 is in this case better than BM1 due to its consideration of the selected harmonics to be suppressed from both loads. However, due to the lack of information of the power grid's configuration, BM2 is not able to match the THD_Vs resulting from the optimal harmonic mitigation using the MPC. The reason why can be seen from the two upper plots in Figure 3.6a, where the APF current with MPC is slightly phase shifted and has a slightly lower amplitude compared to the APF current with BM2. This is mainly because the MPC is explicitly considering the impedances in the system. The resulting APF current from BM1 has lower harmonic amplitudes compared to the MPC and BM2, since it is only compensating for the harmonic currents generated by load 1.

Table 3.5: Study case 1: Configuration and resulting THD_V.

	MPC	BM1	BM2
THD V_{L1}	1.4%	2.9%	1.6%
THD V_{L2}	1.4%	2.6%	1.8%
Load 1 element	6-pulse		
Load 2 element	6-pulse		
Power load 1	0.05 [pu]		
Power load 2	0.05 [pu]		

The two lower plots in Figure 3.6a show the generator currents with har-

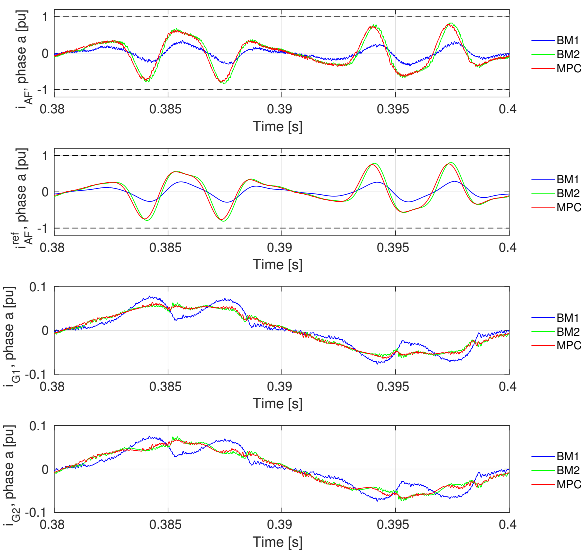

(a) Filter and generator currents.

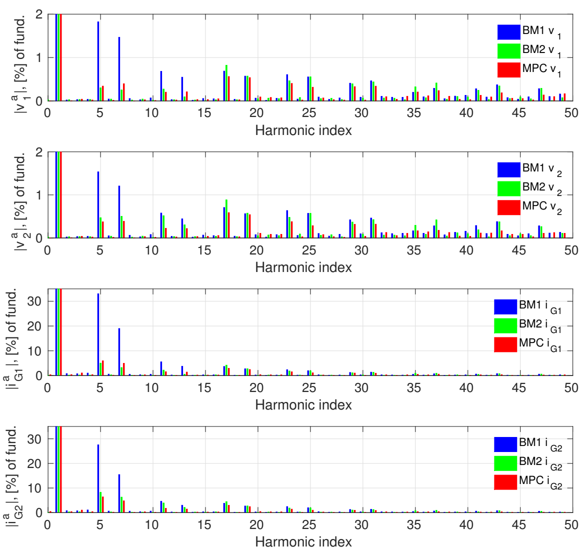

(b) Load voltage and generator current frequency spectra.

Figure 3.6: Study case 1: Two loads with 6-pulse rectifiers and equal power demand, one load connected to each bus.

monic conditioning according to all three methods. As shown, the generator currents are quite similar for BM2 and the MPC, while they are significantly more distorted with BM1. This is as expected, since the BM1 is not compensating for the harmonic load currents at bus 1.

The two upper plots in Figure 3.6b show the frequency spectra of the bus voltages while the two lower plots show the frequency spectra of the generator currents up to the 50th harmonic component. For the bus 1 voltage, the MPC is better than BM1 for almost all the harmonics. Compared to BM2, the MPC gives a slightly higher magnitude for the 5th, 7th and 13th harmonic, however, results in lower magnitudes for all other dominating harmonic components. This is due to the fact that the MPC penalizes filter currents which introduce harmonics that is not part of the harmonic suppression in the grid. This can be seen from (3.9), where all filter currents corresponding to non-zero generator harmonics are penalized. For the bus 2 voltage the MPC seems to result in lower magnitudes than BM1 and BM2 for all dominating harmonic components. As evident, BM1 has the highest magnitudes in both voltage spectra, indicating higher THD_V than both the MPC and BM2. As the load demands from both loads are quite small, the THD_I is quite high for the generator currents, which can be observed from the two lower plots in Figure 3.6b.

3.5.2 Study Case 2

The second study case is a scenario where load 1 has a 12-pulse diode rectifier and load 2 has a 6-pulse rectifier. The power demand from load 1 is set higher than the power demand from load 2, as indicated in Table 3.6, with power demands of 80% and 30% of rated load, respectively. The THD_Vs presented in Table 3.6 show that also in this case the BM2 is providing superior performance compared to BM1, since the harmonic components in load 1 have significant impact on the bus voltages. However, the MPC is able to improve the harmonic mitigation beyond what is achievable with BM2, further decreasing the THD_Vs at both buses. It can be noticed that in this case BM1 violates the ABS classification requirement of THD_V below 5%, and the individual harmonic limits are also exceeded for the 11th and the 13th harmonic voltage components at bus 1, see Figure 3.7b.

As in the previous case, the filter current resulting from BM1 deviates from BM2 and the MPC due to the local filtering approach, which can be seen

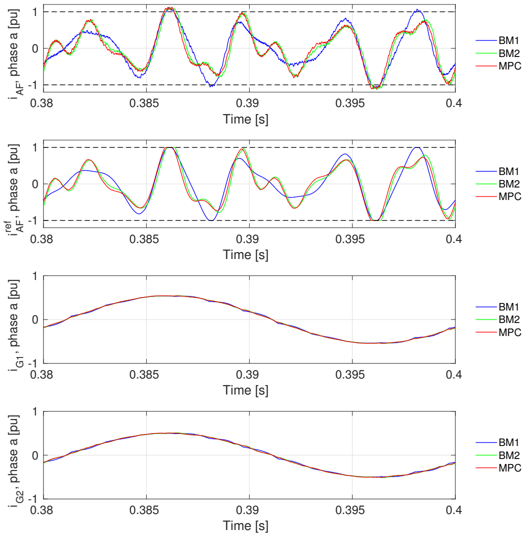

(a) Filter and generator currents.

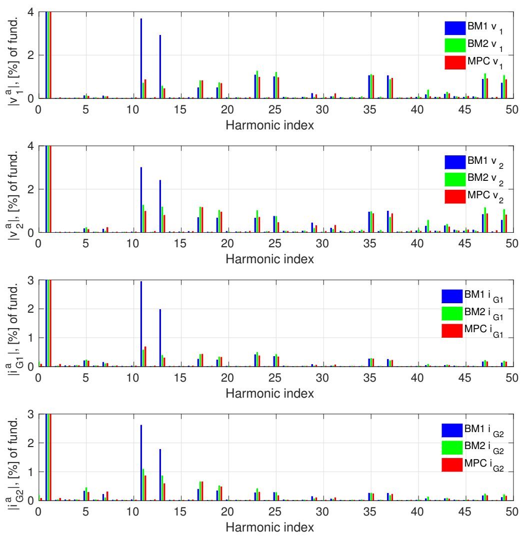

(b) Load voltage and generator current frequency spectra.

Figure 3.7: Study case 2: One load with a 12-pulse rectifier connected to bus 1 and one load with a 6-pulse rectifier connected to bus 2. The power demand from load 1 is higher than the power demand from load 2.

Table 3.6: Study case 2: Configuration and resulting THD_V.

	MPC	**BM1**	**BM2**
THD $\mathbf{V}_{L1}$	2.8%	5.3%	3.1%
THD $\mathbf{V}_{L2}$	2.8%	4.5%	3.4%
Load 1 element	12-pulse		
Load 2 element	6-pulse		
Power load 1	0.8 [pu]		
Power load 2	0.3 [pu]		

from Figure 3.7a. The difference between the filter currents from BM2 and the MPC is also in this case given by a small phase shift and a small difference in amplitude. From the two upper plots in Figure 3.7b it is seen that the MPC has lower magnitudes for all dominating harmonic components in the bus 1 voltage compared to BM2, except the 11th and 37th harmonic components. Hence, the MPC compromises and scarifies the 11th harmonic component in the bus 1 voltage to decrease the THD_V in bus 2 beyond the abilities of BM2. This is seen in the spectra for the bus 2 voltage, where the magnitude of almost all dominating harmonic components are lower for the MPC compared to BM2.

The spectra for the generator currents in the lower two plots in Figure 3.7b show some of the same behavior, resulting in lower THD_Is for both generator currents when using the MPC for harmonic mitigation compared to BM1 and BM2.

3.5.3 Study Case 3

The third study case illustrates the performance of the three different harmonic mitigation approaches with an additional aggregation of single-phase loads on bus 1, resulting in unbalanced conditions. The power demands from bus 1 are 80% for the three-phase 12-pulse load and in total 10% for aggregated single-phase diode rectifier loads (phase a and b). This results in a load current unbalance of about 6% on bus 1. The power demand from the three-phase 6-pulse load in bus 2 is 25%. The resulting THD_Vs for the three different harmonic mitigation methods are given in Table 3.7, and also in this case there are clear distinctions between the methods. As in the previous study cases the MPC conducts the best harmonic mitigation while BM1 conducts the worst. Evidently, BM1 violates also in this case the classification requirement of THD_V below 5%.

Table 3.7: Study case 3: Configuration and resulting THD_V.

	MPC	**BM1**	**BM2**
THD V$_{L1}$	3.9%	6.0%	4.2%
THD V$_{L2}$	3.5%	5.0%	4.0%
Load 1 element	12-pulse + single-phase 2-pulse		
Load 2 element	6-pulse		
Power load 1	0.8 [pu] + 0.1 [pu]		
Power load 2	0.25 [pu]		

Compared to the previous study cases, the difference between the APF reference currents generated by the three methods are now easier to recognize, as illustrated in the two upper plots in Figure 3.8a. Differences between the three APF reference currents in both phase angles and amplitudes are easily recognized from the plot, indicating different results from the harmonic mitigation, which is supported by the resulting THD_Vs in Table 3.7.

The frequency spectra in Figure 3.8b show the presence of zero-sequence harmonics, e.g. 3rd and 9th, which is a result of the unbalanced conditions caused by the single-phase diode rectifier load connected to bus 1. From the spectra of bus voltage 1, the MPC results in lower magnitudes compared to BM2 for all dominating harmonic components, except for the 5th and 11th component. Also from the spectra of bus voltage 2, the MPC has lower dominating harmonic magnitudes than BM2, except for the 5th harmonic component. From both voltage spectra it is easy to see that BM1 results in the worst harmonic mitigation, where the 11th and 13th components are major contributors to the increased THD_V compared to the MPC and BM2. Also in this case the 3% single harmonic voltage limit set by some of the classification entities is violated by BM1.

The results in this section indicate that the use of MPC can provide better system-level harmonic mitigation than both BM1 and BM2. The results also demonstrate that BM2, which is used in this work as a reference for comparison, is not an optimal solution, especially when there is non-negligible impedances between the buses in the system and when the APF current saturation is reached. Furthermore, the results demonstrate that the MPC can achieve better utilization of an APF within its current limitations.

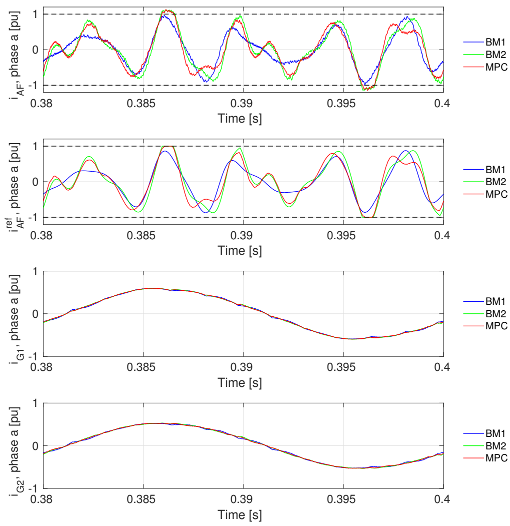

(a) Filter and generator currents.

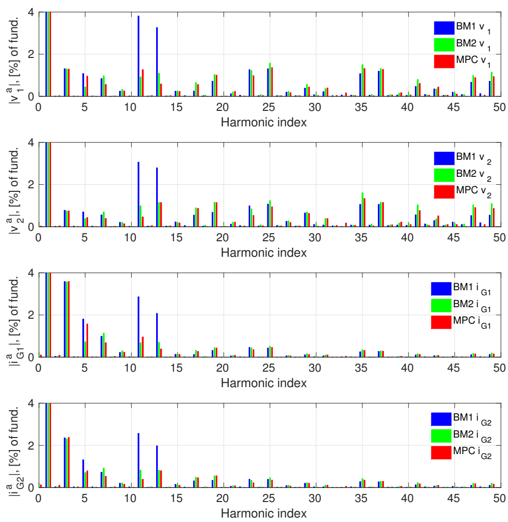

(b) Load voltage and generator current frequency spectra.

Figure 3.8: Study case 3: A three-phase load with a 12-pulse rectifier and a single-phase load with a 2-pulse rectifier connected to bus 1. One three-phase load with a 6-pulse rectifier connected to bus 2. The aggregated power demand from load 1 is higher than the power demand from load 2.

3.6 Conclusion

An approach for system-wide harmonic mitigation using Model Predictive Control (MPC) to generate the current reference for an active power filter (APF) has been presented and implemented in this work. Three case-studies of non-linear load conditions in a ship power system with two separate buses have been implemented in a MATLAB/Simulink model, and the compensation performance obtained with the MPC-based control is compared to two control techniques based on conventional filtering strategies. The THD_Vs obtained with system-oriented on-line optimization with the MPC are the lowest among the three cases investigated. The presented results highlight the advantages of the MPC over conventional approaches; namely its higher degree of freedom when dynamically searching the optimal values by treating all selected harmonics at once without restricting the APF current references by a direct mathematical relation to the load currents, and the ability to optimize within APF current limits (constraints). In particular, the MPC has advantages when the available current from the APF is constrained by the current rating of the converter. Although the results presented in this chapter are obtained in a system with only two separate buses, the MPC algorithm can easily be extended to account for a larger system configuration. Thus, the use of the MPC or another formal optimization technique for online system-wide harmonic mitigation can be clearly beneficial compared to conventional approaches for generating APF current references. This will especially be the case when the complexity of the electrical grid increases, and when the APF operation is constrained by its current ratings. The approach presented in this manuscript can also be applied to other APF topologies, or it can be included in active rectifiers or inverters with multi-functional control capabilities.

CHAPTER 4

In search of the best method for system-wide harmonic compensation in isolated microgrids: MPC vs offline analytical optimization

This chapter, which is based on the reformatted version of [221], investigates two methods for system-wide harmonic mitigation in a microgrid by using a single Active Power Filter (APF). Of the two methods explored in the chapter, one is founded on analytical offline optimization by using a detailed model of the power grid under investigation, while the other is a Model Predictive Controller (MPC) which uses a simplified model of the power system for online optimization. These two techniques are benchmarked against two conventional control methods in five different simulation cases of a two-bus shipboard power system with 12-pulse rectifier loads. In addition to various load conditions, non-idealities such as tranformer saturation and parameter mismatch/uncertainty are studied. Both optimization-based approaches ensure improved utilization of the APF for system-oriented compensation of harmonics compared to the conventional control methods. However, the MPC-based optimization provides the lowest voltage THDs for all investigated cases, due to its online operation and the consideration of nonlinear constraints including the current limitations of the APF in the optimization.

4.1 Introduction

Power electronic converters are today a widely used in modern power systems, with applications ranging from consumer electronics to high voltage transmission schemes. High penetration of power electronics in the power grid, especially by large loads with passive rectifiers as increasingly utilized for variable speed motor drives since the 1980s, introduces non-linear relations between currents and voltages at multiple points in the grid [79, 94]. This non-linear relation will affect the power quality in terms of total harmonic distortion (THD), with various values at different points in the grid, depending on the harmonic loads and the impedances in the system.

Techniques for analyzing and mitigating harmonic voltage and current distortions have been investigated since the early advents of electric power systems. Most of these approaches were based on local harmonics compensation principles [10, 149, 213], and only a few of them reflect the already existing concerns in industry with achieving a system-wide harmonic mitigation [149].

A simple, economical and commonly used approach for harmonic mitigation is to install passive filter solutions with capacitive and/or inductive elements that reduce the impact of harmonic load currents on the rest of the system. For power systems dominated by large non-linear loads with known harmonic spectra, the use of tuned passive harmonic filters, including high-pass filters and wide-band filters, has been a well-established practice [183, 204, 233]. However, despite simple implementation, passive filters have several drawbacks. Passive solutions for suppression of dominant harmonic frequencies are, for instance, susceptible to undesirable series and parallel resonances with the supply and load, since the supply impedance has a strong influence on the passive compensation characteristics of tuned harmonic filters [262]. In addition, passive filters do not always respond correctly to dynamical variations, especially when the installation is exposed to various system parameters and operating points or frequent changes in system configuration, and may be overloaded due to ambient harmonic loads and supply voltage distortions [20]. Furthermore, a set of shunt-connected passive filters cannot be effectively adapted to a wide range of dynamically changing load characteristics, as the amplitude of the harmonic components that are generated by power conversion devices with non-linear characteristics will depend on the load's active power demand.

As a result of recent advances in switching converters, Active Power Filters (APFs) have become a viable solution for real-time harmonic compensation under conditions where passive filters have disadvantages. Due to extensive research activities, the converter design and the local control strategies of

APFs for selective or broadband harmonic mitigation are also well established in literature [10, 99, 159]. The common practice today is to use APFs for local mitigation of harmonic distortions from one single load or suppression of voltage and/or current distortions at one specific location in a power system. However, an APF may be controlled to mitigate harmonic distortions introduced by multiple loads. This implies the need for a system-wide approach to reduce the THD at multiple points in a power system, beyond what can be achieved with local compensation principles that reduce THDs of single loads or single locations.

The potential for system-wide optimization of APF operation was realized in the early phase of research on power conditioning devices, as analyzed in [97, 98], where a single APF was proposed for optimally minimizing harmonic voltage distortion throughout a power distribution grid. The analysis relied solely on current and voltage measurements which were used in non-predictive optimization schemes to calculate the optimal harmonic injection currents for minimizing the THD at all the power grid's nodes. As the approach did not include a model of the power grid under investigation, voltage and current measurements from each node in the power grid were required to obtain the optimal harmonic mitigation. However, the potential for system-wide optimal harmonic mitigation by using one single APF that was implied by the approach from [97, 98], has not received any significant attention in the development of APF control strategies during the last decades. A first approach for system-level harmonic mitigation with one single APF by using Model Predictive Control (MPC) for on-line optimization of the APF current references was recently proposed in [220, 222, 224].

In this work, two approaches towards system-wide optimal harmonic mitigation by a single APF are addressed and studied for a two-bus microgrid system with independent nonlinear 12-pulse loads at both buses. For this system, an explicit analytical solution of the optimal APF compensation for each harmonic current is presented along with an optimal system-wide harmonic mitigation scheme realized as an MPC. The MPC is based on the original idea presented in [220, 222, 224], and shares some of the implementation aspects with the MPCs for system-wide harmonic mitigation of 6-pulse loads presented in [218] and the preliminary analysis of 12-pulse loads presented in [223]. The analytical approach is compared to the MPC-based approach in terms of flexibility and in the light of computational cost, as MPCs often introduce added complexity with stringent real-time requirements but also provides inherent capability for handling constraints. The results from the system-wide harmonic mitigation using both the analytical solution and the MPC are bench-marked against the local harmonic filtering principle, i.e. harmonic mitigation at one single point in the power system (denoted BM1), and an ad-hoc method presented in [202] using 180° phase shifted sum of the harmonic currents from both loads as a reference for the APF (denoted BM2). The observed differences in performance indicates how the system significantly benefits from a mitigation strategy that is designed for system-wide harmonic reduction. Although the investigations in this work are limited to a microgrid, the presented approaches for system-wide harmonic mitigation might also be further expanded to participate in a hierarchical control structure for larger power systems as discussed in [107].

The chapter is organized as follows: In Section 4.2 the microgrid under investigation is presented. Section 4.3 derives and discusses a harmonic mitigation method obtained by offline analytical optimization, while Section 4.4 introduces an online optimal harmonic mitigation approach realized in the framework of MPC. Simulation results are presented and discussed in Section 4.5. Finally, Section 4.6 concludes the chapter.

4.2 The Microgrid Under Investigation

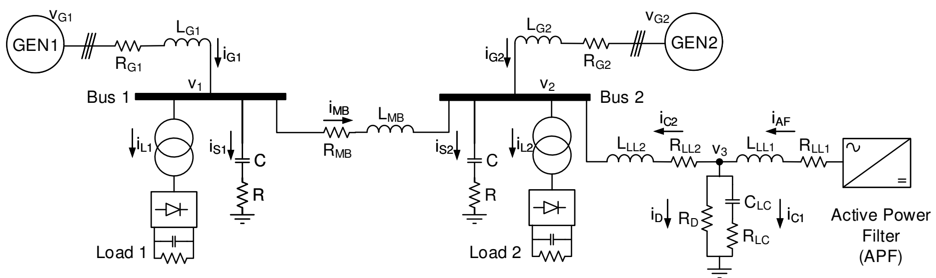

Figure 4.1: Simplified shipboard power system (islanded microgrid) under investigation: Two generators, two buses with loads (Variable Speed Drive (VSD) with 12-pulse rectifiers), an Active Power Filter (APF) for harmonic mitigation, an LCL filter to suppress switching noise from the APF's hysteresis-controlled IGBTs and RC-shunts to model stray capacitance of cables and busbars.

The three-phase three-wire microgrid under investigation is showcased in Figure 4.1. The grid represents a simplified two-bus shipboard power system [181], which in many cases can be seen as an (isolated) islanded microgrid due to, non-constant fundamental frequency, the power system's size and extent and the electrical distances and load flows [65]. Frequency fluctuations is a reality in a shipboard power system, however tends to occur as slow varying oscillations, thus, for conceptual purposes, the nominal frequency is kept constant in this work.

The power system's two buses represent propulsion loads, where the motor drives are realized as VSDs including 12-pulse rectifiers, which are known to produce harmonics of orders 11th, 13th, 23th, 25th ($12k \pm 1, k \in \{1, 2, \ldots\}$) etc. The two buses are connected to their respective switchboards, one at starboard and one at port side of the marine vessel's electrical grid. The two switchboards are connected in an Integrated Power System (IPS) configuration, however, protection schemes, such as circuit breakers (bus-ties) and redundant power flow configurations to ensure power system reliability and continued service in case of single faults are omitted for simplicity. An Active Power Filter (APF) is connected to bus 2 for harmonic mitigation purposes. An LCL filter is installed between bus 2 and the active filter to suppress switching ripples and noise from the APF. An additional damping resistor is connected in parallel to the capacitor of the LCL filter. RC-shunts, which are connected to each switchboard, are included for the purpose of modelling stray capacitance, while the main bus impedance and the generator impedances are representing the equivalent impedance for dominant harmonic currents flowing in the system. The available measurements are the generator currents, $\mathbf{i}_{G1}$ and $\mathbf{i}_{G2}$, the load currents $\mathbf{i}_{L1}$ and $\mathbf{i}_{L2}$, the generator voltages $\mathbf{v}_{G1}$ and $\mathbf{v}_{G2}$ and the APF output current $\mathbf{i}_{AF}$ (used as feedback to the hysteresis controller for controlling the switching of the IGBTs). Table 4.1 lists the power system parameters for the shipboard microgrid in Figure 4.1.

4.3 Analytically Optimized APF Current

One possible approach for realizing optimal harmonic mitigation is to use a detailed model of the power system under investigation and apply analytical (offline) optimization to find an optimal analytical expression of the filter current reference, which will be fed to and tracked by the APF's current controller. The power system showcased in Figure 4.1 includes 11 unknowns, which by using Kirchhoff's current and voltage laws can be expressed by the following 11 equations in the frequency domain for the general harmonic order h and nominal (angular) frequency $\omega = 2\pi f$ (assuming one-phase for

Table 4.1: Power system parameters, notation as given in Figure 4.1 (pu model based on generator rating).

Parameter	Value	Unit
Nominal Voltage (V_{rms})	690	[V]
Nominal Frequency (f)	50	[Hz]
Generator power rating	1	[MVA]
APF DC link	1240	[V]
APF switching frequency	≈ 20	[kHz]
APF hysteresis band	0.10	[pu]
APF current limit	0.15	[pu]
APF DC capacitor	236	[μF]
$L_{G1,2}$	0.2	[pu]
$R_{G1,2}$	$0.1 \cdot L_{G1,2} \cdot \omega$	[pu]
L_{MB}	0.04	[pu]
R_{MB}	$0.1 \cdot L_{MB} \cdot \omega$	[pu]
$C_{S1,2}$	2	[μF]
$R_{S1,2}$	2	[Ω]
$L_{L1,2}$	0.3	[mH]
$R_{L1,2}$	0.03	[Ω]
C_C	30	[μF]
R_C	10	[Ω]
R_D	160	[Ω]

simplicity and omitting time notation (t) for readability):

$$i_{G1,2} = -\frac{v_{1,2}}{R_{G1,2} + jh\omega \cdot L_{G1,2}} \tag{4.1a}$$

$$i_{S1,2} = -\frac{v_{1,2}}{R_{S1,2} - \frac{1}{jh\omega \cdot C_{S1,2}}} \tag{4.1b}$$

$$i_{MB} = \frac{v_1 - v_2}{R_{MB} + jh\omega \cdot L_{MB}} \tag{4.1c}$$

$$i_{C2} = \frac{v_3 - v_2}{R_{L2} + jh\omega \cdot L_{L2}} \tag{4.1d}$$

$$v_3 = \left(R_C - \frac{1}{jh\omega \cdot C_C}\right) \cdot i_{C1} = R_D \cdot i_D \tag{4.1e}$$

$$i_{AF} = i_{C1} + i_{C2} + i_D \tag{4.1f}$$

$$i_{G2} = i_{L2} + i_{S2} - i_{C2} - i_{MB} \tag{4.1g}$$

$$i_{G1} = i_{S1} + i_{L1} + i_{MB} \tag{4.1h}$$

The imaginary operator is given as j. These equations can be solved by a symbolic mathematical software, such as Maple[1], and yield a solution on the form[2]

$$\boldsymbol{\chi} = \boldsymbol{\gamma}\left(\boldsymbol{\rho}, \omega, h, i_{L1}, i_{L2}, i_{AF}\right), \tag{4.2}$$

where the 11 unknowns are collected as

$$\boldsymbol{\chi} = \left[i_{G1}, i_{G2}, i_{S1}, i_{S2}, i_{MB}, i_{C1}, i_{C2}, i_D, v_1, v_2, v_3\right]^\top, \tag{4.3}$$

the power system's parameters (block two and three in Table 4.1) are collected as

$$\begin{aligned} \boldsymbol{\rho} = [&L_{G1}, R_{G1}, L_{G2}, R_{G2}, L_{MB}, R_{MB}, C_{S1}, R_{S1}, \ldots \\ &C_{S2}, R_{S2}, L_{L1}, R_{L1}, L_{L2}, R_{L2}, C_C, R_C, R_D]^\top, \end{aligned} \tag{4.4}$$

i_{L1} and i_{L2} are the load currents and i_{AF} is the APF output current. The main idea of the harmonic mitigation in this work is to keep the switchboard voltages as sinusoidal as possible, avoiding harmonic pollution spreading throughout the power system. Considering individual harmonic components in (4.1), the objective would be to minimize the switchboard voltages, which is analogue to minimizing the (harmonic) generator current components. Thus, the objective for optimal harmonic mitigation of the hth order harmonic component can be stated as

$$\min_{i_{AF}} J\left(\boldsymbol{\rho}, \omega, h, i_{L1}, i_{L2}, i_{AF}\right) = |i_{G1}|^2 + |i_{G2}|^2, \tag{4.5}$$

where the generator currents i_{G1} and i_{G2} are expressed by known variables given by the solution $\boldsymbol{\chi}$ of (4.2). Assuming the optimal APF current is on the form,

$$i_{AF}^c = i_{af}^{re} + j \cdot i_{af}^{im}, \tag{4.6}$$

which will be a valid assumption since complex numbers' include magnitude and phase information, and substituting for i_{AF} in (4.5), by using (4.6), the

[1] http://www.maplesoft.com/

[2] The detailed solution is too large to show in this thesis.

minimization problem can be solved by differentiation with respect to the real and imaginary part of i_{AF}^{c}, i.e.

$$\begin{aligned} &\frac{dJ}{di_{af}^{re}}\left(\boldsymbol{\rho},\omega,h,i_{L1},i_{L2},i_{AF}^{c}\right)=0 \\ &\frac{dJ}{di_{af}^{im}}\left(\boldsymbol{\rho},\omega,h,i_{L1},i_{L2},i_{AF}^{c}\right)=0. \end{aligned} \tag{4.7}$$

The solution of (4.7) yields an optimal APF current on the form

$$\begin{aligned} i_{AF}^{o} &= k_1 \cdot i_{L1}^{h} + k_2 \cdot i_{L2}^{h} \\ &= |k_1(\boldsymbol{\rho},\omega,h)| \cdot i_{L1}^{h} \cdot e^{-j\cdot\theta_1(\boldsymbol{\rho},\omega,h)} \\ &+ |k_2(\boldsymbol{\rho},\omega,h)| \cdot i_{L2}^{h} \cdot e^{-j\cdot\theta_2(\boldsymbol{\rho},\omega,h)}, \end{aligned} \tag{4.8}$$

where $\theta_1 = \angle k_1$, $\theta_2 = \angle k_2$, while i_{L1}^{h} and i_{L2}^{h} are the load currents for the harmonic component h to be mitigated. Considering the configuration in-Figure 4.1, the main difference between the k_1 and k_2 parameters is related to the main bus impedance, as the filter current needed for harmonic mitigation in bus 1 needs to account for the effects of the main bus impedance. Figure 4.2 shows the magnitudes and angles of the k_1 and k_2 parameters in (4.8) relative the main bus inductance L_{MB}. As can be seen, the k_1 parameter in the optimal filter current (Figure 4.2a) is dependent on L_{MB} while the k_2 parameter is not (Figure 4.2b). As expected, both the magnitudes and angles of k_1 and k_2 increases with increased frequency (increased harmonic order). In the following, the analytical approach addressed in this section will be referred to as *analytical controller*.

It is important to highlight that the offline optimization, resulting in an optimal APF current, i_{AF}^{o}, does not take into account the APF's power rating. If for instance the APF output current is being saturated the optimality is no longer valid, as the output current will be limited within the APF's rating. In general, APFs are expensive devices, and the cost is increasing with increasing power rating. Due to this, APFs are seldom over-dimensioned when installed in a power system, which means that APFs are likely to be operated close to or at their maximal power output capabilities. Hence, saturation effects may be an issue, compromising the optimality of the analytical optimal (offline) APF reference current, which calls for an online optimization approach.

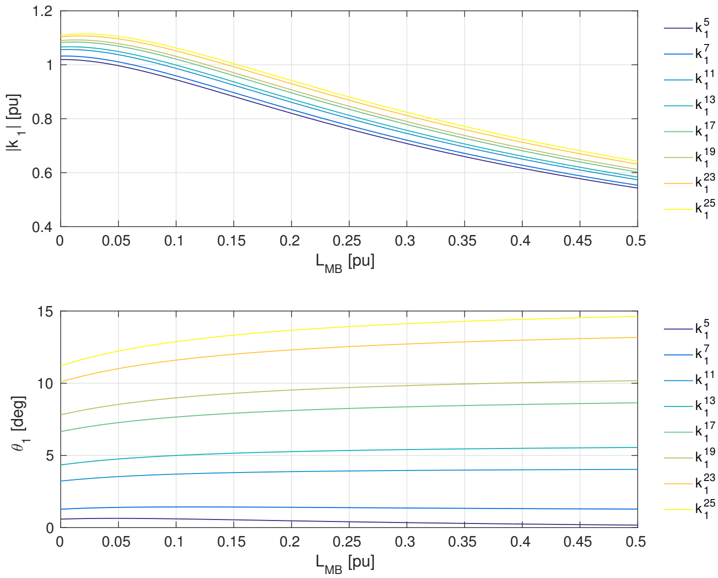

(a) k_1

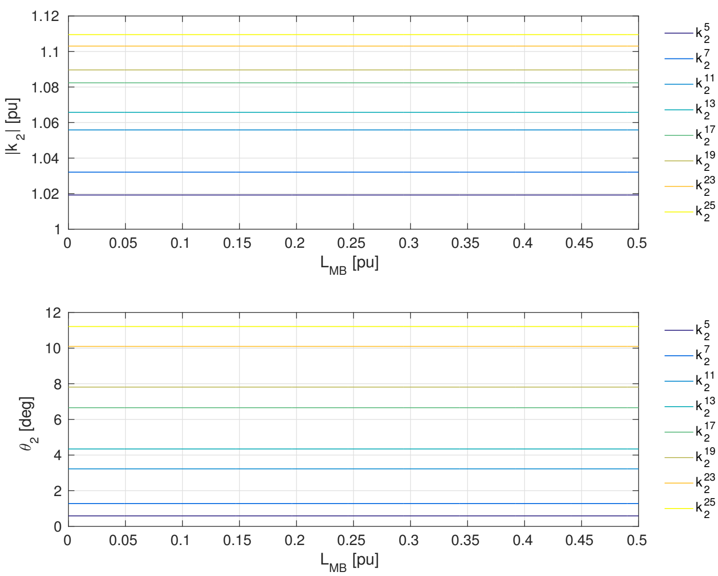

(b) k_2

Figure 4.2: Magnitude and angle of k_1 and k_2 plotted as a function of main bus inductance L_{MB} for harmonic orders $6k \pm 1$, $k \in \{1, 2, 3, 4\}$ (6-pulse rectifier characteristics).

4.4 MPC Generated Filter Current Reference

Another option for optimal harmonic mitigation is to conduct online optimization to calculate an optimal APF current reference. A suitable online optimization scheme is the Model Predictive Control (MPC). An MPC calculates the control action to a process/system using a (usually simplified) model of the process to predict its future behavior. Measurements from the current state of the process are used to initialize the model, and at each sampling interval the control action is obtained by solving online a finite horizon optimal control problem [190]. Depending on the MPC's computational costs, which may introduce a significant time delay that must be accounted for, the control action is extracted from the resulting optimal control vector spanning the MPC's prediction horizon.

The objective of the optimization is formulated as a cost function which is, along with constraints reflecting the physical process' limitations, given to an optimizer. The optimizer tries to optimize control actions using a predefined reference (i.e. desired process behavior), and model output. The total MPC formulation is often written on a standardized form given by

$$\begin{aligned}
\min_{\mathbf{x}(t),\mathbf{z}(t),\mathbf{u}(t)} \quad & V(\mathbf{x}(t),\mathbf{z}(t),\mathbf{u}(t)) = \\
& \quad \int_{t_0}^{t_0+T} l\left(\mathbf{x}(t),\mathbf{z}(t),\mathbf{u}(t)\right) dt \\
\text{s.t.} \quad & \\
& \dot{\mathbf{x}}(t) = \mathbf{f}\left(\mathbf{x}(t),\mathbf{z}(t),\mathbf{u}(t)\right), \\
& \mathbf{g}\left(\mathbf{x}(t),\mathbf{z}(t),\mathbf{u}(t)\right) = 0, \\
& \mathbf{h}\left(\mathbf{x}(t),\mathbf{z}(t),\mathbf{u}(t)\right) \leq 0, \\
& \forall t \in [t_0, t_0+T],
\end{aligned} \tag{4.9}$$

where the process' differential (dynamic) state vector is given by $\mathbf{x}(t)$, the algebraic state vector $\mathbf{z}(t)$, and the optimal control vector $\mathbf{u}(t)$. The scalar function $V(\cdot)$ is the cost (objective) function and the function $l(\cdot)$ is the stage cost. The model's differential states are given by the function $\mathbf{f}(\cdot)$, the algebraic states, and possible equality constraints, are given by the function $\mathbf{g}(\cdot)$, and inequality constraints are given by the function $\mathbf{h}(\cdot)$. The discrete control horizon is defined by T, where t_0 is the initial time instance. Measurements of the physical process are used to initialize the controller, i.e. $\mathbf{x}(t_0)$ and $\mathbf{z}(t_0)$.

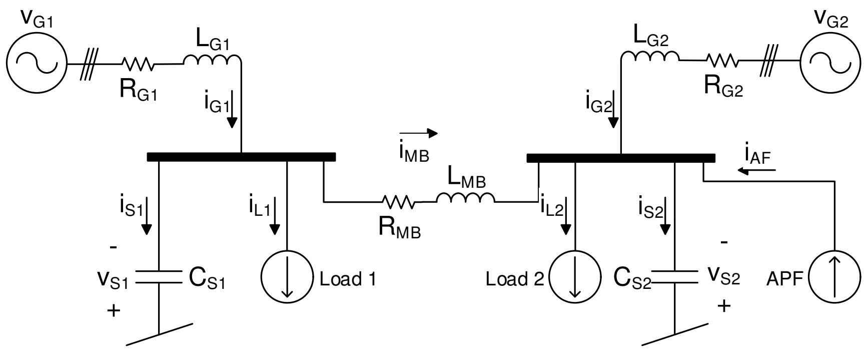

Figure 4.3: Simplified shipboard power system model for the derivation of the MPC.

Figure 4.3 illustrates the simplified MPC model used in this work. Compared to the true system (Figure 4.1) the LCL filter has been ignored and the RC-shunts are replaced by simple C-shunts. In the following the MPC's mathematical model formulation, cost function and constraints will be outlined.

4.4.1 Model Formulation

The power system under investigation is a three-phase three-wire system, thus using the $\alpha\beta$ or the dq transform to describe the system dynamics will reduce the size of the system matrices by 1/3. However, for the purpose of generality and for ensuring simple phase current limitation, the abc form is used to derive the MPC formulation. With regards to Figure 4.3, the power system's dynamics can be stated in the time domain using Kirchhoff's laws as

$$L_{G1,2}\frac{d\mathbf{i}_{G1,2}}{dt} = -R_{G1,2}\mathbf{i}_{G1,2} - \mathbf{v}_{S1,2} \tag{4.10a}$$

$$C_{S1}\frac{d\mathbf{v}_{S1}}{dt} = \mathbf{i}_{G1} - \mathbf{i}_{MB} - \mathbf{i}_{L1} \tag{4.10b}$$

$$L_{MB}\frac{d\mathbf{i}_{MB}}{dt} = \mathbf{v}_{S1} - \mathbf{v}_{S2} - R_{MB}\mathbf{i}_{MB} \tag{4.10c}$$

$$C_{S2}\frac{d\mathbf{v}_{S2}}{dt} = \mathbf{i}_{MB} + \mathbf{i}_{G2} - \mathbf{i}_{L2} + \mathbf{i}_{AF}, \tag{4.10d}$$

which represent 5 dynamic equations for the 5 unknowns in Figure 4.3. The generator voltages have been omitted from the equations as only harmonics are considered, thus assuming the generators are not sources of harmonic pollution.

The load currents, $\mathbf{i}_{L1}$ and $\mathbf{i}_{L2}$, can be expressed as Fourier series,

$$\mathbf{i}_L(t) = \begin{bmatrix} i_{L,a}(t) \\ i_{L,b}(t) \\ i_{L,c}(t) \end{bmatrix} = \begin{bmatrix} \sum_i I_{L,i} \sin\left(i\left(\omega t + \phi_{L,i}\right)\right) \\ \sum_i I_{L,i} \sin\left(i\left(\omega t + \phi_{L,i} - \frac{2\pi}{3}\right)\right) \\ \sum_i I_{L,i} \sin\left(i\left(\omega t + \phi_{L,i} + \frac{2\pi}{3}\right)\right) \end{bmatrix}, \quad \forall i \in \{12k \pm 1 | k = 1, 2, \ldots\}, \tag{4.11}$$

with amplitudes $I_{L,i}$, phases $\phi_{L,i}$ and harmonic orders to be mitigated given by i. The fundamental frequency components are not included in the load current processing as only the harmonic currents are objects for mitigation. The APF currents $\mathbf{i}_{AF}$ are kept as free (unmodeled) variables solely decided by the optimization. With regards to (4.10), the dynamic state vector can be stated as

$$\mathbf{x} = \left[\mathbf{i}_{G1}^\top, \mathbf{i}_{G2}^\top, \mathbf{i}_{MB}^\top, \mathbf{v}_{S1}^\top, \mathbf{v}_{S2}^\top\right]^\top, \tag{4.12}$$

where all the currents and voltages are given in *abc*. The differential equations are added to $\mathbf{f}(\cdot)$ in (4.9). The algebraic state vector can be stated as

$$\mathbf{z} = \left[\mathbf{i}_{L1}^\top, \mathbf{i}_{L2}^\top\right]^\top, \tag{4.13}$$

and the algebraic equations are added to $\mathbf{g}(\cdot)$ in (4.9). The control vector is simply the APF currents, i.e.

$$\mathbf{u} = \mathbf{i}_{AF} = \left[i_{AF,a}, i_{AF,b}, i_{AF,c}\right]^\top. \tag{4.14}$$

4.4.2 Cost Function

The cost function should reflect the objective of the optimization, which in this case will be selective harmonic mitigation of the generator currents. The mitigation is selective as each of the harmonic orders to be suppressed are modeled. A suitable stage cost function may be stated as

$$l\left(\mathbf{x}, \mathbf{z}, \mathbf{u}\right) = \mathbf{i}_{G1}^\top \mathbf{Q}_1 \mathbf{i}_{G1} + \mathbf{i}_{G2}^\top \mathbf{Q}_2 \mathbf{i}_{G2} + \mathbf{u}^\top \mathbf{Q}_u \mathbf{u}, \tag{4.15}$$

where the weights are given as

$$\begin{aligned}&\mathbf{Q}_1 = \mathrm{diag}([q_1, q_1, q_1]),\ \mathbf{Q}_2 = \mathrm{diag}([q_2, q_2, q_2]),\\ &\mathbf{Q}_u = \mathrm{diag}([q_u, q_u, q_u]).\end{aligned} \tag{4.16}$$

The first two parts of (4.15) represent the harmonic generator currents to be mitigated. The third part is added to keep the magnitude of the APF currents as low as possible, thus emphasize utilization of APF current phases to conduct harmonic mitigation, as described in details in [220]. $q_1, q_2 > q_u$ as punishing large filter currents is of lesser importance than minimizing the harmonic pollution. Since the load models, which were stated in (4.11), do not include the fundamental component, the objective is to minimize the generator currents, where perfect harmonic cancellation would yield $\mathbf{i}_{G1} = \mathbf{i}_{G2} = \mathbf{0}^{3\times1}$.

4.4.3 Constraints

The MPC's constraints should reflect the physical process' properties and limitations. In this work the APF's physical limitations are deciding the constraints, and the APF rating can be translated to maximum current output in all three phases [218, 237]. Thus, the constraints can be stated as

$$\begin{aligned}-i_{AF}^{lim} \le i_{AF,a} \le i_{AF}^{lim}\\ -i_{AF}^{lim} \le i_{AF,b} \le i_{AF}^{lim}\\ -i_{AF}^{lim} \le i_{AF,c} \le i_{AF}^{lim},\end{aligned} \tag{4.17}$$

where $i_{AF}^{lim} = 1$ [pu] relative APF rating. The constraints are added to $\mathbf{h}(\cdot)$ in (4.9).

4.5 Results

The power system presented in Figure 4.1 with details given in Table 4.1 is implemented in Matlab/Simulink using the SimPowerSystems library. For simplicity, the generators are assumed to be ideal voltage sources and the nominal frequency is assumed to be constant. The APF is operated with inner loop hysteresis current controllers with 15% hysteresis band and switching frequency of approximately 20kHz. The APF's power rating is set to 15% of the rating of the generators. The simulation step size is set to 2μs. The MPC is implemented using the ACADO (Automatic Control and Dynamic Optimization) toolkit [116], which includes a code generation tool for synthesizing highly efficient C code [117]. The MPC was cross-compiled to Matlab as a mex-function and included in the Simulink implementation of the power system. Details regarding the MPC implementation are listed in Table 4.2. The closed-loop implementation of the MPC with the power system is based on the MPC for system-level harmonic mitigation of 6-pulse loads in [218].

For the purpose of performance assessment of the harmonic mitigation by the MPC and the analytical controller, two benchmarks are applied:

- **BM1**: $\mathbf{i}_{AF}^{h} = \mathbf{i}_{L2}^{h}$
- **BM2**: $\mathbf{i}_{AF}^{h} = \mathbf{i}_{L1}^{h} + \mathbf{i}_{L2}^{h}$

Table 4.2: MPC implementation details.

Parameter	**Value**
Time horizon T	12.5ms
MPC run cycle	100Hz
Discretization N	220
Discretization type	Multiple Shooting
Integrator	Runge-Kutta 4 (RK4)
Hessian Approximation $(\nabla^2_{\mathbf{x}}\mathbf{f}(\cdot))$	Exact Hessian
Solver	qpOASES
Number of iterations	5
Stage cost weights	$q_1 = q_2 = 1000$, $q_u = 1$
AF current limit (APF pu model)	$i_F^{ap} = 1[pu]$

BM1, which performs harmonic mitigation at one single point (in this case bus 2) is considered to be the most common harmonic mitigation practice while using an active filter. BM2, which is an ad-hoc method proposed in [202], is included to provide a more fair comparison with the MPC and the analytical controller than what is achieved with BM1. Five different simulations are addressed:

- **Ideal simulation** - No transformer saturation and exact (and known) system parameters as given in Table 4.1:

1. Both loads have equal power demand.
2. Load 1 has higher power demand than load 2.
3. Load 2 has higher power demand than load 1.

- **Parameter mismatch** - Some of the power system parameters used in the controllers do not correspond to the parameters used in the power system simulation:

  4) Load 1 has higher power demand than load 2.

- **Transformer saturation** - Non-ideal transformers with saturation characteristics according to Figure 4.5:

  5) Load 1 has higher power demand than load 2.

For comparison purposes, simulation 2, 4 and 5 shares the same load demand - an unbalanced load profile where load 1 has a load of 1.2 pu and load 2 has a load of 0.9 pu referred to the generator ratings. In all simulations the harmonics to be mitigated are the 11th, 13th, 23rd and 25th, which corresponds to the four first dominating harmonic orders in a 12-pulse rectifier load. For each case the resulting voltage THDs from each method are presented in tables - all calculated as the mean value using all three phases (*abc*). Simulation 2 and 5 include two figures where the results from the MPC, analytical controller and BM2 are compared.

4.5.1 Ideal Simulation

The first three simulations can be considered as ideal simulations, meaning no transformer saturation and that the control algorithms feeding the APF with a reference current has exact information about the power system parameters, as given in Table 4.1.

Simulation 1:

Table 4.3 shows the configuration of the first simulation; both loads have an equal power demand of 0.25 [pu]. The table also shows the resulting THD values for bus voltage 1 and 2, i.e. $\mathbf{v}_1$ and $\mathbf{v}_2$ as depicted in Figure 4.1. As can be seen, the MPC results in the lowest THD for $\mathbf{v}_2$, however, a slightly worse THD for $\mathbf{v}_1$ compared to the analytical controller. The analytically generated current reference gives overall slightly better results than BM2; with lower THD for $\mathbf{v}_1$ than for BM2, but has slightly higher THD for $\mathbf{v}_2$. BM1, which is considered the common harmonic mitigation method results in the overall worst voltage THDs.

Table 4.3: Simulation 1: Configuration and resulting THD**v**s.

	MPC	**Analytical**	**BM2**	**BM1**
THD $\mathbf{v}_1$	1.7%	1.6%	2.2%	2.8%
THD $\mathbf{v}_2$	1.9%	2.6%	2.5%	2.5%
Power load 1	0.25 [pu]			
Power load 2	0.25 [pu]			

Higher THDs from BM1 and BM2, compared to the MPC and the analytical controller, are expected for a non-saturated APF current reference due to the fact that BM1 and BM2 have no knowledge of the power system and make the APF reference current based on measured harmonics from the load currents. The MPC is re-initialized every run using new measurements, which prevent model errors and potential numerical errors to propagate, ensuring the best performance. The analytical controller does not feature such a property since it is derived offline for a given power system model. Another reason for the MPC's slightly better THD for $\mathbf{v}_2$ is that the MPC is accounting for injection of other harmonics than the harmonics to be mitigated with pure selective harmonic compensation, which can be seen from the stage cost function in (4.15). In other words, APF currents that contribute to harmonics in the generator currents are penalized to achieve the optimal system-level harmonic mitigation of both buses.

Simulation 2:

The configuration of the second simulation is shown in Table 4.4, and the load demands are now set to 1.2 [pu] for load 1 and 0.9 [pu] for load 2. As indicated in the table, the MPC results in the lowest THD for both bus voltages. Also in this case the analytical controller performs better than BM2. BM1 gives the highest THDs, which also violates the maximum allowed voltage THD limit of 5% (measured up to the 50th harmonic) for marine vessels set by the American Bureau of Shipping (ABS) [6].

As can be seen in the two upper plots in Figure 4.4a, the APF's output and reference current is now saturated, as an effect of higher load demands. It

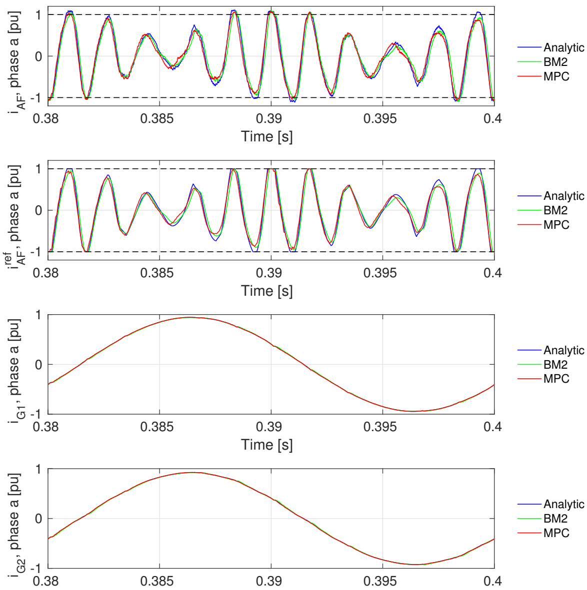

(a) Filter and generator currents for phase a.

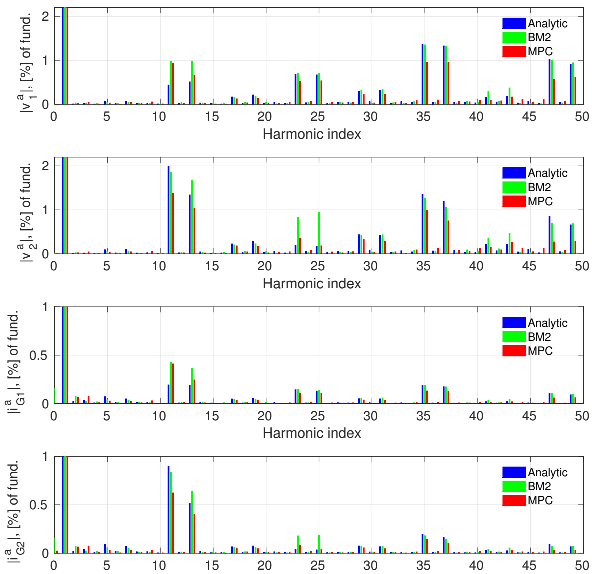

(b) Load voltage and generator current frequency spectra for phase a.

Figure 4.4: Simulation 2: Ideal simulation with 12-pulse loads and load 1 demand of 1.2 [pu] and load 2 demand of 0.9 [pu].

Table 4.4: Simulation 2: Configuration and resulting THD**v**s.

	MPC	**Analytical**	**BM2**	**BM1**
THD $\mathbf{v}_1$	2.1%	2.7%	2.9%	5.8%
THD $\mathbf{v}_2$	2.3%	3.3%	3.5%	4.6%
Power load 1	1.2 [pu]			
Power load 2	0.9 [pu]			

can be seen from the figure that the MPC generated APF current reference is slightly phase-shifted compared to the analytical controller and the BM2. There is also a small difference in amplitude between the three controllers. As indicated in the two lower plots in the same figure, the generator currents are neither in this case pure sinusoidal waveforms.

The upper plot of Figure 4.4b shows that the MPC has a higher magnitude for the 11th and 13th dominating harmonic component compared to the analytical controller. For all other dominating frequency components, the MPC results in the lowest magnitudes. The analytical controller has the lowest magnitudes for the 11th and 13th harmonic component, but are quite similar to BM2's magnitudes for all other dominating frequency components. The investigation of the harmonic components confirms the THD differences for $\mathbf{v}_1$ presented in Table 4.4. For $\mathbf{v}_2$ the MPC results in the lowest magnitudes for all the dominating frequencies, except the 23rd and 25th component, and as the magnitude differences compared to the two other controllers are prominent, the MPC results in a THD which is 1% lower than for the analytical controller and more than 1% lower than for BM2. The same arguments for explaining differences between the controllers apply for the spectra of $\mathbf{i}_{G1}$ and $\mathbf{i}_{G2}$.

As in simulation 1, the THD differences between the MPC and the other controllers may be influenced by model/process mismatch and penalty for harmonic injection into the power system. However, in this case, the saturation of the filter current is the main reason behind the MPC's lower THDs. As the MPC's model includes the APF current limitations, the MPC is able to compensate for saturation effects, which is not the case for the analytical controller, BM1 and BM2.

Simulation 3:

The configuration of the third simulation is shown in Table 4.5, and the load demands are now the opposite of simulation 2, i.e. 0.9 [pu] for load 1 and 1.2 [pu] for load 2. As indicated in the table, also in this case the MPC results in the lowest THDs. The analytical controller results in overall worse THDs compared to BM2; lower THD for $\mathbf{v}_1$, however, higher THD for $\mathbf{v}_2$. BM1 results in the highest THDs, which also in this case violates the maximum voltage THD limit set by ABS for a marine vessel.

Table 4.5: Simulation 3: Configuration and resulting THD**v**s.

	MPC	**Analytical**	**BM2**	**BM1**
THD $\mathbf{v}_1$	2.8%	3.4%	3.6%	6.4%
THD $\mathbf{v}_2$	3.4%	4.3%	3.9%	5.8%
Power load 1	0.9 [pu]			
Power load 2	1.2 [pu]			

Again, the MPC's better performance compared to the other controllers is a result of its ability to handle model/process mismatch, penalty for harmonic injection and its consideration of the APF current limit to avoid effects from APF current saturation.

4.5.2 Parameter Mismatch

The next study case includes parameter mismatch, meaning one or multiple power system parameters used by the controllers deviate from the actual values given in Table 4.1. The parameters used to illustrate parameter mismatch is related to the LCL filter.

Simulation 4:

The configuration of simulation 4 is given in Table 4.6. The load demands are the same as in simulation 2, i.e. 1.2 [pu] for load 1 and 0.9 [pu] for load 2, but the controllers are based on the assumption that the LCL-capacitor (C_C) is 15μF and the LCL-inductors are $L_{L1} = L_{L2} = 0.6$mH, when in reality they are 30μF and 0.3mH, respectively. The resulting voltage THDs shows that the MPC is unaffected by the parameter mismatch, so is BM1 and BM2, which is as expected due to the fact that the MPC, BM1 and BM2 do not have any knowledge of the LCL filter. However, the analytical controller, which relies on correct information about the LCL filter, shows a higher THD for both bus voltages compared to the results from simulation 2.

Table 4.6: Simulation 4: Configuration and resulting THD**vs**.

	MPC	Analytical	BM2	BM1
THD $\mathbf{v}_1$	2.1%	3.0%	2.9%	5.8%
THD $\mathbf{v}_2$	2.3%	3.8%	3.5%	4.6%
Power load 1	1.2 [pu]			
Power load 2	0.9 [pu]			
Parameter mismatch	Power System: $C_C = 30\mu$F, $L_{L1} = L_{L2} = 0.3$mH Controllers: $C_C = 15\mu$F, $L_{L1} = L_{L2} = 0.6$mH			

The results from this simulation underlines the analytical controller's dependency of correct power system information. As the MPC has closed-loop feedback, and does not use a detailed model of the power system, it is not affected by the parameter mismatch. BM1 and BM2 are also unaffected by the parameter mismatch, as they do not rely on any information about the power system.

4.5.3 Transformer Saturation

The last simulation addressed in this work is related to transformer saturation. The previous simulations were simulated using ideal transformer models without saturation.

Simulation 5:

The transformer saturation adopted in this study case is illustrated in Figure 4.5, which shows a distinct saturation characteristic causing a non-linear behaviour of the transformer. The saturation characteristic is chosen for illustrative purposes, and represents therefore a relative low saturation limit. In reality, the saturation limits for many suitable transformers tend to be somewhat higher.

The configuration for simulation 5 is shown in Table 4.7, and once again, for the purpose of comparison, the load demands are set to the same con-

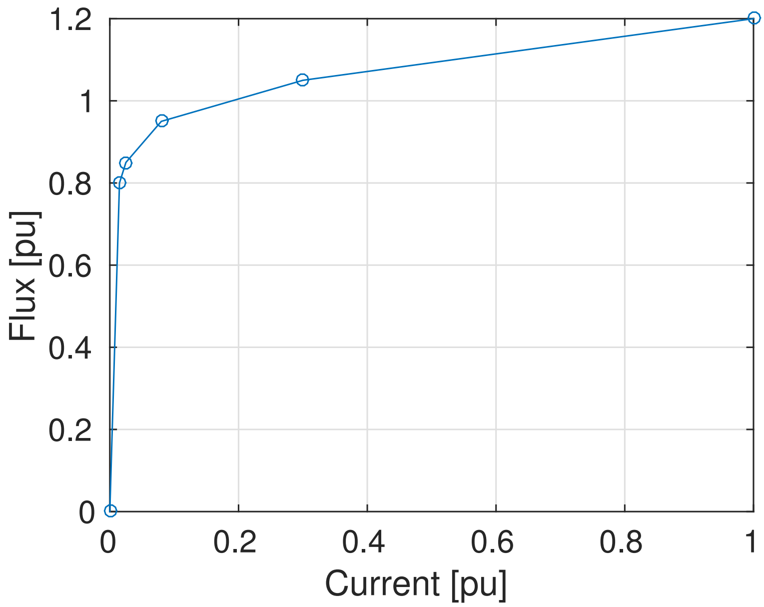

Figure 4.5: Transformer saturation characteristics used in simulation 5.

Table 4.7: Simulation 5: Configuration and resulting THD**v**s.

	MPC	**Analytical**	**BM2**	**BM1**
THD $\mathbf{v}_1$	2.3%	2.7%	2.9%	5.7%
THD $\mathbf{v}_2$	2.4%	3.4%	3.6%	4.5%
Power load 1	1.2 [pu]			
Power load 2	0.9 [pu]			

figuration as used in simulation 2. The resulting bus voltage THDs from the MPC are also in this case lower than the THDs from the analytical controller, BM1 and BM2, and gives the best harmonic mitigation. Compared to simulation 2, the analytical controller and BM2 result in slightly higher THDs for $\mathbf{v}_2$, while the THDs for both buses are reduced for BM1. The MPC seem to be a bit more affected, showing increased THDs for both bus voltages compared to the MPC results in simulation 2.

The two upper plots in Figure 4.6a show the APF output currents in phase a measured after the LCL filter and the APF reference current for the MPC, the analytical controller and BM2. As indicated the APF current resulting from the MPC is slightly phase-shifted compared to the analytical

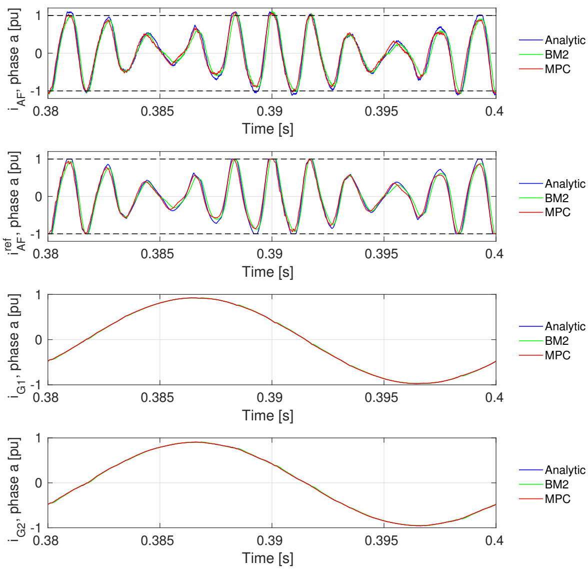

(a) Filter currents and generator currents for phase a.

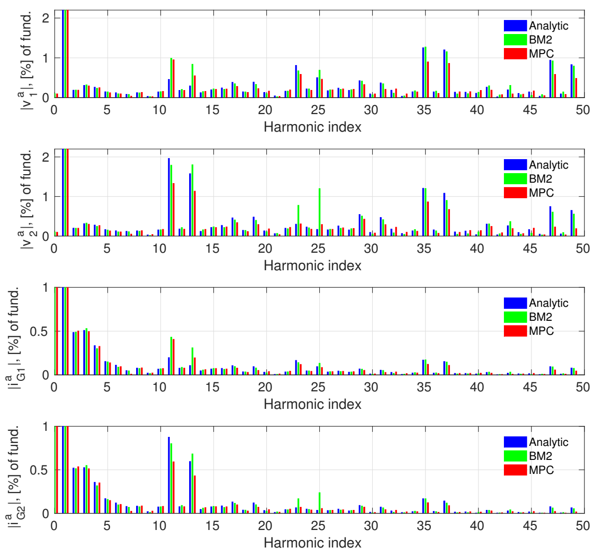

(b) Load voltage and generator current frequency spectra for phase a.

Figure 4.6: Simulation 5: 12-pulse loads with transformer saturation.

controller, and the analytical controller's APF current is slightly phase-shifted compared to BM2's APF current. Also amplitude differences can be seen between the three controllers. The two lower plots in Figure 4.6a show the resulting generator currents, $\mathbf{i}_{G1}$ and $\mathbf{i}_{G2}$.

Figure 4.6b includes the frequency spectra of the bus voltages and generator currents. From the two upper plots, which presents the bus voltage spectra, it can be seen that the MPC results in lower amplitudes for almost all dominating frequency components, which explains the reduced THDs compared to the analytical controller and BM2. For the spectra of bus 1 voltage, the analytical controller has reduced amplitudes for the 11th and 13th component compared to BM2, which is confirmed by the analytical controller's slightly reduced THD. Furthermore, BM2 has higher amplitudes for the 23rd and 25th harmonic component for $\mathbf{v}_2$ compared to the analytical controller, which are main contributors for the increased bus 2 voltage THD.

By examining the THD differences between simulation 2 and simulation 5, the MPC is slightly more affected by the transformer saturation than the three other controllers, which indicates that the transformer saturation affects the MPC's search for the optimal system-level harmonic mitigation. Thus, the result from simulation 2 is not longer achievable as the global optimum to the optimization problem solved by the MPC. As the analytical controller, BM1 and BM2, are not working in the close neighbourhood of the optimal APF current, the transformer saturation has lower impact on the resulting bus voltage THDs.

4.6 Conclusion

Two conceptual methods for optimal system-wide harmonic mitigation using one single APF have been presented. An analytical approach, which is based on offline optimization, and an MPC, which is an online model-based optimization method with predictive abilities, have been developed and implemented. The power system under investigation was a two-bus shipboard (isolated) microgrid with two generators and two 12-pulse loads - one generator and one load connected to each bus. The results of five different simulations, including transformer saturation and parameter mismatch, were presented where the two proposed methods were benchmarked against two conventional mitigation methods. In all simulations the MPC resulted in the lowest total voltage THDs. For the case with parameter mismatch the analytical controller proved to be not very robust, hence resulting in higher THDs than one of the benchmark methods. In addition, due to offline optimization, the analytical controller did not include any information about the filter's rating, thus suffered from saturation when the APFs current limits were reached. This was not the case with the MPC, which demonstrated clear advantages over the analytical controller related to robustness and adaptive behavior, and therefore resulted in the lowest total voltage THD in all presented simulations.

CHAPTER 5

Real-time Model Predictive Control Architecture for System-level Harmonic Mitigation in Power Systems

The design of Model Predictive Control (MPC) schemes, that holds the required real-time properties, for use in systems with fast dynamics are challenging, and an understanding of the system's behavior, to exploit system properties that can benefit real-time implementation is imperative. This chapter, which is based on [214], proposes a real-time MPC implementation for optimal system-wide mitigation of harmonic distortions by optimally controlling one single Active Power Filter (APF) in an electrical grid with multiple buses. The MPC is designed on the basis of repetitive and distributed control, and its objective is to provide an optimal current reference for the APF to track and actuate. Moreover, a novel system architecture, which incorporates the MPC implementation and handles distribution of control action as well as receiving measurements used by the MPC, is proposed to obtain the application's real-time properties. A simulator architecture is implemented with the aim of conducting a Hardware-In-Loop (HIL) simulator test to evaluate the application's real-time properties, as well as the application's use of resources. The results demonstrates that the implementation of the harmonic mitigation application holds the necessary real-time requirements with relatively low resource usage.

5.1 Introduction

Model predictive control (MPC), which is founded on optimization, utilizes a model of the system to online forecast system behavior and optimize the forecast to produce the best control decision at the current time instance

[190]. The model, which is an approximation of the physical system that only represent the dynamics under investigation, is initialized by measurements or estimates of the system's current state. A cost function, defining the objective of the control and constraints, may be applied to reflect the system's physical and operational limitations. At each sampling interval the future control action is obtained by solving online a finite horizon optimal control problem. A range of different MPC schemes have been developed for systems with different properties and requirements, including deterministic as well as stochastic, linear and nonlinear systems. Hence, MPC is not one single method but rather a set of methods and algorithms that forms a control philosophy [22]. A general, but simplified, illustration of MPC is portrayed in Figure 5.1.

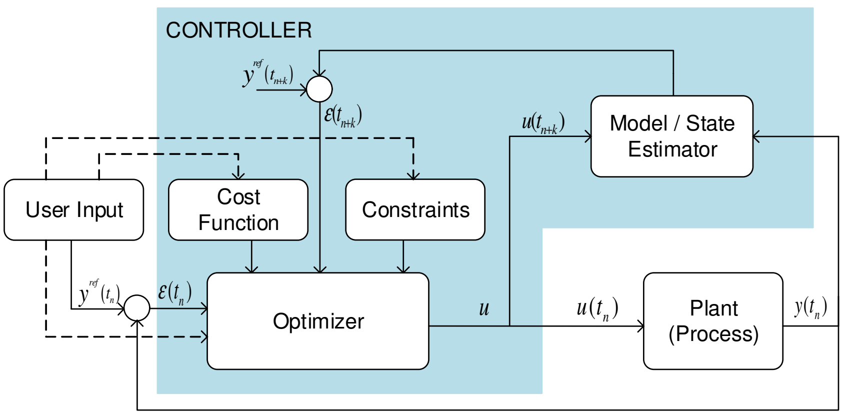

Figure 5.1: Simplified illustration of model predictive control.

Since the early advents of MPC in the process industries, thousands of successful MPC applications have been implemented in the same industries [133, 187, 190]. A lot of research has been directed to the MPC's area of application, and MPC has been investigated within several industries and fields of research in the pursuit of smart control schemes to improve existing non-optimal control strategies or to solve challenging control problems where conventional control theory alone does not provide a sufficient solution. In this regard, MPC is often used as a higher level controller feeding one or multiple lower level controllers with references or set-points to be tracked.

In the field of electrical power engineering, MPC has been frequently investigated as a vital option for optimal control of power converters [26, 43, 44, 45, 140, 195, 196, 199, 252], where the switching of the Power Electronics (PE) devices has been the main focus of control. As examples, in [252] an indirect Finite Control Set (FCS) MPC is investigated for the optimal control of the Modular Multilevel Converter's (MMC) switching, in [130] MPC is applied to power system protection schemes, control of batteries in a peak-shaving application is discussed in [24], frequency control in [77], control of distributed energy resources in [160, 166], and mitigation of harmonic distortions in [218, 220, 222, 223, 224]. Simultaneous optimization and control in real-time is one of the most desirable properties of MPC and still a vast area of application in electrical power engineering where multi-layer control is common practice, and where the common practice is ad-hoc offline optimization strategies [97, 99]. This work proposes a scheme for real-time MPC implementation in a case-study of harmonic profile optimization where the common practice has been the use of offline optimization for the choice of set-points for the converter controllers.

Harmonic distortions, which are any deviation from the pure sinusoidal voltage or current waveform, introduce active power losses and contributes to reactive power in the system [10]. Methods for mitigating harmonic distortion include the use of passive and active filters. Unlike passive filters, the active filters can be controlled, and, depending on the control philosophy, be able to adapt to changes in the harmonic distortion spectra. This is a desirable functionality, especially in power systems with dynamic load profiles. The most applied control philosophy for active filters involves the mitigation of harmonic distortion at a specific location in the power system. However, as active filters can be controlled to dynamically track a current reference, a single active filter can be designed to track a current reference that can optimize the harmonic profile of the entire system. This task can be performed in real-time by a tailor-designed MPC. This chapter's main contribution lies in the real-time system framework and implementation of an MPC designed for such a task, in contrast with the state of the art solution based on offline optimization for set-point definition.

The real-time implementation of a Continuous Control Set (CCS) MPC application for optimal mitigation of harmonic distortions as discussed in [218, 220, 222, 223, 224] will be treated in detail in this work. By exploiting the periodic nature of the voltage and current waveforms, a repetitive MPC control philosophy is selected and we propose a dedicated real-time framework that holds sufficient real-time properties. Hardware-in-Loop (HIL) simulation experiments are conducted to verify the system architecture with regards to the MPC's execution cost and the time delay introduced by the framework and the communication link. The new framework enables reliable and fast nonlinear MPC to be implemented in this challenging application by using standard optimization frameworks and industry standard computer technology without resorting to hard real-time systems and formal verification.

The chapter is organized as follows: The problem formulation and adopted control philosophies are addressed in section 5.2, section 5.3 presents the system architecture and the implementation of the MPC and its framework and middleware. Furthermore, section 5.4 presents a HIL test of the system architecture. Finally, section 5.5 concludes the work.

5.2 Problem Formulation

The MPC uses a model, or a state estimator, of the system to predict future behavior and be able to calculate the best possible control action to control the system to meet a desired objective while, at the same time, comply with the system's physical and operational constraints. In the following, the derivation of the MPC and its model on standard form for the optimal harmonic mitigation application, as introduced in [218, 223] for a two-bus shipboard power system, will be discussed. The different hardware layers and adopted control philosophy will be introduced.

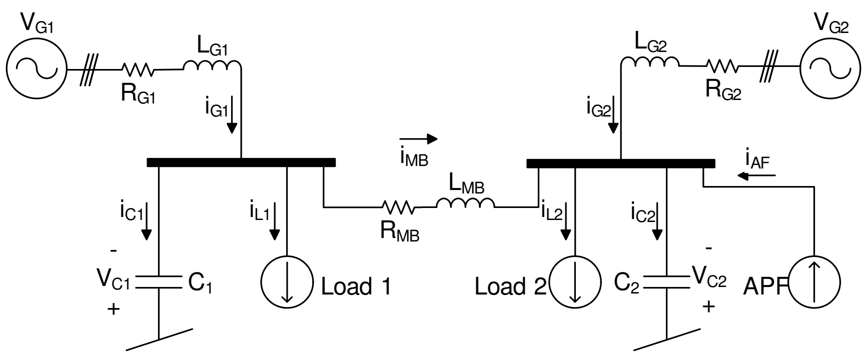

Figure 5.2: Simplified model of a two-bus shipboard power system: Propulsion loads and Active Power Filter (APF) modeled as ideal current sources, generators modeled as ideal voltage sources. Shunt capacitors are included for the purpose of modeling cable capacitance and provide bus voltages [218].

5.2.1 MPC Formulation

Although the concept is general, for simplicity of presentation a simplified model of a two-bus shipboard power system, which is illustrated in Figure 5.2, is used in the design of the MPC's internal model. According to Kirchhoff's laws, the model's dynamic equations can be stated as

$$
\begin{aligned}
L_{G1}\frac{d\mathbf{i}_{G1}}{dt} &= -R_{G1}\mathbf{i}_{G1} - \mathbf{v}_{C1} && \text{(5.1a)}\\
C_1\frac{d\mathbf{v}_{C1}}{dt} &= \mathbf{i}_{G1} - \mathbf{i}_{MB} - \mathbf{i}_{L1} && \text{(5.1b)}\\
L_{MB}\frac{d\mathbf{i}_{MB}}{dt} &= \mathbf{v}_{C1} - \mathbf{v}_{C2} - R_{MB}\mathbf{i}_{MB} && \text{(5.1c)}\\
C_2\frac{d\mathbf{v}_{C2}}{dt} &= \mathbf{i}_{MB} + \mathbf{i}_{G2} - \mathbf{i}_{L2} + \mathbf{i}_{AF} && \text{(5.1d)}\\
L_{G2}\frac{d\mathbf{i}_{G2}}{dt} &= -R_{G2}\mathbf{i}_{G2} - \mathbf{v}_{C2}, && \text{(5.1e)}
\end{aligned}
$$

where t represents the continuous time. The vectors $\mathbf{v}$ and $\mathbf{i}$ represent the three-phase voltages and currents, respectively, given in the *abc* frame. Assuming the generators are not sources of harmonic distortion, the fundamental components (voltages and currents) are left out of (5.1), as only the dynamics originating from the harmonic distortion introduced by the loads are subjects for optimization. The propulsion loads ($\mathbf{i}_{L1}$ and $\mathbf{i}_{L2}$) can be modeled as Fourier series,

$$
\begin{aligned}
\mathbf{i}_{Lj}(t) = &\begin{bmatrix} \sum_i I^a_{L,j,i}\sin\left(i\left(\omega t + \phi^a_{L,j,i}\right)\right) \\ \sum_i I^b_{L,j,i}\sin\left(i\left(\omega t + \phi^b_{L,j,i} - \frac{2\pi}{3}\right)\right) \\ \sum_i I^c_{L,j,i}\sin\left(i\left(\omega t + \phi^c_{L,j,i} + \frac{2\pi}{3}\right)\right) \end{bmatrix}, \\
&\forall i \in \mathcal{H}, j \in \{1,2\},
\end{aligned} \tag{5.2}
$$

where $\mathcal{H}$ is the set of harmonic orders to be mitigated, $\omega = 2\pi f$ with f as the fundamental frequency, $I^k_{j,i}$ and $\phi^k_{L,j,i}$ are harmonic amplitudes and phases, respectively, for phases $k \in \{a,b,c\}$. The active filter's current constraints can be represented as

$$
i^k_{\min} \le i^k_{AF} \le i^k_{\max}, \tag{5.3}
$$

with phases $k \in \{a, b, c\}$. Assuming a balanced filter yields $i^k_{\max} = -i^k_{\min}$ $\forall k$, and $i^k_m = i^l_m$ $\forall (k,l)|_{k \neq l} \in \{a, b, c\}$ with $m \in \{\min, \max\}$. The harmonic mitigation problem can now be written on standard MPC form,

$$
\begin{aligned}
\min_{\mathbf{x}(t),\mathbf{z}(t),\mathbf{u}(t)} \quad & V(\mathbf{x}(t), \mathbf{z}(t), \mathbf{u}(t)) = \\
& \int_{t_0}^{t_0+T} l\left(\mathbf{x}(t), \mathbf{z}(t), \mathbf{u}(t)\right) dt \\
\text{s.t.} \quad & \\
& \dot{\mathbf{x}}(t) = \mathbf{f}\left(\mathbf{x}(t), \mathbf{z}(t), \mathbf{u}(t)\right), \\
& \mathbf{g}\left(\mathbf{x}(t), \mathbf{z}(t), \mathbf{u}(t)\right) = 0, \\
& \mathbf{h}\left(\mathbf{x}(t), \mathbf{z}(t), \mathbf{u}(t)\right) \leq 0, \\
& \qquad \forall t \in [t_0, t_0 + T]
\end{aligned} \tag{5.4}
$$

with initial time instance t_0 and horizon length T, dynamic equations $\mathbf{f}(\cdot)$, algebraic equations $\mathbf{g}(\cdot)$ and inequality constraints $\mathbf{h}(\cdot)$. By dropping the time notation t, the dynamic state vector $\mathbf{x}$, algebraic state vector $\mathbf{z}$ and control vector $\mathbf{u}$ are stated as

$$
\begin{aligned}
\mathbf{x} &= \left[\mathbf{i}_{G1}^\top, \mathbf{i}_{G2}^\top, \mathbf{i}_{MB}^\top, \mathbf{v}_{C1}^\top, \mathbf{v}_{C2}^\top\right]^\top \\
\mathbf{z} &= \left[\mathbf{i}_{L1}^\top, \mathbf{i}_{L2}^\top\right]^\top \\
\mathbf{u} &= \mathbf{i}_{AF}.
\end{aligned} \tag{5.5}
$$

The objective function, which specifies the objective of the optimization, is $V(\cdot)$ with the convex stage cost function

$$
l\left(\mathbf{x}, \mathbf{z}, \mathbf{u}\right) = \mathbf{i}_{G1}^\top \mathbf{Q}_1 \mathbf{i}_{G1} + \mathbf{i}_{G2}^\top \mathbf{Q}_2 \mathbf{i}_{G2} + \mathbf{u}^\top \mathbf{Q}_u \mathbf{u}. \tag{5.6}
$$

The first and second term in (5.6) represent the quadratic contribution of harmonic currents drawn from the generators, while the last part is included to penalize the use of large (high amplitude) active filter currents. $\mathbf{Q}_1$, $\mathbf{Q}_2$ and $\mathbf{Q}_\mathbf{u}$ are diagonal weight matrices, where $Q_{1,ii}, Q_{2,ii} \geq Q_{\mathbf{u},ii}$ for all $i \in \{1, 2, 3\}$ as minimizing the harmonic currents is of greater importance than penalizing the utilization of large active filter currents. As evident from (5.1)-(5.6), all three phases are decoupled from each other, which allows the use of independent distributed MPCs, one for each phase, according to [253]. This is a desired property, which might be crucial in the pursue of meeting the application's real-time demands. In the rest of this work the MPC will be treated as a single-phase MPC, according to the phase decoupling of the three-phase MPC formulation presented by (5.1)-(5.6).

5.2.2 Control and Hardware Layers

MPC is often used as higher level controller feeding one or multiple lower level controllers with setpoints or references (trajectories) to track, which forms a multi-layered solution involving both hardware and software. A simplified schematic of the control- and hardware layers for the optimal harmonic mitigation application discussed in this work is showcased in Figure 5.3. As can be seen in the figure, the MPC is part of the higher level control layer and interacts with the lower level control layer. The lower level control layer, which consist of the Active Power Filter (APF) controller and measurement processing, interacts with the MPC in the higher level control layer and the power system in the hardware layer. The amplitude and phase information from the harmonics to be mitigated are provided by FFT, or a suitable estimator. Other available measurements, which might involve impedance estimates, the main bus and generator currents and voltages, are also provided by the lower level control layer. Furthermore, the APF controller is fed with an optimal current reference calculated by the MPC. In this work the design of the higher level control layer will be treated, in which incorporates the lower level control layer as well as the hardware layer.

5.2.3 Control Philosophy

Maybe the most used control philosophy, where MPC is involved as a higher level controller, is to extract one or few points from the MPC's output control vector, which is fed to one or multiple lower level controllers and used as setpoints. The points extracted depends on the MPC's computational cost, i.e. if the MPC's time horizon is 10 seconds, with discretization of 10 steps (1step = 1s), and the MPC's time consumption is 1.5s, then the second point might be used as control action. This control philosophy is not suitable for the harmonic mitigation application presented in this work

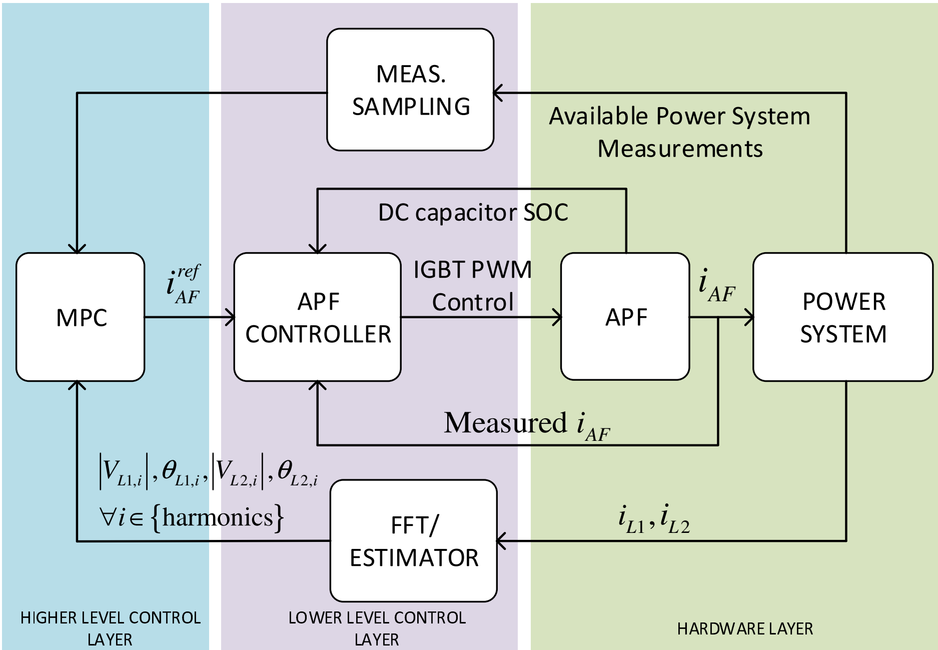

Figure 5.3: Multi-layered control- and hardware architecture for the optimal harmonic mitigation application using MPC: The MPC in the higher level control layer interacts with the lower control layer, while the lower layer control layer interacts with the hardware layer.

due to the inherent fast dynamics. The MPC must be able to provide a new setpoint/reference to the APF control at a specific time instance to assure harmonic mitigation properties. If the setpoint update is too slow, the active filter may inject harmonics contributing to a higher THD, thus failing to meet the designed control objective of harmonic mitigation.

Another control philosophy for CCS-MPCs, which is adopted in this work, is repetitive control. Instead of using only one or few points from the MPC's optimal future control vector, the whole vector is used to form a reference for the active filter to track. The MPC's optimization horizon can be designed to span one fundamental period, in which, due to the optimization problem's nature, give interesting properties that can be used for fault handling: If for instance the MPC fails to deliver a new control vector to the APF control within a finite deadline, the old control vector might be used once more for the next period. How to utilize this property of repetitive control will be discussed in more details later on.

5.3 System Architecture and Implementation

To obtain the required real-time properties for an MPC controlling a stiff system with fast dynamics might prove to be a challenge. Even if the MPC is able to meet the necessary real-time demands, the middleware, which is responsible for connecting the MPC to the rest of the system, might introduce additional critical latency which combined with the MPC's computational costs fail to assure the real-time demands. As important as thorough MPC design and tuning, the middleware should be designed to interact with the MPC and the rest of the system without unnecessary overhead. In the following the MPC implementation and the system architecture, including the middleware, is discussed. Moreover, a simple simulator architecture is proposed for the purpose of verifying the control system's real-time properties.

5.3.1 MPC Implementation

There exist many suitable software solutions and libraries for nonlinear MPC implementation, and two examples are CasADi [14] and the ACADO toolkit [116]. These simplifies the implementation since they provide an abstraction layer between the MPC specification and the numerical optimization software. In this work the ACADO toolkit is used due to its fast prototyping properties and real-time support [117]. ACADO comes with a higher-level C++ interface, where the MPC's model and specification are written in standard form. From this C++ interface, a highly efficient C code can be generated for the MPC. This approach has been adopted in this work using the MPC on standard form in (5.4), and the generated C code has been embedded in a larger system which will be discussed below.

To achieve the needed real-time properties, the discretization and optimization horizon, as well as integrator and Nonlinear Programming (NLP) solver, have to be chosen with care. These design parameters will be treated separately in the following:

5.3.1.1 Optimization Horizon

The control philosophy adopted in this work is of repetitive control. Repetitive control means that controls reappear in a repetitive manner, which

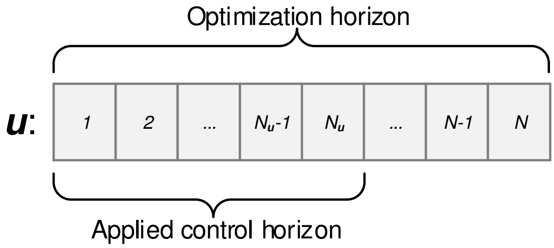

Figure 5.4: Visual representation of the control vector length: Optimization horizon discretization steps N, applied control steps $N_{\mathbf{u}}$, $N > N_{\mathbf{u}}$.

indeed is the case for harmonic currents. Harmonic currents introduce fast nonlinear dynamics, which requires a lot of computational effort. Therefore, instead of using one single step from each optimal future control vector calculated by the MPC, which is an often applied practice in MPC designs, a whole fundamental period of control steps (i.e. active filter currents) will be used. This requires the optimization horizon to be larger than one fundamental period (20ms for 50Hz), enabling an overlap between fundamental horizons. Such an overlap is important for keeping future changes in account, and assure optimality between fundamental periods. Moreover, by using a control vector which spans one fundamental period, the repetitive nature of the harmonic currents allows to reuse the same control vector (assuming approximately constant fundamental frequency) if the MPC fails to deliver a new control vector within the required deadline. A visualized representation of the applied control horizon and optimization horizon is given in Figure 5.4. If the fundamental frequency is not constant, the optimization horizon should be long enough to enclose the freqency variations' fundamental periods. This work assumes a fundamental frequency close to 50Hz, thus the optimization horizon is chosen to be 22ms and the applied control horizon is 20ms.

5.3.1.2 Discretization

The discretization should be chosen to represent the fastest dynamics under consideration, while on the other hand be chosen to satisfy real-time demands as an increased number of discretization steps introduce additional computational costs. Assuming a fundamental frequency of 50Hz, and assuming harmonics up to the 50th order, the Shannon-Nyquist sampling theorem (to avoid aliasing) states that the sampling frequency should be chosen as $2 \cdot 50\text{Hz} \cdot 50 = 5000\text{Hz}$. This gives a step size of 0.2ms, and for a 22ms optimization horizon a discretization of 110 steps is needed.

The discretization type (or method) is responsible to convert the MPC on standard form to NLP form, which can be solved by a suitable NLP solver. The most common discretization methods are single shooting, multiple shooting and collocation [22]. Multiple shooting is a refinement of single shooting. Unlike single shooting, which integrates a differential state throughout the horizon as one trajectory, multiple shooting divides the optimization horizon into elements. The elements are integrated separately, which gives better numerical stability and robustness due to decoupling of the elements. State constraints are enforced on each segment junction to ensure continuity between the elements throughout the horizon. Multiple shooting forms a larger NLP problem than single shooting, but, on the other hand, enables parallelization of element integration routines, which might give an advantage in the pursuit of real-time properties. Collocation, as with multiple shooting, divides the optimization horizon into elements, however, the state trajectories in a collocation scheme are approximated by polynomials on each control interval within the optimization horizon. Each polynomial is parametrized by interpolating points, which have the same dimension as the state space formulation and are extra decision variables in the NLP scheme. Even though the size of the NLP problem increases compared to multiple shooting, the polynomial approximations of the state trajectories often become easier to solve [22, 220], especially with highly nonlinear system equations, and the system matrices are often sparse which could be exploited by a sparse QP solver.

Both multiple shooting and collocation are good candidates for discretization type for the MPC application presented in this work, however, collocation is not yet supported by the code generation feature in ACADO. Hence, multiple shooting is chosen as the discretization type.

5.3.1.3 Integrator

The problem formulation presents a stiff nonlinear system, thus using a common integrator such as the Runge-Kutta of order 4 (RK4) will require a high number of integration steps. The RK4 integrator was implemented for the problem formulation in (5.4), and required 1500 integration steps to converge. Even with that high number of steps the solution was not sufficiently accurate. In addition, the high number of integration steps destroyed the real-time properties of the MPC. In this work the implicit Runge-Kutta Radau IIA of order 3 (RIIA3), which is an integrator that is able to handle stiff systems [102], is chosen with $2N$ (220) integrator steps.

5.3.1.4 NLP Solver

There exist a range of different NLP solvers with different properties that might fit the MPC proposed in this work. ACADO's code generation feature is currently supporting qpOASES [81] and FORCES [67], which are both Quadratic Programming (QP) solvers. qpOASES is an active set online QP solver, and ACADO provides different condensing techniques when using qpOASES to exploit the structure of the system matrices. FORCES is an interior point QP solver that exploit sparsity in the system matrices. As only qpOASES is open source, with available source code that can easily be embedded in a larger framework, the qpOASES solver is chosen in this work. Table 5.1 summarizes the implementation details of the MPC.

Table 5.1: MPC Implementation details.

Parameter	Value
Software	ACADO
Optimization horizon (T)	22ms
Applied control horizon	20ms
Discretization steps (N)	110
Applied control vector discretization steps ($N_{\mathbf{u}}$)	100
Discretization type	Multiple Shooting
Hessian approximation ($\nabla^2\mathbf{f}$)	Gauss-Newton
Integrator type	Implicit Runge Kutta Radau IIA 3 (IRK RIIA3)
Number of integration steps	220 ($2N$)
NLP solver	qpOASES
Number of iterations	2

5.3.2 MPC Framework and Architecture

In the design of a system architecture and framework, which comply with real-time demands, aspects such as threading, communication (middleware) and scheduling and execution of tasks with cross-thread synchronization need to be considered. In the wake of *Industrial Internet of Things* (IIoT), event-based architectures have gained a lot of attention. Unlike cyclic execution, which runs with a predefined cycle frequency, event-based architectures trigger on events, or signals, meaning that an event-based thread is in hibernation (latent) until an event arrives and triggers execution of the tread. Both cyclic and event-based architectures have desired properties that can be exploited in the design of the system architecture for the harmonic mitigation application addressed in this work. An example of desired property of the event-based architecture is minimal resource use, i.e. memory and CPU, while for a cyclic architecture is fast response. This is because an event-based thread that is latent (sleeping) does not consume processing resources, while a cyclic thread is running whether it is doing any work or not, which adds to the resource use. However, as the cyclic thread is constantly running, it does not have any invoking delay, which might be the case for an event-based thread, depending on the occupied system resources and processor scheduling at the time instant the event mechanism calls for task scheduling.

Figure 5.5 portrays the system architecture for the main controller, i.e. the controller running the MPC with suitable middleware and framework. In this work the term middleware is defined as communication between devices, while framework is defined as internal mechanisms that constitutes cross-thread communication and synchronization, internal memory allocation and information sharing. The blocks in Figure 5.5 represents threads, and for each tread a state-machine based on Unified Modelling Language (UML) [87] is presented. Cross-thread signals (events) are presented as connections between the threads. The communication (interaction) to the rest of the system (Figure 5.3) is also presented as arrows from and to the main controller block. In the following the blocks (threads) in Figure 5.5 will be treated separately. Thread names are referred to with bold font, while states and signals use italic font.

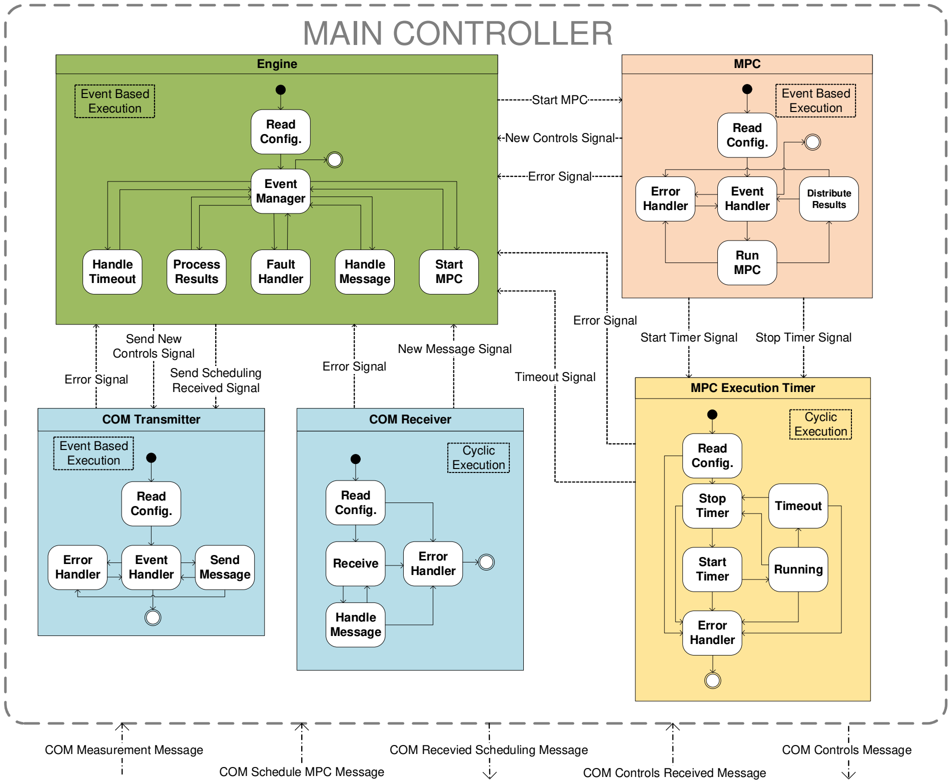

Figure 5.5: Simplified schematic of the main controller architecture. The different blocks (either cyclic or event-based execution) represents threads. The signals between the blocks are internal event-based signals. The arrows connected to the main controller block represents communication links with other devices, such as the simulator in Figure 5.6.

5.3.2.1 Engine

The **Engine** thread is the main component in the MPC framework; it is an event-based thread and act as an event manager, meaning receiving events from the other threads and determine appropriate actions, which are then distributed to the other threads as new events. As can be seen from Figure 5.5, the initial state in the **Engine**'s state-machine is responsible for reading configuration. This configuration is given as a XML file during startup, and includes configuration related to the MPC (parameters), the communication link (**COM Transmitter** and **COM Receiver** thread) and the **MPC Execution Timer** thread. The read configuration is then stored in the shared memory to be loaded by the other threads. As the **Engine** thread is the only thread reading the XML configuration file, all other threads are initialized after the Engine thread finishes reading and storing the configuration. After reading the configuration, the **Engine** goes to the *Event Manager* state and awaits events. Depending on the received events, the **Engine** may take different states. The *Handle Timeout* state handles the timeout of the MPC, i.e. if the execution of the MPC takes longer time than specified in the configuration file. An appropriate action is then to send the previously computed control vector to the active filter, which can be reused due to the repetitive nature of the filter currents and the applied horizon length equals one fundamental period. Another state is the *Process Results* state, which handles the resulting control vector after the MPC finishes. The control vector is then checked (length, discretization and amplitude) before being sent to the active filter controller through the **COM Transmitter** thread. The *Fault Handler* state handles faults from the different threads. Examples of faults could be communication error or the MPC is unable to provide a new control vector due to infeasibility. An appropriate action for communication error would be to check the return codes (error messages) from the erroneous sockets for further diagnostics to find the reason behind the errors. As a last resort the communication sockets might be closed and the communication threads reinitialized. For MPC infeasibility, depending on the cause, an appropriate action could be to rerun the MPC with new measurements, while sending the previously computed control vector to the active filter controller. The *Handle Message* state handles all messages received over the communication link, which is delivered by the **COM Receiver thread**. If a *Schedule MPC* message is received, a reply message is made and signalled to the **COM Transmitter** thread to be sent. This reply message can be omitted if a reliable protocol, such as TCP over Ethernet, is used. The last state, *Start MPC*, signals the MPC thread to start (if new measurements are available), and reallocates memory for a new control vector.

5.3.2.2 MPC

The **MPC** thread is also an event-based thread which is started when receiving a *Start MPC* signal from the **Engine** thread. As can be seen from Figure 5.5, the **MPC** thread has also a *Read Configuration* state, which reads the configuration from internal memory stored by the **Engine** thread. After the configuration is read, the *Event Handler* state is invoked. When receiving a *Start MPC* signal from the **Engine** thread, the state *Run MPC* is invoked. In this state a *Start Timer* signal is sent to the **MPC Execution Timer** thread before the MPC is run. When the MPC finishes, a *Stop Timer* event is signalled the **MPC Execution Timer** thread, before invoking the *Distribute Results* state. In this state the resulting control vector is stored in the controller's internal memory before signalling to the **Engine** thread that new controls are available. After this, a transition to the *Event Handler* state is made. In case of errors, which may result from the MPC (infeasibility, solver failure, etc.), the **MPC** thread enters the *Error Handler* state, which performs local diagnostics and signals an error message to be handled by the **Engine** thread. After the error message is sent, the **MPC** thread transitions back to the *Event Handler* state.

5.3.2.3 MPC Execution Timer

This thread is a cyclic thread which is invoked by the **MPC** thread. Its main function is to time the execution of the MPC. As with the previous threads, the **MPC Execution Timer** thread reads the configuration during startup, then enters the *Stop Timer* state. When signalled by the **MPC** thread, the **MPC Execution Timer** thread enters the *Start Timer* state, in which resets and start the timer before entering the *Running State*. If a *Stop Timer* signal is sent from the **MPC** thread before the timer times out, a transition to the *Stop Timer* state is made. On the other hand, if the timer times out, relative a predefined setpoint in the configuration, a transition to the *Timeout* state is made, which signals a *Timeout* signal to the **Engine** thread. Also this thread has an *Error Handler* state, which handles errors related to the timer object used. If the error is not solved locally, an *Error* signal is sent to the **Engine** thread for further investigation and appropriate actions to solve the error.

5.3.2.4 COM Transmitter

This event-based thread is responsible for sending information to other devices, i.e. handles external outgoing communication. As with the other threads this thread has also a *Read Configuration* state, which reads configuration related to the communication link. The communication link itself could be i.e Ethernet or serial connection. After the configuration is read, the thread enters the *Event Handler* state, and awaits events sent by the **Engine** thread. If events are received, i.e. a *Send New Controls* or *Send Scheduling Received* signal, the *Send Message* state is entered, which sends the message before transitioning back to the *Event Handler* state. Examples of messages are *COM Received Scheduling* and *COM Controls*, as depicted in Figure 5.5. As communication links may break down or fail, the thread also includes an *Error Handler* state. If the error is not solved locally, an *Error* signal is sent to the *Engine* thread for further action.

5.3.2.5 COM Receiver

This thread is a cyclic thread that check the communication link for new messages in a cyclic behavior. As with the other thread this thread also has a *Read Configuration* state which is entered after thread initialization. After the configuration is read the thread transitions to the *Receive* state. If a new message is received over the communication link, the thread enters the *Handle Message* state, which parses the message and copies its content to an appropriate data structure which is stored in the controllers internal memory. A *New Message* event is then signalled to the **Engine** thread, in which processes the message. Example of messages are *COM Measurement* and *COM Schedule MPC*, as depicted in Figure 5.5. As with the **COM Transmitter** thread, also this thread has an *Error* state in which communication errors will be handled. If the error is not resolved, an *Error* signal is sent to the **Engine** thread for further action.

5.3.3 Simulator Architecture

To test and verify the architecture of the main controller discussed in the previous section, a simulator architecture is proposed in Figure 5.6. As in the previous section, the different threads (blocks) will be separately discussed in the following. The **COM Transmitter** and **COM Receiver** threads adopt the same functionality as for the communication threads in the main controller in Figure 5.5.

5.3.3.1 Engine

The simulator's **Engine** thread is like the **Engine** thread in Figure 5.5, although simpler. It is an event-based thread and acts as an event manager. The states *Read Configuration* and *Handle Message* work just like the

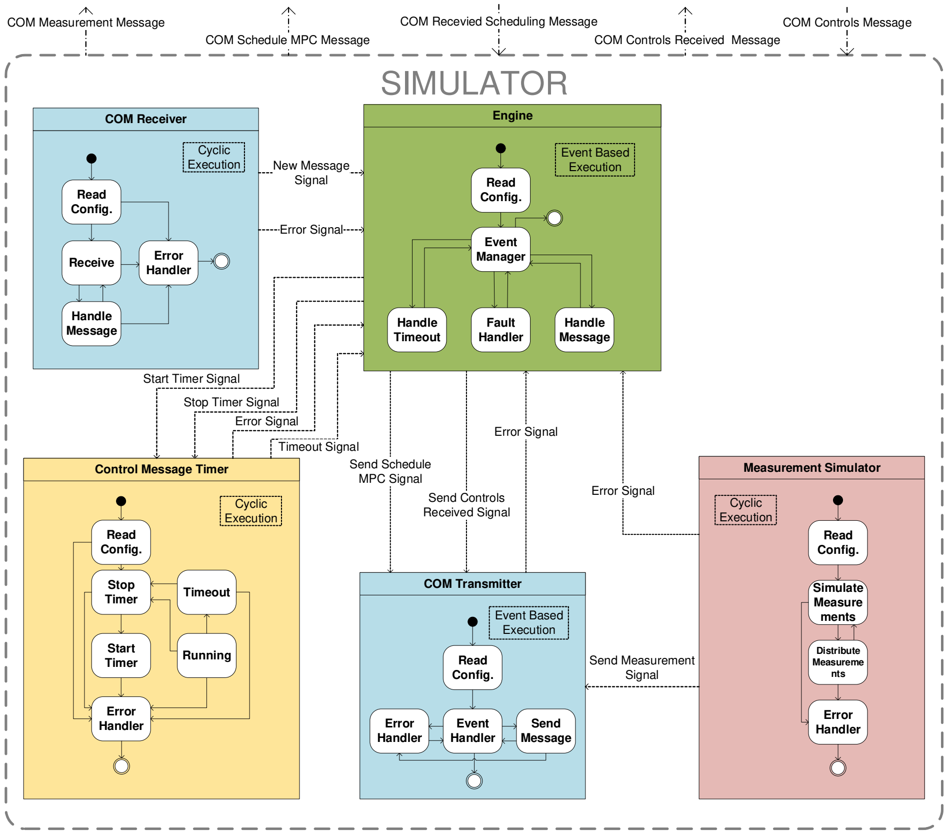

Figure 5.6: Simplified schematic of the simulator architecture, which includes measurement generation. The different blocks (either cyclic or event-based execution) represents threads. The signals between the blocks are internal event-based signals. The arrows connected to the simulator block represents communication links with other devices, such as the main controller in Figure 5.5.

coinciding threads in the main controller's **Engine** thread, except that the *Handle Message* state has functionality devoted for the types of messages that is received by the simulator's **COM Receiver** thread. As an example, if a *COM Controls* Message is received, depending on the communication protocol, a reply message should be sent to the main controller indicating the new control vector was received. Furthermore, the *Fault Handler* state is responsible for resolving errors that are not resolved locally by corresponding threads. The **Engine** thread also has a *Handle Timeout* state, in which is entered if the **Control Message Timer** thread distributes a *Timeout* event. Such an event is distributed if the time difference between sending a *COM Schedule MPC* message and receiving a *COM Controls* message exceeds a predefined threshold.

5.3.3.2 Measurement Simulator

The **Measurement Simulator** thread is a cyclic thread responsible for generating measurements that are distributed to the main controller through the **COM Transmitter** thread. The first state is the *Read Configuration* state, which reads the configuration that specifies how the measurement should be generated, e.g. which harmonic orders to generate, amplitude bands, phase bands and rate of change. After the configuration is read, a transition to the *Simulate Measurements* state is made, and in this state the measurements are generated. After the measurements are generated the *Distribute Measurements* state is entered, which packs the measurements in a suitable data structure that is sent over the communication link by the **COM Transmitter** thread by invoking a *Send Measurement* event signal. The **Measurement Simulator** thread also has an *Error Handler* state, in which handles errors related to the timer used for generating the measurements. If errors are not solved locally an *Error* signal is sent to the **Engine** thread for further investigation.

5.3.3.3 Control Message Timer

The **Control Message Timer** thread is also a cyclic thread. Its main function is to calculate the time difference between sending a *COM Schedule MPC* message over the communication link and receiving a new *COM Controls* message. The thread's state machine has the same structure as the **MPC Execution Timer** in Figure 5.5.

5.3.4 Synchronization of Measurements

Available measurements, which are sampled different places in the grid, are sent to the main controller after proper processing (noise suppressing and validation) to be used by the MPC. However, if not all the measurements are consistent, i.e. all the measurements are not sampled synchronously, leading to the MPC receives and uses some new measurement along with old measurements, the controls obtained from the MPC cannot be guaranteed to be valid. Thus, synchronization of the measurements are quite important for the MPC to provide a valid control vector. A proper synchronization procedure of the measurement devices might result in unnecessary high communication traffic and communication delay, thus might lead to measurement being invalid when reaching the MPC. As the measurements should be filtered to suppress measurement noise in the lower level control layer in Figure 5.3, an estimator such as a Kalman filter [35] can be used, which has both predictive as well as noise suppression capabilities. The filter's prediction capabilities allows to predict measurements at a desired time instance when measurements do not arrive simultaneously. As the design of measurement processing systems falls outside the scope of this work, this will not be discussed any further.

5.3.5 Communication Link

The communication link, which is supervised by the **COM Receiver** and **COM Transmitter** threads, is quite important for this type of application. The communication link must allow fast distribution of much data. For instance, if 100 active filter reference points (float representation with 32 bits) are to be distributed at least every 20ms, this means $\frac{100 \cdot 32\text{b}}{0.02\text{s}} = 160\text{kb/s}$, or 20kB/s. Even though this transmission rate does not include additional message overhead, which is protocol dependent, an RS-232 serial communication link is excluded. An alternative serial link that can be used is RS-485, but a more appropriate solution that has the needed transmission rate, and at the same time offers flexibility and N-to-N connection, is Ethernet with protocols such as TCP or UDP. Unlike the TCP protocol, in which can guarantee that the messages arrives their destination as long as the communication link is alive, UDP is a *best effort* protocol, where the arrival of important messages, such as the *COM Schedule MPC* and *COM Controls* messages in Figure 5.5 and 5.6, must be confirmed by separate reply messages (for this example the *COM Received Scheduling* and *COM Controls Received* messages). In this sense UDP has lower overhead compared to TCP, as the developer can decide which messages should be sent by *best effort* and which messages need arrival confirmation, however, arrival confirmation requires implementation of extra logic and functionality that handles reply messages and redistributes messages if confirmation is not received. UDP is widely used in the industry for communication between distributed control nodes and systems, and plays an important role in cloud based IIoT middleware without centralized servers.

5.3.6 Implementation Aspects

In this work, the MPC framework in Figure 5.5 and the simulator in Figure 5.6 were implemented in C++ with libraries from Qt [118, 235] for event management, with Linux as target platform. The threads are implemented as high priority threads. The communication link is realized using UDP over Ethernet. The message protocol is designed using JSON, which offers great properties in the design and prototyping of communication structure. JSON is promoted as a low-overhead alternative to XML, with great debugging and logging properties due to human-readable text to transmit data objects consisting of attribute-value pairs. JSON messages are also easily parsed and processed, and corrupt messages can easily be detected due to the JSON message identifiers, which encloses one message structure.

5.4 Hardware in the Loop Test

Hardware in the Loop (HIL) simulation tests are conducted with two computers connected to a local Ethernet network. One of the computers acts as the main controller running the MPC and its framework, while the other computer runs the simulator, as discussed in the previous section. The specifications of the two computers are listed in Table 5.2, and the HIL setup is showcased in Figure 5.7.

Table 5.2: Details of Main Controller and Simulator used in HIL test.

Main Controller	Simulator
Lenovo Thinkpad T440s	Lenovo Thinkpad P50
8GB memory (DDR3, 1600MHz)	24GB memory (DDR4, 2133MHz)
Intel® Core™	Intel® Core™
i7-4600U CPU @ 2.10GHz × 4	i7-6820HQ CPU @ 2.70GHz × 8
Graphics:	Graphics:
Intel® Haswell Mobile	Quadro M2000M/PCIe/SSE2
64-bit Ubuntu 16.04 LTS	64-bit Ubuntu 16.04 LTS
Low latency kernel:	Low latency kernel:
4.4.0-22 x86_64	4.4.0-22 x86_64

The parameters in the MPC's internal model is, according to Figure 5.2, listed in Table 5.3. As can be seen, the APF's power rating is set to 10% of the generator rating, which is a relative small filter. With a voltage level

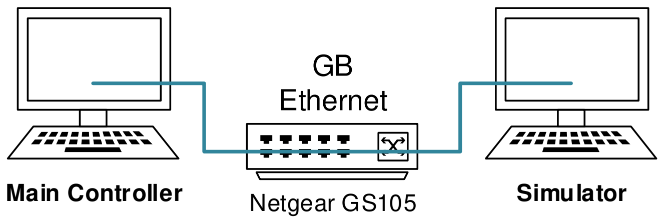

Figure 5.7: Hardware in loop setup: Two computers, one acting as the main controller running the MPC and its framework and the other running the simulator, connected to a local Gb Ethernet network.

of 690V this corresponds to current limits of $i_{\max} = -i_{\min} = \sqrt{2} \cdot \frac{50\text{kVA}}{690\text{V}} \approx$ 102.48A (peak current) in (5.3). Furthermore, the fundamental frequency is set to 50Hz, and the harmonics to be mitigated are the first four significant harmonic orders in a 6-pulse rectifier, i.e. 5th, 7th, 11th and 13th. The other electrical parameters are adopted from [218, 223].

Table 5.3: Power system model parameters, according to Figure 5.2.

Parameter	**Value**
RMS voltage	690V
Generator ratings	500kVA
APF rating	50kVA
L_{G1}, L_{G2}	30.309mH
R_{G1}, R_{G2}	9.512mΩ
L_{MB}	60.619µF
R_{MB}	1.904mΩ
C_1, C_2	2µF
Fundamental frequency (f)	50Hz
Harmonic orders to be mitigated	5th, 7th, 11th, 13th

The simulator, with architecture showcased in Figure 5.6, is responsible for generating the measurements that the MPC is using for optimal harmonic conditioning. The generated FFT amplitudes and phases, for the load currents in Figure 5.2, are shown in Figure 5.8. The measurements are designed to provide a dynamic spectra of the harmonics to be mitigated, with the intention to provide both low and high levels of harmonic pollution that

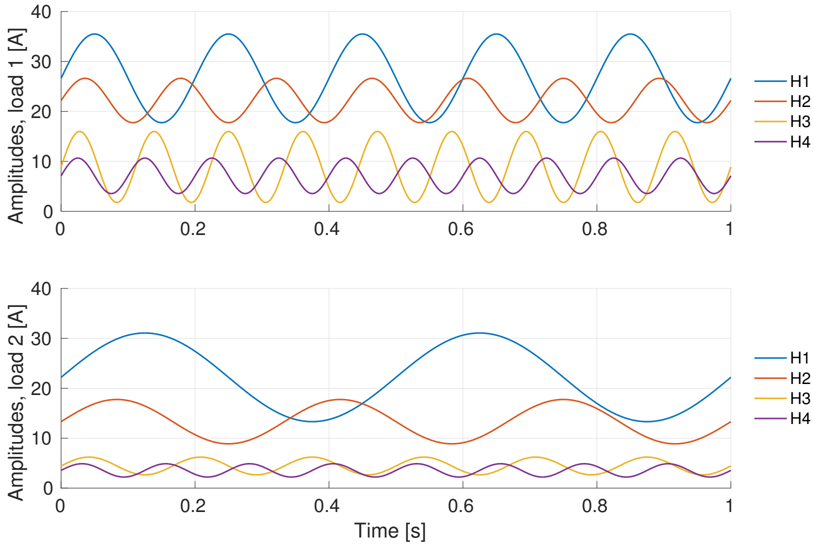

(a) FFT amplitudes.

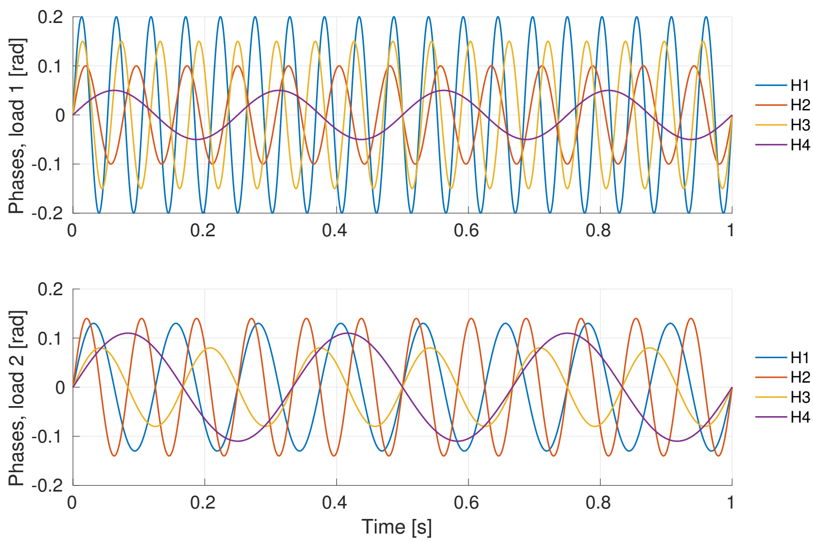

(b) FFT phases.

Figure 5.8: Simulated FFT amplitudes and phases for the four harmonic orders (H) to be mitigated: H1=5th, H2=7th, H3=11th and H4=13th.

challenges the MPC in different ways that might affect the MPC's computational costs. Hence, the measurements are not extracted from a physical (or simulated) power system, but designed to challenge the MPC's real-time properties. As the simulator does not provide closed-loop control, due to the fact that the HIL test is designed to test the MPC's real-time properties and not the harmonic mitigation capabilities (which has been thoroughly explored in [218, 223]), thus the state trajectories (voltages and currents) from the previous run of the MPC is used to initialize the states before a new run.

A HIL test was performed with 100.000 MPC runs, and the results are shown in Figure 5.9 and summarized in Table 5.4. Figure 5.9a shows the MPC's time consumption, which was calculated by the **MPC Execution Timer** thread in Figure 5.5, and the time between scheduling an MPC run and receiving the control vector (indicated in the figure by *Receiver side*) calculated by the **Control Message Timer** thread in Figure 5.6. The difference between these timers represents the pipeline in the figure, including transmission delays and framework delays. The additional latency experienced by the receiver side, which is shown as spikes in Figure 5.9a for the pipeline, might be related to other high priority background processes running on the controllers, additional latency introduced by the framework and/or by the switch in the HIL setup in Figure 5.7.

Table 5.4: HIL results summary of Figure 5.9.

Time measurement	**Avg.** [ms]	**Max** [ms]	**Min** [ms]	**Histogram Peak** [ms]
MPC	8.74	12.77	5.02	8.80
Receiver side	9.53	14.47	8.70	9.55
Pipeline	0.79	3.31	0.47	0.77

Figure 5.9b portrays a histogram of the time consumptions in Figure 5.9a. As can be seen in the figure, the time consumption of the MPC, the receiver side and the pipeline all give single characteristic peaks in the histogram, which represent consistent time consumption within stochastic distributions. Table 5.4 summarizes Figure 5.9, and as the receiver side's maximum time consumption is below 20ms, there is no need to reuse any control vectors. Hence, the real-time properties of the MPC and the architecture in Figure 5.5 and 5.6 for this HIL test are assured.

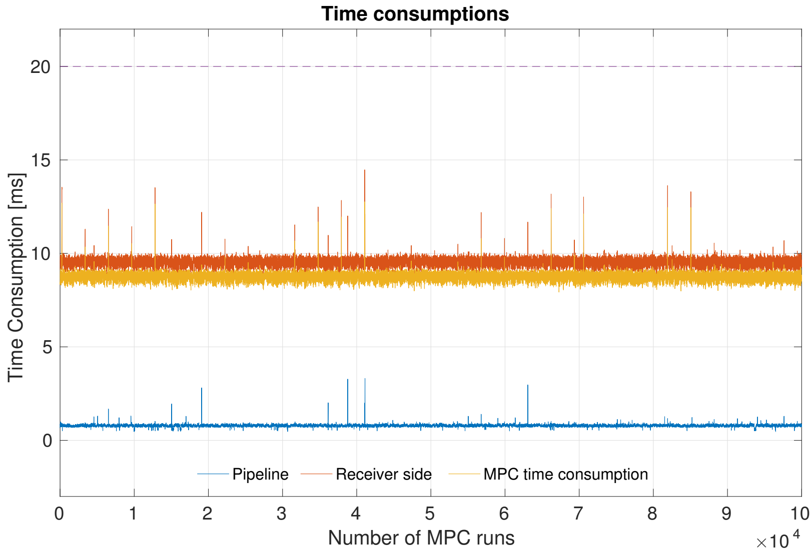

(a) Time consumptions of the HIL test.

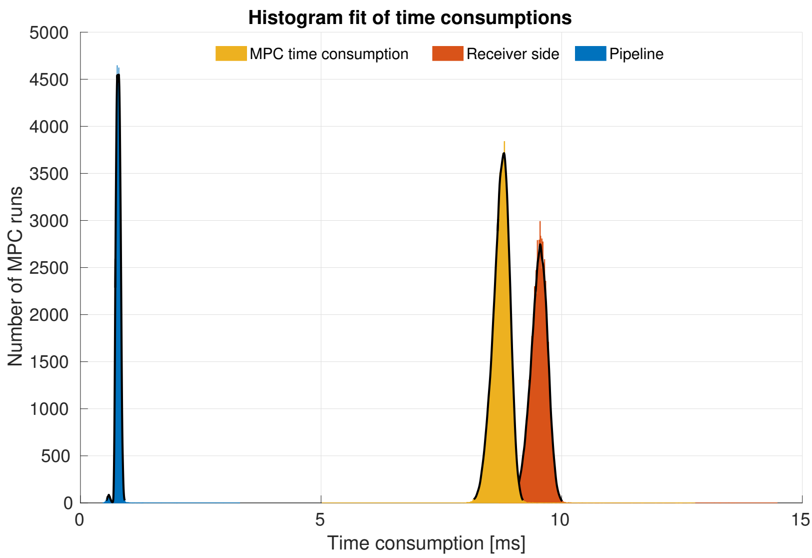

(b) Histogram fit of time consumptions from the HIL test.

Figure 5.9: Results of the HIL test: Time consumption of the MPC, of the pipeline and the time between scheduling an MPC run and receiving the control vector from the simulator side.

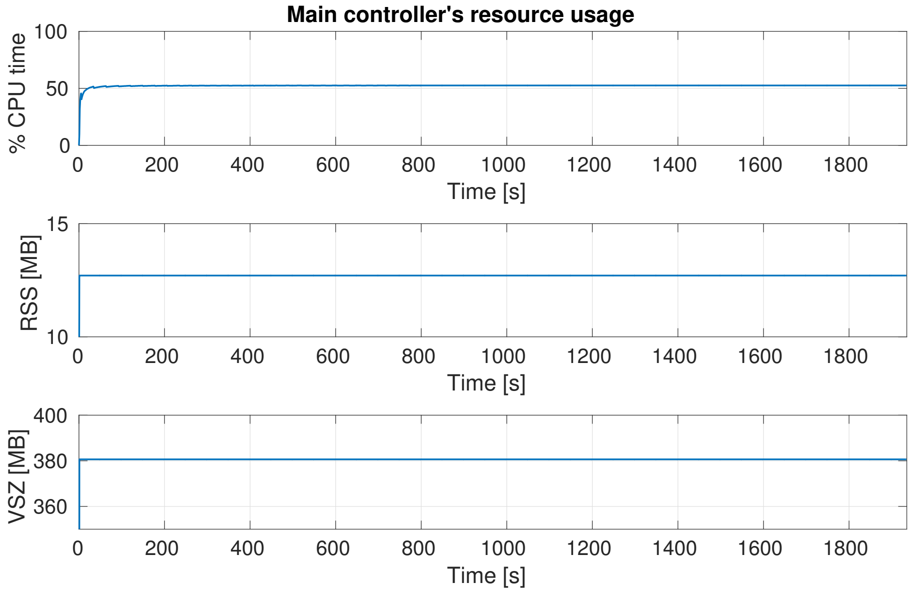

Figure 5.10: The main controller's resource usage during HIL test, sampled at 1Hz. From above: i) % CPU time, which is the CPU time used by the application divided by the time the application has been running, ii) RSS (resident set size) is the non-swapped physical memory (RAM) that the application currently is using, iii) VSZ (virtual set size) is the memory size assigned to the application and represents how much memory the application has available for its execution usage (allocated address space).

Figure 5.10 shows the resource use of the main controller during the HIL test, sampled at 1Hz. The upper plot shows the percentage of CPU time used by the application, the plot in the middle shows the physical memory currently used by the application (RSS), while the lower plot shows the total memory the application has allocated for its execution (VSZ). From the plots it is evident that the application running on the main controller is quite steady in its resource usage. The % CPU time settles around 52.5%. The RSS and VSZ are constant throughout the HIL test, 12.7MB and 380.6MB respectively.

5.5 Conclusion

MPC applications for systems with fast dynamics are challenging, and put stringent requirements on the implementation, which relates to the design and the internal mechanisms of the MPC as well as its framework and middleware connecting the MPC application to the physical system. In this work a novel MPC application for optimal harmonic mitigation has been presented, and the system design and architecture for obtaining the necessary real-time properties has been discussed and implemented. To obtain the required real-time properties, the design of the MPC has been centered around the repetitive control philosophy, which enables the utilization of larger parts of the calculated control vector compared to conventional MPC designs, which uses only one or few steps from the obtained control vector. The proposed system architecture uses both cyclic and event-based threads with the aim of minimizing the resource usage. Furthermore, a simulator was designed to verify the MPC's and the framework's real-time properties, a HIL test using two computers connected to a dedicated Ethernet link was conducted. The results show that the proposed system architecture assures the system's real-time demands with consistent and relatively low resource usage. Even though the results indicates that the application, with the proposed architecture, holds the required real-time properties, this work is only centered around the higher level control layer in Figure 5.3. Hence, future work has to be conducted for realizing the lower level control layer, thus enabling possibilities for experimental tests where the complete system is considered

Part III

Energy Management

CHAPTER 6

Approaches to Economic Energy Management in Diesel-Electric Marine Vessels

Recently, the efficiency of diesel-electric marine vessels has been subject for discussion with focus on improving fuel efficiency, reducing the environmental footprint from emissions of greenhouse gases, as well as reducing running hours and maintenance costs. This chapter, which is based on the reformatted version of [215], presents an analysis of load profiles extracted from three different vessels during operation; a ferry, a Platform Supply Vessel (PSV) and a seismic survey vessel. The analysis of the extracted data shows that the loadings of the diesel engines are typically quite low, and do not fall within the optimal loading range of diesel engines' Specific Fuel Oil Consumption (SFOC) curves. Furthermore, three different power plant configurations are proposed and compared, which include fixed speed (diesel-engine-generators) gensets, variable speed gensets and implementation of an Energy Storage System (ESS). Moreover, Energy Management System (EMS) algorithms based on Mixed Integer Linear Programming (MILP) are proposed as a suitable strategy for optimal unit commitment in the power generation. The results yielded from the MILP algorithms are compared to EMS algorithms based on logic such as if/else statements. The results indicate that optimal EMS algorithms in combination with a revised vessel configuration can increase the operational efficiency, in terms of fuel savings and reduction in genset running hours.

6.1 Introduction

The world's maritime fleet, due to widespread use of fossil fuels, is currently an unnecessary large contributor to greenhouse gases and other emissions. Moreover, many marine vessels are not operated in an optimal way, where the fuel consumption is in line with the power demand. As up to 90% of a vessel's power generation capability may at some point be locked into the propulsion units [139, 218], and the fact that the propulsion demands tend to be highly dynamic for a wide range of different marine operations in varying weather conditions, often more diesel engine generators (gensets) than actually needed to supply the consumers are online. However, running more gensets than needed, i.e. the online power generation capability exceeds the power demand with remarkable margins, often causes the loading of each genset to be lowered with the effect of moving the Specific Fuel Oil Consumption (SFOC, $\frac{\mathrm{g}}{\mathrm{kWh}}$) away from its optimum [54, 227]. To run more gensets than needed (spinning reserve), often with open bus ties, is for some types of operation a redundancy requirement from stakeholders with the purpose of preventing partial or total loss of (vital) power in occurrences of faults and component failures. The remaining healthy power bus with its enabled gensets are supposed to, with no further delays, replace the power demand from the faulty power bus. Such requirements are particularly enforced for Dynamic Positioned (DP) operations during safety critical operations denoted as consequence class 2 according to regulations by the International Marine Organization (IMO) and national authorities [176, 186].

Loss of power can have severe consequences, which may not only cause severe material and environmental damage and put human lives at risk, but may also lead to economic penalties for the vessel's operational responsible, in terms of financial claims and exclusion from pending or future contracts. Stories from multiple vessels' crew indicate that non-optimal unit commitment, in the sense of having more gensets online than needed (exceeding required spinning reserves) with non-optimal loadings, is a widespread practice introduced by distrust of the Power Management System (PMS) and a risk of not being able to supply the vessel's, and thus the given operation's, required (and vital) load demands. Examples of such demands may be navigation and bridge systems as well as loads originating from propulsion units and winches during e.g. DP, heavy lifts and anchor handling operations. One can speculate that also lack of knowledge and incentives allows the crew in non-safety critical operations to operate with open bus ties with multiple gensets enabled, which cultivates non-optimal unit commitment, wasting fuel and increasing the emission of greenhouse gases.

The benefit of optimizing the power generation, and at the same time minimize fuel consumption by running gensets with optimal loadings relative their lowest SFOC, is not only limited to achieve cost-efficient operations. By minimizing the fuel consumption the emission of greenhouse gases is also reduced, which, due to the global goals of reducing environmental footprints, is an increasingly important requirement. January 1st 2015 IMO implemented Emission Controlled Areas (ECA), which specify stringent requirements for allowed emission of NO_x, SO_x and particle matter for selected areas [128]. In the near future, due to the stringent emission requirements near shore, it might also be expected that marine vessels are required to conduct emission-free approaches to harbor, which calls for energy storage and more advanced control algorithms, thus taking steps towards All Electric Ships (AES).

The use of ESS can enable emission-free approaches to harbor, but can also facilitate optimal power generation in terms of optimal loading of gensets. In situations where the online genests are running with low loading conditions, the ESS can be charged, which allows for an increase in generator loadings towards optimal SFOCs. With a fully charged ESS, one or multiple gensets may be shut down and their supply of power substituted by discharge of the ESS. There exist a range of different Energy Storage Systems (ESS), ranging from mechanical, thermal and chemical to electrical systems. Some examples are Battery Storage System (BESS), Pumped Hydro Storage (PHS), Compressed Air Energy Storage (CAES), Superconductive Magnetic Energy Storage (SMES), fuel-cells, flywheels and super-capacitors [11, 21, 120, 169, 265]. For a marine vessel it has also been proposed to use the DP system and the vessel's position as a short-term energy storage [133]. The differences between ESS technologies can be generalized and listed as capacity, charge and discharge rates, weight, cost (including maintenance) and expected lifetime. The type of ESS should be chosen relative to the application. For example, in peak-shaving applications high charge/discharge rates of the ESS may be more critical than high capacity, while high capacity might be more critical in situations where the ESS is substituting a genset. Implementation of ESS can take many forms and can be part of both AC and DC distribution systems [143, 218]. Even though the employment of ESS can be beneficial for overall efficiency, and adds to power redundancy and flexibility, the control of the ESS and the generator scheduling (also called unit commitment) is critical to achieve optimal power generation with reduced fuel consumption and emissions.

Examples of optimal control schemes that have been employed for power and energy management applications are Model Predictive Control (MPC) and Linear/Nonlinear Programming (LP/NLP) algorithms. In [100] an LP algorithm is applied to control the power balance in a vessel with diesel-electric power generation and batteries, where the efficiency of each diesel engine is regarded in the objective function. The output of the LP scheme dictates the amount of power delivered from each genset and the power flow to or from the battery. A Mixed Integer Nonlinear Programming (MINLP) approach for optimal sizing of ESS and economic dispatch of controllable units for a shipboard power system is explored in [15]. In [210] an MPC for real-time power management in a marine vessel with different power generation devices, including batteries, fuel-cells and gas turbines, is addressed. [19] includes a generator dispatching algorithm based on optimization (LP) in the EMS design for power sharing purposes. An optimal power management system strategy based on dynamic programming, which includes ESS and emission limitations, is addressed in [134]. Another approach, based on theoretical optimization, is addressed in [264], which optimizes the efficiency of AES with dc hybrid power system and ESS. Unlike optimal scheduling of gensets and control of ESS, also the demand-side can be controlled by adjusting the power consumption of the electric propulsion units. Such an approach, which is based on dynamic programming, is explored in [135]. Some of the applied optimal power management and optimal control strategies in the automotive industry might also be applicable for marine vessels [136, 142, 167, 168, 173, 244, 246]. It is also expected that further development of ESS for these industries will enable even more cost-effective solutions for the maritime industry as well. It should be mentioned that the energy management of the power plant of an advanced ship is a highly multi- and inter-disciplinary challenge, involving the fields of internal combustion engines, electric power generation and distribution, battery technology, control engineering, and maritime operations, safety, rules and regulations.

The main scientific contribution in this work is the analysis of experimental vessel data from normal operation to shed light on the potential for employing ESS and optimization-based unit commitment (generator scheduling). Moreover, three Mixed Integer Linear Programming (MILP) EMS algorithms are proposed for optimal scheduling of fixed-speed gensets, i) with ESS, ii) without ESS and iii) without ESS and substitution of one fixed-speed genset to a variable-speed genset. Furthermore, the algorithms are assessed on the load profiles extracted from the real vessel data and compared with logic-based EMS algorithms, that utilize if/else statements, with the same objectives. In this way, the impact of the ESS and EMS on the vehicle operation can be predicted.

The chapter is organized as follows: Section 6.2 presents and discusses load profiles and power generation profiles extracted from three different vessels in operation. Section 6.3 presents three different power generation configurations along with corresponding EMS algorithms based on MILP. Section 6.4 evaluates the proposed MILP algorithms, along with logic-based algorithms, on the data extracted from the three vessels to conduct a theoretical study exploring the differences between the three proposed configurations. Finally, section 6.5 concludes the chapter.

6.2 Data Extracted from Vessels in Operation

Operational data from three different vessels, i) a ferry, ii) a Platform Supply Vessel (PSV) and iii) a seismic vessel, have been collected. The collected data are extracted using the vessels' Integrated Automation Systems (IAS), and include generator loadings and, except the data collected from the ferry, propulsion loads. All three vessels have diesel-electric propulsion systems, and as the emergency generators were not in use during the period the data were sampled, these have been omitted from the analysis. The loads from each propulsion unit, if available, have been added for each vessel for visualization purposes. The vessels' names are kept anonymous, as well as specific device and component names, which was a requirement set by the stakeholders owning the data used in this work. The sampling frequency used to log the experimental data is limited to ≤ 1 Hz. Hence, with this low sampling frequency, fast high-frequency dynamics such as harmonics and fast transients are not captured. It is not in the scope of this work to analyze such dynamics but to assess a long-time trending of the vessels' load profiles in the search of configurations and algorithms that cultivate fuel efficiency. For the collected operational data from the three vessels under investigation, the grid configuration relative to the different operational profiles the vessels exhibit, i.e. open or closed bus-ties, is not known. In the following, the collected operational profiles from each vessel will be visualized and discussed.

6.2.1 Ferry

The first vessel under investigation is a ferry with power plant configuration given in Table 6.1. As can be seen from the table, the vessel has two smaller gensets (G2 and G3) and two larger gensets (G1 and G4), and has two propulsion units, one at the stern and one at the bow. The sampling of the data set was started around 13:00 pm and stopped around the same time the following day, with sampling frequency of 1 Hz, spanning a 24 hour horizon. The vessel's load profile and generated power profiles from each genset are visualized in Figure 6.1.

Table 6.1: Ferry configuration and data set information.

Parameter/Component	**Value/Rating** (each)
Machinery:	
2× Diesel engine	1200 kW
2× Diesel engine	640 kW
Propulsion system:	
2× (twin-propeller) rudder-propeller	1200 kW
Data set:	
Length	≈24 hr
Sampling frequency	1 Hz

The ferry uses, at minimum, about 25 minutes for each crossing, and conducts 40 crossings within the sampled 24 hour horizon. In this sense, the ferry exhibits two different operation profiles, i.e. transit (crossings) and docking. Figure 6.1a, which portrays the vessel's load profile over the 24 hours horizon, shows quite varying load profiles for each crossing. In the start of the horizon, from about 1 to 3 hours, the ferry is a bit delayed, hence, does not slow down when approaching harbor. Instead, the ferry maintains speed as long as possible and reverses the propulsion units, with high Revolutions Per Minute (RPM), to slow down, which is clearly visible in the figure by the high power peaks stretching above 1.5 MW. In fact, this type of approach requires an additional genset to be started, which can be seen in Figure 6.1b where genset 3 (G3) is brought online after 1 hour and after 2.5 hours into the sampled data horizon. This approach is not an economical approach, as an additional genset is started, and is only conducted when the ferry is delayed.

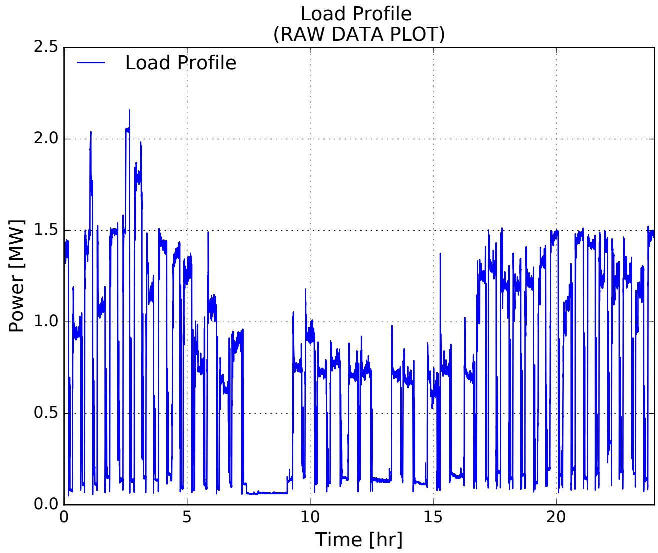

(a) Load profile.

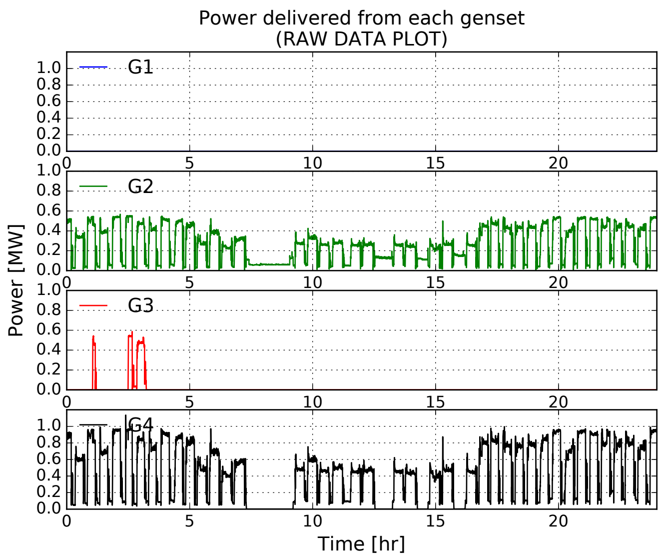

(b) Power delivered from each genset.

Figure 6.1: Measured data from ferry (approximately 25 minutes duration for each crossing): (a) shows the vessel's load profile while (b) shows the power generated by (and delivered from) each genset.

Furthermore, before starting the night crossings, the ferry takes a break with, among other things, a crew shift. This is visualized in Figure 6.1a between approximately 7 and 9 hours into the data set. The night crossings are scheduled with more time between each crossings, hence the ferry can conduct the crossing with a slower pace. This is seen in Figure 6.1a between approximately 9 and 15 hours, where the load profile is overall reduced, and is confirmed by the power delivered from each genset in Figure 6.1b. After the night, the morning rush and the daytime scheduling of the crossings starts, around 17 hours, which requires the ferry to increase the pace of each crossing. This is again confirmed by the load profile in Figure 6.1a and the power delivered from each genset in Figure 6.1b.

From Figure 6.1b one can see that each genset, which is online, takes a range of different loadings. The smaller genset G2, which is online during the whole operational horizon, has in average a loading of 263 kW, which corresponds to approximately 42% of the genset's total rating. Moreover, during the break, only G2 is online, with a loading of approximately 60 kW (9.4%). The genset rating is even lower while in harbor between the crossings, with as low as 21 kW (3.3%). Also the larger G4 genset takes a range of different loadings, ranging from about 37 kW (3.1%) to 1136 kW (94.7%). A summary of the minimum, maximum and average loadings, calculated from the online gensets, are listed in Table 6.2. A low rating of the gensets, in addition to have poor SFOCs, increase sooting of the prime movers and might lead to increased frequency of the engines' service (maintenance) intervals. Clearly, the ferry could benefit of an ESS to handle the low power demands while docking in harbor, and also keep the running gensets close to their optimal loading conditions by coordinating starting and stopping (scheduling) of gensets in accordance with the ESS' charge and discharge cycles. An ESS would also be able to supply additional power for fast approach to harbor if the ferry is delayed, thus, with the right power and capacity rating, eliminating the need for starting an additional genset.

6.2.2 Platform Supply Vessel (PSV)

The next vessel under investigation is a Platform Supply Vessel (PSV). This vessel can be seen as a multi-purpose vessel that can conduct a range of different offshore operations. Such operations might for instance involve dynamic positioning (or station keeping) as well as winching and pumping operations, with highly dynamic load profiles. The power plant configura-

Table 6.2: Ferry: Maximum, minimum and average genset loadings.

Genset	Min. power	Max. power	Avg. power
G1	0 kW (0.0%)	0 kW (0.0%)	0 kW (0.0%)
G2	21 kW (3.3%)	567 kW (88.6%)	263 kW (41.1%)
G3	40 kW (6.3%)	587 kW (91.7%)	355 kW (55.5%)
G4	37 kW (3.1%)	1136 kW (94.7%)	517 kW (43.1%)

tion of the PSV treated in this work is listed in Table 6.3. Also this vessel has four gensets, two smaller (G2 and G3) and two larger (G1 and G4). The vessel has five propulsion units, ranging from azipull to bow- and azimuth thrusters. The data set spans a 1056 hours horizon (44 days), and is sampled with a frequency of 0.2 Hz. The vessel's total load profile, as well as the propulsion load profile and power delivered from each genset are portrayed in Figure 6.2.

Table 6.3: PSV configuration and data set information.

Parameter/Component	**Value/Rating** (each)
Machinery:	
2× Diesel engine	2350 kW
2× Diesel engine	994 kW
Propulsion system:	
2× Azipull	2200 kW
2× Bow thruster	880 kW
1× Bow azimuth (retractable)	880 kW
Data set:	
Length	≈1056 hr
Sampling frequency	0.2 Hz

The total load profile as well as the propulsion load profile is visualized in Figure 6.2a. The difference between the total load profile and the propulsion load profile, which can be seen in the lower plot in Figure 6.2a, constitutes the auxiliary load demands, as well as power losses related to power conversion and the distribution grid. Unlike the ferry discussed in the previous section, the characterization of the different operational profiles is not clear from the PSV's load profile. In fact, during the sampling of the data from the PSV, the different operations were not logged, and thus unknown for

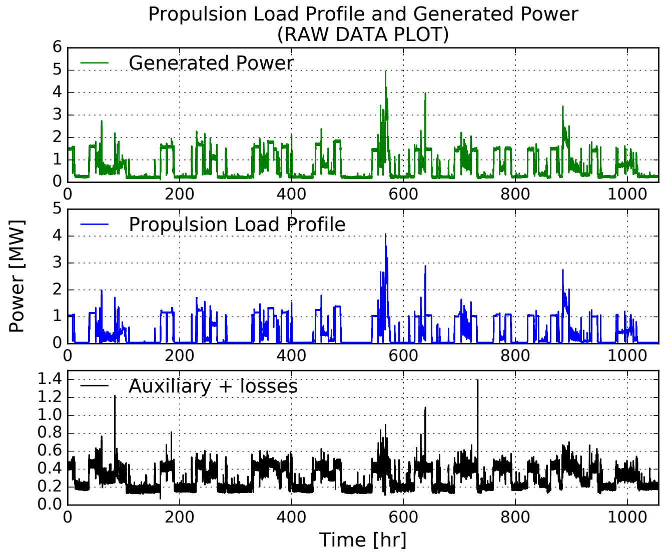

(a) Generated power and propulsion load profile.

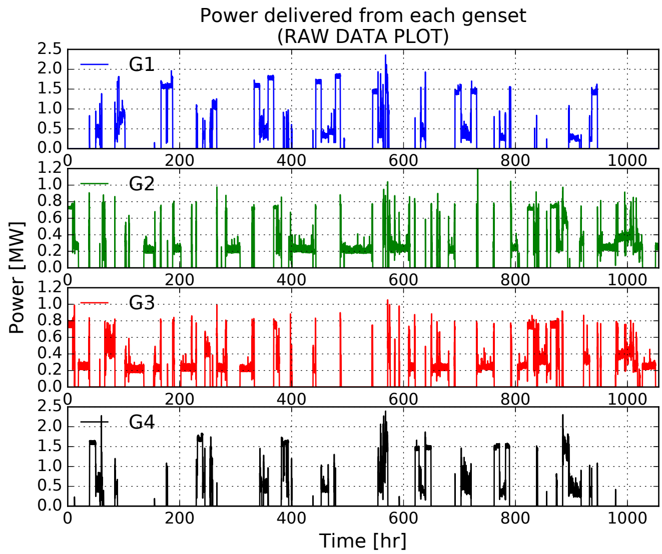

(b) Power delivered from each genset.

Figure 6.2: Measured data from PSV: (a) shows the vessel's generated power profile, propulsion load profile and the auxiliary load profile, while (b) shows the power generated by (and delivered from) each genset.

the data set presented in this work. However, from the load profile, one can clearly see some of the same behavior as with the ferry's operational profile while in harbor, where the load demand is reduced. The PSV's data set also includes some peaks, especially around 570 hours into the data horizon, which is manifested in both the propulsion load profile and the auxiliary load profile in the lower plot in Figure 6.2a. For the highest peak in the propulsion load profile, about 4138 kW is locked in the propulsion system, which corresponds to about 61.9% of the vessel's main power generation capacity. The total load demand at this time instance is about 4977 kW (74.4%), and only genset 1 and 4 (G1 and G4) are supplying the load demand, which can be seen in Figure 6.2b.

Furthermore, the scheduling of the gensets, as well as the individual genset loadings, for the whole data set horizon, are presented in Figure 6.2b. As can be seen from the figure, the loading of each genset is quite dynamic, and the gensets are scheduled (started and stopped) to fit the varying aggregated load demand. The main findings from Figure 6.2b, which include maximum and minimum power, as well as average power, delivered from each genset while online, are listed in Table 6.4. As shown in the table, all gensets are at one point overloaded, exceeding 100% of rating. It is not known which kind of operation(s) caused the overloading of the gensets. The lowest genset loading is found for G4, with a loading of 5.2% relative to its rating. In addition, optimal SFCOs for diesel engines tend to be with loadings between 60-100% [7], thus the average delivered power from each genset, which are found to be below 40%, does not cultivate fuel efficiency. Hence, it is speculated that also this vessel would benefit of an ESS and a more advanced unit commitment strategy to keep the genset loadings close to the optimal loading dictated by each diesel engine's SFOC curve.

Table 6.4: PSV: Maximum, minimum and average genset loadings.

Genset	Min. power	Max. power	Avg. power
G1	138 kW (5.9%)	2360 kW (100.4%)	892 kW (38.0%)
G2	77 kW (7.7%)	1198 kW (120.5%)	333 kW (33.5%)
G3	61 kW (6.1%)	1054 kW (106.0%)	346 kW (34.8%)
G4	123 kW (5.2%)	2394 kW (101.9%)	887 kW (37.7%)

6.2.3 Seismic survey vessel

The last vessel under investigation is a seismic survey vessel. Such vessels usually tow enormous amounts of equipment, e.q. 8-12 streamer sets which can span up to 10 km each, while conducting offshore seismic survey operations. In addition, the canons used to generate sound waves for exploring the different layers of the geological formations use compressed air. Hence, high propulsion and compressor loads often constitute the main load demands in many of the seismic survey vessel's operational profiles. The seismic survey vessel treated in this work has four gensets of equal rating. The vessel's propulsion system consists of five propulsion units, including Controlled Pitch Propellers (CPP), bow and stern thrusters and a retractable azimut thruster. The data set is sampled during seismic operation, spans 1066 hours (44.4 days), and is sampled with a frequency of 0.2 Hz. The configuration of the vessel, as well as data set information, are listed in Table 6.5. The vessel's total load profile, propulsion load profile, compressor load profile and power delivered from each genset are portrayed in Figure 6.3.

Table 6.5: Seismic survey vessel configuration and data set information.

Parameter/Component	**Value/Rating** (each)
Machinery:	
4× Diesel engine	3060 kW
Propulsion system:	
2× Controlled pitch propeller	4800 kW
1× Bow thruster	830 kW
1× Stern thruster	830 kW
1× Bow azimuth (retractable)	850 kW
Data set:	
Length	≈1066 hr
Sampling frequency	0.2 Hz

The total load profile, i.e. power delivered by the gensets, the propulsion load profile and the compressor load profile are visualized in Figure 6.3a. The lower plot in the figure is the difference between the power delivered by the generators and the sum of the propulsion and compressor load profile, and represents additional (auxiliary) loads, as well as power losses in components in the distribution system. From the figure one can see that

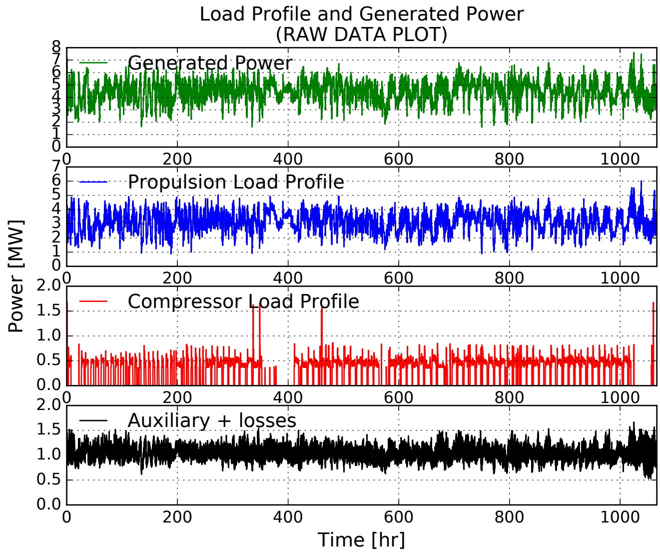

(a) Generated power and propulsion load profile.

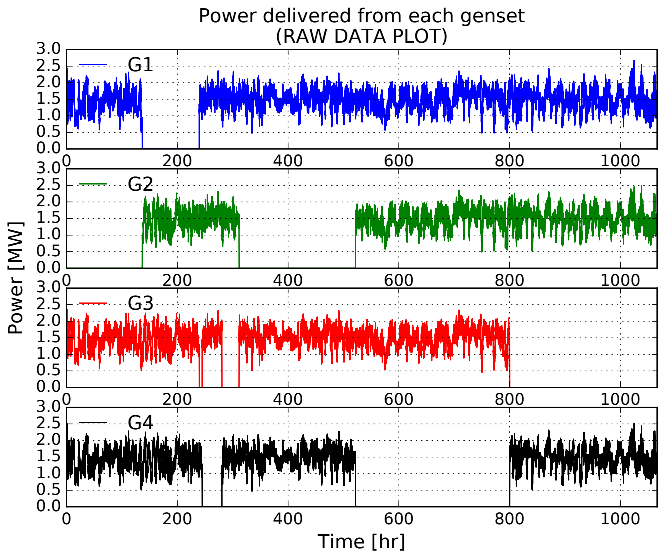

(b) Power delivered from each genset.

Figure 6.3: Measured data from seismic survey vessel during seismic operation: (a) shows the vessel's generated power profile, propulsion load profile, compressor load profile and the auxiliary load profile, while (b) shows the power generated by (and delivered from) each genset.

the total load demand (generated power) is more stable than for the load profiles for the ferry and the PSV. Also the propulsion load profile is more stable, as the vessel performs a fixed low-speed towing operation of seismic equipment. The stable load profiles confirms that the seismic vessel exhibit few different operational profiles during the period the data were sampled. Even though the propulsion loads are the main contributors in the total load profile, the compressor load profile is significant. As shown in Figure 6.3a, the compressor load has a distinct pattern, which shows that the vessel's compressors are started to fill tanks with compressed air, and stopped when the tanks are full. The number of compressors started determines the amplitude of the compressor load profile. The auxiliary power demand is also quite stable, and higher than the auxiliary load in the PSV. The high auxiliary load is expected due to power demand of the long tail of seismic measurement equipment the vessel is towing.

The individual generated power and scheduling of each genset are visualized in Figure 6.3b. The figure confirms the stable load profiles in Figure 6.3a. Also, compared to the PSV data set, the gensets are almost not scheduled at all (started and stopped). Gensets G1-G2 are scheduled two times each during the horizon, while the G3 and G4 gensets are scheduled three times. The low scheduling frequency is expected, due to the stable (and high) load profile. Table 6.6 lists some of the main findings from Figure 6.3b; the maximum, minimum and average loadings of each genset. As can be seen, the minimum loadings of each genset are higher than for both the ferry and the PSV. Moreover, the maximum loadings of the gensets are lower compared to the PSV. The average loadings are higher than for the PSV, meaning a more efficient fuel utilization, relative to the optimal SFOCs. However, with a suitable and proper dimensioned ESS, as well as more advanced Energy Management System (EMS) algorithms, it is speculated that the genset loadings could be kept closer to the optimal SFOC, thus cultivate more fuel-efficient operations.

6.3 EMS Algorithms

The main difference between a PMS and an EMS is that a PMS controls the vessel's power plant at instantaneous time with the purpose of stabilizing voltage and frequency and meet load demands, while an EMS often considers events in past and present along with future predictions/estimates. An Energy Management System (EMS) is often considered as part of a

Table 6.6: Seismic survey vessel: Maximum, minimum and average genset loadings.

Genset	Min. power	Max. power	Avg. power
G1	474 kW (15.5%)	2675 kW (87.4%)	1481 kW (48.4%)
G2	490 kW (16.0%)	2497 kW (81.6%)	1478 kW (48.3%)
G3	462 kW (15.1%)	2323 kW (75.9%)	1490 kW (48.7%)
G4	468 kW (15.3%)	2520 kW (82.4%)	1466 kW (47.9%)

Power Management System (PMS) that includes ESS and/or different types of power producers along with additional supervisory functionality. Some EMS/PMS today include decision support, however, scheduling of gensets is often considered a manual operation and conducted by the crew. As genset scheduling is a difficult task, where multiple aspects must be addressed, the way of manually scheduling the gensets often introduces human errors and poor decisions that do not support fuel efficiency and minimal environmental footprint through reduced emissions. With implementation of ESS, the complexity of the EMS/PMS increases, and with additional objectives, such as reducing and synchronizing the total number of running hours for all gensets, the process of scheduling the gensets manually in an optimal way becomes difficult for a human operator. This gives foundation for applying more advanced decision support tools and scheduling algorithms, where all important objectives and aspects are considered. In the following, the objectives of such algorithms are discussed and Mixed Integer Linear Programming (MILP) [38] is proposed as a viable option for EMS along with logic-based algorithms.

6.3.1 Objectives and models

The overall objective of an EMS/PMS it to supply the load demand, thus ensuring that all online consumers, and especially consumers that are critical for a given operation, experience a stable and reliable supply of power. With the implementation of an ESS also capacity and charge/discharge cycles must be supervised. Moreover, the system should cultivate fuel efficiency, thus reducing the fuel costs, and keep the emission of greenhouse gases to a minimum. Minimizing emission is especially important for maintaining a sustainable environment and for keeping the emissions below required levels set by the ECA zones introduced by IMO [128]. For the vessels treated in this work, service and maintenance of diesel engines are required after every 1000 running hours, which include, among other things, an expensive oil change. Thus, additional objectives could be to reduce the number of running hours for each genset and synchronizing the number of running hours so that service of multiple engines can be scheduled at a time - saving both maintenance costs and downtime.

Depending on the type of algorithm used in the EMS to handle all the objectives stated above, a model of the system must be developed. An MPC algorithm includes dynamic states, thus is able to capture dynamics in the systems, which are used to provide predictive abilities in the optimization scheme. Such dynamics may relate to starting and stopping of gensets, as well as ESS dynamics. Even though such a strategy provides an interesting aspect of control, many factors are unknown, or tend to unfold as stochastic distributions, which can prove challenging to implement in practice. In this work, a MILP strategy is adopted, which is based on optimization of linear algebraic models. The linear algebraic models used in this work are based on power- and energy balances. A power balance usually considers the instantaneous generated power relative to the load demand, while energy balance provides predictive abilities that consider e.g. the State Of Charge (SOC) of ESS. Three different MILP algorithms are proposed for energy management of a vessel with 4 gensets with following configurations:

1) 4 fixed speed gensets
2) 3 fixed speed gensets and 1 variable speed genset
3) 4 fixed speed gensets and an ESS

The fixed speed gensets are assumed to have optimal SFOC with a loading of 80% (relative to its rating). Furthermore, the variable speed genset has an operational range relative loadings of 10-90%. The ESS has a given maximum and minimum capacity (kWh), and also constraints for maximum charge and discharge rates (kW). Furthermore, dynamics related to starting and stopping delays of gensets are neglected. All EMS algorithms assumes closed bus-tie operations. The mathematical notation used to present the MILP algorithms is given in Table 6.7. In the following the MILP algorithms treated in this work, as well as logic-based algorithms constituting EMS/PMS, are discussed.

Table 6.7: Mathematical notation and description.

Notation	Description
k	Discrete time step
$P_L(k)$	Load power demand at time k (kW)
$P_{g,i}^{\max}$	Maximum power capability for genset i (kW)
$P_{g,i}^{\min}$	Minimum power capability for genset i (kW)
$P_{g,i}^{\text{opt}}$	Optimal SFOC power loading of genset i (kW)
$P_{g,i}(k)$	Power capability for genset i at time k (kW)
$E_{g,i}^{\text{opt}}(k)$	Energy capability for genset i when online at time k, assuming optimal loading
$E_{ess}^{\max}$	Maximum energy capacity of ESS (kWh)
$E_{ess}^{\min}$	Minimum energy capacity of ESS (kWh)
$E_{ess}(k)$	ESS energy capacity at time k (kWh)
$P_{ess}^{\max}$	Maximum power rating (> 0) of ESS (kW) (Maximum discharge power)
$P_{ess}^{\min}$	Minimum power rating (< 0) of ESS (kW) (Maximum charge power)
$P_{ess}(k)$	ESS power at time k (kW)
$Q_{\text{fuel},i}(k)$	Fuel consumption for genset i at time k (kg)
$T_{g,i}(k)$	Number of running hours for genset i
$S_{g,i}(k)$	Number of starts/stops of genset i
Δt	Maximum time between every run of algorithm (s)
y_i	Integer decision variable for scheduling genset i
q_p, q_s, q_t	Objective weights for power balance, number of starts/stops and running hours, respectively
$J(k)$	Objective function for time k

6.3.2 Mixed Integer Linear Programming (MILP) Algorithms

A MILP algorithm is an LP algorithm, with an objective function, inequality and equality constraints, where some of the decision variables (manipulated variables) are integers [38, 175]. The MILP formulations uses the minimum number of starts/stops and running hours, considering all gensets, i.e.

$$\begin{aligned} T_g^{\min}(k) &= \min\{T_{g,i}(k)\}, \\ S_g^{\min}(k) &= \min\{S_{g,i}(k)\}. \end{aligned} \tag{6.1}$$

In the following, the three MILP formulations for the three configurations listed above are treated separately.

6.3.2.1 4 fixed speed gensets

$$\begin{aligned} \min_{y_i} \quad & J(k) = q_p \sum_i \left(P_{g,i}(k)\right) \\ & \qquad + q_t \sum_i \Big(T_{g,i}(k) - T_g^{\min}(k)\Big) \cdot y_i \\ & \qquad + q_s \sum_i \Big(S_{g,i}(k) - S_g^{\min}(k)\Big) \cdot y_i, \\ \text{subject to} \quad & \\ & P_{g,i}(k) = y_i \cdot P_{g,i}^{\text{opt}}, \\ & \sum_i \left(P_{g,i}(k)\right) \geq P_L(k), \\ & y_i \in \{0, 1\}, \\ & i \in \{\text{gensets}\}, \end{aligned} \tag{6.2}$$

where y_i are the decision variables. The reason why $T_g^{\min}(k)$ and $S_g^{\min}(k)$ are subtracted from the gensets' running hours and number of starts/stops, respectively, is because minimizing the power production is the main objective, and should not be overshadowed by the accumulated running hours and number of starts/stops. In addition, the subtractions introduce equalization of running hours and number of starts/stops. $P_{g,i}^{\text{opt}}$ is used in the first set of equality constraints in (6.2) to enforce all running fixed speed gensets in the power calculation to have approximately optimal loading conditions as an approximation to schedule gensets.

6.3.2.2 3 fixed speed gensets and 1 variable speed genset

$$
\begin{aligned}
\min_{y_i, P_{g,j}(k)} \quad & J(k) = q_p \sum_i \left(P_{g,i}(k)\right) \\
& \quad + q_t \sum_i \Big(T_{g,i}(k) - T_g^{\min}(k)\Big) \cdot y_i \\
& \quad + q_s \sum_i \Big(S_{g,i}(k) - S_g^{\min}(k)\Big) \cdot y_i, \\
\text{subject to} \quad & \\
& P_{g,j}(k) = y_j \cdot P_{g,j}^{\text{opt}}, \\
& P_{g,l}(k) \le P_{g,l}^{\max}, \\
& P_{g,l}(k) \ge 0, \\
& \sum_i \left(P_{g,i}(k)\right) \ge P_L(k), \\
& y_j \in \{0, 1\}, \\
& i \in \{\text{gensets}\}, \\
& j \in \{\text{fixed speed gensets}\}, \\
& l \in \{\text{variable speed gensets}\},
\end{aligned}
\tag{6.3}
$$

where y_j and $P_{g,l}$ are the decision variables. Note that the minimum equality constraint for the variable speed gensets is set to 0. This is because if an additional integer variable is introduced to determine if the variable speed genset should run, i.e. $y_l \cdot P_{g,l}^{\min} \le y_l \cdot P_{g,l} \le P_{g,l}^{\max}$, the problem would become nonlinear, thus not supported by linear programming solvers. Thus the following evaluation of the results yielded from the MILP is adopted:

$$
\begin{aligned}
& \textbf{if } P_{g,l}(k) < P_{g,l}^{\min} \textbf{ and } P_{g,l}(k) > 0\textbf{:} \\
& \quad P_{g,l}(k) = P_{g,l}^{\min} \\
& \textbf{else:} \\
& \quad \text{use } P_{g,l}(k) \text{ from MILP} \\
& \textbf{endif}
\end{aligned}
\tag{6.4}
$$

6.3.2.3 4 fixed speed gensets and an ESS

With the implementation of an ESS a mode variable is introduced to distinguish between charging and discharging of the ESS:

$$
\begin{aligned}
\min_{y_i, P_{ess}(k)} \quad J(k) = {} & q_p \sum_i \left(P_{g,i}(k)\right) \\
& + q_t \sum_i \left(T_{g,i}(k) - T_g^{\min}(k)\right) \cdot y_i \\
& + q_s \sum_i \left(S_{g,i}(k) - S_g^{\min}(k)\right) \cdot y_i, \\
\text{subject to} \quad & \\
& \textbf{if } \text{mode} == \text{"charge"}\textbf{:} \\
& \quad P_{ess}(k) \leq 0 \\
& \quad P_{ess}(k) \geq P_{ess}^{\min} \\
& \textbf{else if } \text{mode} == \text{"discharge"}\textbf{:} \\
& \quad P_{ess}(k) \leq P_{ess}^{\max} \\
& \quad P_{ess}(k) \geq 0 \\
& \textbf{endif} \\
& P_{g,i}(k) = y_i \cdot P_{g,i}^{\text{opt}}, \\
& \sum_i \left(P_{g,i}(k)\right) + P_{ess}(k) \geq P_L(k), \\
& y_i \in \{0, 1\}, \\
& i \in \{\text{gensets}\},
\end{aligned}
\tag{6.5}
$$

where y_i and $P_{ess}(k)$ are the decision variables. $P_{ess}(k) > 0$ is defined as positive power flow from the ESS (discharge), while $P_{ess}(k) < 0$ determines charging of the ESS. The introduced mode (charge and discharge) is determined by the caller of the algorithm, and is decided relative to the ESS' capacity, i.e.

$$
\begin{aligned}
&\textbf{if } E_{ess}(k-1) - P_{ess}^{\max} \cdot \frac{\Delta t}{3600} \leq E_{ess}^{\min}\textbf{:} \\
&\quad \text{mode} = \text{"charge"} \\
&\textbf{else if } E_{ess}(k-1) - P_{ess}^{\min} \cdot \frac{\Delta t}{3600} \geq E_{ess}^{\max}\textbf{:} \\
&\quad \text{mode} = \text{"discharge"} \\
&\textbf{endif}
\end{aligned}
\tag{6.6}
$$

6.3.3 Logic Algorithms

Logic-based algorithms are often adopted in industry for control of various systems and processes. EMS/PMS is not an exception. Logic-based algorithms are usually intuitive, however, often requires a high number of nested logic statements to achieve the desired results. This makes logic-based algorithms complex, hard to construct and debug. For a genset scheduling algorithm, which uses the rating of each individual genset to construct logic with the objective of supplying the load demand with minimum number of gensets online, and with minimum online total power generation capability, the rating of the gensets are crucial to get the logic right. This can cause dependencies that may not be fulfilled if one or multiple gensets were to change rating. To account for such dependencies, the logic structure in the algorithm becomes even more complex, which increases the chance of failing to meet the desired objective. In this work three logic-based algorithms are implemented, relative to the three configurations presented earlier, with the objective of supplying the load demands with minimal online power generation capability. The logic-based algorithms use the gensets' optimal loading conditions to construct nested if-else statements relative the load profile, starting from the genset(s) with the lowest rating with optimal loading conditions. A small example of how the logic structure is implemented, with the configuration of 4 fixed speed gensets and genset ratings according to Table 6.1, is given below in (6.7). $P_g^{\sum}(k)$ denotes the sum of the (intended) generated power (assuming optimal loading conditions) from selected gensets.

$$
\begin{aligned}
&\textbf{if } P_L(k) == 0 \textbf{ :}\\
&\quad P_g^{\sum}(k) = 0\\
&\textbf{else if } P_L(k) \leq P_{g,2}^{\text{opt}} \textbf{ :}\\
&\quad P_g^{\sum}(k) = P_{g,2}^{\text{opt}}\\
&\textbf{else if } P_L(k) \leq P_{g,1}^{\text{opt}} \textbf{ :}\\
&\quad P_g^{\sum}(k) = P_{g,1}^{\text{opt}}\\
&\textbf{else if } P_L(k) \leq P_{g,2}^{\text{opt}} + P_{g,3}^{\text{opt}} \textbf{ :}\\
&\quad P_g^{\sum}(k) = P_{g,2}^{\text{opt}} + P_{g,3}^{\text{opt}}\\
&\qquad\qquad\vdots\\
&\textbf{else :}\\
&\quad P_g^{\sum}(k) = P_{g,1}^{\text{opt}} + P_{g,2}^{\text{opt}} + P_{g,3}^{\text{opt}} + P_{g,4}^{\text{opt}}
\end{aligned}
\tag{6.7}
$$

6.4 Results

The proposed EMS algorithms, both MILP and logic-based, are in this section applied to the experimental data extracted from the three vessels to analyze the three proposed configurations and for various operational profiles. The MILP algorithms are implemented in Python using the Pulp framework that acts as an interface to solvers such as CPLEX. The rating of the gensets are kept the same as listed in Table 6.1 - 6.5. For all the MILP algorithms the weights in the cost functions are chosen by trial and error according to

$$
\begin{aligned}
q_p &= 10^6\\
q_t &= \begin{cases} 10, & \text{if } \max\{T_{g,i}\} - \min\{T_{g,i}\} \geq 50\\ 0, & \text{otherwise} \end{cases}\\
q_{ss} &= \begin{cases} 10^3, & \text{if } \max\{S_{g,i}\} - \min\{S_{g,i}\} \geq 100\\ 0, & \text{otherwise} \end{cases}
\end{aligned}
\tag{6.8}
$$

The penalties related to running hours and number of starts/stops are not effectuated until the difference of the genset with lowest number and the genset with highest number exceeds a threshold. This is to avoid unnecessary scheduling in situations where the differences in number of running hours and starts/stops, considering all gensets, are marginal.

For all three vessels the second genset, G2, is chosen as variable speed genset for configuration 2, and marked as G2* in the following. The operation range of the variable speed gensets are set to loadings between 10% and 90%, and are assumed to follow the SFOC curve in Figure 6.4b. The fixed speed gensets are assumed to follow the SFOC curve portrayed in Figure 6.4a, with optimal loading of about 90%. The EMS algorithms for all vessels will be run

- every 10 minutes,
- or if the load demand exceeds the online power supply capability,
- or if the ESS exceeds its capacity limits.

The ESS is assumed to have a capacity of C kWh and power constraints of $\pm C$ kW. The ESS capacities for the three different vessels treated in this work have been chosen relative the capacity of existing ESS applications in similar vessels. Furthermore, the ESS is assumed to have an operation range between 30% and 100% capacity. For a fair comparison of the three configurations, the start capacity of the ESS is set to 30%. The load demands to be met are, for each data set, calculated as the sum of the supplied power from each individual genset from the experimental data. To validate and compare the results from the three different configurations, with both MILP and logic-based EMS algorithms, three performance targets are used:

- Total fuel consumption throughout the data set horizon for all gensets: $\sum_i Q_{\text{fuel},i}$
- Running hours for all gensets: $\sum_i T_{g,i}$
- Number of starts/stops for all gensets: $\sum_i S_{g,i}$

The first item in the list above is especially important, as reducing the total fuel consumption, and thus minimizing the emissions, considering all gensets, is the main objective of the EMS. For comparison, the total fuel consumption and total number of running hours, as well as number

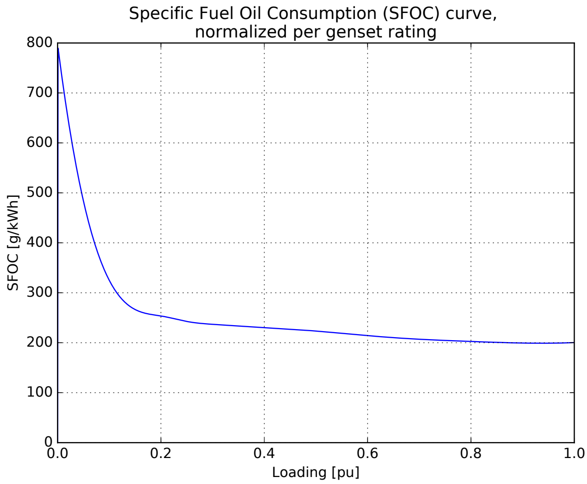

(a) Normalized (brake) SFOC for fixed speed genset operation.

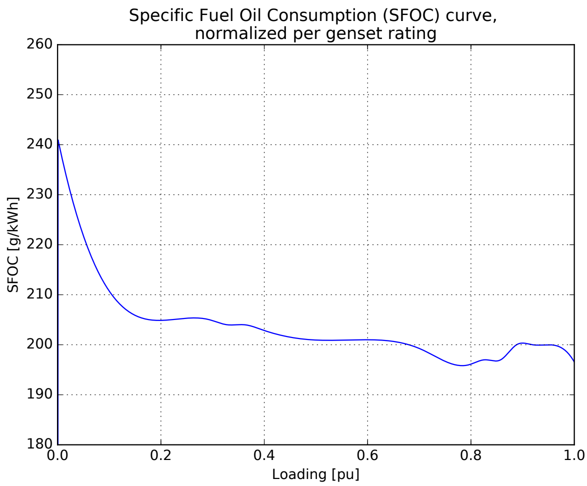

(b) Normalized (brake) SFOC for variable speed genset operation.

Figure 6.4: (Brake) Specific Fuel Oil Consumption (SFOC) curves for fixed speed and variable speed genset operation adopted in this work, normalized relative to the per unit genset loading. The SFOC curves are based on acceptance and certification tests for fixed speed and variable speed operations of gensets and are provided by a leading genset supplier. Optimal loading for the fixed speed SFOC is about 90% with SFOC of 199 $\frac{\text{g}}{\text{kWh}}$, and the variable speed SFOC is about 80% with SFOC of 196 $\frac{\text{g}}{\text{kWh}}$.

of starts/stops, have been calculated from the operational data and listed in Table 6.8. The results presented are affected by uncertainties, and the main uncertainties are considered to be the adopted SFOC curves and the accuracy of the sampled data from the three vessels. The SFOC curves used in this work have been constructed from a manufacturer's acceptance and certification tests of a single genset type for fixed speed and variable speed operation, and have been normalized (w.r.t. loading) to fit a range of different gensets with different ratings according to the three vessels' power plants treated in this work. The power measurements do also include uncertainties due to, among other things, measurement noise and sampling. The sampling frequencies used are small ($\leq$ 1Hz) due to the amount of logged data for long data collection horizons, and also due to limitations in the logging systems used. Such low sampling frequencies do also introduce uncertainties and do not account the fast dynamics in the power systems. Hence, the result presented in this section is regarded to be an indication of how alternative EMS/PMS strategies affect the performance targets listed above. In the following, each vessel with the three proposed configurations will be treated separately, and a load-sharing strategy with equal loading (% of relative individual genset ratings) of the running gensets are adopted.

6.4.1 Ferry

The EMS configuration of the ferry is listed in Table 6.9. As can be seen, the maximum ESS capacity is set to 670 kWh. The total energy demand (E_L) throughout the ferry's data set is 17.24 MWh, thus the optimal genset scheduling (unit commitment) would yield $\sum_i E_{g,i}^{\text{opt}} = E_L$ MWh, where the online gensets have optimal loadings.

The EMS results using the three different configurations for the load demand extracted from the operational data are listed in Table 6.10. As the ESS capacity in the end of the EMS analysis might be above minimum capacity, the added fuel consumption that has been used to charge the ESS beyond minimum capacity has to be subtracted from the total fuel consumption results to assure fair comparisons between the configuration. This has been done in the last row in Table 6.10 (denoted $\sum_{30\%}$), where $200\frac{\text{g}}{\text{kWh}}$ fuel has been subtracted from the total fuel consumptions to bring the ESS capacity down to 30%. Comparing the three different configurations, and the use of MILP and logic-based algorithms, the lowest total fuel consumption, $\sum_i Q_{\text{fuel},i}$, can be found for configuration 3 using the logic-

Table 6.8: Performance targets extracted from the real vessel data.

		$T_{g,i}$ (hours)	$S_{g,i}$	$Q_{\text{fuel},i}$ (kg)
FERRY	G1	0.00	0	0.00
	G2	23.98	0	1405.98
	G3	0.88	2	83.71
	G4	20.48	5	2358.82
	$\sum$	45.34	7	3848.52
PSV	G1	266.11	34	53104.27
	G2	433.72	47	33084.15
	G3	433.87	38	34275.50
	G4	220.78	33	45783.06
	$\sum$	1354.49	152	166246.99
SEISMIC	G1	963.40	2	317683.71
	G2	719.33	2	236924.51
	G3	764.06	3	253209.37
	G4	752.10	3	246001.21
	$\sum$	3198.90	10	1053818.79

Table 6.9: EMS information and configuration for the ferry.

Parameter	**Value**
Total load energy demand, E_L	17.24 MWh
Optimal loading, fixed speed gensets	90%
Load range, variable speed genset	10-90%
ESS max. capacity, $E_{ess}^{\max}$	670 kWh (100%)
ESS min. capacity, $E_{ess}^{\min}$	201 kWh (30%)
ESS start capacity, $E_{ess}(0)$	201 kWh (30%)
ESS discharge rating, $P_{ess}^{\max}$	670 kW (1C)
ESS charge rating, $P_{ess}^{\min}$	-670 kW (-1C)

based algorithm. The difference in total fuel consumption when comparing the MILP and the logic-based algorithm for this configuration is marginal, and both algorithms indicate fuel savings of 10.2% compared to the total fuel consumption calculated from the real vessel data in Table 6.8. The highest total fuel consumption can be found for configuration 1 using the

Table 6.10: Ferry: EMS results with rating of gensets according to Table 6.1

		LOGIC			MILP		
		$T_{g,i}$ (hours)	$S_{g,i}$	$Q_{\text{fuel},i}$ (kg)	$T_{g,i}$ (hours)	$S_{g,i}$	$Q_{\text{fuel},i}$ (kg)
CONFIG 1	G1	9.57	63	1449.46	17.59	121	2500.29
	G2	24.00	1	1575.97	14.97	109	954.12
	G3	9.56	98	675.50	0.93	56	84.78
	G4	0.00	0	0.00	0.81	22	144.55
	$\sum$	43.13	162	3700.93	34.30	308	3683.74
CONFIG 2	G1	9.57	63	1776.34	2.97	44	579.80
	G2*	18.92	445	785.31	18.92	445	785.32
	G3	9.56	98	933.32	9.56	98	933.32
	G4	0.00	0	0.00	6.60	43	1196.59
	$\sum$	38.06	606	3494.96	38.06	630	3495.04
CONFIG 3	G1	2.57	23	513.09	10.66	86	2193.66
	G2	18.89	75	2117.60	11.29	100	1274.39
	G3	7.90	82	875.90	0.04	6	4.40
	G4	0.00	0	0.00	0.17	1	35.89
	$\sum$	29.36	180	3506.59	22.16	193	3508.35
	$\sum_{30\%}$	-	-	3457.37	-	-	3457.51

logic-based algorithm, which indicates fuel savings compared to Table 6.8 of 3.8%. The MILP algorithm for the same configuration indicates fuel savings of 4.3%, however, at the expense of increasing the number of starts/stops. The difference in total fuel consumptions for configuration 2, comparing the two algorithms, is also marginal, and both algorithms indicate fuel savings of 9.2%. Furthermore, configuration 3 with MILP results in the lowest number of total running hours, $\sum_i T_{g,i}$ (51.1% reduction compared to Table 6.8), while the logic-based algorithms for configuration 1 results in the highest number of running hours(4.9% reduction compared to Table 6.8). Configuration 2, which includes a variable speed genset, is the configuration with the highest number of starts/stops, $\sum_i S_{g,i}$. The highest number of starts/stops for a single generator is the variable speed generator, G2*, in configuration 2 for both algorithms, yielding 445 starts/stops for the whole horizon. This corresponds to an average of 18.54 starts/stops per hour, i.e. 3.24 minutes between each start/stop. The logic-based algorithm for configuration 2 has slightly lower number of total starts/stops, which is due to the MILP algorithm's objective of synchronizing running hours and number of starts/stops for all gensets.

The results presented in Table 6.10 indicate that it could be most beneficial to employ an ESS (configuration 3) to reduce the fuel consumption and the total number of running hours, where the lowest total number of running hours, $\sum_i T_{g,i}$, is obtained by the MILP algorithm. However, the number of starts/stops exceeds what is presented in Table 6.8, which is expected due to minimizing the online power supply capability (spinning reserve).

It can be discussed whether high scheduling frequencies (i.e. high number of starts/stops) are beneficial, due to wear and tear of the gensets and increased fuel consumption during acceleration towards ideal working state. Assuming the cooling liquid from the running gensets flows through the engine blocks of the gensets that are not running, one prevents cold starts of the gensets. Furthermore, assuming an AC distribution network, the gensets are not exposed to any significant loadings before the gensets' voltages and frequencies match the distribution grid and the gensets are connected to the distribution bus, which will support fast acceleration of the genset to ideal states. For many gensets the acceleration phase will last for 20-30 seconds, and with no significant loads the fuel consumption during such a phase would be limited. The gensets' starters and starter relays would be subject for wear and tear with increased scheduling frequency. However, an assessment regarding how the scheduling frequency affects wear and tear of single components, and affects the fuel consumption of single gensets, lays outside the scope of this work.

6.4.2 Platform Supply Vessel (PSV)

The EMS configuration of the PSV is listed in Table 6.11. As can be seen, the maximum ESS capacity is in this case set to 1000 kWh, which is slightly higher than the ESS for the ferry. The total energy demand (E_L) throughout the PSV's data set is 728.49 MWh, which is calculated from the operational data's approximately 1056 hours long horizon. As earlier, the optimal genset scheduling (unit commitment) would yield $\sum_i E_{g,i}^{\text{opt}} = E_L$ MWh.

The EMS results using the three different configurations for the load demand extracted from the operational data are listed in Table 6.12. Comparing the three different configurations, and the use of MILP and logic-based

Table 6.11: EMS information and configuration for the PSV.

Parameter	**Value**
Total load energy demand, E_L	728.49 MWh
Optimal loading, fixed speed gensets	90%
Load range, variable speed genset	10-90%
ESS max. capacity, $E_{ess}^{\max}$	1000 kWh (100%)
ESS min. capacity, $E_{ess}^{\min}$	300 kWh (30%)
ESS start capacity, $E_{ess}(0)$	300 kWh (30%)
ESS discharge rating, $P_{ess}^{\max}$	1000 kW (1C)
ESS charge rating, $P_{ess}^{\min}$	-1000 kW (-1C)

Table 6.12: PSV: EMS results with rating of gensets according to Table 6.3.

		LOGIC			**MILP**		
		$T_{g,i}$ (hours)	$S_{g,i}$	$Q_{\text{fuel},i}$ (kg)	$T_{g,i}$ (hours)	$S_{g,i}$	$Q_{\text{fuel},i}$ (kg)
CONFIG 1	G1	43.28	202	14688.83	37.28	142	12692.98
	G2	1029.67	251	98023.73	346.92	1134	45721.62
	G3	320.05	1156	43951.77	1002.79	285	96253.69
	G4	0.67	16	226.03	6.68	142	2222.03
	$\sum$	1393.67	1625	156890.36	1393.66	1703	156890.32
CONFIG 2	G1	43.28	202	16046.08	37.20	136	14009.72
	G2*	966.54	9533	74833.77	966.54	9533	74833.91
	G3	320.04	1156	55523.63	320.05	1156	55523.88
	G4	0.67	16	234.97	6.75	138	2271.35
	$\sum$	1330.54	10907	146638.45	1330.54	10963	146638.86
CONFIG 3	G1	27.23	178	11330.65	21.17	62	8868.53
	G2	558.77	1152	99477.98	428.42	1202	76352.20
	G3	194.13	774	34506.14	328.37	1204	58508.42
	G4	0.04	2	18.61	3.81	64	1576.91
	$\sum$	780.18	2106	145333.38	781.77	2532	145306.05
	$\sum_{30\%}$	-	-	145305.37	-	-	145293.80

algorithms, the MILP algorithm for configuration 3 (with ESS) results in the lowest total fuel consumption, $\sum_i Q_{\text{fuel},i}$ (12.6% fuel savings compared to Table 6.8), while configuration 1, with both MILP and logic-based algorithms, results in the highest fuel consumption (5.6% fuel savings compared to Table 6.8). Both algorithms for configuration 2 indicate fuel savings, compared to Table 6.8, of 11.8%. The main difference between the MILP and logic-based algorithms for configuration 1 and 2 relates to total number of starts/stops, $\sum_i S_{g,i}$, where the MILP algorithm has the highest number for both configurations compared to the logic-based algorithms. As discussed earlier, this is because the MILP algorithms synchronize the number of running hours and starts/stops for all gensets. The total number of running hours, $\sum_i T_{g,i}$, are about the same comparing the MILP algorithm and the logic-based algorithm in both configurations (1 and 2), indicating an increase of 2.9% for configuration 1 and a reduction of 1.8% for configuration 2 compared to Table 6.8. For configuration 3, the logic-based algorithm has slightly lower total number of running hours compared to the MILP algorithm (reduction of 42.4% for the logic-based algorithm and a reduction of 42.3% for the MILP algorithm compared to Table 6.8). The logic-based algorithm also results in a lower total number of starts/stops compared to the MILP algorithm.

Furthermore, the genset with the highest number of starts/stops is the variable speed genset, G2* for configuration 2 using both the MILP and logic-based algorithm, with 9533 starts/stops. This is approximately 9.03 starts/stops per hour, i.e. 6.65 minutes between each start/stop. Comparing the results in Table 6.12 with the results extracted from the operational data presented in Table 6.8, all proposed configurations with both MILP and logic-based algorithms results in lower total fuel consumption, however, for configuration 1 the total number of running hours exceeds the total number of running hours extracted from the operational data. As with the ferry, the numbers of starts/stops exceed what is presented in Table 6.8, which is expected due to minimizing the online power supply capability.

The results in Table 6.12 indicate that it would also for this vessel be beneficial to employ an ESS to reduce the fuel consumption. The MILP algorithm provides a slightly lower total fuel consumption, however, the logic-based algorithm for this configuration yields better results than the MILP algorithm considering running hours and total number of starts/stops. Even though the results indicate significant fuel savings, the reduced number of running hours for configuration 3 is also of interest from a maintenance/service perspective.

6.4.3 Seismic Survey Vessel

The EMS configuration of the seismic survey vessel is listed in Table 6.13. As can be seen, the maximum ESS capacity is also in this case set to 1000 kWh. The total energy demand (E_L) is calculated from the operational data with horizon length of approximately 1066 hours and is 4731.17 MWh. As earlier, the optimal genset scheduling (unit commitment) would yield $\sum_i E_{g,i}^{\text{opt}} = E_L$ MWh.

Table 6.13: EMS information and configuration for the seismic survey vessel.

Parameter	**Value**
Total load energy demand, E_L	4731.17 MWh
Optimal loading, fixed speed gensets	90%
Load range, variable speed genset	10-90%
ESS max. capacity, $E_{ess}^{\max}$	1000 kWh (100%)
ESS min. capacity, $E_{ess}^{\min}$	300 kWh (30%)
ESS start capacity, $E_{ess}(0)$	300 kWh (30%)
ESS discharge rating, $P_{ess}^{\max}$	1000 kW (1C)
ESS charge rating, $P_{ess}^{\min}$	-1000 kW (-1C)

The EMS results using the three different configurations for the load demand extracted from the operational data are listed in Table 6.14. The EMS results from the seismic survey vessel show that configuration 2, with a variable speed genset installed, results in the lowest total fuel consumption, $\sum_i Q_{\text{fuel},i}$, 10.3% reduction compared to Table 6.8 for both algorithms. The total number of running hours for the same configuration is equal for both algorithms, indicating a reduction of 31.9% compared to Table 6.8. The main difference between the algorithms for this configuration is related to number of starts/stops, where the MILP algorithm provides a higher number than the logic based algorithm. For configuration 3, the logic-based algorithm results in lower number of starts/stops, total fuel consumption and total running hours compared to the MILP algorithm, and it is speculated that the MILP algorithm uses too much effort to equalize the number of running hours and starts/stops, which impairs the results. For this configuration, the logic-based algorithm indicates an reduction in total running hours of 38.8% compared to Table 6.8, while the MILP algorithm indicates a 37.7% reduction. For total fuel consumption, the logic-based algorithm indicates fuel savings of 8.9% compared to Table 6.8, while the MILP algorithm indicates fuel savings of 8.6%. The configuration with the highest fuel consumption is configuration 1: The logic-based algorithm has slightly higher fuel consumption than the MILP algorithm (both algorithms indicate fuel savings of 6.4% compared to Table 6.8). The total number of running hours are almost identical for both algorithms in configuration 1 (reduction of 29.2% compared to Table 6.8), however, the number of starts/stops is higher for the MILP algorithm than for the logic-based algorithm. The genset with the highest number of starts/stops is the variable speed G2* genset in configuration 2 for both algorithms, with 16253 starts/stops. This corresponds to an average of 15.25 starts/stops per hour, i.e. about 3.94 minutes between each start/stop. As indicated from the results in Table 6.14, all three configurations with both algorithms result in lower fuel consumptions and have lower numbers of running hours than what is stated in Table 6.8, however, the total numbers of starts/stops are higher.

The load profile from the seismic survey vessel is quite different compared to the ferry and the PSV, with a more stable load profile without rapid power peaks of high magnitude. Thus, to investigate the benefit of the three different configurations further, the third genset, G3, is reduced to half of its rating to give more flexibility for the algorithms to utilize in the unit commitment. The results from this analysis are listed in Table 6.15.

As can be seen from the results in Table 6.15, also in this case configuration 2 results in the lowest total fuel consumption, $\sum_i Q_{\text{fuel},i}$. The difference between the algorithms when comparing total number of running hours and total fuel consumption for this configuration is marginal, both algorithms indicate a reduction in total number of running hours of 29.2% and a reduction in total fuel consumption of 10.5% compared to Table 6.8. However, the MILP algorithm results in a higher total number of starts/stops of gensets. As before, configuration 1 results in the highest fuel consumption, with approximately the same total fuel consumption for both algorithms, both indicating fuel savings of 8.1% compared to Table 6.8. Also the total number of running hours for this configuration is approximately the same comparing both algorithms, indicating a reduction of 29.2%, the same as configuration 2, compared to Table 6.8. For configuration 3, the logic-based algorithm results in lower total number of running hours and total fuel consumption compared to the MILP algorithm. Comparing the results from configuration 3 with Table 6.8, both algorithms indicate fuel savings of 10.4%. For the total number of running hours, the logic-based algorithm

Table 6.14: Seismic survey vessel: EMS results with rating of gensets according to Table 6.5.

		LOGIC			MILP		
		$T_{g,i}$ (hours)	$S_{g,i}$	$Q_{\text{fuel},i}$ (kg)	$T_{g,i}$ (hours)	$S_{g,i}$	$Q_{\text{fuel},i}$ (kg)
CONFIG 1	G1	154.20	1278	60476.90	213.34	1940	89986.58
	G2	1066.34	1	467960.75	259.98	1940	108671.47
	G3	1044.77	175	457445.95	906.93	1303	397904.02
	G4	0.00	0	0.00	884.75	1497	389311.28
	$\sum$	2265.13	1454	985883.59	2265.01	6680	985873.36
CONFIG 2	G1	153.90	1280	81900.09	43.21	742	22823.31
	G2*	979.88	16253	293285.97	979.88	16253	293286.55
	G3	1044.77	177	570172.17	1043.28	183	569361.20
	G4	0.00	0	0.00	112.17	742	59888.51
	$\sum$	2178.55	17710	945358.23	2178.55	17920	945359.57
CONFIG 3	G1	3.95	136	1855.01	518.51	4003	249510.74
	G2	1066.34	1	527606.45	698.90	3433	337118.90
	G3	887.7	11715	430485.33	356.51	4004	172495.42
	G4	0.00	0	0.00	418.62	4004	204598.99
	$\sum$	1958.00	11852	959946.78	1992.54	15444	963724.05
	$\sum_{30\%}$	-	-	959806.78	-	-	963583.91

results in a reduction of 37.3%, while the MILP algorithm results in a reduction of 37.1% compared to Table 6.8. The difference between the algorithms for this configuration is related to total number of starts/stops, where the logic-based algorithm conducts more starts/stops of gensets compared to the MILP algorithm. Furthermore, all configurations with both algorithms result in lower fuel consumption compared to Table 6.14. For configuration 2 and 3, the total number of running hours are higher than what is stated in Table 6.14, while the total numbers of starts/stops are lower for configuration 2 using both algorithms with reduced rating of the G3 genset, and configuration 3 using the MILP algorithm. The genset with the highest number of starts/stops is now the G3 genset in configuration 3 using the logic-based algorithm, now with 11601 starts/stops. This corresponds to an average of 10.88 starts/stops per hour, i.e. about 5.51 minutes between each start/stop. Comparing the results in Table 6.15 with the results extracted

Table 6.15: Seismic survey vessel: EMS results with rating of G3 set to 1530 kW.

		LOGIC			**MILP**		
		$T_{g,i}$ (hours)	$S_{g,i}$	$Q_{\text{fuel},i}$ (kg)	$T_{g,i}$ (hours)	$S_{g,i}$	$Q_{\text{fuel},i}$ (kg)
CONFIG 1	G1	788.03	1413	369825.75	1035.09	129	487750.64
	G2	1066.34	1	502360.39	459.85	3899	216103.81
	G3	410.16	2856	95786.14	410.05	2870	95762.11
	G4	0.60	14	243.98	360.02	3900	168594.68
	$\sum$	2265.13	4284	968216.26	2265.01	10798	968211.23
CONFIG 2	G1	788.02	1423	432667.83	344.22	4089	188989.64
	G2*	1065.46	217	397763.78	1065.46	217	397764.36
	G3	410.05	2870	112572.95	410.05	2870	112572.95
	G4	0.60	14	319.57	444.39	4088	243998.52
	$\sum$	2264.12	4524	943324.13	2264.12	11264	943325.47
CONFIG 3	G1	384.82	6218	209866.93	184.83	1926	99955.36
	G2	1066.34	1	582583.79	993.72	183	540386.38
	G3	554.23	11601	151611.34	549.78	2689	149667.19
	G4	0.02	2	8.36	284.91	1926	154807.74
	$\sum$	2005.42	17822	944070.43	2013.22	6724	944816.67
	$\sum_{30\%}$	-	-	943939.19	-	-	944685.43

from the operational data presented in Table 6.8, it is evident that all proposed configurations with both MILP and logic-based algorithms results in lower total fuel consumption and total number of running hours. As before, the number of starts/stops exceeds what is presented in Table 6.8, which is expected due to minimizing the online power supply capability (spinning reserve), thus running the gensets with more optimal loadings which cultivate fuel savings.

The EMS results presented for the seismic vessel in Table 6.14 and Table 6.15 indicate that for this kind of load profile the use of a variable speed genset could be more beneficial than the two other configurations when comparing fuel consumptions. However, the largest reduction in total number of running hours is indicated by configuration 3.

6.5 Conclusion

This work has presented three different load profiles extracted from three different marine vessels during operation, and the operational data have been presented and analysed in terms of genset loadings. To achieve a fuel-efficient operation, where the fuel consumption and the emission of greenhouse gases are in line with the load demand, the gensets should be running with optimal loadings, which is dictated by the diesel gensets' SFOC curves. To achieve optimal loadings of the gensets in the unit commitment, it is imperative that no more gensets than what is required to meet the load demand are running, meaning a minimal spinning reserve. In addition, with fixed speed gensets, the implementation of a variable speed genset or an ESS would further benefit the unit commitment by introducing flexibility in the power generation, and thus be able to further move the loadings of the fixed speed generators towards optimal loadings.

Three different configurations of the vessels were introduced; i) 4 fixed speed gensets, ii) 3 fixed speed gensets and 1 variables speed genset, and iii) 4 fixed speed gensets and one ESS. Both MILP-based and logic-based EMS algorithms were implemented and presented for the three different power plant configurations. The algorithms were run using the real load demands extracted from the three vessels during operation. The results of the EMS analysis showed that, with the load profiles presented in this work, the unit commitment would benefit most of the implementation of an ESS in terms of fuel savings and reduction in number of running hours for the ferry and the PSV. The seismic vessel would benefit most from a variable speed genset, seen from a fuel saving perspective, however, the lowest total number of running hours was obtained with the use of an ESS. A further implementation to improve the results obtained in configuration 3 could include optimal sizing of the ESS by including it in the EMS optimization algorithm's objective function for offline analysis as treated in this work. If the ESS is based on battery packs, also optimizing the battery packs' lifetime, with higher C-ratings, by minimizing battery-cycling would make an interesting aspect for further work. The difference between the MILP-based and logic-based algorithms were also discussed. The MILP algorithms enable ease in implementation, and possibilities for multiple objectives, such as synchronization of running hours and number of starts/stops of gensets.

Even though the analysis presented in this work indicates that the efficiency of unit commitment can be improved by a configuration modification in the power plant and applying more advanced EMS algorithms, further research that includes genset dynamics must be conducted. Moreover, an assessment of the investment costs (CAPEX) related to installing an ESS, and the increased complexity of the total system, need further attention. In addition, even though unit commitment strategies, as presented and discussed in this work, indicate possibilities for further optimizing marine operations, the rules and requirements set by classification entities and vessels' employers might dictate stringent requirements related to spinning reserve(online power supply capability) and segregation of the vessel's power system assuring safety in error prone situations. Thus, additional work related to ensuring the safety of operations with a minimal online power supply capacity must be conducted, where rules and regulations are implemented in the EMS algorithms.

CHAPTER 7

Concluding Remarks and Recommendation for Future Work

Among many incentives and driving forces, the increased focus on emissions of greenhouse gases and particle matter, along with a tougher and more demanding offshore market, has brought the discussions about the marine vessel's efficiency to the table. The efficiency of a marine vessel involves many aspects, and involves a broad range of disciplines. Moreover, as discussed in Chapter 2, the evolution of the shipboard electrical power system has brought us to a scenario of an increasing number of power system components that are highly dependent on automation and hierarchical control design. This is in clear contrast with the early stages of the evolution, where the power system applications consisted of few and large human-controlled power system units. The main contribution of the thesis has been centered around this aspect, where optimal control strategies for two intertwined topics, one requiring lower level control and one higher level control, within the marine vessel's power system are investigated: Optimal harmonic mitigation and optimal unit commitment as part of EMS. The two topics are motivated by increasing the shipboard power system's efficiency. In the following, concluding remarks and recommendations for future work will be given for each of these topics as treated in Part II and III of the thesis.

Part II: Harmonic Mitigation

Chapter 3 introduced system-wide harmonic mitigation using one single APF, where an MPC was employed to generate optimal APF current references that were fed to the local APF control. The proposed control strategy was benchmarked against conventional (local) filtering methods using a two-bus shipboard power system with 6-and 12-pulse rectifier loads as test system. Three simulation cases with different load configurations were conducted, and the MPC showed clear advantages compared to the conventional methods, especially in situations with saturated filter currents, and resulted in better harmonic mitigation.

In **Chapter 4**, a system-wide harmonic mitigation method, also using one single APF, based on offline analytical optimization was proposed and compared with the MPC introduced in the previous chapter. The MPC and the offline analytical optimization approach were benchmarked and compared with two conventional (local) harmonic mitigation strategies using a two-bus shipboard power system with 12-pulse rectifier loads: Five different simulation cases with different load configurations were conducted, and non-idealities such as transformer saturation and parameter mismatch/uncertainty were introduced to more clearly highlight the differences between the methods in as realistic conditions as possible. The results showed that the MPC demonstrated clear advantages compared to the other methods, giving the lowest (voltage) THDs in all simulation cases. The offline analytical optimization approach resulted in lower THDs compared to the conventional (local) filtering methods in all simulation cases, except for the case with parameter mismatch. In this case the analytical approach proved to be not very robust due to its inherently strong dependence on the model of the power system used during the offline analytical optimization calculations, and lacked dynamic and adaptive properties.

In **Chapter 5**, a real-time system architecture with a single-phase MPC implementation for system-level harmonic mitigation using one single APF was proposed. The single-phase MPC was designed on the basis of repetitive and distributed control, as the three-phase MPC formulations in Chapter 3 and 4. The proposed system architecture utilized (internal and external) event-based communication in a configurable component-oriented structure, to cultivate minimal use of computational resources in efforts to increase the real-time properties needed for the system-level harmonic mitigation strategy. A suitable simulator was implemented, and the total system was tested with a HIL setup using two desktop computers. The HIL simulation confirmed that the proposed system architecture implementation met the real-time requirements for the proposed harmonic mitigation strategy, with consistent and relatively low resource usage.

The system-level harmonic mitigation strategy with one single APF, utilizing MPC to generate optimal APF filter current references, has shown promising results in the work conducted in this thesis. However, the harmonic mitigation approach using MPC has its challenges, such as model complexity for larger power systems, high computational costs and is sensitive to measurement noise and delays. Thus, work remains to industrialize such a strategy. Hence, recommendations for future work are:

- Design and conduct experimental verification of the proposed system-level harmonic mitigation strategy using MPC and a single APF. This requires implementation of necessary instrumentation, processing and synchronization procedures, along with low-overhead power system component- and instrumentation interfaces.
- Use the Harmonic Coupled Norton Equivalent (HCNE) Model [12] instead of the Classical Norton Model (which is used in this work) to model the load currents in the MPC to increase model accuracy by allowing cross-coupling between harmonic current components.
- Design of adaptive, approximate power system models to use in the MPC design for large and complex multi-bus power systems, with the goal of reducing the dimension of the MPC's system matrices, thus reducing computational costs.
- Investigate the potential to utilize already existing power system components in the system-level harmonic mitigation strategy to eliminate the need for installing an APF. Such components could potentially be an active rectifier unit (part of an active motor drive unit) with suitable dimensioned internal energy storage, that could be controlled, or hold functionality, to conduct system-level harmonic mitigation.

Part III: Energy Management

In **Chapter 6**, three shipboard power system load profiles from three different vessels during operation, a ferry, a PSV and a seismic survey vessel, were analyzed in terms of genset loadings. From the analysis it was evident that the gensets in the three vessels were running with non-optimal loads relative the optimal loading conditions specified by the gensets' SFOC curves. Non-optimal genset loading conditions contribute to lower fuel utilization, where the emission of greenhouse gases is not in line with the load demand. To achieve more optimal genset loading conditions in the unit commitment, two different strategies were proposed and implemented. One based on MILP and the other based on logics. Moreover, three different power system configurations were proposed; i) four fixed-speed gensets, ii) three fixed-speed gensets and one variable-speed genset, and iii) four fixed-speed gensets and an ESS. The proposed unit commitment algorithms were run with the three proposed power system configurations using the load profiles from the three vessels extracted during operation. The results indicated that all vessels would benefit of smarter unit commitment strategies, both in terms of reduced fuel consumption and reduced total genset running hours. Moreover, the ferry and the PSV would further benefit of an ESS to increase the genset loadings toward optimal loading conditions specified by the individual gensets' SFOC curves. The seismic survey vessel, which had a more stable load profile, would benefit most from the configuration with three fixed-speed gensets and one variable-speed genset. For all vessels the reduction in fuel consumption and total genset running hours were achieved at the cost of increasing the total number of genset starts/stops. Increasing the number of starts/stops will increase wear and tear of an electrical genset start system, and increased compressor loads for a genset start system using compressed air. Increased wear and tear of auxiliary systems, such as an electrical genset start system, can be avoided by right dimensioning.

As the results portrayed, a vessel's power system configuration, its power producer units and energy storage(s) should be carefully designed and dimensioned with regards to the vessel's intended operations, and the units and energy storage(s) carefully controlled to achieve a fuel-efficient power generation with minimal emissions. Even though the results in this analysis indicated potential fuel savings and reduced emissions by applying smarter unit commitment strategies and redesigning the power configurations, more work must be conducted to strengthen the analysis by including various stakeholder requirements. In addition, different sizes and types of power producers and energy storages must be considered to find the optimal power system solution for a given vessel. Hence, recommendations for future work are listed as follows:

- Include various stakeholder requirements in the EMS analysis, such as class rules and regulations, charterer/employer requirements and environmental regulations, which affect the shipboard power system and its power production. This means that also *active* rules and requirements along with power system reconfigurations must be logged and time stamped during the extraction of real vessel data during operation.

- Include power producer unit dynamics in the EMS analysis, and optimize power producer unit types, sizes and ratings, along with capacity and ratings of potential energy storage(s), to find an optimal power system configuration to achieve maximal fuel savings and reduction in genset running hours for a given vessel's load profile. An additional objective would be to minimize ESS cycling and deep discharge to maximize the lifetime of ESS based on batteries.

- Assessment of the investment costs (CAPEX) related to installing an ESS, and the increased complexity in the total system, compared to potential fuel savings and reduced genset running hours, i.e. operational costs (OPEX).

References

[1] *A Brief History of the T2 Tanker*. Accessed: 2015-08-06. URL: http://www.t2tanker.org/t2-history.html.

[2] *A Glimpse Into BB-40' Early Years*. Accessed: 2015-07-03. URL: http://www.ussnewmexico.net/old-updates/.

[3] *ABB: The step forward, Onboard DC Grid*. Accessed: 2015-09-22. URL: http://new.abb.com/docs/librariesprovider91/articles/lm00614-onboard-dc-grid-brochure_june2014_1.pdf?sfvrsn=2.

[4] ABS. URL: http://ww2.eagle.org/.

[5] ABS. *Guide for Dynamic Positioning Systems*. Nov. 2013. URL: http://ww2.eagle.org/.

[6] *ABS: Guidance Notes on Control of Harmonics in Electrical Power Systems*. May 2006.

[7] Alf Kåre Ådnanes. *Maritime electrical installations and diesel electric propulsion*. ABB, 2003.

[8] Vilmar Æsøy and Dag Stenersen. 'Low Emission LNG Fuelled Ships for Environmental Friendly Operations in Arctic Areas'. In: *ASME 2013 32nd International Conference on Ocean, Offshore and Arctic Engineering*. American Society of Mechanical Engineers. 2013, V006T07A028–V006T07A028.

[9] Seon-Ju Ahn, Jin-Woo Park, Il-Yop Chung, Seung-Il Moon, Sang-Hee Kang and Soon-Ryul Nam. 'Power-sharing method of multiple distributed generators considering control modes and configurations of a microgrid'. In: *IEEE Trans. Power Del.* 25.3 (2010), pp. 2007–2016.

[10] H. Akagi, E.H. Watanabe and M. Aredes. *Instantaneous Power Theory and Applications to Power Conditioning*. IEEE Press Series on Power Engineering. Wiley, 2007.

[11] S. Alahakoon and M. Leksell. 'Emerging energy storage solutions for transportation – A review: An insight into road, rail, sea and air transportation applications'. In: *2015 International Conference on Electrical Systems for Aircraft, Railway, Ship Propulsion and Road Vehicles (ESARS)*. Mar. 2015, pp. 1–6.

[12] C.F.M. Almeida and N. Kagan. 'Harmonic coupled Norton equivalent model for modeling harmonic-producing loads'. In: *14th International Conference on Harmonics and Quality of Power (ICHQP), 2010*. IEEE. 2010, pp. 1–9.

[13] *America's First Aircraft Carrier - USS Langley*. Accessed: 2015-07-03. URL: http://www.navalhistory.org/2014/03/20/americas-first-aircraft-carrier-uss-langley-cv-1-warfighting-first-platforms-people.

[14] Joel Andersson. 'A General-Purpose Software Framework for Dynamic Optimization'. PhD thesis. Department of Electrical Engineering (ESAT/SCD) and Optimization in Engineering Center (Kasteelpark Arenberg 10, 3001-Heverlee, Belgium): Arenberg Doctoral School, KU Leuven, Oct. 2013.

[15] Amjad Anvari-Moghaddam, Tomislav Dragicevic, Lexuan Meng, Bo Sun and Josep M Guerrero. 'Optimal Planning and Operation Management of a Ship Electrical Power System with Energy Storage System'. In: *42nd Annual Conference of the IEEE Industrial Electronics Society (iecon'16)*. IEEE Press. 2016.

[16] *Association of the United States Navy: USS Langley - The Navy's First Carrier*. Accessed: 2015-07-03. URL: http://www.ausn.org/NewsPublications/NavyMagazine/MagazineArticles/tabid/2170/ID/8239/USS-Langley--The-Navys-First-Carrier.aspx.

[17] BJ Baliga, MS Adler, PV Gray, RP Love and Nathan Zommer. 'The insulated gate rectifier (IGR): A new power switching device'. In: *International Electron Devices Meeting, 1982*. Vol. 28. IEEE. 1982, pp. 264–267.

[18] M.E. Baran and N.R. Mahajan. 'DC distribution for industrial systems: opportunities and challenges'. In: *IEEE Trans. Ind. Appl.* 39.6 (Nov. 2003), pp. 1596–1601.

[19] E Barklund, Nagaraju Pogaku, Milan Prodanović, C Hernandez-Aramburo and Tim C Green. 'Energy management in autonomous microgrid using stability-constrained droop control of inverters'. In: *IEEE Transactions on Power Electronics* 23.5 (2008), pp. 2346–2352.

[20] Subhashish Bhattacharya, Po-Tai Cheng and Deepak M Divan. 'Hybrid solutions for improving passive filter performance in high power applications'. In: *IEEE Trans. Ind. Appl.* 33.3 (1997), pp. 732–747.

[21] F. A. Bhuiyan and A. Yazdani. 'Energy storage technologies for grid-connected and off-grid power system applications'. In: *Electrical Power and Energy Conference (EPEC), 2012 IEEE*. Oct. 2012, pp. 303–310.

[22] L.T. Biegler. *Nonlinear Programming: Concepts, Algorithms, and Applications to Chemical Processes*. Society for Industrial and Applied Mathematics (SIAM), 2010.

[23] T. I. Bø et al. 'Real-time Marine Vessel and Power Plant Simulator'. In: *ASME 34th International Conference on Ocean, Offshore and Arctic Engineering (OMAE2015) in St. John's, Newfoundland, Canada*. 2015.

[24] Torstein Ingebrigtsen Bø. 'Scenario- and Optimization-based Control of Marine Electric Power Systems'. PhD thesis. Department of Engineering Cybernetics: Norwegian University of Science and Technology, Mar. 2016.

[25] Math Bollen, Mark Stephens, S Djokic, K Stockman, B Brumsickle, J Milanovic, J Romero Gordón, R Neumann, G Ethier, F Corcoles et al. 'Voltage dip immunity of equipment and installations'. In: *Prepared by the members of CIGRE/CIRED/UIE Joint Working Group C* 4 (2010).

[26] C. Bordons and C. Montero. 'Basic Principles of MPC for Power Converters: Bridging the Gap Between Theory and Practice'. In: *IEEE Industrial Electronics Magazine* 9.3 (Sept. 2015), pp. 31–43.

[27] Bimal K Bose. 'Power electronics-an emerging technology'. In: *IEEE Transactions on Industrial Electronics* 36.3 (1989), pp. 403–412.

[28] Bimal K Bose. 'Power electronics and motor drives recent progress and perspective'. In: *IEEE Transactions on Industrial Electronics* 56.2 (2009), pp. 581–588.

[29] B.K. Bose. 'Power electronics-a technology review'. In: *Proceedings of the IEEE* 80.8 (Aug. 1992), pp. 1303–1334.

[30] B.K. Bose. *Power Electronics And Motor Drives: Advances and Trends*. Elsevier Science, 2010.

[31] Aviva Brecher and David Arthur. *Review and Evaluation of Wireless Power Transfer (WPT) for Electric Transit Applications*. Tech. rep. 2014.

[32] *Brief History of Diesel-Electric Submarines.* Accessed: 2015-08-12. URL: http://www.pmbatteries.com.au/batteries/history-of-diesel-electric-submarines.

[33] D. M. Brod and A. W. Novotny. 'Current Control of VSI-PWM Inverters'. In: *IEEE Trans. Ind. Appl.* IA-21.4 (June 1985), pp. 562–570.

[34] A. K. Broen, M. Amin, E. Skjong and M. Molinas. 'Instantaneous frequency tracking of harmonic distortions for grid impedance identification based on Kalman filtering'. In: *2016 IEEE 17th Workshop on Control and Modeling for Power Electronics (COMPEL).* June 2016, pp. 1–7.

[35] Robert Grover Brown and Patrick Y C Hwang. *Introduction to random signals and applied kalman filtering: with MATLAB exercises and solutions; 3rd ed.* New York, NY: Wiley, 1997.

[36] *Bureau Veritas: Rules for the Classification of Steel Ships: Part C - Machinery, Electricity, Automation and Fire Protection.* July 2014.

[37] WB Carter. 'The Ljungström System of Electric Drive'. In: *Journal of the American Society for Naval Engineers* 28.3 (1916), pp. 708–728.

[38] Enrique Castillo, Antonio J Conejo, Pablo Pedregal, Ricardo Garcia and Natalia Alguacil. *Building and solving mathematical programming models in engineering and science.* Vol. 62. John Wiley & Sons, 2011.

[39] A.P. Chalkley. *Diesel engines for land and marine work.* D. Van Nostrand, 1912.

[40] Lin-Gen Chen, Jun-Lin Zheng, Feng-Rui Sun and Chih Wu. 'Power, power density and efficiency optimization for a closed cycle helium turbine nuclear power plant'. In: *Energy Conversion and Management* 44.15 (2003), pp. 2393 –2401.

[41] EU Commission et al. 'The Paris protocol: A blueprint for tackling global climate change beyond 2020'. In: *COM (2015)* 81 (2015).

[42] P. Cortés, M. P. Kazmierkowski, R. M. Kennel, D. E Quevedo and J. Rodríguez. 'Predictive Control in Power Electronics and Drives'. In: *IEEE Trans. Ind. Electron.* 55.12 (Dec. 2008), pp. 4312–4324.

[43] Patricio Cortes, José Rodríguez, Patrycjusz Antoniewicz and Marian Kazmierkowski. 'Direct power control of an AFE using predictive control'. In: *IEEE Trans. Power Electron.* 23.5 (2008), pp. 2516–2523.

[44] Patricio Cortés, Gabriel Ortiz, Juan I Yuz, José Rodríguez, Sergio Vazquez and Leopoldo G Franquelo. 'Model predictive control of an inverter with output filter for UPS applications'. In: *IEEE Trans. Ind. Electron.* 56.6 (2009), pp. 1875–1883.

[45] Patricio Cortés, Marian P Kazmierkowski, Ralph M Kennel, Daniel E Quevedo and José Rodríguez. 'Predictive control in power electronics and drives'. In: *IEEE Trans. Ind. Electron.* 55.12 (2008), pp. 4312–4324.

[46] *Corvus Energy: CASE STUDY: Norled AS, MF Ampere, Ferry.* Accessed: 2015-08-20. URL: http://files7.webydo.com/42/421998/UploadedFiles/a4465574-14ff-4689-a033-08ac32adada1.pdf.

[47] Grant Covic, John T Boys et al. 'Modern trends in inductive power transfer for transportation applications'. In: *IEEE Journal of Emerging and Selected Topics in Power Electronics* 1.1 (2013), pp. 28–41.

[48] Joseph J Cunningham. 'Manhattan Electric Power Distribution, 1881-1901'. In: *Proceedings of the IEEE* 103.5 (2015), pp. 850–858.

[49] Frederick Dalzell. *Engineering Invention, Frank J. Sprague and the U.S. Electrical Industry.* MIT Press, 2010.

[50] Kent Davey. 'Ship Component in Hull Optimization'. In: *Marine Technology Society Journal* 39.2 (2005), pp. 39–46.

[51] Paul A. David and Julie Ann Bunn. 'The economics of gateway technologies and network evolution: Lessons from electricity supply history'. In: *Information Economics and Policy* 3.2 (1988), pp. 165 – 202.

[52] Philip S Dawson. *British Superliners of the Sixties: A Design Appreciation of the Oriana, Canberra and QE2.* London: Conway Martime Press, 1990.

[53] Philip S Dawson. *Canberra: In the Wake of a Legend.* Conway Maritime Press, 1997.

[54] Eleftherios K Dedes, Dominic A Hudson and Stephen R Turnock. 'Assessing the potential of hybrid energy technology to reduce exhaust emissions from global shipping'. In: *Energy Policy* 40 (2012), pp. 204–218.

[55] N.-Q Dinh and J. Arrilaga. 'A Salient-Pole Generator Model for Harmonic Analysis'. In: *IEEE Trans. Power Syst.* 16.4 (Nov. 2001), pp. 609–615.

[56] K.C. Divya and Jacob Østergaard. 'Battery energy storage technology for power systems - An overview'. In: *Electric Power Systems Research* 79.4 (2009), pp. 511 –520.

[57] DNV. *Dynamic Positioning Systems.* Rules for Classification of Ships, Part 6, Chapter 7. July 2014. URL: http://www.dnv.com.

[58] DNV. *Failure Mode and Effect Analysis (FMEA) of Redundant Systems.* DNV-RP-D102. Jan. 2012. URL: http://www.dnv.com.

[59] DNV-GL. URL: https://www.dnvgl.com/.

[60] DNV-GL. *Recommended Practice: Safety, operation and performance of grid-connected energy storage systems.* DNVGL-RP-0043. Dec. 2015. URL: https://www.dnvgl.com/.

[61] DNV-GL. *The ReVolt – A new inspirational ship concept.* Accessed: 2015-09-26. 2015. URL: https://www.dnvgl.com/technology-innovation/revolt/index.html.

[62] *DNV-GL: Highlight Projects in the LNG as Fuel History.* Accessed: 2015-08-24. URL: https://www.dnvgl.com/Images/LNG\%20as\%20fuel\%20highlight\%20projects_new_tcm8-6116.pdf.

[63] *DNV-RU-SHIP-Pt4Ch8: Part 4 Systems and components, Chapter 8 Electrical installations.* October 2015.

[64] *DNVGL-OS-D201: Offshore standards, Electrical Installations.* July 2015.

[65] N. Doerry. 'Naval Power Systems: Integrated power systems for the continuity of the electrical power supply.' In: *IEEE Electrification Magazine* 3.2 (June 2015), pp. 12–21.

[66] Norbert H Doerry and David H Clayton. 'Shipboard electrical power quality of service'. In: *Electric Ship Technologies Symposium, 2005 IEEE.* IEEE. 2005, pp. 274–279.

[67] Alexander Domahidi and Juan Jerez. *FORCES Professional*. embotech GmbH (http://embotech.com/FORCES-Pro). July 2014.

[68] W.H. Donnelly. *Nuclear Power and Merchant Shipping*. Nuclear Power and Merchant Shipping v. 7. U.S. Atomic Energy Commission, Division of Technical Information, 1964.

[69] D.H. Dyal, B.B. Carpenter and M.A. Thomas. *Historical Dictionary of the Spanish American War*. Gale virtual reference library. Greenwood Press, 1996.

[70] *Edison vs. Westinghouse: A Shocking Rivalry*. Accessed: 2015-07-01. URL: http://www.smithsonianmag.com/history/edison-vs-westinghouse-a-shocking-rivalry-102146036/?no-ist.

[71] *Electric Generator*. Accessed: 2015-06-29. URL: http://edison.rutgers.edu/generator.htm.

[72] *Engineering and Technology History Wiki: Edison's Electric Light and Power System*. Accessed: 2015-06-29. URL: http://ethw.org/Edison's_Electric_Light_and_Power_System.

[73] T. Ericsen. 'Future navy application of wide bandgap power semiconductor devices'. In: *Proceedings of the IEEE* 90.6 (June 2002), pp. 1077–1082.

[74] T. Ericsen. 'Power Electronic Building Blocks - A systematic approach to power electronics'. In: *IEEE Power Engineering Society Summer Meeting, 2000*. Vol. 2. 2000, 1216–1218 vol. 2.

[75] T. Ericsen, N. Hingorani and Y. Khersonsky. 'Power electronics and future marine electrical systems'. In: *Petroleum and Chemical Industry Technical Conference, 2004. Fifty-First Annual Conference 2004*. Sept. 2004, pp. 163–171.

[76] T. Ericsen and A. Tucker. 'Power Electronics Building Blocks and potential power modulator applications'. In: *Conference Record of the 1998 Twenty-Third International Power Modulator Symposium, 1998*. June 1998, pp. 12–15.

[77] Anne Mai Ersdal, Davide Fabozzi, Lars Imsland and Nina F Thornhill. 'Model predictive control for power system frequency control taking into account imbalance uncertainty'. In: *Proc. IFAC World Congr.* Vol. 19. 2014, pp. 981–986.

[78] Christian Esposito and Mario Ciampi. 'On Security in Publish / Subscribe services: A Survey'. In: *Communications Surveys & Tutorials, IEEE* 17.2 (2015), pp. 966–997.

[79] I.C. Evans, A.H. Hoevenaars and P. Eng. 'Meeting Harmonic Limits on Marine Vessels'. In: *IEEE Electric Ship Technologies Symposium, 2007. ESTS '07.* May 2007, pp. 115–121.

[80] H. Faÿ. *Dynamic Positioning Systems: Principles, Design and Applications.* Technip, 1990.

[81] H.J. Ferreau, C. Kirches, A. Potschka, H.G. Bock and M. Diehl. 'qpOASES: A parametric active-set algorithm for quadratic programming'. In: *Mathematical Programming Computation* 6.4 (2014), pp. 327–363.

[82] P.E. Fontenoy. *Submarines: An Illustrated History of Their Impact.* Weapons and warfare series. ABC-CLIO, 2007.

[83] Jack Foran. *The Day They Turned The Falls On: The Invention Of The Universal Electrical Power System.* Accessed: 2015-07-01. URL: http://library.buffalo.edu/projects/cases/niagara.htm.

[84] A Fowler. 'Closed-cycle diesel engine for underwater power'. In: (1984).

[85] A Fowler. 'Closed-cycle diesel engines as underwater power generators'. In: *North East Coast Institution of Engineers & Shipbuilders Transactions* 106.2 (1990).

[86] A Fowler. 'Closed cycle diesel propulsion systems'. In: *Institute of Marine Engineers Transactions* 102.Part 2 (1990).

[87] Martin Fowler. *UML distilled: a brief guide to the standard object modeling language.* Addison-Wesley Professional, 2004.

[88] N. Friedman. *U.S. Submarines Through 1945: An Illustrated Design History.* Illustrated Design Histories Series. Naval Institute Press, 1995.

[89] Gianluca Frison, D. Kwame Minde Kufoalor, Lars Imsland and John Bagterp Jørgensen. 'Efficient Implementation of Solvers for Linear Model Predictive Control on Embedded Devices'. In: *Proceedings of 2014 IEEE International Conference on Control Applications (CCA).* 2014, pp. 1954–1959.

[90] Alejandro Garces, Marta Molinas and Pedro Rodriguez. 'A generalized compensation theory for active filters based on mathematical optimization in ABC frame'. In: *Electric Power Systems Research, Elsevier Journal* 90.0 (2012), pp. 1 –10.

[91] R. Gardiner and A. Greenway. *The Golden Age of Shipping: The Classic Merchant Ship, 1900-1960*. Conway's history of the ship. Conway Maritime Press, 1994.

[92] William H Garzke and Robert O Dulin. *Battleships: Axis and Neutral Battleships in World War II*. Vol. 3. Naval Institute Press, 1985.

[93] T. Geyer, G. Papafotiou and M. Morari. 'Model Predictive Control in Power Electronics: A Hybrid Systems Approach'. In: *44th IEEE Conference on Decision and Control 2005, and 2005 European Control Conference. CDC-ECC '05*. Dec. 2005, pp. 5606–5611.

[94] Stephen Gleaves and Guido Perla. *Electric Propulsion, It's time to get onboard*. Maritime Reporter and Engineering News. 2009.

[95] *GlobalSecurity: T2-SE-A1 AO-49 Suamico / AO-65 Pecos*. Accessed: 2015-08-06. URL: http://www.globalsecurity.org/military/systems/ship/t2-tanker.htm.

[96] Michael J Gouge. 'Closed cycle gas turbine nuclear power plant for submarine propulsion'. In: *Naval engineers journal* 107.6 (1995), pp. 35–41.

[97] W. M. Grady, M. J. Samotyj and A. H. Noyola. 'Minimizing network harmonic voltage distortion with an active power line conditioner'. In: *IEEE Trans. Power Del.* 6.4 (1991), pp. 1690–1697.

[98] W. M. Grady, M. J. Samotyj and A.H. Noyola. 'The application of network objective functions for actively minimizing the impact of voltage harmonics in power systems'. In: *IEEE Trans. Power Del.* 7.3 (1992), pp. 1379–1386.

[99] W Mack Grady, Marek J Samotyj and Antonio H Noyola. 'Survey of active power line conditioning methodologies'. In: *Power Delivery, IEEE Transactions on* 5.3 (1990), pp. 1536–1542.

[100] Hugo Grimmelius, Peter de Vos, Moritz Krijgsman and Erik van Deursen. 'Control of hybrid ship drive systems'. In: *10th international conference on computer and IT applications in the maritime industries. Berlin: Technische Universitat Hamburg-Harburg*. 2011.

[101] Giuseppe Guidi and Jon Are Suul. 'Minimization of converter ratings for MW-scale inductive charger operated under widely variable coupling conditions'. In: *2015 IEEE PELS Workshop on Emerging Technologies: Wireless Power (WoW)*. IEEE. 2015, pp. 1–7.

[102] Ernst Hairer and Gerhard Wanner. 'Stiff differential equations solved by Radau methods'. In: *Journal of Computational and Applied Mathematics* 111.1-2 (1999), pp. 93 –111.

[103] A. A. Halacsy and G. H. von Fuchs. 'Transformer invented 75 years ago'. In: *Electrical Engineering* 80.6 (June 1961), pp. 404–407.

[104] Jeff Hammarlund. 'Oregon's role as an energy innovator: A historical perspective'. In: *Oregon's Future 3 (1), 10.(2002)* (2002).

[105] M.R. Hanna. *Voltage transformation*. US Patent 1,026,391. May 1912.

[106] H Franklin Harvey Jr and WE Thau. 'Electric Propulsion of Ships'. In: *American Institute of Electrical Engineers, Transactions of the* 44 (1925), pp. 497–522.

[107] M. M. Hashempour, M. Savaghebi, J. C. Vasquez and J. M. Guerrero. 'A Control Architecture to Coordinate Distributed Generators and Active Power Filters Coexisting in a Microgrid'. In: *IEEE Transactions on Smart Grid* 7.5 (Sept. 2016), pp. 2325–2336.

[108] R.E. Hebner, K. Davey, J. Herbst, D. Hall, J. Hahne, D.D. Surls and A. Ouroua. 'Dynamic Load and Storage Integration'. In: *Proceedings of the IEEE* 103.12 (Dec. 2015), pp. 2344–2354.

[109] Robert E. Hebner et al. 'Technical cross-fertilization between terrestrial microgrids and ship power systems'. In: *Journal of Modern Power Systems and Clean Energy* (2015), pp. 1–19.

[110] C.C. Herskind, M.M. Morack and IEEE Industry Applications Society. *A History of Mercury-arc Rectifiers in North America*. IEEE, 1987.

[111] *History of Electricity*. Accessed: 2015-06-30. URL: http://www.electricalfacts.com/Neca/Science/electricity/history.shtml.

[112] T. Hoevenaars, I. Evans and A. Lawson. 'New marine harmonic standards'. In: vol. 16. 1. Jan. 2010, pp. 16–25.

[113] Thomas Hone and Trent Hone. *Battle Line: The United States Navy, 1919-1939*. Naval Institute Press, 2006.

[114] J.H. Horlock. *Advanced Gas Turbine Cycles: A Brief Review of Power Generation Thermodynamics*. Elsevier Science, 2013.

[115] LR Horne. *Electric propulsion of ships*. North East Coast Institution of Engineers and Shipbuilders, 1939.

[116] B. Houska, H.J. Ferreau and M. Diehl. 'ACADO Toolkit – An Open Source Framework for Automatic Control and Dynamic Optimization'. In: *Optimal Control Applications and Methods* 32.3 (2011), pp. 298–312.

[117] B. Houska, H.J. Ferreau and M. Diehl. 'An Auto-Generated Real-Time Iteration Algorithm for Nonlinear MPC in the Microsecond Range'. In: *Automatica* 47.10 (2011), pp. 2279–2285.

[118] S. Huang. *Qt 5 Blueprints*. Community experience distilled. Packt Publishing, 2015.

[119] Harlow A Hyde. *Scraps of Paper: The Disarmament Treaties Between the World Wars*. Harlow Andrew Hyde, 1988.

[120] Hussein Ibrahim, Adrian Ilinca and Jean Perron. 'Energy storage systems – Characteristics and comparisons'. In: *Renewable and sustainable energy reviews* 12.5 (2008), pp. 1221–1250.

[121] IMCA. URL: http://www.imca-int.com/.

[122] IMCA. *A Guide to DP Electrical Power and Control Systems*. IMCA M 206. Nov. 2010. URL: http://www.imca-int.com.

[123] IMCA. *Guidelines for The Design and Operation of Dynamically Positioned Vessels*. IMCA M 103 Rev. 1. Dec. 2007. URL: http://www.imca-int.com.

[124] IMCA. *International Guidelines for The Safe Operation of Dynamically Positioned Offshore Supply Vessels*. IMCA 182 MSF Rev. 2. Apr. 2015. URL: http://www.imca-int.com.

[125] IMO. URL: http://www.imo.org/.

[126] IMO. *Guidelines for Vessels with Dynamic Positioning Systems*. MSC / Circ.645. June 1994. URL: http://www.imo.org.

[127] International Maritime Organization (IMO). *Third IMO Greenhouse Gas Study 2014*. International Maritime Organization (IMO), 2014.

[128] *International Maritime Organization: Prevention of Air Pollution from Ships*. Accessed: 2015-08-21. URL: http://www.imo.org/en/OurWork/Environment/PollutionPrevention/AirPollution/Pages/Air-Pollution.aspx.

[129] Sándor Jeszenszky. *Electrostatics and Electrodynamics at Pest University in the id-19th Century*. Accessed: 2015-07-01. URL: http://ppp.unipv.it/Collana/Pages/Libri/Saggi/Volta\%20and\%20the\%20History\%20of\%20Electricity/V\%26H\%20Sect2/V\%26H\%20175-182.pdf.

[130] L. Jin, R. Kumar and N. Elia. 'Model Predictive Control-Based Real-Time Power System Protection Schemes'. In: *IEEE Trans. Power Syst.* 25.2 (May 2010), pp. 988–998.

[131] T. A. Johansen and A. J. Sørensen. 'Experiences with HIL simulator testing of power management systems'. In: *MTS Dynamic Positioning Conference, Houston, TX*. 2009.

[132] T.A. Johansen. 'Toward Dependable Embedded Model Predictive Control'. In: *IEEE Syst. J.* in press.99 (2014), pp. 1–12.

[133] Tor Arne Johansen, Torstein I Bo, Eirik Mathiesen, Aleksander Veksler and Asgeir J Sorensen. 'Dynamic Positioning System as Dynamic Energy Storage on Diesel-Electric Ships'. In: *IEEE Transactions on Power Systems* 29.6 (2014), pp. 3086–3091.

[134] F. D. Kanellos. 'Optimal Power Management With GHG Emissions Limitation in All-Electric Ship Power Systems Comprising Energy Storage Systems'. In: *IEEE Transactions on Power Systems* 29.1 (Jan. 2014), pp. 330–339.

[135] F. D. Kanellos, G. J. Tsekouras and N. D. Hatziargyriou. 'Optimal Demand-Side Management and Power Generation Scheduling in an All-Electric Ship'. In: *IEEE Transactions on Sustainable Energy* 5.4 (Oct. 2014), pp. 1166–1175.

[136] Sami H Karaki, Rabih Jabr, Riad Chedid and Ferdinand Panik. *Optimal Energy Management of Hybrid Fuel Cell Electric Vehicles*. Tech. rep. SAE Technical Paper, 2015.

[137] M. P. Kaźmierkowski and L. Malesani. 'Current Control Techniques for Three-Phase Voltage Source PWM Converters: A Survey'. In: *IEEE Trans. Ind. Electron.* 45.5 (Oct. 1998), pp. 691–703.

[138] A. Khaligh and Zhihao Li. 'Battery, Ultracapacitor, Fuel Cell, and Hybrid Energy Storage Systems for Electric, Hybrid Electric, Fuel Cell, and Plug-In Hybrid Electric Vehicles: State of the Art'. In: *IEEE Trans. Veh. Technol.* 59.6 (July 2010), pp. 2806–2814.

[139] S. Kim, S. Choe, S. Ko and S. Sul. 'A Naval Integrated Power System with a Battery Energy Storage System: Fuel efficiency, reliability, and quality of power.' In: *IEEE Electrification Magazine* 3.2 (June 2015), pp. 22–33.

[140] Samir Kouro, Patricio Cortés, René Vargas, Ulrich Ammann and José Rodríguez. 'Model predictive control – A simple and powerful method to control power converters'. In: *IEEE Trans. Ind. Electron.* 56.6 (2009), pp. 1826–1838.

[141] Benjamin Kroposki, Robert Lasseter, Toshifumi Ise, Satoshi Morozumi, S Papatlianassiou and Nikos Hatziargyriou. 'Making microgrids work'. In: *IEEE Power and Energy Magazine* 6.3 (2008), pp. 40–53.

[142] O. Laldin, M. Moshirvaziri and O. Trescases. 'Predictive Algorithm for Optimizing Power Flow in Hybrid Ultracapacitor/Battery Storage Systems for Light Electric Vehicles'. In: *IEEE Transactions on Power Electronics* 28.8 (Aug. 2013), pp. 3882–3895.

[143] Andrey Lana, K Tikkanen, Tuomo Lindh and Jarmo Partanen. 'Control of directly connected energy storage in diesel electric vessel drives'. In: *15th International Power Electronics and Motion Control Conference (EPE/PEMC), 2012*. IEEE. 2012, DS1e–7.

[144] R.H. Lasseter. 'MicroGrids'. In: *Power Engineering Society Winter Meeting, 2002. IEEE*. Vol. 1. 2002, 305–308 vol.1.

[145] Matti Lehti, Pertti Hyvarinen and Timo Tissari. 'The new generation of propulsion drive systems'. In: *All Electric Ship 2003 Conference*. 2003, pp. 13–14.

[146] P. Lezana, R. Aguilera and D.E. Quevedo. 'Model Predictive Control of an Asymmetric Flying Capacitor Converter'. In: *IEEE Trans. Ind. Electron.* 56.6 (June 2009), pp. 1839–1846.

[147] *Lighting the Steam Ship Columbia with Edison's First Commercial Light Plant*. Accessed: 2015-06-29. URL: http://www.ieeeghn.org/wiki/images/f/fe/Edison_-_lighting_the_steamship_columbia_with_edisons_first_commercial_light_plant.pdf.

[148] K.V. Ling, S.P. Yue and J.M. Maciejowski. 'A FPGA implementation of model predictive control'. In: *American Control Conference, 2006.* June 2006, 6 pp.–.

[149] P. J. A Ling and C. J. Eldridge. 'Designing 21st Century Electrical Systems that Incorporate System-wide Harmonic Conditioning'. In: *IEEE - IASTED International Conference on Power Quality in High Technology Competition, Florida, 1997.* 1997.

[150] *Lloyd's Register: General Information for the Rules and Regulations for the Classification of Ships.* July 2014.

[151] J Lopes, CL Moreira and AG Madureira. 'Defining control strategies for microgrids islanded operation'. In: *IEEE Trans. Power Syst.* 21.2 (2006), pp. 916–924.

[152] Nie Luo, G.H. Miley, Kyu-Jung Kim, Rodney Burton and Xinyu Huang. 'NaBH4/H2O2 fuel cells for air independent power systems'. In: *Journal of Power Sources* 185.2 (2008), pp. 685 –690.

[153] John M. Maber. *Electrical Supply in Warships; A brief History.* Crown Copyright/MoD (1980), Accessed: 2015-09-26. URL: http://www.worldnavalships.com/forums/showthread.php?t=12722.

[154] Gaston Maggetto and Peter Van den Bossche. 'Inductive Automatic Charging–The Way to Safe, Efficient and User-Friendly Electric Vehicle Infrastructure'. In: *Electric Vehicle Symposium EVS-18.* 2001, pp. 20–24.

[155] *March 20, 1800: Volta describes the Electric Battery.* Accessed: 2015-08-11. URL: http://www.aps.org/publications/apsnews/200603/history.cfm.

[156] *Marine Engineering.* v. 8. Marine Publishing Company, 1903.

[157] Martin Doppelbauer. *The invention of the electric motor 1800-1854.* Accessed: 2015-09-27. URL: http://www.saint-petersburg.com/famous-people/moritz-hermann-von-jacobi/.

[158] E. Mathiesen, B. Realfsen and M. Breivik. 'Methods for reducing frequency and voltage variations on DP vessels'. In: *MTS Dynamic Positioning Conference, Houston, TX.* 2012.

[159] Paolo Mattavelli. 'A closed-loop selective harmonic compensation for active filters'. In: *IEEE Trans. Ind. Appl.* 37.1 (2001), pp. 81–89.

[160] E. Mayhorn, K. Kalsi, J. Lian and M. Elizondo. 'Model Predictive Control-Based Optimal Coordination of Distributed Energy Resources'. In: *2013 46th Hawaii International Conference on System Sciences (HICSS)*. Jan. 2013, pp. 2237–2244.

[161] W.M. McBride. *Technological Change and the United States Navy, 1865–1945*. Johns Hopkins Studies in the History of Technology. Johns Hopkins University Press, 2000.

[162] Neil McCart. *P&O's Canberra - The Ship That Shaped The Future*. Kingfisher Railway Publications, 1989.

[163] T. McCoy. 'Electric Ships Past, Present, and Future [Technology Leaders]'. In: *IEEE Electrification Magazine* 3.2 (June 2015), pp. 4–11.

[164] T.J. McCoy. 'Trends in ship electric propulsion'. In: *Power Engineering Society Summer Meeting, 2002 IEEE*. Vol. 1. July 2002, 343–346 vol.1.

[165] T. McNichol. *AC/DC: The Savage Tale of the First Standards War*. Wiley, 2011.

[166] E. D. Mehleri, H. Sarimveis, L. G. Papageorgiou and N. C. Markatos. 'Model Predictive Control of distributed energy resources'. In: *2012 20th Mediterranean Conference on Control Automation (MED)*. July 2012, pp. 672–678.

[167] Scott Jason Moura, Hosam K Fathy, Duncan S Callaway and Jeffrey L Stein. 'A stochastic optimal control approach for power management in plug-in hybrid electric vehicles'. In: *Control Systems Technology, IEEE Transactions on* 19.3 (2011), pp. 545–555.

[168] Cristian Musardo, Giorgio Rizzoni, Yann Guezennec and Benedetto Staccia. 'A-ECMS: An adaptive algorithm for hybrid electric vehicle energy management'. In: *European Journal of Control* 11.4 (2005), pp. 509–524.

[169] Vincenzo Musolino, Luigi Piegari and Enrico Tironi. 'Storage systems for transportation, land handling and naval applications'. In: *Electrical Systems for Aircraft, Railway and Ship Propulsion (ESARS), 2012*. IEEE. 2012, pp. 1–9.

[170] *NAVSEA Design Practices and Criteria Manual, Electrical Systems for Surface Ships, Chapter 300*. Naval Sea Systems Command (NAVSEA). NAVSEA T9300-AF-PRO-020.

[171] *New home for Queen Elizabeth 2*. Accessed: 2015-08-17. URL: http://travel.cnn.com/new-home-queen-elizabeth-2-764401.

[172] *New Invention to Transform Shipbuilding*. Accessed: 2015-06-30. URL: http://query.nytimes.com/mem/archive-free/pdf?res=980CEEDE143EE033A25750C0A9669D946897D6CF.

[173] AnhTu Nguyen, Jimmy Lauber and Michel Dambrine. 'Optimal control based algorithms for energy management of automotive power systems with battery/supercapacitor storage devices'. In: *Energy Conversion and Management* 87 (2014), pp. 410–420.

[174] *Nikola Tesla Inventor*. Accessed: 2015-06-30. URL: http://nikolatesla-inventor.com/INVENTIONS/index.html.

[175] Jorge Nocedal and Stephen Wright. *Numerical optimization*. Springer Science & Business Media, 2006.

[176] Norwegian Maritime Authority (NMD). URL: https://www.sjofartsdir.no/en/ (visited on 02/08/2016).

[177] *Office of the Historian: The Washington Naval Conference, 1921-1922*. Accessed: 2015-08-06. URL: https://history.state.gov/milestones/1921-1936/naval-conference.

[178] Torill Grimstad Osberg and Tomas Heber Tronstad. 'Propelling Ships for the Future-Gas Engines Today, Fuel Cells Tomorrow'. In: *Marine Engineering* 44.6 (2009), pp. 922–933.

[179] A. Oudalov, D. Chartouni and C. Ohler. 'Optimizing a Battery Energy Storage System for Primary Frequency Control'. In: *IEEE Trans. Power Syst.* 22.3 (Aug. 2007), pp. 1259–1266.

[180] A. Oudalov, R. Cherkaoui and A. Beguin. 'Sizing and Optimal Operation of Battery Energy Storage System for Peak Shaving Application'. In: *IEEE Lausanne Power Tech, 2007*. July 2007, pp. 621–625.

[181] M.R. Patel. *Shipboard Electrical Power Systems*. Shipboard Electrical Power Systems. Taylor & Francis, 2011.

[182] *Peace Treaty of Versailles, Articles 159-213: Military, Naval and Air Clauses*. Accessed: 2015-08-12. URL: http://net.lib.byu.edu/~rdh7/wwi/versa/versa4.html.

[183] S. M. Peeran and C. W. P. Cascadden. 'Application, Design, and Specification of Harmonic Filters for Variable Frequency Drives'. In: *IEEE Trans. Ind. Appl.* 31.4 (Aug. 1995), pp. 841–847.

[184] *PEO Ships Electric Ships Office: History*. Accessed: 2015-06-30. URL: http://www.navsea.navy.mil/teamships/PEOS_ElectricShips/ESO_History.aspx.

[185] Ola Persson, Christina Östberg, Joakim Pagels and Aleksandra Sebastian. 'Air contaminants in a submarine equipped with air independent propulsion'. In: *Journal of Environmental Monitoring* 8.11 (2006), pp. 1111–1121.

[186] Petrolium Safety Authority (PTIL) Norway. URL: http://www.psa.no/?lang=en_US (visited on 02/08/2016).

[187] Helfried Peyrl, Hans Joachim Ferreau and Dimitris Kouzoupis. 'A Hybrid Hardware Implementation for Nonlinear Model Predictive Control'. In: *IFAC-PapersOnLine* 48.23 (2015). 5th IFAC Conference on Nonlinear Model Predictive Control NMPC, Seville, Spain, 17-20 September 2015, pp. 87 –93.

[188] N. Polmar and K.J. Moore. *Cold War Submarines: The Design and Construction of U.S. and Soviet Submarines*. Brassey's, 2004.

[189] *QE2 History*. Accessed: 2015-08-17. URL: http://www.chriscunard.com/qe2_history.php.

[190] J.B. Rawlings and D.Q. Mayne. *Model Predictive Control: Theory and Design*. Nob Hill Pub., 2009.

[191] G.T. Reader, I.J. Potter, E.J. Clavelle and O.R. Fauvel. 'Low power Stirling engine for underwater vehicle applications'. In: *Proceedings of the 1998 International Symposium on Underwater Technology*. Apr. 1998, pp. 411–416.

[192] G.F. Reed, B.M. Grainger, A.R. Sparacino and Zhi-Hong Mao. 'Ship to Grid: Medium-Voltage DC Concepts in Theory and Practice'. In: *IEEE Power and Energy Magazine* 10.6 (Nov. 2012), pp. 70–79.

[193] H-J Reuss. 'Trials and tribulations of the marine diesel.' In: *Motor Ship* 84.1000 (2003), pp. 32–33.

[194] P.F. Ribeiro, B.K. Johnson, M.L. Crow, A. Arsoy and Y. Liu. 'Energy storage systems for advanced power applications'. In: *Proceedings of the IEEE* 89.12 (Dec. 2001), pp. 1744–1756.

[195] S. Richter, S. Mariéthoz and M. Morari. 'High-speed online MPC based on a fast gradient method applied to power converter control'. In: *Proceedings of the 2010 American Control Conference*. June 2010, pp. 4737–4743.

[196] M. Rivera, A. Wilson, C. A. Rojas, J. Rodriguez, J. R. Espinoza, P. W. Wheeler and L. Empringham. 'A Comparative Assessment of Model Predictive Current Control and Space Vector Modulation in a Direct Matrix Converter'. In: *IEEE Trans. Ind. Electron.* 60.2 (Feb. 2013), pp. 578–588.

[197] S.M. Robinson. *Electric Ship Propulsion*. Simmons-Boardman publishing Company, 1922.

[198] LH Roddis, JW Simpson et al. *The Nuclear Propulsion Plant of the USS Nautilus SSN-571*. Society of Naval Architects and Marine Engineers, 1954.

[199] Jose Rodriguez, Marian P Kazmierkowski, Jose R Espinoza, Pericle Zanchetta, Haitham Abu-Rub, Hector A Young and Christian A Rojas. 'State of the art of finite control set model predictive control in power electronics'. In: *IEEE Trans. Ind. Informat.* 9.2 (2013), pp. 1003–1016.

[200] Rolls-Royce-Marine. *Rolls-Royce Drone Ships Challenge $375 Billion Industry: Freight*. Accessed: 2015-09-26. 2014. URL: http://www.bloomberg.com/news/articles/2014-02-25/rolls-royce-drone-ships-challenge-375-billion-industry-freight.

[201] Frank Jr. Rowsome. *The Birth of Electric Traction, the extraordinary life of inventor Frank Julian Sprague*. IEEE History Center Press, 2013.

[202] A. Rygg, E. Skjong and M. Molinas. 'Handling System Harmonic Propagation in a Diesel-Electric Ship with an Active Filter'. In: *ESARS 2015 Conference on Electrical Systems for Aircraft, Railway, Ship Propulsion and Road Vehicles*. Mar. 2015.

[203] saint-petersburg.com. *Moritz Hermann von Jacobi*. Accessed: 2015-09-26. URL: http://www.saint-petersburg.com/famous-people/moritz-hermann-von-jacobi/.

[204] Zainal Salam, Tan Perng Cheng and Awang Jusoh. 'Harmonics mitigation using active power filter: A technological review'. In: *Elektrika Journal of Electrical Engineering* 8.2 (2006), pp. 17–26.

[205] Kjell Martin Sandaker et al. 'Use of natural gas as fuel for ships'. In: *19th World Petroleum Congress*. World Petroleum Congress. 2008.

[206] S. Sandler. *World War II in the Pacific: An Encyclopedia*. Garland Military History of the United States. Garland Pub., 2001.

[207] Gunter Sattler. 'Fuel cells going on-board'. In: *Journal of Power Sources* 86.1-2 (2000), pp. 61–67.

[208] Mike Schuler. *Introducing ISLA BELLA - World's First LNG-Powered Containership Launched at NASSCO)*. Accessed: 2015-08-25. 2015. URL: http://gcaptain.com/isla-bella-worlds-first-lng-powered-containership-launched-at-nassco/\#.VdwXkPntlBc.

[209] *Seatrade Award for DNV GL classed Ampere, world's first fully electric vessel*. Accessed: 2015-08-20. URL: https://www.dnvgl.com/news/seatrade-award-for-dnv-gl-classed-ampere-world-s-first-fully-electric-vessel--24038.

[210] Gayathri Seenumani. 'Real-time power management of hybrid power systems in all electric ship applications'. PhD thesis. The University of Michigan, 2010.

[211] Siemens. *Electrical Propulsion Systems*. Accessed: 2015-12-22. URL: http://w3.siemens.no/home/no/no/sector/industry/marine/pages/electrical_propulsion_systems3.aspx.

[212] *Siemens: BlueDrive PlusC*. Accessed: 2015-09-22. URL: https://w3.siemens.no/home/no/no/sector/industry/marine/Documents/Orig.BDPC_16pages.pdf.

[213] G. K. Singh. 'Power system harmonics research: a survey'. In: *European Transactions on Electrical Power* 19.2 (2009), pp. 151–172.

[214] E. Skjong, T. Johansen and M. Molinas. *Real-time Model Predictive Control Architecture for System-level Harmonic Mitigation in Power Systems*. Submitted for publication.

[215] E. Skjong, T. Johansen, M. Molinas and A. J. Sørensen. 'Approaches to Economic Energy Management in Diesel-Electric Marine Vessels'. In: *IEEE Trans. Transport. Electrific.* 3.1 (2017), pp. 22–35.

[216] E. Skjong, S. Gale, M. Molinas and T. A. Johansen. 'Data-Driven decision support tool for power quality measures in marine vessel power system'. In: *2016 IEEE Transportation Electrification Conference and Expo (ITEC)*. June 2016, pp. 1–8.

[217] E. Skjong, R. Volden, E. Rødskar, M. Molinas, T. A. Johansen and J. Cunningham. 'Past, Present, and Future Challenges of the Marine Vessel's Electrical Power System'. In: *IEEE Trans. Transport. Electrific.* 2.4 (Dec. 2016), pp. 522–537.

[218] E. Skjong, J. A. Suul, A. Rygg, T. A. Johansen and M. Molinas. 'System-Wide Harmonic Mitigation in a Diesel-Electric Ship by Model Predictive Control'. In: *IEEE Trans. Ind. Electron.* 63.7 (July 2016), pp. 4008–4019.

[219] E. Skjong, E. Rødskar, M. Molinas, T.A. Johansen and J. Cunningham. 'The Marine Vessel's Electrical Power System: From its Birth to Present Day'. In: *Proceedings of the IEEE* 103.12 (Dec. 2015), pp. 2410–2424.

[220] Espen Skjong, Marta Molinas and Tor Arne Johansen. 'Optimized current reference generation for system-level harmonic mitigation in a diesel-electric ship using non-linear model predictive control'. In: *2015 IEEE International Conference on Industrial Technology (ICIT)*. IEEE Conference Publications. 2015, pp. 2314–2321.

[221] Espen Skjong, Jon Are Suul, Tor Arne Johansen and Marta Molinas. *In search of the best method for system-wide harmonic compensation in isolated microgrids: MPC vs offline analytical optimization*. Submitted for publication.

[222] Espen Skjong, Miguel Ochoa-Gimenez, Marta Molinas and Tor Arne Johansen. 'Management of harmonic propagation in a marine vessel by use of optimization'. In: *2015 IEEE Transportation Electrification Conference and Expo (ITEC)*. IEEE. 2015, pp. 1–8.

[223] Espen Skjong, Jon Are Suul, Marta Molinas and Tor Arne Johansen. 'Optimal Compensation of Harmonic Propagation in a Multi-Bus Microgrid'. In: *International Conference on Renewable Energies and Power Quality (ICREPQ'16), Renewable Energy and Power Quality Journal (RE&PQJ)*. 2016, pp. 1–6.

[224] Espen Skjong, Marta Molinas, Tor Arne Johansen and Rune Volden. 'Shaping the Current Waveform of an Active Filter for Optimized System Level Harmonic Conditioning'. In: *Proceedings of the 1st International Conference on Vehicle Technology and Intelligent Transport Systems*. 2015, pp. 98–106.

[225] E.C. Smith. *A short history of naval and marine engineering*. Cambridge University Press; Reissue edition (October 31, 2013), 1938.

[226] Gordon Smith. *World War 1 at Sea: United States Navy*. Accessed: 2015-08-12. URL: http://www.naval-history.net/WW1NavyUS.htm.

[227] Siri Solem, Kjetil Fagerholt, Stein Ove Erikstad and Øyvind Patricksson. 'Optimization of diesel electric machinery system configuration in conceptual ship design'. In: *Journal of Marine Science and Technology* 20.3 (2015), pp. 406–416.

[228] Asgeir J. Sørensen. 'A survey of dynamic positioning control systems'. In: *Annual Reviews in Control* 35.1 (2011), pp. 123 –136.

[229] *SS Columbia (1880)*. Accessed: 2015-06-29. URL: https://en.wikipedia.org/wiki/SS_Columbia_(1880).

[230] Volker Staudt, Roman Bartelt and Carsten Heising. 'Fault Scenarios in DC Ship Grids: The advantages and disadvantages of modular multilevel converters.' In: *IEEE Electrification Magazine* 3.2 (2015), pp. 40–48.

[231] Z.S. Steiner. *The Lights that Failed: European International History, 1919-1933*. Oxford history of modern Europe. Oxford University Press, 2005.

[232] R. P. Stratford. 'Harmonic Pollution on Power Systems - A Change in Philosophy'. In: *IEEE Trans. Ind. Appl.* (Oct. 1980).

[233] Ray P Stratford. 'Harmonic pollution on power systems - A change in philosophy'. In: *IEEE Trans. Ind. Appl.* IA-16.5 (1980), pp. 617–623.

[234] C. Sulzberger. 'First Edison Lights at Sea: The SS Columbia Story, 1880-1907 [History]'. In: *Power and Energy Magazine, IEEE* 13.1 (Jan. 2015), pp. 92–101.

[235] M. Summerfield. *Advanced Qt Programming: Creating Great Software with C++ and QT 4*. Prentice Hall open source software development series. Addison-Wesley, 2011.

[236] L.M. Surhone, M.T. Timpledon and S.F. Marseken. *War of Currents: George Westinghouse, Thomas Edison, Direct Current, Electric Power, Alternating Current, Nikola Tesla*. Betascript Publishing, 2010.

[237] Jon Are Suul. 'Control of Grid Integrated Voltage Source Converters under Unbalanced Conditions'. PhD thesis. Department of Electrical Power Engineering: Norwegian University of Science and Technology, Mar. 2012.

[238] N. Tesla and Westinghouse Electric & Manufacturing Company. *Transmission of Power; Polyphase System: Tesla Patents*. General Books LLC, 1893.

[239] 'The Columbia'. In: *Scientific American* 42.21 (May 1880), p. 326.

[240] *The Cunard Liner Queen Elizabeth 2: From the Desk of the Chief Engineer*. Accessed: 2015-08-17. URL: http://www.qe2.org.uk/engine.html.

[241] *The invention of the electric motor 1856-1893*. Accessed: 2015-06-30. URL: http://www.eti.kit.edu/english/1390.php.

[242] *The Pacific War Online Encyclopedia: T2-SE-A1 Class, U.S. Tankers*. Accessed: 2015-08-06. URL: http://pwencycl.kgbudge.com/T/2/T2-SE-A1_class.htm.

[243] D.E. Thomas. *Diesel: Technology and Society in Industrial Germany*. University of Alabama Press, 2004.

[244] Siang Fui Tie and Chee Wei Tan. 'A review of energy sources and energy management system in electric vehicles'. In: *Renewable and Sustainable Energy Reviews* 20 (2013), pp. 82–102.

[245] R.W. Tolf. *The Russian Rockefellers: The Saga of the Nobel Family and the Russian Oil Industry*. Hoover Institution publications. Hoover Institution Press, Stanford University, 1976.

[246] Laura Tribioli, Michele Barbieri, Roberto Capata, Enrico Sciubba, Elio Jannelli and Gino Bella. 'A real time energy management strategy for plug-in hybrid electric vehicles based on optimal control theory'. In: *Energy Procedia* 45 (2014), pp. 949–958.

[247] J Turso, T Dalton, S McCullough, C Mako, C Bottorff, W Ainsworth, S Foster, R Peden and D Johnson. *USS Makin Island Auxiliary Propulsion System: Identification and Accommodation of System-Level Interactions*.

[248] National Research Council (U.S.). Panel on Wartime Uses of the United States Merchant Marine. *The Role of the U.S. Merchant Marine in National Security: Project Walrus Report*. National Academy of Sciences. National Research Council. Publication. National Academy of Sciences-National Research Council, 1959.

[249] *U.S. Navy: Energy, Environment & Climate Chage*. Accessed: 2015-08-21. URL: http://greenfleet.dodlive.mil/files/2010/04/MakinIslandEnvironmentFactsheet_v2.pdf.

[250] *USS New Mexico (BB-40) Association: History*. Accessed: 2015-07-03. URL: http://bb40ussnewmexico.com/history/.

[251] T.L. Vandoorn, B. Renders, L. Degroote, B. Meersman and L. Vandevelde. 'Active Load Control in Islanded Microgrids Based on the Grid Voltage'. In: *IEEE Trans. Smart Grid* 2.1 (Mar. 2011), pp. 139–151.

[252] M. Vatani, B. Bahrani, M. Saeedifard and M. Hovd. 'Indirect Finite Control Set Model Predictive Control of Modular Multilevel Converters'. In: *IEEE Trans. Smart Grid* 6.3 (May 2015), pp. 1520–1529.

[253] A. N. Venkat, I. A. Hiskens, J. B. Rawlings and S. J. Wright. 'Distributed MPC Strategies With Application to Power System Automatic Generation Control'. In: *IEEE Trans. Control Syst. Technol* 16.6 (Nov. 2008), pp. 1192–1206.

[254] Andrea Vicenzutti, Daniele Bosich, Giovanni Giadrossi and Giorgio Sulligoi. 'The Role of Voltage Controls in Modern All-Electric Ships: Toward the all electric ship.' In: *IEEE Electrification Magazine* 3.2 (2015), pp. 49–65.

[255] A. Vine. *A Very Strange Way to Go to War: The Canberra in the Falklands*. Aurum Press, Limited, 2014.

[256] *Volta's Life and Works*. Accessed: 2015-08-11. URL: http://www.alessandrovolta.info/life_and_works_8.html.

[257] *What Makes a Warship: Engines*. Accessed: 2015-08-06. URL: http://worldofwarships.com/en/news/common/warship-engines/.

[258] Edward C Whitman. 'Air-Independent Propulsion'. In: *Undersea Warfare* 4.1 (2001), p. 1231.

[259] Thomas Wildenberg. *Auke Visser's Other Esso Related Tankers Site*. Accessed: 2015-08-12. URL: http://www.aukevisser.nl/others/id339.htm.

[260] *World Submarine History Timeline, Part One: 1580-1869*. Accessed: 2015-08-11. URL: http://www.submarine-history.com/NOVAone.htm.

[261] *World Submarine History Timeline, Part Two: 1870-1914*. Accessed: 2015-08-11. URL: http://www.submarine-history.com/NOVAtwo.htm.

[262] C.-J Wu, J.-C. Chiang, S.-S. Yen, C.-J. Liao, J.-S. Yang and T.-Y. Guo. 'Investigation and Mitigation of Harmonic Amplification Problems Caused by Single-tuned Filters'. In: *IEEE Trans. Power Del.* 13.3 (July 1998), pp. 800–806.

[263] Fang Xu, Hong Chen, Weiwei Jin and Yueting Xu. 'FPGA implementation of nonlinear model predictive control'. In: *The 26th Chinese Control and Decision Conference (2014 CCDC),* May 2014, pp. 108–113.

[264] Bijan Zahedi, Lars E Norum and Kristine B Ludvigsen. 'Optimized efficiency of all-electric ships by dc hybrid power systems'. In: *Journal of Power Sources* 255 (2014), pp. 341–354.

[265] Zhibin Zhou, Mohamed Benbouzid, Jean Frédéric Charpentier, Franck Scuiller and Tianhao Tang. 'A review of energy storage technologies for marine current energy systems'. In: *Renewable and Sustainable Energy Reviews* 18 (2013), pp. 390–400.

[266] Edwin Zivi. 'Design of robust shipboard power automation systems'. In: *Annual Reviews in Control* 29.2 (2005), pp. 261 –272.